Electrochemical Studies of Polarisable Liquid/Liquid Interfaces

by

Alan Andrew Stewart

Doctor of Philosophy

University of Edinburgh

1990

To my parents and Anne.

Acknowledgement

I wish to thank Dr. Hubert Girault for his guidance and encouragement throughout the past three years. I am also very grateful for the help and financial assistance I have recieved from Dr. Jerry M^{c}Aleer and MediSense (U.K.) Inc. I would also like to acknowledge the help of the technical staff in the department of chemistry, especially the electronic workshop.

I want to thank the past and present members of the physical electrochemistry group at Edinburgh, in particular Alan Brown for his help with some of the diagrams. Finally I wish to thank all my friends for the good times and helping me out of the bad ones.

Abstract

The interface between two immiscible electrolyte solutions (ITIES) has been investigated for cyclic/linear sweep voltammetry of ion transfer, facilitated ion transfer and electron transfer.

Approximate analytical solutions have been derived for the different geometries of liquid/liquid interfaces which are known, i.e. planar, spherical/hemispherical, micro-hole and micropipette interfaces, for both reversible and quasi-reversible charge transfer. For planar ITIES the solution is the same as for linear diffusion for electron transfer at a metal/electrolyte interface. For spherical and hemispherical ITIES new solutions have been derived which allow a kinetic analysis to be carried out on cyclic voltammetric results, without the need to use extremely high sweep rates. The solution for a spherical interface is then used to approximate a solution for a micro-hole interface by applying the approximation that microdisc and spherical electrodes are equivalent when the ratio of the radii of the spherical electrode to the microdisc electrode is $2/\pi$. This approximation is also used to evaluate a solution for ion transfer across an interface supported at the tip of a micropipette, where the system is also fully characterised experimentally, for voltammetry. Using a similar numerical method as applied to the above problems a solution was evaluated for electron transfer across a planar ITIES for both reversible and quasi-reversible reactions. For all of these approximate solutions the trends found are the same as those seen from experimental results.

A method is also presented for the kinetic analysis of "steady-state" voltammetric waves for facilitated ion transfer across an ITIES supported at the tip of a micropipette. The technique is then used to evaluate the rate of K^+ transfer facilitated by BD18C6 and Li^+ transfer facilitated by both ETH1810 and 2,9-dibutyl -1,10-phenanthroline.

The use of liquid/liquid interfaces is also investigated as an assay method for catecholamines. As well as using ion transfer at ITIES as a method to determine catecholamines the use of emzyme coupled reactions in conjunction with standard redox electrochemistry or liquid/liquid electrochemistry, is also discussed.

Symbols and units.

The following symbols and abbreviations have been used throughout.

$\alpha_{t.c.}$ charge transfer coefficient for electron transfer.
A electrode area, cm^2
a_i activity of ion, i
BTPPA bis[triphenyl(phosphoranylidene)]ammonium

c^* bulk concentration
CE counter electrode
CV crystal violet
COMT catechol-*O*-methyl transferase

D diffusion coefficient, cm^2s^{-1}
DA dopamine
DB18C6 dibenzo-18-crown-6
DCE 1,2-dichloroethane

E epinephrine
ETH1810 see text

F Faraday's constant

KTPBCl potassium tetrakis[chlorophenyl]borate
k electrochemical rate constant

MAO mono amine oxidase
MeDA 3-methoxydopamine

NaTPB sodium tetraphenylborate
NE norepinephrine
η Kinematic viscosity
ppm parts per million

R universal gas constant

SCE saturated calomel electrode
SAM S-adenosylmethionine

TBA tetrabutyl ammonium
TEA tetraethyl ammonium
TMA tetramethyl ammonium
TPAs tetraphenyl arsonium

WE working electrode

z_i charge on ion, i

Table Of Contents

Chapter 1
Introduction

The first studies of liquid/liquid interfaces, by electrochemical methods, were carried out in 1902 by Nernst and Riesenfeld [1], for the determination of transport numbers of ions in organic solvents. These were carried out by passing a current through a water/phenol/water system. Studies, of this type, using concentration cells, and studies to determine the origin of the potential difference in these cells [2-5] dominated the interest in liquid/liquid interfaces until the late 1930's. Around this time the study of the structure and the potential distribution [6,7] across these interfaces came to the fore, and indeed the debate on these topics still continues today. It was not until it was discovered, by Gavach *et al* [8], that the interface between two immiscible electrolyte solutions (ITIES) was polarisable that much of the current interest in this area began. This has meant that many of the techniques used to study electron transfer at metal/ electrolyte interfaces could be applied to the study of both ion and electron transfer at liquid/liquid interfaces. The development of the electrochemistry of ITIES from this date onwards will be discussed more fully in chapter 2.

Several different geometries of liquid/liquid interfaces are known. The standard interface being a large planar ITIES, usually a disc with a diameter greater than 50μm, however spherical or hemispherical interfaces, i.e. dropping electrolyte electrodes and hanging electrolyte drop electrodes, are also possible. As well large scale ITIES, micro ITIES have also been developed, which are similar to the the metal/electrolyte micro electrodes which have been developing since the mid 1970's [9]. An ITIES equivalent to a microdisc electrode has recently been reported [10] where the interface is supported at a

hole in a very thin sheet of polymer. Another microITIES is where the interface is suspended at the tip of a micropipette has also been reported [11], however there is no equivalent system for a solid/electrolyte interface. A schematic diagram of these geometries of liquid/liquid interfaces is shown in figure 1.1. All of these geometries of liquid interfaces have been studied by cyclic voltammetry, however analytical solutions for all have not been reported. In chapter 3 the cyclic voltammetric responses of these different ITIES will be discussed in more detail for both ion and electron transfer, for reversible and quasi-reversible systems. Approximate analytical solutions for cyclic voltammetry are also presented.

The study of ITIES has been applied to several different areas, however an area which has a large potential is their use for the sensing and determination of ions in solutions [12], particularly for amperometric devices. One of the advantages of an ITIES as a sensing device is that it introduces a different type of electrochemical selectivity. Instead of the resolution of different species in solution by their redox potentials, as at metallic electrodes, analysis at the ITIES relies on the characteristic transfer potentials of the species, between the two liquids. This then allows the resolution of anions and cations which have oxidation/reduction potentials which are very similar, since the potentials at which they will cross an ITIES will be very far apart. This technique can also be used for the detection of ions which have redox potentials which cannot be attained at metal electrodes. As well as having this new type of selectivity it is also possible to introduce selective molecules into the organic phase which will selectively complex ions, so altering their transfer potentials and allowing these ions to be detected. This technique, known as facilitated ion transfer, will be

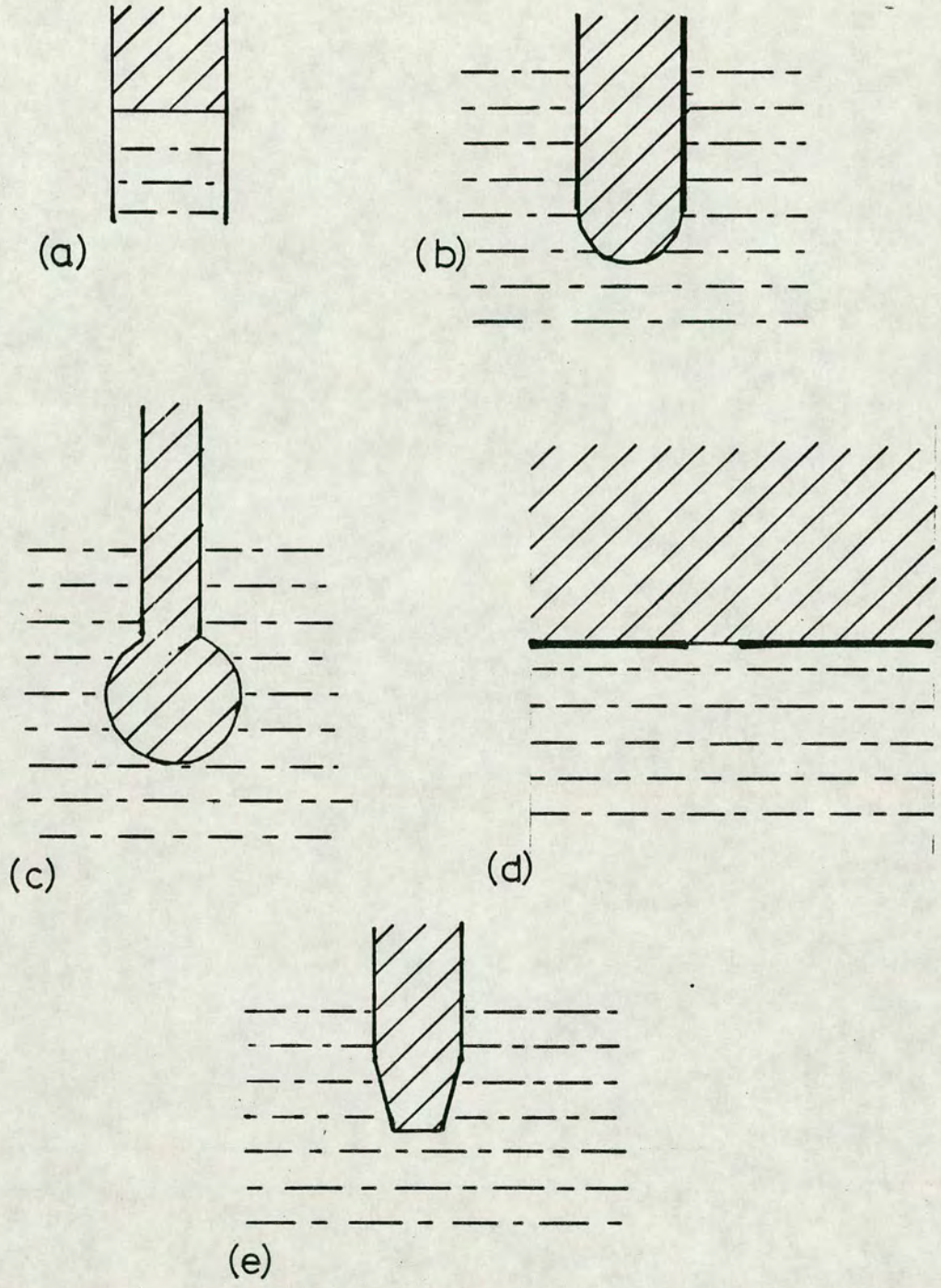

Figure 1.1 Diagram showing the different geometries of liquid/liquid interfaces. (a) planar interface (to scale), (b) hemispherical (half scale), (c) spherical interface (half scale), (d) micro disc interface (1mm: 2μm), (e) micropipette interface (1mm: 2μm).

discussed in chapter 2, and a method to evaluate the kinetics of the global transfer of an ion from one phase to the other will be given in chapter 4.

The selectivity introduced by normal ion transfer at an ITIES will also be investigated as a method to determine catecholamines in solution. This technique is particularly applicable to these biological molecules since the major interfering species, to detecting catecholamines, by conventional redox electrochemistry, are anions whereas catecholamines are cations, and as mentioned earlier, separation of anions from cations by ion transfer at an ITIES is relatively straightforward. This will be discussed in chapter 5, along with the possibility of coupling enzymes with electrochemistry as a method to detect catecholamines.

Chapter 2
Methodology, Theory and Experimental Procedures For Charge Transfer At ITIES

2.1 Resume Of Charge Transfer at Liquid/Liquid Interfaces Since 1968

As described in the introduction until 1968 the study of liquid/liquid interfaces had been confined mainly to studies of the origins of potential differences between two liquid phases and the structure and distribution of the potential at these interfaces. After this date the study of charge transfer reactions came to the fore, due to the discovery by Gavach *et al* [1] that liquid/liquid interfaces could be made polarisable. Consequently many of the techniques that are used to study charge transfer reactions at metal/electrolyte interfaces could be used to study charge transfer reactions at liquid/liquid interfaces.

Much of the motivation behind the electrochemical studies of charge transfer at liquid/liquid interfaces was due to the similarities that could be drawn between them and biological interfaces. Thus a single liquid/liquid interface could be used as an analogy to one half of a biological interface, for the study of either ion or electron transfer across these interfaces.

Initially most of the studies at the interface between two immiscible electrolyte solutions, or ITIES, as they are known, were carried out by controlled current techniques, i.e. chronopotentiometry [13-16]. The reason why these were predominant was due to the large amount of ohmic drop across the organic phase, which distorted any attempts to use controlled potential techniques.

In 1976 Koryta *et al* [17] attempted to use a three electrode configuration at a dropping electrolyte electrode (analogous to a dropping mercury electrode) for a polarographic type study, the type of cell used is shown in figure 2.1.1. Here a reference electrode (Ag/AgBr) and a platinum auxilary electrode were placed in the aqueous, dropping, phase and the organic phase contained only a platinum electrode. Thus the system was analogous to a normal metal/electrolyte system where the working electrode is the organic phase. However due to the large ohmic drop, often referred to as iR drop, no proper analysis of these results could be carried out. In 1977 Z. Samec *et al* [18] used a four electrode system, and a four electrode potentiostat, to examine the transfer of tetramethyl ammonium (TMA^+) across a water/nitrobenzene interface, by cyclic voltammetry. This system is shown schematically in figure 2.1.2, and it greatly decreased the ohmic drop by controlling the potential difference, between the two phases, by means of two reference electrodes in Luggin capillaries, which were positioned very close to either side of the interface. However the use of this 4-electrode system did not completely remove the effects of iR drop in the organic phase, and indeed it was reported, in this reference, that the transfer of TMA^+ was a kinetically controlled process, which has been subsequently found not to be the case, and the origin of these "kinetics" were in fact iR effects.

In 1979 Samec *et al* [19] showed that it was possible to compensate for the effects of ohmic drop in a 4-electrode system by means of a positive feedback loop, in a manner similar to that used at a three electrode configuration, and this allowed the problem of organic phase resistance to be almost totally solved.

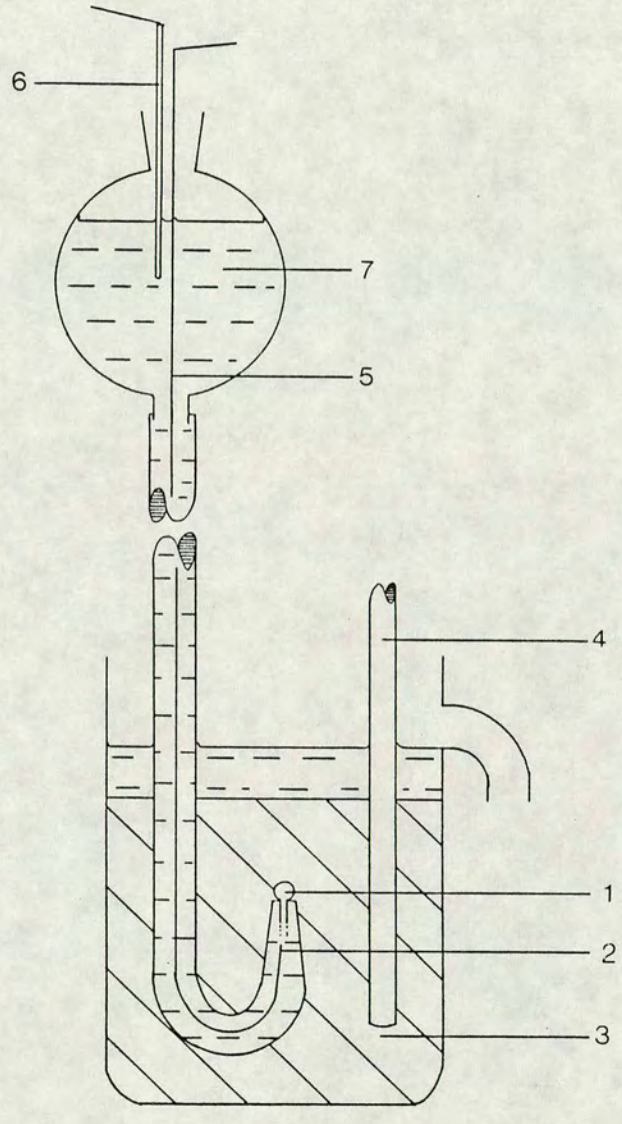

Figure 2.1.1 Schematic diagram of three electrode dropping electrolyte system used by Koryta *et al.* (1) dropping electrode, (2) Ag/AgBr reference electrode, (3) nitrobenzene electrolyte, (4) platinum electrode, (5) insulated lead to Ag/AgBr electrode, (6) auxiliary electrode, (7) aqueous electrolyte.

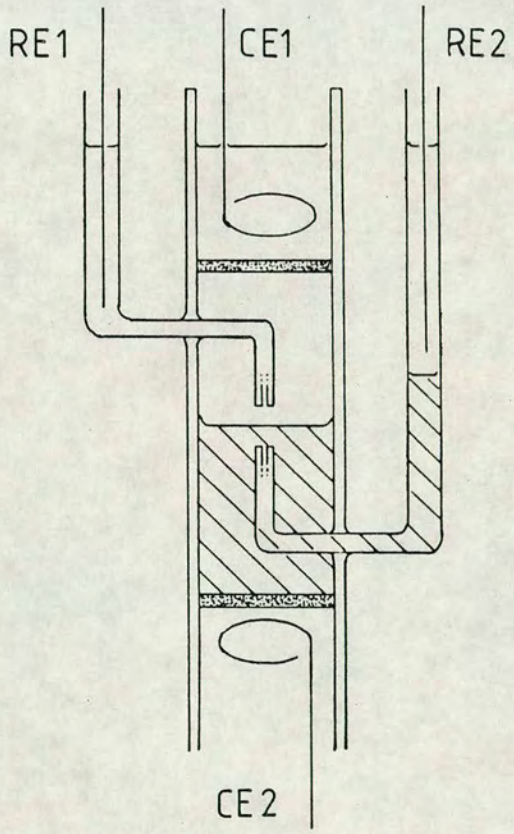

Figure 2.1.2 Schematic diagram of 4-electrode used by Samec *et al.* RE1 and RE2, Ag/AgCl reference electrodes, CE1 and CE2, counter platinum wire electrode. Lower phase contains the nitrobenzene solution.

The use of 4-electrode potentiostats, with iR compensation, opened up the study of charge transfer at ITIES by conventional controlled potential techniques.

Throughout the 1980's many potentiostatic techniques have been used to study charge transfer at ITIES e.g. linear sweep/cyclic voltammetry [19], polarography [20,21], chronoamperometry/coulometry [22], A.C. voltammetry [23] and impedance [24], and differential pulse stripping voltammetry [25]. These polarisable ITIES have been used to study ion transfer[15], facilitated ion transfer[26] and electron transfer[27]; these systems will be discussed, along with the techniques used, later in this chapter.

Recently studies of ITIES have also moved away from the more traditional geometries of these interfaces with the development of micro liquid/liquid interfaces. These new geometries of electrodes, now possible with micro ITIES, will be discussed in 2.4.

2.2 Comparison Between Charge Transfer At Metal/Electrolyte Interfaces and ITIES

Much of the theory and terminology which has been developed for metal/electrolyte interfaces can be directly transferred to charge transfer at ITIES. There are however some differences which should be noted.

2.2.1 Potentials

At metal/electrolyte interfaces the potential difference arises due to the occupied and unoccupied electronic energy levels within the metal or semi-conductor phase and in the redox active species in solution. Whereas at liquid/liquid interfaces the potential difference arises from the Gibbs free

energy of transfer, or partition, of the ions between the two phases, $\Delta G_{t,i}^{\alpha \rightarrow \beta}$, which is in turn related to the solvation energies of the ion in each phase. For each ion it is possible to define a standard Gibbs energy of transfer from phase α to phase β, $\Delta G_{t,i}^{o,\alpha \rightarrow \beta}$. However for individual ions this is not a directly measurable quantity, but it is possible to evaluate the standard Gibbs energy of transfer of a salt, by measuring the difference in energies of solution of the salt in both phases. It is then only possible to evaluate the standard ionic Gibbs energy of transfer from the relationship

$$\Delta G_{MX,t}^{o,\alpha \rightarrow \beta} = \Delta G_{M,t}^{o,\alpha \rightarrow \beta} + \Delta G_{X,t}^{o,\alpha \rightarrow \beta} \qquad (2.2.1)$$

by making an assumption on how $\Delta G_{MX,t}^{o,\alpha \rightarrow \beta}$ can be related to the individual ionic components. Several different assumptions have been made, the most common one being the Grunwald assumption [28] i.e.

$$\Delta G_{t,TPAs}^{o,\alpha \rightarrow \beta} = \Delta G_{t,TPB}^{o,\alpha \rightarrow \beta} = 1/2\ \Delta G_{t,TPAsTPB}^{o,\alpha \rightarrow \beta} \qquad (2.2.2)$$

(TPAs = tetraphenylarsonium, TPB = tetraphenylboron) The basis of this assumption is the similarity between the two ions, i.e. size, symmetry and the way that the charge is masked under the phenyl groups in each case, thus suggesting that their energies of solvation would be similar. Therefore from the value of $\Delta G_{t,TPAsTPB}^{o,\alpha \rightarrow \beta}$ it is possible to evaluate values of $\Delta G_{t,i}^{o,\alpha \rightarrow \beta}$. This is an unrealistic assumption since the charge on these species will not be totally masked by the phenyls and, due to the opposite charges, the ions will both be solvated to different degrees.

As mentioned earlier the potential differences arise from the variations in $\Delta G_{t,i}^{o,\alpha \rightarrow \beta}$ and from these values it is possible to evaluate the potential difference between the two phases, i.e. the Galvani Potential difference, at

equilibrium. At thermodynamic equilibrium

$$\tilde{\mu}_i^{\alpha} = \tilde{\mu}_i^{\beta} \qquad (2.2.3)$$

where

$$\tilde{\mu}_i^{\alpha} = \mu_i^{\alpha} + z_i F \varphi^{\alpha} \qquad (2.2.4)$$

the chemical and the electrical potentials, respectively, of an ion in phase α. A similar expression can be written of phase β. The chemical difference can be expanded to

$$\mu_i^{\beta} - \mu_i^{\alpha} = \mu_i^{o,\beta} + RT\ln a_i^{\beta} - \mu_i^{o,\alpha} - RT\ln a_i^{\alpha} \qquad (2.2.5)$$

which can be related to the standard Gibbs energy of transfer by

$$\mu_i^{o,\beta} - \mu_i^{o,\alpha} = \Delta G^{o,\alpha\rightarrow\beta} \qquad (2.2.6)$$

Thus it can be written

$$\Delta^{\beta}_{\alpha}\varphi = \varphi^{\beta} - \varphi^{\alpha} = -\Delta G^{o,\alpha\rightarrow\beta}/z_i F + RT/z_i F \ln(a_i^{\alpha}/a_i^{\beta}) \qquad (2.2.7)$$

By defining a standard potential of transfer

$$\Delta^{\beta}_{\alpha}\varphi_i^{o} = -\Delta G^{o,\alpha\rightarrow\beta}/z_i F \qquad (2.2.8)$$

we obtain

$$\Delta^{\beta}_{\alpha}\varphi = \Delta^{\beta}_{\alpha}\varphi_i^{o} + RT/z_i F \ln(a_i^{\alpha}/a_i^{\beta}) \qquad (2.2.9)$$

This is analogous to the Nernst equation for metal/electrolyte interfaces, and if a formal potential term is introduced, in place of the standard potential, then it is possible to rewrite the Nernst equation in terms of the concentrations in each phase. In future all Galvani potential differences will be written as E, E^{o}, $E^{o'}$ etc. for $\Delta^{\beta}_{\alpha}\phi$, $\Delta^{\beta}_{\alpha}\phi^{\circ}$ and $\Delta^{\beta}_{\alpha}\phi^{o'}$ etc. Thus it is possible to define standard Galvani potential differences in the same way that it is possible to define standard

electrode potentials at metal/ electrolyte interfaces. However they are different in that the former refers potentials to the Grunwald assumption, and the latter assumes that the free energy of the reaction $H^+ + e^- \rightleftharpoons 1/2H_2$ is zero.

2.2.2 "Polarisation Windows"

Again by analogy with metal/electrolyte interfaces it is possible to define a range over which the interface behaves in a polarisable manner. For a metal/electrolyte interface the potential range over which the metallic electrode behaves in this way is limited by the material of the solid electrode, the solvents used and the species in the solution, i.e. it is governed by the rates of oxidation and reduction of the different components in solution. At an ITIES however these factors do not arise since, except in the special case of electron transfer, the process does not involve the oxidation or reduction of the species in solution. Thus the range of polarisability of the interface is governed by different criteria i.e. the different potentials which are required to be applied to cause the ions in either phase to cross the interface. Therefore it is necessary to have supporting electrolyte ions in each phase which are at extremes in the potential range hence yielding a working range which is as large as possible. This is done by having hydrophilic salts as the supporting electrolyte in the aqueous phase, and conversely having hydrophobic salts in the organic phase. Some of the more common salts used in the aqueous phase are $MgCl_2$ and LiCl, and for the organic phase TBATPB (tetrabutylammonium tetraphenylboron), or TBATPBCl (tetrabutylammonium tetrakis[chlorophenyl]boron). However more exotic organic phase supporting electrolyte ions have been investigated and have been found to produce much larger "potential windows". These are of particular interest in extending the positive ($\Delta^o_w\phi$) end of the window, since changing the organic supporting electrolyte has no effect on lengthening the negative limit. This has been shown [29] to be due to the aqueous phase

limiting this end and thus producing very hydrophobic organic anions has no effect, although they do exist, i.e. tetrakis[pentafluorophenyl]borate ($TPFTPB^-$) and tetrakis[di-3,5-trifluoromethylphenyl]borate ($TDTFMPB^-$). The hydrophobic cations which have been used are bis[triphenylphosphoranylidene] ammonium ($BTPPA^+$) or crystal violet (CV^+), and the use of these for organic phase supporting electrolytes allow almost all aqueous phase ions to transfer within a polarisable range. The structures of these very hydrophobic ions are shown in figure 2.2.1.

2.2.3 Mass Transports

As with metal/electrolyte interfaces there are three main types of mass transport that can occur at an ITIES, i.e. migration, convection and diffusion.

2.2.3.1 Migration

Migration is the movement of a charged species in solution under the influence of an electric field, i.e. a potential gradient. This is the main mechanism by which charge passes through the bulk of the solution, to counter the flow of electrons in the external circuit. However this type of mass transport may only play a negligible part in the transport of the electroactive species since any ionic species in solution can carry this charge. Thus if a large concentration of a supporting electrolyte is used then only negligible amounts of the electroactive species are transported by this method.

2.2.3.2 Convection

Convection is the movement of a species in solution due to mechanical forces, e.g. vibration of the electrochemical cell, density gradients due to temperature fluctuations. However on the time scale of most of the techniques which are used, these convective motions can be eliminated with careful

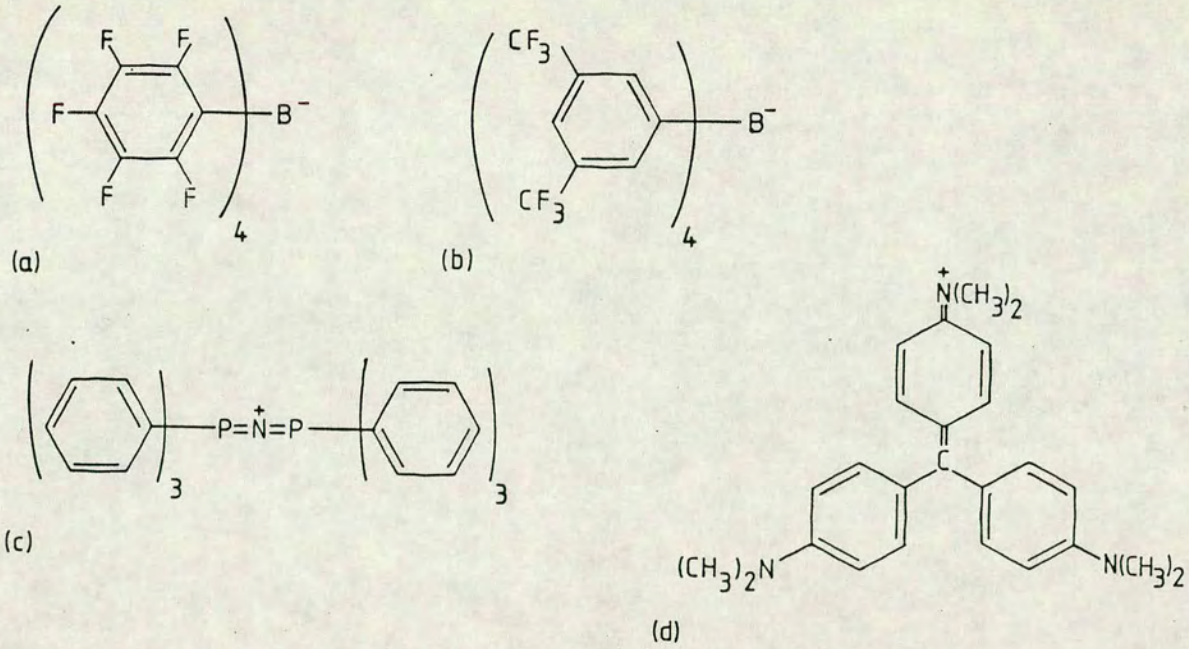

Figure 2.2.1 Diagrams of the hydrophobic ions (a) $TPFPB^-$, (b) $TDTFMPB^-$, (c) $BTPPA^+$, (d) CV^+.

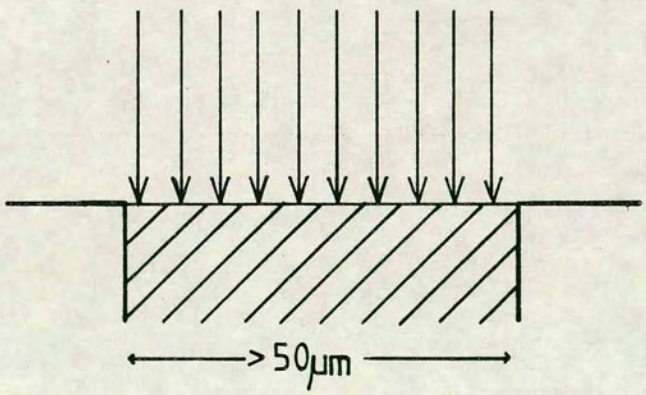

Figure 2.2.2 Diagram showing linear diffusion to a planar electrode.

experimental techniques. There are some techniques where this convective motion of the species is deliberately introduced i.e. rotating disc, wall jet electrodes and dropping polarography, however these techniques will not be discussed here.

2.2.3.3 Diffusion

Diffusion is the movement of a species due to a concentration gradient in solution, where the species will try to move down this gradient so as to produce a uniform concentration throughout the solution. This is the most important form of mass transfer in an electrochemical cell, since the concentration of the electroactive species changes, with time, at the electrochemical interface due to either oxidation or reduction, or due to charge transfer to the other phase at an ITIES. This therefore sets up a concentration gradient, which induces the electroactive species to diffuse so as to restore the uniformity of the concentrations. It is this concentration gradient which controls the arrival and removal of electroactive reactants and products at the interface , and this in turn governs the current which flows across the interface at the applied potential.

The movement of these species by diffusion can be described by Fick's Laws of diffusion, which describe the flux of a substance and its concentration as a function of time and position. The flux being the net mass transfer rate of the electroactive species in units of amount per unit time per unit area.

The flux of the species to an interface is very dependent upon the geometry of the interface being examined. If the interface is a flat semi-infinite plane, then the transfer at the interface is said to be linear or planar, see figure 2.2.2. However as the size of this interface is decreased to micrometer dimensions the diffusion is no longer described as planar, due to the enhanced effect of

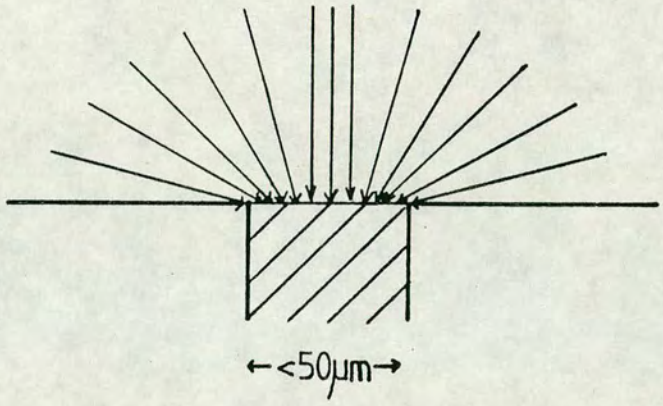

Figure 2.2.3 Diagram showing diffusion to a microdisc electrode with a contribution of edge effects.

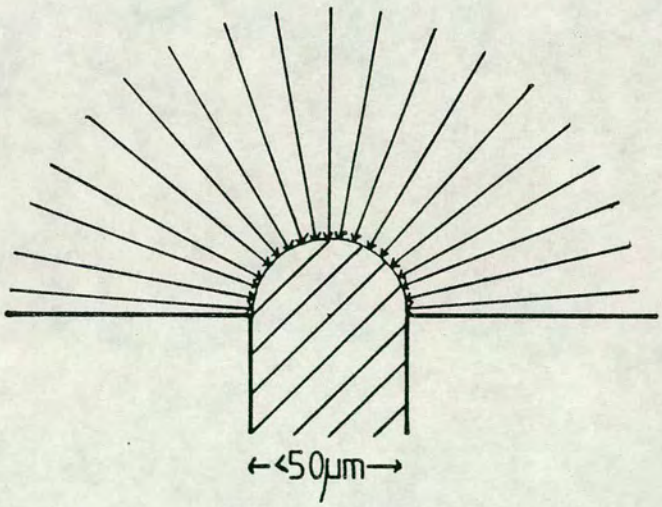

Figure 2.2.4 Diagram showing diffusion to a hemi-spherical electrode.

diffusion to the edge of the electrode, see figure 2.2.3. This greatly complicates the mathematical treatment of the flux to the electrode and it is very difficult to solve these equations for electrochemical problems. If the interface is spherical, or hemispherical, then the diffusion is said to be spherical, see figure 2.2.4, and Fick's laws have been derived for such a case. Due to the similarity between the types of diffusion found at spherical and at microplane (usually microdisc) electrodes approximate solutions for the diffusion to micro disc electrodes are derived from the solutions for spherical diffusion, this will be explained more fully in 3.3.2.

For linear diffusion the flux J_i is described as the number of moles of the electroactive species, i, to pass a given location per second per cm^2 of area normal to the axis of diffusion. The flux is proportional to the concentration gradient and is given by Fick's first law for linear diffusion

$$-J(x,t) = D_i[\partial c_i(x,t)/\partial x)] \qquad (2.2.10)$$

x being the distance from the plane being examined. From this it is possible to derive an expression for the variation of concentration at a location, x, with time

$$\partial c_i(x,t)/\partial t = D_i[\partial^2 c_i(x,t)/\partial x^2] \qquad (2.2.11)$$

which is Fick's second law of linear diffusion.

For spherical diffusion the flux can be defined in the same way as for a planar electrode i.e.

$$-J_i(r,t) = D_i[\,\partial c_i(r,t)/\partial r\,] \qquad (2.2.12)$$

with r being the radial distance of the plane from the centre of the sphere. From the above expression it is possible to derive Fick's second law of spherical diffusion i.e.

$$\partial c_i(r,t)/\partial t = D_i[\,\partial^2 c_i(r,t)/\partial r^2 + 2/r\ \partial c_i(r,t)/\partial r\,] \qquad (2.2.13)$$

The flux of an electroactive species, i, at the interface is related to the current at the surface by the expression, for linear diffusion,

$$-J_i(0,t) = i/nFA = D_i[\,\partial c_i(x,t)/\partial x\,]_{x=0} \qquad (2.2.14)$$

and a similar expression can be derived for spherical diffusion for $r=r_o$, r_o being the radius of the spherical / hemispherical interface.

It is the evaluation of the surface concentration with time, e.g. $c_i(0,t)$ for linear diffusion, for the electroactive products and reactants which is the major problem in producing solutions for the current, or the potential, for almost all electrochemical techniques which rely on diffusion for mass transfer. The solution of these problems will be treated in more detail in chapter3.

2.3 Electrochemical Methods Used to Study Charge Transfer At ITIES

As mentioned earlier in this chapter many of the techniques which are used to study charge transfer at metal/ electrolyte interfaces, can be applied to charge transfer at ITIES. Presented here are the different techniques which have been used to study the three different types of charge transfer possible at liquid/liquid interfaces.

2.3.1 Ion Transfer

2.3.1.1 Cyclic Voltammetry

After the initial use of the four electrode potentiostat, with iR drop compensation, cyclic voltammetry was one of the first potentiostatic techniques to be investigated.

It was shown for reversible ion transfer that the cyclic voltammograms produced showed similar properties to those found for reversible ion transfer at a metal/electrolyte interface, [21]. Thus for processes controlled by linear diffusion the forward peak current, i_p, should be proportional to the square root of the potential scan rate and the potential difference between the current peaks and the half peak potential should be independent of scan rate. From these criteria of reversibility it should be possible to use cyclic voltammetry as a technique to check the reversibility of ion transfer, and also the Randles-Sevcik relationship should hold i.e.

$$i_p = 0.4463 z_i F A c^* (nF/RT)^{1/2} D^{1/2} \nu^{1/2}$$

This then allows cyclic voltammetry to be used as a method to evaluate the

diffusion coefficients of the ions which are being transferred and also to evaluate the concentration of a species which is in solution, for diffusion limited transfers. As well as this it should be possible to evaluate formal, or standard, Galvani potential differences of transfer from the relationship

$$\Delta_{\alpha}^{\beta}\phi_{i,1/2} = \Delta_{\alpha}^{\beta}\phi_{i}^{o} + RT/z_{i}F \ln(\gamma_{i}^{\alpha}D_{i}^{\beta} / \gamma_{i}^{\beta}D_{i}^{\alpha})$$

which is analogous to the half wave potential of charge transfer at metal/electrolyte interfaces. However estimates of the values of the activity coefficients must be made which are heavily dependent on the degree of ion pairing in a particular solvent. The ratio of the diffusion coefficients must also be approximated to the inverse ratio of the viscosities of both solvents, as predicted by Walden's rule which can be written as

$$D_o/D_w = \eta_w/\eta_o$$

Due to these reasons great care must be taken when using this analysis.

Before carrying out analysis of any data from cyclic voltammetry of ITIES it must be certain that the correct amount of iR drop compensation has been applied, since, as mentioned earlier, the effects of ohmic drop are the same as those of kinetically controlled charge transfer reactions. Cyclic voltammetry has been used to examine the transfer of a wide range of ions e.g. alkali metal ions [19,30], tetra alkylammonium ions [31]. It has also been used to demonstrate the usefulness of ITIES as an analytical tool in the quantitative analysis of biologically active species i.e. catecholamines [32], tetracycline antibiotics [33] and acetylcholine [34,12].

Hence cyclic voltammetry for ion transfer at an ITIES shows the same characteristics as electron-transfer at a metal/electrolyte interface, and thus

can be used in the same manner for analytical purposes, provided the precautions mentioned above are kept in mind.

2.3.1.2 Polarography

In the same way as it has been possible to transfer the theory of cyclic voltammetry from metallic/electrolyte interfaces to ITIES it has been possible to transfer polarographic techniques. It is possible to make a dropping electrolyte electrode in the same way as a dropping mercury electrode [21] can be made. Since the boundary conditions for diffusion are identical in each case, i.e. spherical diffusion, the theories can be directly transformed. However most treatments involving spherical diffusion do not take into account the solubility of the product within the drop, which is what occurs at an ITIES. Thus for a correct analysis the effect of diffusion within the drop should be taken into account, however for the lifetime of the drop, during polarography, the effect of any diffusion within the drop is minimal. Thus analysis of the current response in the usual manner is acceptable i.e.

$$\log_{10}((i_l - i)/i) \textit{ vs. } E$$

gives a linear relationship, with a slope of *c.a.* 58mVdecade^{-1}, and allows the evaluation of the $E_{1/2}$, for the ion transfer reaction. Many of the ions studied by cyclic voltammetry have also been studied by polarography.

2.3.1.3 Differential Pulse Stripping Voltammetry

For electrochemistry at a metal/electrolyte interface, one of the best techniques to resolve the current responses of two species in solution, which have very similar oxidation/reduction potentials, is by differential pulse voltammetry. If this technique is combined with anodic stripping then the advantages of very sensitive and highly selective techniques combine to produce a powerful electroanalytical tool. As has been described in 2.3.1.2

polarography can be used at ITIES using a hanging electrolyte electrode, suggesting that such an electrode could be used for stripping analysis in the same way as at a hanging mercury drop electrode. Thus a hanging electrolyte drop electrode can be used for differential pulse stripping voltammetry. This was first demonstrated by Marecek and Samec [35] for the determination of acetylcholine, and it was shown that it was possible to determine quantities of acetylcholine down to 0.5ppm. They also demonstrated that for a reversible process it is possible to analyse the shape of the current potential curve in the same way as A.C. or square wave or derivative voltammetry i.e.

$$i/i_p = 4P/(1+P)^2$$

where i_p is the peak current and P is given by

$$P = \exp[(z_i F/RT)(E-E_{1/2})]$$

$E_{1/2}$ being the polarograph half wave potential, and hence $E_p=E_{1/2}$. Therefore differential-pulse stripping voltammetry at ITIES is as powerful an electroanalytical technique as at a mercury drop electrode.

2.3.1.4 A.C. Voltammetry

Since cyclic voltammetry and linear sweep voltammetry at ITIES show the same characteristics as at metal/electrolyte interfaces, it would be expected that A.C. voltammetry could be transposed in the same manner. This is indeed the case, with the peak current of an A.C. voltammogram being at the same potential as $E_{1/2}$ evaluated from either cyclic voltammetry or polarography, and also the peak width at half peak height is found to be 90/n mV, which is as expected for a reversible process. A.C. voltammetry at ITIES has been used to evaluate the standard Galvani potential differences for a number of ions, from

$E_{1/2}$ measurements [12]. In addition to this it can be used as an electroanalytical tool since it provides good resolution of individual ions, so solutions containing several ions can be analysed, and with very low detection limits.

2.3.1.5 Chronoamperometry/coulometry

Chronoamperometry has been investigated at ITIES [11] and again it has been shown to behave as for a polarisable interface, with the current-time transient, for a reversible process, behaving as predicted by the Cottrell equation. If a constant time current-potential relationship is investigated the standard S-shaped wave is produced which, on analysis, can be shown to have reversible characteristics, and thus another technique to evaluate $E_{1/2}$ is available. Due to high values of uncompensated cell resistance, this technique is unsuitable to carry out measurements at short times, and thus rate constants at short times are difficult to measure.

Recently Shao and Girault [36], have used chronocoulometry to measure the rates of acetylcholine transfer across a water/ 1,2-dichloroethane interface. This technique circumvents the problems encountered at short times since they investigate the time domain (1-10Hz). They have applied the theory for metal/electrolyte interfaces directly to ion transfer at ITIES, and the values of standard rate constants that they have evaluated are the same order of magnitude as those evaluated by other steady state techniques.

Therefore either of these techniques can be directly transposed from charge transfer at metal/electrolyte interfaces to ion transfer at ITIES.

2.3.2 Facilitated Ion Transfer

As described in 2.2.1 the transfer of an ion across an ITIES depends on the

solvation properties of the ion in both phases i.e. the standard transfer potential is related only to the solvation energies of the ion in each phase. It is however possible to alter the solvation energy of the ion by having a specific ion complexing agent in one or other of the phases, and this can result in a significant shift in the transfer potential of the ion. The complexing agents are usually neutral compounds, ionophores, which are generally hydrophobic macrocyclic compounds, either natural or synthetic, e.g. nonactin, valinomycin, dibenzo-18-crown-6.

If the transfer of the metal ion M^{z+}, in phase α, is facilitated by the transfer of neutral ligand (L), in phase β, there are a number of possible reaction schemes which can be considered, i.e.

$$\begin{array}{ccc} M^{z+,\alpha} + mL^{\alpha} & \overset{K_a^{\alpha}}{\rightleftharpoons} & ML_m^{z+,\alpha} \\ \Big\| K_{M^{z+}}^{\alpha,\beta} & \Big\| K_L^{\alpha,\beta} & \Big\| K_{ML^{z+}}^{\alpha,\beta} \\ M^{z+,\beta} + mL^{\beta} & \underset{K_a^{\beta}}{\rightleftharpoons} & ML_m^{z+,\beta} \end{array}$$

with $K_i^{\alpha,\beta}$ being the distribution coefficient

$$K_i^{\alpha,\beta} = a_i^{\beta}/a_i^{\alpha} \qquad (2.3.6)$$

and K_a is the homogeneous association constant, for phase α or β i.e.

$$K_a^{\alpha/\beta} = a_{ML^+}/a_{M^+}a_L \qquad (2.3.7)$$

The transfer of M^{z+} can proceed via any of these schemes, although some are more likely than others, depending on the system being studied.

For reversible transfers the Galvani potential difference between the phases α and β is given by

$$\Delta^{\beta}_{\alpha}\varphi = \Delta^{\beta}_{\alpha}\varphi^{o} + RT/z_iF \ln a^{\alpha}_{M^{+z}} / a^{\beta}_{M^{+z}}$$

$$= \Delta^{\beta}_{\alpha}\varphi_{ML^{+z}} + RT/z_iF \ln a^{\alpha}_{ML^{+z}_{m}} / a^{\beta}_{ML^{+z}_{m}} \qquad (2.3.8)$$

The most common treatment of ion transfer is by considering the simplified reaction scheme, for a 1:1 stoichiometry,

$$M^{+(\alpha)} \rightleftharpoons M^{+(\beta)}$$

$$M^{+(\beta)} + L^{(\beta)} \rightleftharpoons ML^{+(\beta)}$$

The Galvani potential difference for this is as given above i.e.

$$\Delta^{w}_{o}\phi_{M^+} = \Delta^{w}_{o}\phi^{\circ}_{M^+} + RT/F \ln a^{(o)}_{M^+} / a^{(w)}_{M^+} \qquad (2.3.9)$$

which can be rewritten as

$$\Delta^{w}_{o}\varphi_{M^+} = \Delta^{w}_{o}\varphi^{o'}_{M^+} + RT/F \ln(c_{LM^+}/K_a c_L c_{M^+})$$

where K_a is the association constant as defined above, only in this case it is written in terms of concentrations, not activities, due to the introduction of the Formal Galvani potential difference.

Again in order to simplify the system most experiments are carried out so that the concentration of M^{z+} in the aqueous phase is in excess, thus only the diffusion of the ionophore and the ionophore-metal complex need be considered. This being the case, at the half wave potential, the following applies

$$(c_{LM}/c_L)_{x=0} = (D_L/D_{LM^+})^{1/2} \qquad (2.3.10)$$

and thus the half wave potential is given by

$$\Delta_o^w\varphi_{1/2,LM^+} = \Delta_o^w\varphi^{o'} + RT/zF \ln(D_L/D_{LM^+}) - RT/F \ln(K_a c_{M^+}) \qquad (2.3.11)$$

This allows the evaluation of the association constant, K_a, for a complexation, provided the other parameters are known, i.e. assuming that $D_L=D_{LM^+}$, and that the formal transfer potential can be evaluated from extraction data. As well as being able to evaluate the association constant the use of ionophores also allows the quantitative determination of ions which normally transfer outside the potential window.

In the same way as it is possible to show that the complexation of an ion alters the transfer potential of that ion, a more specific case can be regarded. This is facilitated proton transfer, where the transfer is achieved by the protonation of a basic group on a hydrophobic molecule, not necessarily a cyclic compound. Thus a proton association constant can be evaluated for the organic phase, as the ion-ionophore association constant was evaluated in the previous case. As described in 2.3.1.1 for low dielectric solvents care must be taken in the use of half wave potentials to carry out any kind of quantitative analysis due to ion-pairing effects in the organic phase, however this can be taken into account and an expression for the half wave potential can be found.

If the species which is transferred ion-pairs with the anion TPB^-, tetraphenylborate, this expression is

$$\Delta^{o}_{w\varphi 1/2} = \Delta^{o}_{w\varphi M} + RT/2F \ln (D_{ML^+TPB^-}/D_L) + RT/F \ln(K_{LM^+}a_{M^+}) + RT/F \ln(a_{TPB^-}) \qquad (2.3.12)$$

Therefore if significant ion pairing exists it would be expected that the half wave potential should move ≃30mV per decade change in concentration of TPB^-, given that the activity of TPB^- in a low dielectric solvent is

$$c_{TPB} = [K_d c_{TBA^+TPB^-}]^{1/2} \qquad (2.3.13)$$

Most of the techniques which have been used to study simple ion transfer at an ITIES have also been applied to facilitated ion transfer. The most commonly used one being cyclic voltammetry [37], and again, for a reversible process, all of the characteristics associated with cyclic voltammetry at a metal/electrolyte interface, described in 2.3.1.1, are found to hold for this case. As well as cyclic voltammetry, differential pulse stripping voltammetry has been used [25], and it has shown that using this technique allows the quantitative analysis of ions which would normally not cross inside the "potential window". However care must be taken if using this technique to analyse a solution containing several different ions since the ionophore does not necessarily specifically complex one ion. The specificity towards different ions can be observed by looking at the association constants of the ionophores for the different ions.

The stoichiometry of these complexation reactions is also an important factor, particularly in relation to industrial metal ion extraction processes, and it has been possible to use electrochemical techniques to evaluate this. This has

been done by Homolka *et al* [38] by analysising the peak shape of convolution potential sweep voltammograms.

Facilitated ion transfer at an ITIES thus has several analytical applications. Evaluation of K_a, quantitative analysis of solutions, and evaluation of the stoichiometry of these complexations. These involve the simple analysis of the ion transfers by standard electrochemical techniques.

2.3.3 Electron Transfer

As mentioned earlier in this chapter, charge transfer at an ITIES is important due to the analogies to biological systems, where the transfer is across hydrophilic membranes. To date most of the work at ITIES has involved the study of ion transfer, however it has also been shown that electron transfer can occur at a liquid/liquid interface. This was first demonstrated by Guainazzi *et al* [39], where aqueous Cu(II) was reduced to Cu metal using tetrabutylammonium hexacarbonyl vanadate(-1) in 1,2-dichloroethane by passing a current across the interface. It was subsequently shown by Samec *et al* [16] that electron transfer could also be observed for the system ferro-/ferri- cyanide in water, and ferrocene/ferrocinium in nitrobenzene. Electron transfer has been mainly studied by cyclic voltammetry.

The general reaction scheme for electron transfer is shown below

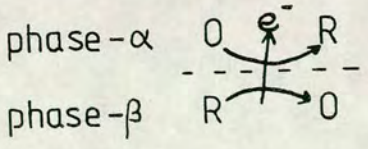

i.e. $O_\alpha + R_\beta \rightleftharpoons R_\alpha + O_\beta$.

At equilibrium this gives the expression

$$\Delta G_{O_\alpha / R_\beta} + RT\ln(a^\alpha_R a^\beta_O / a^\alpha_O a^\beta_R) + zF\Delta^\alpha_\beta\varphi = 0 \qquad (2.3.14)$$

From this equation a standard Galvani potential for electron transfer can be written

$$\Delta^\alpha_\beta\varphi^0_{O_\alpha/R_\beta} = -\Delta G_{O_\alpha/R_\beta}/zF = -1/zF\ [(\mu^0 O_\beta + \mu^0 R_\alpha) - (\mu^0 O_\alpha + \mu^0 R_\beta)] \qquad (2.3.15)$$

and thus a Nernst equation

$$\Delta^\alpha_\beta\varphi = \Delta^\alpha_\beta\varphi^0 + RT/z_iF\ \ln(a^\alpha_O a^\beta_R / a^\alpha_R a^\beta_O) \qquad (2.3.16)$$

Thus electron transfer at an ITIES can be treated in the same way as ion transfer at an ITIES, and can be investigated by similar techniques. A theory for cyclic voltammetry of electron transfer at ITIES for both reversible [40] and quasi-reversible reactions is presented in Chapter 3 and it illustrates the effects of the relative concentrations of the reactants and products in each phase, and it will be shown that it is difficult to apply normal "rules" for cyclic voltammetry to electron transfer.

2.4 Microelectrodes

Microelectrodes are electrodes such that at least one dimension is small enough that the properties of the electrode are a function of its size. Research into such electrodes was first carried out in the late 1960's and the 1970's by Fleishmann and co-workers [41]. Later these electrodes began to be utilised for electroanalytical and bioelectrochemical studies [42,43].

The properties of microelectrodes which make them important devices for electrochemical studies are :-

(1) enhanced rates of mass transport to and from electrodes which reduces contributions from transient diffusional contributions and thus tends to give steady-state mass transport

(2) reduction of contribution of iR drop effects due to the small currents which are being passed

(3) reduction in effects from charging currents due to the decrease in surface area of the electrode

(4) small physical size of the electrode which allows *in vivo* analysis and also the study of nucleation processes.

These properties have led to several new experimental techniques being developed, and also different electrochemical responses to standard techniques.

Several different geometries of solid microelectrodes have been studied i.e. spherical [44], hemispherical [44], line/band [47], wire [47], disc [45] and ring electrodes [46]. Different geometries mean that different diffusion processes control the arrival of the electroactive species at the electrode surface, and hence different responses are found.

Until 1986 there were no reports of micro liquid/liquid interfaces, however in this year Taylor and Girault [11] presented a short note on the response of an ITIES which are suspended at the tip of a micropipette. This therefore combines the advantages of ITIES, as a different selective process for electroactive species, with the advantages of microelectrodes. For an ITIES at a micropipette they however reported an unusual asymmetric diffusion profile,

due to the diffusion into the pipette being radially from the bulk of the solution. However the diffusion to the interface from inside the pipette is restricted by the walls of the pipette resulting in linear diffusion. A full characterisation of linear sweep and cyclic voltammetry at a pipette will be given in chapter 3. This type of micro electrode has no analogous solid microelectrode geometry due to the asymmetry of the diffusion.

A second type of micro liquid/liquid interface has been reported by Campbell and Girault [10], where the ITIES is supported at a microhole in a very thin polymer film. These holes were produced by laser micro-machining the polymer film with U.V. radiation, and it allows not only the production of single holes but also regular arrays of holes, i.e. micro array ITIES. These electrodes show an analogous steady-state response to transfer of the ion from both phases and can therefore be considered in the same way as a solid microdisc electrode. When, instead of single hole ITIES, an array of microholes ITIES is used it has been shown that the current produced is greatly enhanced compared to a large planar ITIES of the same surface area. Thus this should allow the analysis of trace amounts of ions to give a much larger response than previously achieved at ITIES.

Thus it is possible to combine the advantages outlined for solid micro electrodes and the different electroactive properties of ITIES, to produce powerful analytical tools to study charge transfer reactions across a liquid/liquid interface, and also to quantitatively measure low concentrations of ions in solution.

2.5 Experimental Techniques

2.5.1 Experiments At ITIES

2.5.1.1 Large Planar ITIES

For all experiments at a large planar ITIES, a four electrode system was used. The design of cell used is shown in figure 2.5.1. In this cell the interface was not planar, but there is a curvature due to surface tension effects, however the curvature is very slight and the interface can be assumed to be planar. The interface in the cell is adjusted such that it is close to the organic reference Luggin capillary to minimise the effect of iR drop through the organic phase.

For voltammetric experiments the potential difference between the two phases is controlled by means of a 4-electrode potentiostatic system. This four electrode potentiostat consisted of a normal three electrode potentiostat (Southampton University), where only the reference and counter electrode terminals are used, and an "in house" built zerostat. This zerostat holds the potential of the phase, whose reference and counter electrodes are connected to it, at a virtual zero potential, with respect to the other phase. The potential is applied to the 3-electrode potentiostat, which normally controls the potential of the organic phase, and thus the potentials that are quoted at large ITIES are of the water phase with respect to the organic phase i.e. $\Delta_o^w\phi$. The current which is measured is that which flows between the two counter electrodes and is output from the zerostat. This system allows foriR compensation by feeding back a proportion of the output signal to the input of the potentiostat, full iR compenstation being achieved when the electronics go into oscillation. Due to this oscillation of the electronics it is therefore not possible to fully compensate and thus the compensation is set such that it is slightly less than

that required for oscillation. This is detected by outputing the current signal to an oscilloscope, (Gould 1425).

The controlled potential program is supplied by a PPR1 Waveform Generator (Hi-Tek, U.K.) and the potential and current output signals were monitored on an X-Y recorder (Advance Bryans Instruments, Series 60000).

For chronopotentiometric experiments the same potentiostat/zerostat system was used with the reference and working electrodes of the potentiostat connected via a resistor of appropriate size in order to produce a constant current source. The zerostat was set to output ΔE, not i as previously, with the reference and counter electrodes attached to the common and counter electrode sockets in the zerostat. Again the output was monitored on an X-Y recorder, however with the time base in operation.

For all experiments the cell was contained within a grounded Faraday cage.

2.5.1.2 Micro ITIES

Micropipettes were made from Kwik-Fill capillaries (1.5 mm o.d., 0.86 i.d., Clark Electromedical Instruments, Reading, England) pulled with a vertical pipette puller (Kopf 720, Tujunga, USA). The puller was adjusted to provide pipettes with a short shank and a fine tip, since the resistance of the shank of the pipette is directly proportional to its length, thus keeping the resistance within the pipette to a minimum. The pipette was then polished on an optically flat glass of pipette beveller (K.T. Brown Type, B.V.-10, USA). During polishing the resistance of the pipette was continually monitored, the best tips being produced when the resistance has decreases by 5-10% from its initial value. However using this technique it is very difficult to produce flat circular sections, these can only be obtained on a trial and error basis by carefully

breaking the tip of the pipette. These pipettes are then filled with the aqueous phase by back filling with a syringe and a very fine needle, the point of the pipette filling by capillary action. The cell was operated in a two electrode mode with only a reference electrode in either phase. It is possible to do this and not alter the potential of the reference electrodes due to the small currents which are being passed. A schematic diagram of the experimental cell is shown in figure 2.5.2. It consists of a glass U-tube which contains the organic reference phase, in contact with the organic phase. The organic phase is covered with an aqueous layer to limit any evaporation of the organic solvent during the experiment. The micropipette, containing the aqueous phase is then immersed in the organic phase, with the tip of the pipette being positioned, by micrometer control, as close as possible to the interface between the organic phase and the reference phase. This is done to reduce any iR drop through the organic phase, and the gap is normally less than 1mm. During the experiment the tip is monitored with a zoom microscope (Olympus, SZH, maximum magnification 384x) together with a colour video attachment (Sony CCD camera, DXC-102). This constant observation is necessary to ensure that the interface remains located at the tip of the pipette. The video screen was used to manually measure the inner diameter of the pipette *in situ* having precalibrated the zoom lens with a microscope graticule. The error on the radius was thus estimated to be of the order of 5%.

The voltage program was again supplied by a PPR1 Waveform Generator, and current was measured by a battery powered current follower based on a high-input impedance FET operational amplifier (Burr Brown OAP 104). For these micropipette experiments the phase within the pipette was held at virtual zero, with respect to the bulk phase, normally the organic phase, and the potential is quoted as the organic phase with respect to the aqueous phase

Figure 2.5.2 Two electrode cell used for micropipette experiments.

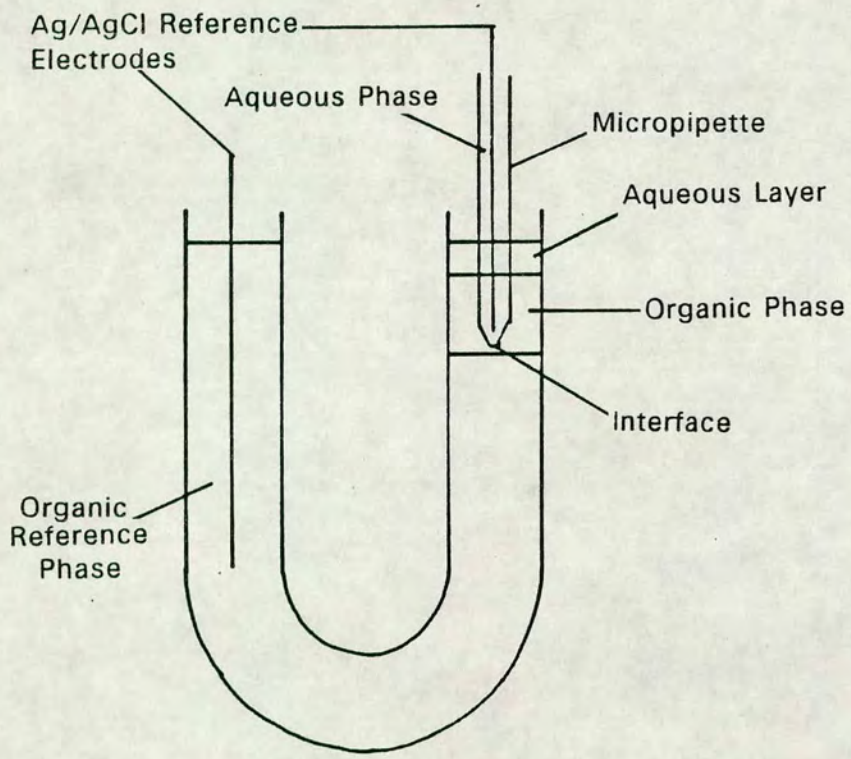

Figure 2.5.1 Schematic diagram of the 4-electrode cell used in all large scale ITIES experiments.

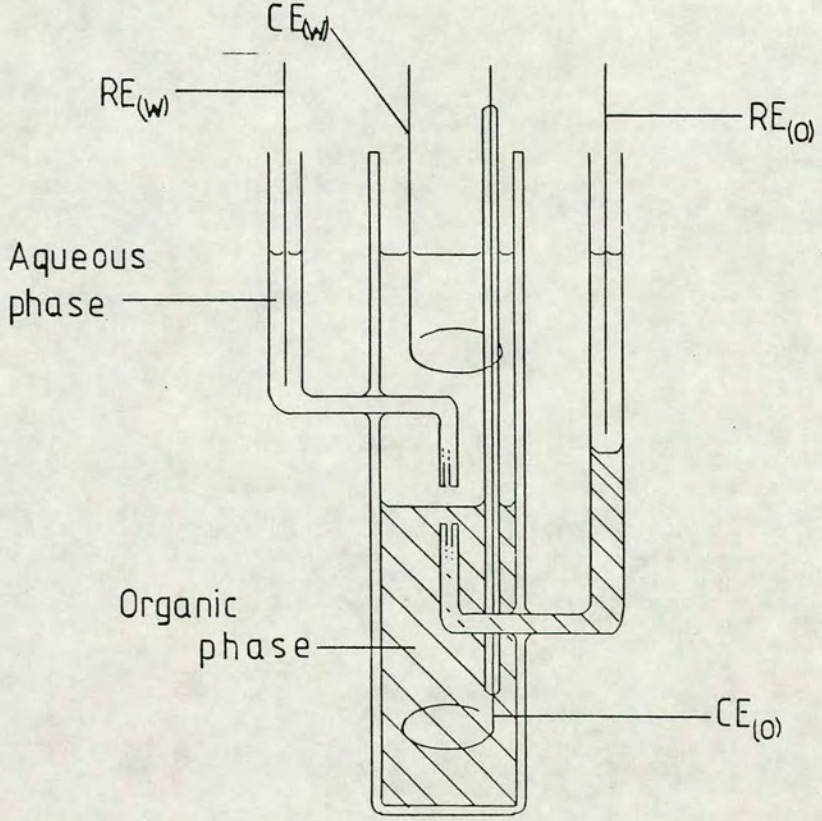

(0V) i.e. $\Delta_w^o\phi$. This is the opposite of that used for large ITIES, this is due to the potentiostat used for large ITIES inverting the potential which is input.

2.5.2 Experiments At Metal/Electrolyte Interfaces

For voltammetric experiments at metal/electrolyte interfaces the potential waveform was supplied as in 2.5.1, and recorded similarly on an X-Y recorder, with a three electrode configuration using a three electrode potentiostat (Southampton University), except for experiments with microelectrodes. The electrodes used were Pt disc (Russel Electrodes, Auchtermuchty, Scotland), and carbon disc (Metrohm).

For microelectrode experiments a 25µm diameter Pt disc electrode was used. This was made by fusing the 25µm diameter Pt wire (99.9%, Johnson Mathey, England) in a bead of soft soda glass, this was then fused onto a narrow (3mm i.d. glass tube). A back contact was made onto the Pt wire by melting solder and running it down the glass tube and this was then contacted on an insulated copper cable, (see figure 2.5.3). The microelectrode experiments were carried out in a two electrode mode, again using the current follower as described in 2.5.1, with the microdisc electrode attached directly to the waveform generator, and a reference electrode attached to the current follower.

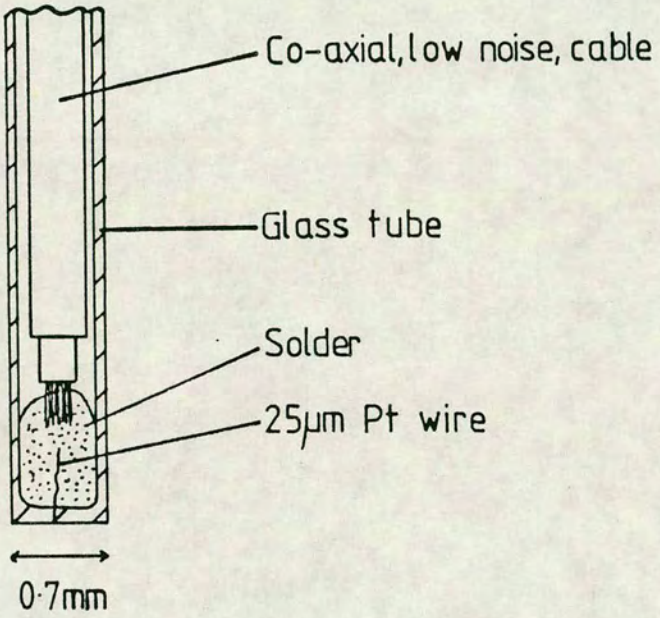

Figure 2.5.3 Schematic diagram of a platinum disc (r=12.5μm) microelectrode.

2.5.3 Reference Electrodes

The reference electrodes used were Ag/AgCl, Ag/Ag_2SO_4, Ag/AgBr, Ag/AgTPB and a saturated calomel electrode.

The silver/silver salt reference electrodes were all made in a similar manner. Silver wire (99.99%, Goodfellow, England) is connected to the anode of a 9V battery and placed in an aqueous solution of a soluble salt, of the silver salt required i.e. NaCl, $MgSO_4$ etc. A counter electrode is then attached to the cathode of the battery via a 1kΩ resistor. Thus 10mA is forced to flow, which slowly coats an insoluble layer of the required silver salt on the silver wire. For micropipette experiments 125µm silver wire is used and for other experiments 0.5mm wire is used. The Calomel electrode was supplied by Russel Electrodes (Auchtermuchty, Scotland).

2.5.4 Chemicals

The following chemicals were used as supplied:-

Lithium Chloride (Fluka, *purum*)

Potasium Chloride (F.S.A., A.R)

Sodium Chloride (F.S.A., A.R.)

Lithium Sulphate (Fluka, *purum*)

Tetrabutylammonium Chloride (Fluka, *purum*)

Tetrabutylammonium Bromide (Fluka, *purum*)

Bis(triphenylphosphoranylidene)ammonium Chloride (Aldrich, 99%+)

3-Hydroxytyramine Hydrochloride (Dopamine Hydrochloride) (Fluka, *puriss*)

Noradrenaline Hydrochloride (Fluka, *purum*)

Ascorbic Acid (Vitamin C) (Aldrich, 99%+)

Crystal Violet (Aldrich, 95%)

Potassium Tetrakis(4-chlorophenyl)borate (Lancaster Synthesis, 98%+)

Sodium Tetraphenylborate (Aldrich, 99.5%+)

4-*O*-Methyldopamine Hydrochloride (Aldrich, 99%)

Potassium Ferrocyanide (BDH, AnalaR)

Dibenzo-18-Crown-6 (Aldrich, 98%)

Benzo-15-crown-5 (Aldrich, 98%)

The solvents used were :-

H_2O (Millipore, Milli-Q SP Reagent Water System)

1,2-dichloroethane (BDH, AnalaR)

Nitrobenzene (BDH, AnalaR)

Organic salt were prepared by simple metathesis reactions as described below.

Tetrabutylammonium tetraphenylborate (TBATPB) was prepared by mixing equimolar aqueous solutions of tetrabutylammonium bromide (TBABr) and sodium tetraphenylborate (NaTPB), the resulting precipitate of TBATPB is filtered and washed thoroughly with water, to remove any sodium bromide. The filtrate

was then recrystalised from acetone and dried under vacuum. Tetraethylammonium tetraphenylborate (TEATPB), crystal violet tetraphenylborate (CVTPB) and bis(triphenylphosphoranylidene)ammonium tetraphenylborate (BTPPATPB) are all prepared in the same way, from the corresponding salts of the respective cations.

The $BTPPA^+$ and TBA^+ salts of tetrakis(4-chlorophenyl) borate were prepared in the same manner as above, however in this case the equimolar solvents were made up in a methanol:water mixture (2:1), and the recrystallisation solvent used is methanol.

N,N-dicyclohexyl-n',N-diisobutyl-cis-cyclohexane-1,2-carboxamide (ETH1810) and 2,9-dibutyl-1,10-phenanthroline were generously prepared and donated by MediSense (UK) Inc.

2.5.5 Computation

All computation was carried out on the University of Edinburgh main frame computer system (EMAS, Edinburgh Multi Access System) with diagrams being produced on the university's printing and plotting facilities. All programs are written in FORTRAN 77 and compiled using an Amdahl Fortran 77 compiler version 2.2.

Chapter 3
Cyclic/Linear Sweep Voltammetry At An ITIES

3.1 Cyclic Voltammetry For Planar Diffusion

3.1.1 Reversible Ion Transfer at an ITIES

For a reversible ion transfer at a planar ITIES of the type $I_\alpha \rightleftharpoons I_\beta$, the boundary conditions are the same as those for an electron transfer at a metal/electrolyte interface of the same geometry. Thus the boundary conditions are

$$[\partial c_\alpha(x,t)/\partial t] = D_\alpha[\partial^2 c_\alpha(x,t)/\partial x^2] \qquad (3.1.1)$$

$$[\partial c_\beta(x,t)/\partial t] = D_\beta[\partial^2 c_\beta(x,t)/\partial x^2] \qquad (3.1.2)$$

$$t = 0\ ,\ x \geq 0 : c_\alpha = c_\alpha^*\ ;\ c_\beta = c_\beta^*\ (\approx 0) \qquad (3.1.3)$$

$$t \geq 0,\ x \to \infty : c_\alpha \to c_\alpha^*\ ;\ c_\beta \to 0 \qquad (3.1.4)$$

$$t > 0,\ x = 0 : D_\alpha[\partial c_\alpha/\partial x] = -D_\beta[\partial c_\beta/\partial x] \qquad (3.1.5)$$

$$c_\alpha(0,t)/c_\beta(0,t) = \exp[(nF/RT)(E-E^\circ)] \qquad (3.1.6)$$

assuming that only I_α is present initially in the phase α. These boundary conditions can be treated in a manner similar to that used by Nicholson and Shain [48], to evaluate expressions for $c_\alpha(0,t)$ and $c_\beta(0,t)$.

For cyclic voltammetry the potential function with time is given by

$$0 < t \leq \lambda : E = E_i - \nu t \qquad (3.1.7)$$

$$\lambda \leq t : E = E_i - 2\nu\lambda + \nu t \qquad (3.1.8)$$

These expressions for E can be substituted into (3.1.6) to yield

$$c_\alpha(0,t)/c_\beta(0,t)=\exp[(nF/RT)(E_i-E^\circ-\nu t)] \quad : 0 < t \leq \lambda \qquad (3.1.9)$$

$$c_\alpha(0,t)/c_\beta(0,t)=\exp[(nF/RT)(E_i-E^\circ+\nu t-2\nu\lambda)] \quad : t \geq 0 \qquad (3.1.10)$$

In turn these equations can be simplified using the following substitutions

$$\theta=\exp[(nF/RT)(E_i-E^\circ)] \qquad (3.1.11)$$

$$\sigma=\nu nF/RT \qquad (3.1.12)$$

and can be expressed as

$$c_\alpha(0,t)/c_\beta(0,t) = \theta S_\lambda(t) \qquad (3.1.13)$$

with $S_\lambda(t)$ defined as

$$S_\lambda(t) = \begin{cases} e^{-\sigma t} & : t \leq \lambda \\ e^{\sigma t-2\sigma\lambda} & : t \geq \lambda \end{cases} \qquad (3.1.14)$$

By taking the Laplace transforms of the boundary conditions (3.1.1) - (3.1.4) expressions for the transformed concentrations of I_α and I_β can be obtained

$$\bar{c}_\alpha(x,s) = c_\alpha^*/s + A(s)\exp[-(s/D_\alpha)^{1/2}x] \qquad (3.1.15)$$

$$\bar{c}_\beta(x,s) = -A(s)\exp[-(s/D_\alpha)^{1/2}x] \qquad (3.1.16)$$

The flux to a planar electrode can be given as

$$-J_\alpha(0,t) = i(t)/nFA = D_\alpha[\partial c_\alpha(x,t)/\partial x]_{x=0} \qquad (3.1.17)$$

i.e. Fick's 1st law of planar diffusion, which can be transformed to

$$\bar{i}(0,s)/nFA = D_\alpha[\partial \bar{c}_\alpha(x,s)/\partial x]_{x=0} \qquad (3.1.18)$$

The partial derivative in this expression can be solved by taking the derivative of (3.1.15) with respect to x, which gives

$$[\partial \bar{c}_\alpha(x,s)/\partial x]_{x=0} = -A(s)(s/D_\alpha)^{1/2} \qquad (3.1.19)$$

Which can then be substituted into eqn (3.1.18) resulting in

$$A(s) = -(\bar{i}(0,s)/nFAD_\alpha)(D_\alpha/s)^{1/2} \qquad (3.1.20)$$

This expression for A(s) can then be substituted into eqns. (3.1.15) and (3.1.16) to give

$$\bar{c}_\alpha(x,s)=c^*_\alpha/s \; -(\bar{i}(0,s)/nFAD_\alpha)(D_\alpha/s)^{1/2}\exp[-(s/D_\alpha)^{1/2}x] \qquad (3.1.21)$$

$$\bar{c}_\beta(x,s)=(\bar{i}(s)/nFAD_\beta)(D_\beta/s)^{1/2}\exp[-(s/D_\beta)^{1/2}x] \qquad (3.1.22)$$

For x=0, i.e. the surface concentration, the equation for I_α reduces to

$$\bar{c}_\alpha(0,s) = c_\alpha^*/s - (\bar{i}(0,s)/nFAD_\alpha)(D_\alpha/s)^{1/2} \qquad (3.1.23)$$

By inversion of (3.1.23), to real space, and application of the convolution theorem we get

$$c_\alpha(0,t) = c_\alpha^* - (1/nFA(\pi D_\alpha)^{1/2}) \int_0^t i(\tau)/(t-\tau)^{1/2}\, d\tau \qquad (3.1.24)$$

and by a similar procedure an expression for $c_\beta(0,t)$ can be obtained

$$c_\beta(0,t) = (1/nFA(\pi D_\beta)^{1/2}) \int_0^t i(\tau)/(t-\tau)^{1/2}\, d\tau \qquad (3.1.25)$$

By then making the substitution $f(\tau) = i(\tau)/nFA$ eqns. (3.1.24) and (3.1.25) become

$$c_\alpha(o,t) = c_\alpha^* - 1/(\pi D_\alpha)^{1/2} \int_0^t f(\tau)/(t-\tau)^{1/2}\, d\tau \qquad (3.1.26)$$

$$c_\beta(0,t) = 1/(\pi D_\beta)^{1/2} \int_0^t f(\tau)/(t-\tau)^{1/2}\, d\tau \qquad (3.1.27)$$

The surface concentrations can then be substituted into (3.1.14) to give

$$\int_0^t f(\tau)/(t-\tau)^{1/2}\, d\tau = c_\alpha^*(\pi D)^{1/2}/(1+\theta S_\lambda(t)) \qquad (3.1.28)$$

for $D_\alpha=D_\beta=D$.

This expression allows us to obtain the current - time curves, and in order to obtain current - potential curves the calculations must be made with respect

to σt,and not t, since σt is dimensionless and proportional to the potential i.e.

$$\sigma t = nF\nu t/RT = (nF/RT)(E_i - E) \qquad (3.1.29)$$

This is done by making the following change of variables

$$\tau = z/\sigma \qquad (3.1.30)$$

$$f(t) = g(\sigma t) \qquad (3.1.31)$$

thus (3.1.28) becomes

$$\int_0^{\sigma t} g(z)/(\sigma(\sigma t - \tau))^{1/2}\, dz = c_\alpha^*(\pi D)^{1/2}/(1+ S_{\sigma\lambda}(\sigma t)) \qquad (3.1.32)$$

In order to be able to use numerical methods to evaluate the integral (3.1.32) it must be made dimensionless, and this is done by the substitution

$$g(\sigma t) = c_\alpha^*(\pi D\sigma)^{1/2}\chi(\sigma t) \qquad (3.1.33)$$

therefore (3.2.33) becomes

$$\int_0^{\sigma t} \chi(z)/(\sigma t - z)^{1/2}\, dz = 1/(1+ \theta S_{\sigma\lambda}(\sigma t)) \qquad (3.1.34)$$

with the current being given by

$$i(\sigma t) = nFAc_\alpha^*(\pi D\sigma)^{1/2}\chi(\sigma t) \qquad (3.1.35)$$

Equation (3.1.34) can be solved for $\chi(\sigma t)$ as a function of potential by numerical integration. The range of the integration must be split into a range σt=0 to σt=M with N equally spaced subintervals by a change of variables thus

$$z = \delta v \qquad (3.1.36)$$

$$n = \sigma t/\delta \qquad (3.1.37)$$

where δ is the length of the dimensionless subinterval i.e. δ=M/N and n is the serial number of the subinterval. Therefore (3.1.34) becomes

$$\int_0^n \chi(\delta v)/(n-v)^{1/2}\, dv = 1/(1+ \theta S_{\delta\lambda}(\delta n)) \qquad (3.1.38)$$

This can be integrated by parts to give

$$\int_0^n \chi(\delta n)/(n-v)^{1/2}\, dv = 2\left[\chi(0)n^{1/2} + \int_0^n (n-v)^{1/2}\, d[\chi(\delta n)]\right] \qquad (3.1.39)$$

The integral on the R.H.S. of (3.1.39) is a Riemann-Stieltjes integral, which can be replaced by its finite sum, and with elimination of i=0 and i=n we get

$$\int_0^n \chi(\delta n)/(n-v)^{1/2} dv = 2\left[\chi(1)n^{1/2} + \sum_{i=1}^{n-1} (n-i)^{1/2}\, [\chi(i+1)-\chi(i)]\right] \qquad (3.1.40)$$

Thus the resulting numerical solution to eqn. (3.1.34) is

$$2\delta^{1/2}\left[\chi(1)\sqrt{n} + \sum_{i=1}^{n-1} (n-i)^{1/2}\, [\chi(i+1)-x(i)]\right] = 1/(1+\xi\theta S_{\delta\lambda}(\delta n)) \qquad (3.1.41)$$

This equation defines N algebraic equations in the unknown function $\chi(n)$, where each n^{th} equation involves the n-1 previous unknowns. These equations can therefore be solved successively for the values of $\chi(\sigma t)$ by computation. The program used to carry this out is given in Appendix 1.1.

The evaluation of (3.1.41) computationally can be split into two relatively simple parts; the first involves the evaluation of the number of integral steps which will be required to cover the potential range chosen and the second involves the evaluation of the finite sum and consequently the dimensionless current function $\chi(n)$.

The former is very simple, however some important points must be kept in mind when deciding on the input parameters, for the potential range to be covered. In a manner similar to that used in ref. [48] all potential values will be quoted relative to E^o, thus the potential at any given integration point is given

by

$$n(E-E^{*}) = RT/F \ln(\theta S_{\sigma\lambda}(\sigma t)) \qquad (3.1.42)$$

From the relationship given in (3.1.10) the initial potential of the scan is given by

$$n(E_i-E^{*}) = RT/F \ln\theta \qquad (3.1.43)$$

and thus choosing θ fixes the start potential $n(E_i-E^{o})$. However care must be taken when choosing this value due to the relationship given in (3.1.13), as for t=0, $c_{\alpha}(0,t)/c_{\beta}(t,0)=\theta$, and thus in choosing θ the initial ratio of reactant to product is set, and from boundary condition (3.1.3) this should be limiting to infinity. Therefore if we do not use values of θ that are large enough we will see some instability in the current function over the first few integration steps. However it should be noted that above a certain value of θ this instability will be seen to disappear due to the precision of the computing. Having chosen a value of θ which is suitable it is then possible to evaluate the number of integration points, knowing the scan limit, using

$$n = ((-(F/RT)(E_{\lambda}-E^{\circ}) + \ln\theta)/\delta) \times 2 \qquad (3.1.44)$$

which for symmetrical scan limits about E^{o} can be reduced to

$$n = 4\ln\theta/\delta \qquad (3.1.45)$$

The second part of the computation involves the evaluation of the finite sum. If we examine this sum for different values of n we get :-

$$n=1: \ 2\sqrt{\delta}\ \chi(1)\ \Lambda 1$$

$$n=2: \ 2\sqrt{\delta}\ [\chi(1)\Lambda 2 + \Lambda 1(\chi(2)-\chi(1))] = 2\sqrt{\delta}\ [\chi(2)\Lambda 1 + \chi(1)(\Lambda 2-\Lambda 1)]$$

$$n=3: \ 2\sqrt{\delta}\ [\chi(3)\Lambda 3 + \chi(2)(\Lambda 2-\Lambda 1) + \chi(1)(\Lambda 3-\Lambda 2)]$$

Thus it can be seen that there is a pattern emerging for the coefficients of $\chi(i)$

of the general form

$$2\sqrt{\delta}\ [\chi(n)(\sqrt{1}-\sqrt{0}) + \chi(n-1)(\sqrt{2}-\sqrt{1}) + ..$$

$$..... +\chi(2)(\sqrt{n-1} - \sqrt{n-2}) + \chi(1)(\sqrt{n} - \sqrt{n-1})\ ] \quad (3.1.46)$$

These coefficients can be evaluated computationally, and this is done in lines 34-40. It is then possible to evaluate the sum of the previous n-1 values of χ with their relevant coefficients, and then evaluate $\chi(n)$.

Figure 3.1.1 shows a plot of $\sqrt{\pi}\chi(\sigma t)$ *vs.* $n(E-E^{\circ})$ and table 3.1.1 shows the values of $\sqrt{\pi}\chi(\sigma t)$ evaluated by this method. They are identical to those evaluated by Nicholson and Shain [48].

3.1.2 Quasi-Reversible Ion Transfer At An ITIES

As well as being able to apply the above treatment to reversible charge transfer reactions, it is possible to use a similar treatment for kinetically controlled reactions.

For this case the boundary conditions are the same as presented in 3.1.1, however here the ratio of the surface concentrations is not controlled by a Nernstian relationship. Eqn (3.1.6) should be replaced by

$$i(t)/nFA = D_{\alpha}[\,\partial c_{\alpha}(x,t)/\partial x\,]_{x=0} = k_f c_{\alpha}(0,t) - k_b c_{\beta}(0,t) \qquad (3.1.47)$$

give that the reaction being examined is

$$\text{I}_{\alpha} \underset{k_b}{\overset{k_f}{\rightleftharpoons}} \text{I}_{\beta}$$

It is assumed that the kinetics can be described by the Butler-Volmer relationship and therefore the following substitutions can be made into (3.1.47).

$$k_f = \exp[\,-(\alpha nF/RT)(E-E^{\circ})\,] \qquad (3.1.48)$$

$$k_b = \exp[\,(1-\alpha)(nF/RT)(E-E^{\circ})\,] \qquad (3.1.49)$$

Table 3.1.1 Table showing the variation of the dimensionless current parameter, $\chi(\sigma t)$, as a function of potential, $n(E-E^{o})$, for the reversible cyclic voltammogram in figure 3.1.1

$n(E-E^{o})/V$	$\sqrt{\pi}\,\chi(\sigma t)$	$n(E-E^{o})/V$	$\sqrt{\pi}\,\chi(\sigma t)$
0.1200	0.0093	-0.1500	0.2144
0.1002	0.0197	-0.1200	0.1903
0.0799	0.0418	-0.1002	0.1706
0.0601	0.0843	-0.0799	0.1401
0.0501	0.1175	-0.0601	0.0906
0.0450	0.1381	-0.0501	0.0541
0.0401	0.1601	-0.0450	0.0315
0.0349	0.1854	-0.0401	0.0085
0.0301	0.2115	-0.0349	-0.0184
0.0249	0.2406	-0.0301	-0.0459
0.0200	0.2691	-0.0249	-0.0764
0.0149	0.2994	-0.0200	-0.1063
0.0100	0.3275	-0.0149	-0.1379
0.0049	0.3554	-0.0100	-0.1673
0.0000	0.3795	-0.0049	-0.1965
-0.0049	0.4005	0.0000	-0.2218
-0.0100	0.4185	0.0049	-0.2440
-0.0149	0.4315	0.0100	-0.2632
-0.0200	0.4407	0.0149	-0.2773
-0.0249	0.4452	0.0200	-0.2877
-0.0301	0.4461	0.0249	-0.2933
-0.0349	0.4436	0.0301	-0.2953
-0.0401	0.4381	0.0349	-0.2938
-0.0450	0.4306	0.0401	-0.2893
-0.0501	0.4210	0.0450	-0.2828
-0.0601	0.3992	0.0501	-0.2743
-0.0799	0.3535	0.0601	-0.2543
-0.1002	0.3123	0.0799	-0.2122
-0.1200	0.2804	0.1002	-0.1744
-0.1500	0.2450	0.1200	-0.1456

Figure 3.1.1 Cyclic voltammogram for the numerical solution of a reversibl reaction at a planar electrode. Current values are presented as the dimensionless parameter $\chi(\sigma t)$

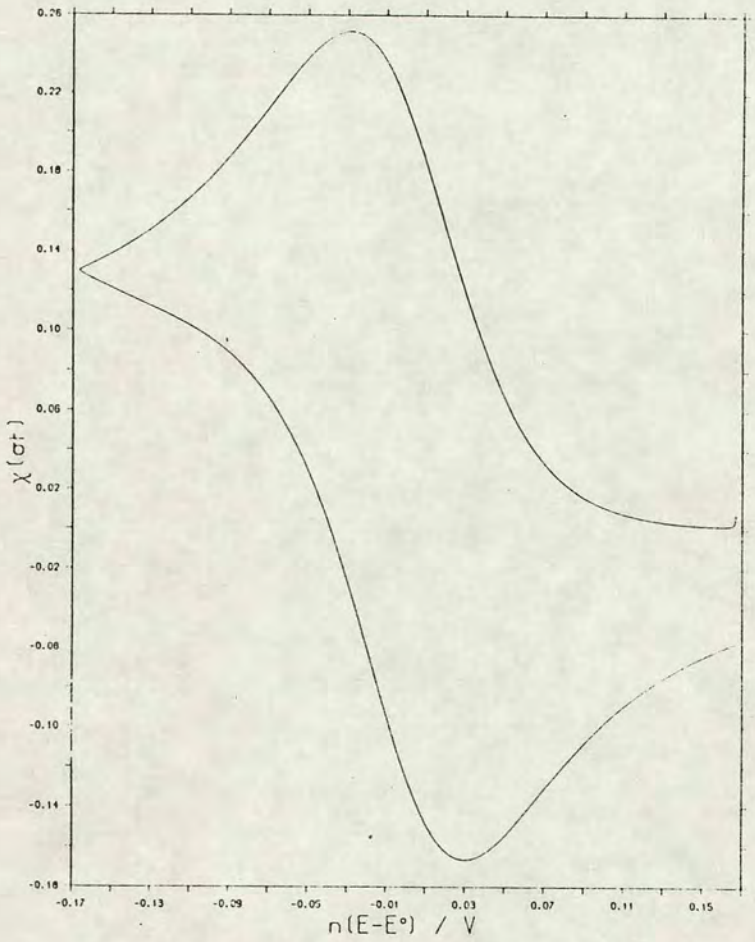

The potential-time expression being the same as in 3.1.1 and by making the same substitutions, ie. $S_\lambda(t)$ as in (3.1.13) and $\theta=c_\alpha^*/c_\beta^*$, eqn. (3.1.47) becomes

$$i(t)/nFA = k(\theta S_\lambda(t))^\alpha[\, c_\alpha(0,t) - c_\beta(0,t)\theta S_\lambda(t)\,] \quad (3.1.50)$$

The expressions for the surface concentrations $c_\alpha(0,t)$ and $c_\beta(0,t)$ can be derived in the same manner as for the reversible case i.e. eqns. (3.1.24) and (3.1.25), and they can be substituted into (3.1.49) to give

$$i(t)/nFA = k(\theta S_\lambda(t))^\alpha\Big[c_\alpha^* - 1/(nFA(\pi D)^{1/2})\int_0^t i(\tau)/(t-\tau)^{1/2}\, d\tau$$

$$-\theta S_\lambda(t)\Big[\, c_\beta - 1/(nFA\sqrt{(\pi D)})\int_0^t i(\tau)/\sqrt{(t-\tau)}\, d\tau\,\Big]\Big] \quad (3.1.51)$$

Assuming that $D_a=D_b$ and that $f(t)=i(t)/nFA$ eqn. (3.1.50) becomes

$$f(t)(\theta s_\lambda(t))^\alpha/kc_\alpha^* = 1 - S_\lambda(t) +$$

$$(\theta S_\lambda(t)-1/c_\alpha^*(\pi D)^{1/2})\int_0^t f(\tau)/(t-\tau)^{1/2}\, d\tau \quad (3.1.52)$$

As in 3.1.1 it is necessary to make a change of variables to obtain a the current as a function of potential,these changes are as in eqns. (3.1.30) and (3.1.31) and they result in the expression

$$\chi(\sigma t)(\theta S_{\sigma\lambda}(\sigma t))^\alpha\psi^{-1} = 1 + S_{\sigma\lambda}(\sigma t) +$$

$$+ (\theta S_{\sigma\lambda}(\sigma t)-1)\int_0^{\sigma t}\chi(z)/(\sigma t-z)^{1/2}\, dz \quad (3.1.53)$$

where $\chi(\sigma t)$ is defined as in (3.1.33) and ψ is given by

$$\psi = k/(\pi D\sigma)^{1/2} \quad (3.1.54)$$

It is now possible after making a change of variables, i.e. eqns. (3.1.36) and (3.1.37) to replace the integral in eqn. 3.1.53 by its finite sum as in 3.1.1. Thus is the final form of the expression for the dimensionless current $\chi(\sigma t)$ is

$$\chi(\sigma t)\{\theta S_{\delta\lambda}(\delta n))^{\alpha/\psi} = 1 + S_{\delta\lambda}(\delta n) + \qquad (3.1.55)$$

$$+ 2\delta^{1/2}(\theta S_{\delta\lambda}(\delta n) - 1)\left[\dot{\chi}(1)n^{1/2} + \sum_{i=1}^{n-1}(n-i)^{1/2}[\chi(i+1)-\chi(i)]\right]$$

which can be solved in the manner that is described in 3.1.1.

The program used to solve this expression for $\chi(\sigma t)$ is presented in Appendix 1.2. This expression for kinetically controlled charge transfer was first presented by Nicholson [49] and the results obtained from the above solution are compared with those reported in this paper. A table showing the variation of ΔE_p with ψ is shown in table 3.1.2 and the cyclic voltammograms associated with this are presented in figure 3.1.2.These voltammograms agree exactly with those reported in reference [49].

3.1.3 Experimental Results For Planar Diffusion to An ITIES

The transfer of tetraethylammonium, (TEA^+). across the interface between water and 1,2 dichloroethane was investigated for the cell

Ag/AgCl/TPBNa(1mM),NaCl(10mM)/CVTPB(1mM)
//LiCl(1mM),TEACl(15μM)/AgCl/Ag

using a large planar ITIES, as described in 2.5.1.1. Cyclic voltammograms are presented in figures 3.1.3(a) and (b). The former figure shows a scan including the full potential window for this cell, the later shows a set of cyclic voltammograms, showing a sweep rate dependence. These cyclic voltammograms have full iR compensation. It can be seen from figure 3.1.3 (b) , as discussed in chapter2, that increasing the sweep rate has no effect on ΔE or

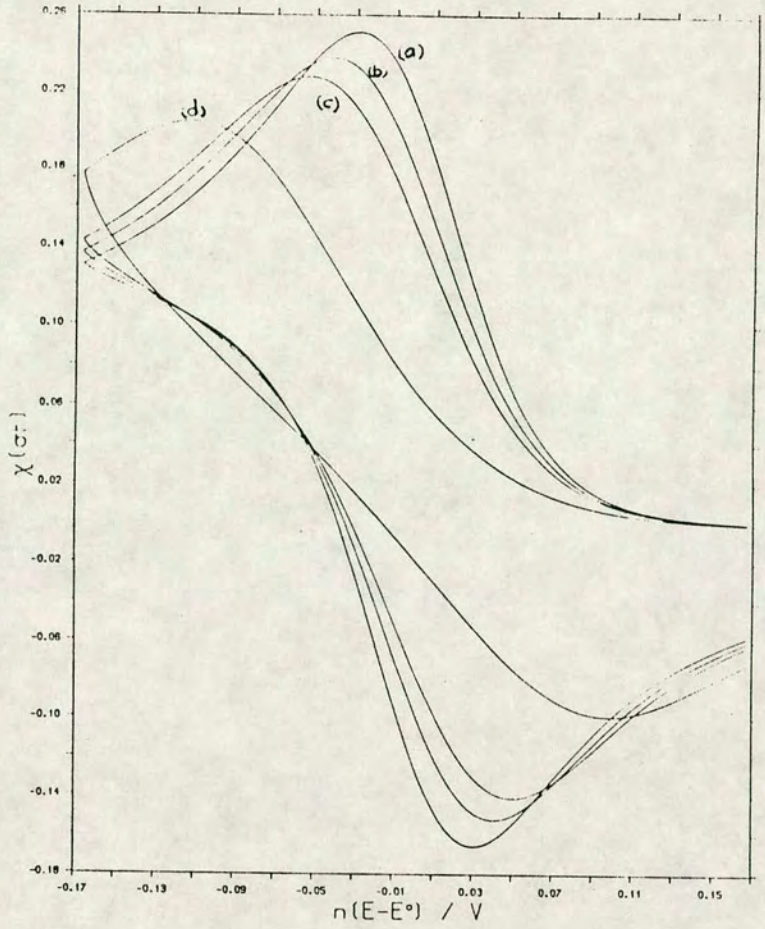

Figure 3.1.2 Cyclic voltammograms for the numerical solution of a quasi-reversible reaction at a planar electrode, for varying values of the kinetic parameter, ψ. (a) ψ=20, (b) ψ=1, (c) ψ=0.5, (d) ψ=0.1.

ψ	ΔE_p/mV
20	60.1
1	83.2
0.5	104.4
0.1	221.5

Table 3.1.2 Table showing the variation of ΔE_p, i.e. the peak to peak separation, with the kinetic parameter, ψ, for quasi-reversible cyclic voltammetry.

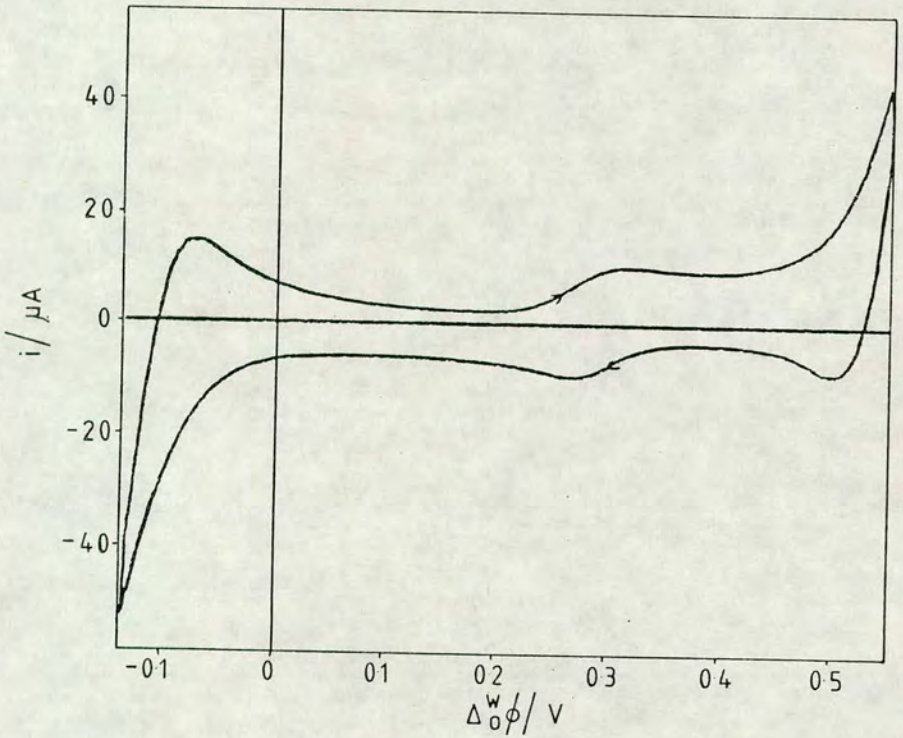

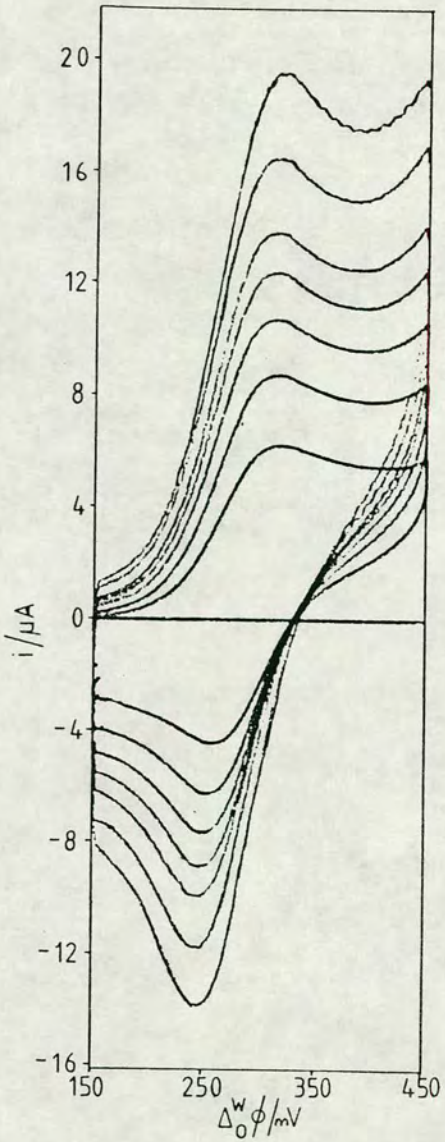

Figure 3.1.3 (a) Cyclic voltammogram showing TEA^+ transfer at a large planar ITIES for the cell shown in section 3.1.3. The full potential window for this system is shown. (ν=100mVs^{-1}). (b) Cyclic voltammograms showing the sweep rate dependence of TEA^+ transfer, as for (a). ν=20,40,60,80,100,140,180mVs^{-1}.

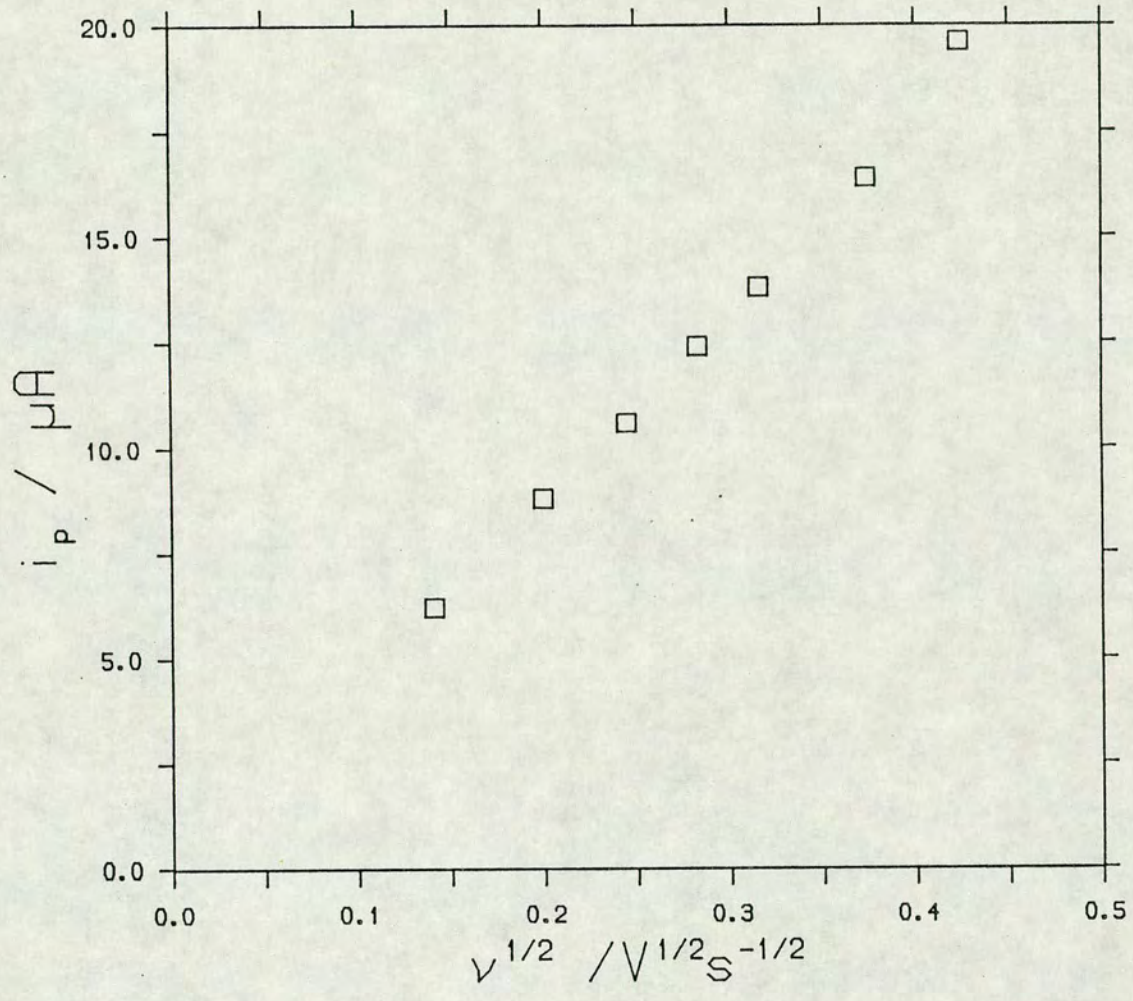

Figure 3.1.4 Plot of peak current, i_p, against $\nu^{1/2}$ for the cyclic voltammograms shown in figure 3.1.3 (b).

on the position of $E_{1/2}$. Thus TEA^+ ion transfer is a reversible reaction. If however the same voltammograms were to be recorded without iR compensation increasing ν would increase ΔE_p and also the $E_{1/2}$ would alter. The plot of i_p *vs.* $\nu^{1/2}$ is shown in figure 3.1.4 and from the gradient of the linear relationship the diffusion coefficient of TEA^+ was calculated to be $5.1 \times 10^{-6} cm^2 s^{-1}$, using the Randles-Sevcik relationship, see 2.3.1.1.

These results therefore show that the preceding treatment of cyclic voltammetry at planar electrodes is applicable to ion transfer at ITIES. However the effects of iR must be noted when kinetic analyses are to be carried out.

3.2 Cyclic/ Linear Sweep Voltammetry For Spherical Diffusion

3.2.1 Reversible Ion Transfer

As described in chapter 2 the diffusion of ions to a microhole ITIES can be approximated to spherical diffusion and therefore an approximate analytical solution for a spherical electrode can be applied to provide an approximate solution to this problem [56]. Hence the following solution is presented. The boundary conditions, which are the same as found at a hemispherical metal/electrolyte interface e.g. a mercury drop electrode, are given by

$$[\partial c_\alpha(r,t)/\partial t] = D_\alpha[(\partial^2 c_\alpha(r,t)/\partial r^2)+(2/r)(\partial c_\alpha(r,t)/\partial r)] \qquad (3.2.1)$$

$$[\partial c_\beta(r,t)/\partial t] = D_\alpha[(\partial^2 c_\beta(r,t)/\partial r^2)+(2/r)(\partial c_\beta(r,t)/\partial r)] \qquad (3.2.2)$$

$$t = 0,\ r \geq r_o : c_\alpha = c_\alpha^* \ ;\ c_\beta = c_\beta^* \ (\approx 0) \qquad (3.2.3)$$

$$t \geq 0,\ r \to \infty : c_\alpha \to c_\alpha^* \ ;\ c_\beta \to 0 \qquad (3.2.4)$$

$$t > 0,\ r = r_o : D_\alpha [\partial c_\alpha/\partial r] + D_\beta[\partial c_\beta/\partial r] = 0 \qquad (3.2.5)$$

$$c_\alpha(r_o,t)/c_\beta(r_o,t) = \exp[(nF/RT)(E-E^\circ)] \qquad (3.2.6)$$

These boundary conditions have been solved for the surface concentrations, $c_\alpha(r_o,t)$ and $c_\beta(r_o,t)$ where r_o is the radius of the hemisphere, by application of Laplace transformations, in a manner which was first carried out by G. Mamantov [50] in 1953. Since these boundary conditions have been solved for this problem, the solution has been applied to different techniques, i.e. chronopotentiometry [51], constant potential electrolysis [52], and a.c. polarography [53], but not to cyclic voltammetry.

For cyclic voltammetry the potential-time function is as given in eqns (3.1.7) and (3.1.8), and when these are substituted into the Nernst relationship (3.2.6) we obtain

$$c_\alpha(r_o,t)/c_\beta(r_o,t) = \theta S_\lambda(t) \qquad (3.2.7)$$

where the definitions of θ, $S_\lambda(t)$ and σ are the same as in eqns. (3.1.11-12) and (3.1.14).

For completeness the solution of the above stated boundary conditions for $c_\alpha(r_o,t)$ and $c_\beta(r_o,t)$ is presented.

In order to simplify the calculations the following change of variables can be made

$$u(r,t) = rc_\alpha^* - rc_\alpha(r,t) \qquad (3.2.8)$$

$$v(r,t) = rc_\beta(r,t) - rc_\beta^* \qquad (3.2.9)$$

The resulting Laplace transforms of each, when combined with the transforms of Fick's Law are

$$\bar{u}(r,s) = \gamma(s)\ \exp(r_o-r)(s/D_\alpha)^{1/2} \qquad (3.2.10)$$

$$\bar{v}(r,s) = \delta(s)\ \exp(r_o-r)(s/D_\beta)^{1/2} \qquad (3.2.11)$$

In this case the Laplace transform of the current is given by

$$\bar{i}(s) = nFAD_\alpha[\,\partial\bar{c}_\alpha(r,s)/\partial r\,]_{r=r_o} = -nFAD_\beta[\,\partial\bar{c}_\beta(r,s)/\partial r\,]_{r=r_o} \qquad (3.2.12)$$

In order to eliminate the partial derivative from eqn. (3.2.12) the following routine is carried out.

Manipulation of (3.2.8) results in

$$[\,\partial c_\alpha(r,t)/\partial t\,] = u(r,t)/r^2 - (1/r)[\,\partial u(r,t)/\partial r\,] \qquad (3.2.13)$$

the Laplace transform of which is

$$[\,\partial \bar{c}_\alpha(r,s)/\partial r\,] = \bar{u}(r,s)/r^2 - (1/r)[\,\partial \bar{u}(r,s)/\partial r\,] \qquad (3.2.14)$$

From eqn. (3.2.10) we get

$$[\,\partial \bar{u}(r,s)/\partial r\,] = -\gamma(s)(s/D_\alpha)^{1/2}\exp(r_o-r)(s/D_\alpha)^{1/2} \qquad (3.2.15)$$

Then with substitution of eqns (3.2.10) and (3.2.15) into (3.2.14) for $r=r_o$ results in

$$[\,\partial \bar{c}(r_o,s)/\partial r)\,]_{r=r_o} = \gamma(s)/r_o[\,(s/D_\alpha)^{1/2} + 1/r_o\,] \qquad (3.2.16)$$

It is then possible to evaluate the integration constant $\gamma(s)$ by substituting (3.2.16) into (3.2.12) i.e.

$$\gamma(s) = (\bar{i}(s)/nFAD_\alpha)[\,r_o/((1/r_o)+(s/D_\alpha)^{1/2})\,] \qquad (3.2.17)$$

This can then be used in eqn. (3.2.10), bearing in mind that $r=r_o$, to give

$$\bar{u}(r,s) = \bar{i}(s)/nFAD_\alpha\ (r_o/((s/D_\alpha)^{1/2} + (1/r_0))) \qquad (3.2.18)$$

Rearrangement of (3.2.8) and then taking its Laplace transform we get

$$\bar{c}_\alpha(r_o,s) = c_\alpha^*/s - \bar{u}(r,s)/r_o \qquad (3.2.19)$$

into which we substitute u(r,s) from (3.2.17) resulting in

$$\bar{c}_\alpha(r_o,s) = c_\alpha^*/s - \bar{i}(s)/nFAD_\alpha\ [\,1/((s/D_\alpha)^{1/2}+(1/r_o))\,] \qquad (3.2.20)$$

It is interesting to note here that eqn. (3.2.20) limits to the expression for planar diffusion as $r\to\infty$, as would be expected for a sphere with a very large radius, since the curvature of the surface decreases as the radius increases.

The reverse transform of eqn. (3.2.20) is carried out, with the application of the convolution theorem and this gives an expression for $c_\alpha(r_o,t)$

$$c_\alpha(r_o,t)=c_\alpha^*-(1/nAF\sqrt{D_\alpha})\int_0^t i(\tau)\left[1/(\pi(t-\tau))^{1/2} - a\exp[a^2(t-\tau)]\operatorname{erfc}[a(t-\tau)^{1/2}]\right]d\tau \qquad (3.2.21)$$

A similar treatment as carried out on eqn.(3.2.8) can be applied to eqn. (3.2.9) to produce a solution for the $c_\beta(r_o,t)$, with $c_\beta^*=0$, thus making eqn. (3.2.9)

$$v(r,t) = rc_\beta(r,t) \qquad (3.2.22)$$

The resulting expression being

$$c_\beta(r_o,t)=(1/nFA\sqrt{D_\beta})\int_0^t i(\tau)\left[1/(\pi(t-\tau))^{1/2} - a_\beta\exp[a_\beta^2(t-\tau)]\operatorname{erfc}[a_\beta(t-\tau)^{1/2}]\right]d\tau \qquad (3.2.23)$$

These expressions for the surface concentrations can then be substituted into the Nernst relationship (3.2.7), for $D_\alpha=D_\beta$ and by defining the function

$$G(t-\tau)=[1/(\pi(t-\tau))^{1/2}]-a\exp[a^2(t-t)]\operatorname{erfc}[a(t-\tau)^{1/2}] \qquad (3.2.24)$$

with $a=\sqrt{D}/r_o$. This equation becomes

$$\int_0^t f(\tau)G(t-\tau)d\tau = D^{1/2}c_\alpha^*/(1+\theta S_\lambda(t)) \qquad (3.2.25)$$

with f(t)=i(t)/nFA. If (3.2.24) is subsequently split to give

$$G(t-\tau) = 1/(\pi(t-\tau))^{1/2} - H(t-\tau) \qquad (3.2.26)$$

$$H(t-\tau) = a\exp[a^2(t-\tau)]\operatorname{erfc}[a(t-\tau)^{1/2}] \qquad (3.2.27)$$

eqn. (3.2.25) becomes

$$\int_o^t f(\tau)/(\pi(t-\tau))^{1/2}d\tau - \int_0^t f(\tau)H(t-\tau)d\tau = D^{1/2}c_\alpha^*/(1+\theta s_\lambda(t)) \qquad (3.2.28)$$

In this case as in the planar diffusion case it is necessary to make a change of variables in order to obtain current-potential curves. These changes are the

same as eqns. (3.1.30) and (3.1.31) and it results in eqn. (3.2.28) becoming

$$1/(\pi\sigma)^{1/2}\int_0^{\sigma t} g(\sigma t)/(\sigma t-z)^{1/2}dz \quad -\int_0^{\sigma t} g(\sigma t)\varphi\exp[\,\varphi(\sigma t-z)\,]\mathrm{erfc}[\,\varphi(\sigma t-z)^{1/2}\,]dz$$

$$= (Dc_\alpha^*)^{1/2}/(1+\theta S_{\sigma\lambda}(\sigma t)) \quad (3.2.29)$$

with $\phi=a/\sqrt{\sigma}$.

Also as in the planar case the integral must be made dimensionless in order to allow it to be evaluated numerically and thus the following substitution is made

$$g(\sigma t) = c_\alpha^* (D\sigma)^{1/2}\psi(\sigma t) \qquad (3.2.30)$$

where $\psi(\sigma t)$ is the dimensionless current. This results in eqn.(3.2.29) becoming

$$1/(1+\theta S_{\sigma\lambda}(\sigma t))=\int_0^{\sigma t} \psi(z)/(\sigma t-z)^{1/2}dz$$

$$-\int_0^{\sigma t} \psi(z)\varphi\exp[\,\varphi^2(\sigma t-z)\,]\mathrm{erfc}[\,\varphi(\sigma t-z)^{1/2}\,]dz \qquad (3.2.31)$$

This expression can be solved for $\psi(\sigma t)$ as a function of σt by using a manner similar to that for the planar cases, with the same change of variables, i.e. (3.1.36) and (3.1.37), to give for this case

$$1/(1+\theta S_{\sigma\lambda}(\delta n))=(\delta/\pi)^{1/2}\int_0^{n} \psi(\delta n)/(n-v)^{1/2}dv$$

$$-\delta\int_0^{n} \psi(\delta v)\varphi\exp[\,\alpha^2(n-v)\,]\mathrm{erfc}[\,\alpha(n-v)^{1/2}\,]dv \qquad (3.2.32)$$

The first integral can be solved as for the same integral in the planar case, see eqn. (3.1.39) with $\psi(n)$ replacing $\chi(n)$.

The second integral can then be replaced by its corresponding finite sum

$$\int_0^{n}\psi(\delta v)\varphi\exp(\alpha^2(n-v))\mathrm{erfc}(\alpha(n-v)^{1/2})dv$$

$$= \varphi\Big[\sum_{i=1}^{n-1}\psi(i)\exp(\alpha^2(n-v))\mathrm{erfc}(\alpha(n-v)^{1/2})\Big] \qquad (3.2.33)$$

Thus eqn. (3.2.32) can be expressed as

$$1/(1+\theta S_{\delta\lambda}(\sigma n)) = 2(\delta/\pi)^{1/2}\Big[\psi(1)\sqrt{n} + \sum_{i=1}^{n-1}(n-i)^{1/2}[\psi(i+1)-\psi(i)]\Big]$$

$$- \delta\varphi\Big[\sum_{i=1}^{n-1}\psi(i)\exp(\alpha^2(n-i))\mathrm{erfc}(\alpha(n-i)^{1/2})\Big] \qquad (3.2.34)$$

This can now be solved for ϕ by computational methods.

As explained above the first finite sum in (3.2.33) can be evaluated as in the planar case with it resulting as an expression with a sum involving the previous n−1 unknown values of $\phi(i)$ and the unknown value $\phi(n)$. The second finite sum (3.2.33) is a simple Reimann type evaluation of the corresponding integral and is evaluated for the previous n−1 values of $\phi(i)$, with the product of the $\exp(x^2)\mathrm{erfc}(x)$, $x=\phi\sqrt{\delta}\sqrt{n-i}$, function. In the replacement of the integral by this finite sum it is assumed that $\psi=0$ and thus i=0 is not evaluated.

The evaluation of the function

$$\exp(x^2)\mathrm{ercf}(x) \qquad (3.2.35)$$

for x<=2 is carried out by using the normal routines. However for large values of x, it is not possible to evaluate the exponential as it is outside computational limits. This product $\exp(x^2)\mathrm{erfc}(x)$ can then be evaluated by exploiting the expression for erfc(x) for x>2, i.e.

$$\mathrm{erfc}(x) = e^{-x}/\pi^{1/2}x)\ [1-(1/2x^2)+(1.3/(2x^2)^2)\ -(1.3.5/(2x^2)^3)+\ldots]$$

and thus (3.2.36) can be evaluated as

$$\exp(x^2)\mathrm{erfc}(x) = (1/(\pi^{1/2}x)[1-(1/2x^2)+(1.3/(2x^2)^2)\ -(1.3.5/(2x^2)^3)+\ldots..]$$

The program which solves this routine is shown in Appendix 1.3. From equation

ν / Vs^{-1}	ΔE / mV
10	88.77
10^2	68.21
10^3	61.27
10^4	59.22
10^5	58.45
10^6	58.19

Table 3.2.1 Table showing the effect of increasing the sweep rate on the peak separation of cyclic voltammograms for spherical diffusion. These numerical results are for $D=1x10^{-5}cm^2s^{-1}$ and $r=5x10^{-4}cm$.

3.2.34 it can be seen that this expression for spherical diffusion will collapse to the corresponding expression for planar diffusion (eqn. 3.1.41) as ϕ limits to zero, i.e. very small diffusion coefficients, large values of r_o or high sweep rates. It has been shown, see table 3.2.1, that for a 5μm radius electrode and a species with a diffusion coefficient of $1x10^{-5}$ cm^2s^{-1}, that this occurs for sweep rates greater than 10^4 Vs^{-1} i.e. $\Delta E \simeq 59mV$.

3.2.2 Comparison of The Solution In 3.2.1 With Reinmuth's Spherically Corrected Linear Diffusion Solution

In 1957 Reinmuth [54] presented a correction factor by which it was possible to correct the current obtained from the planar diffusion solution, for spherical diffusion. Reinmuth carried this out by solving the same boundary conditions as given in 3.2.1, by using Laplace transformations of Fick's 2nd Law of spherical diffusion, for both species, and by making a change of variables as in eqns. (3.2.8) and (3.2.9). This results in an expression for $u(r_o,t)$ and $v(r_o,t)$ of

$$u(r_o,t)=v(r_o,t)=r_oc_o[\,(1-\exp(-\sigma t))/(1+\theta\exp(-\sigma t))\,] \quad (3.2.36)$$

θ being defined as in section 3.1.1. Given that the current at a spherical electrode is

$$i=nFAD(\partial c/\partial r)_{r=r_o}=nFADu(r_o,t)/r_o^2-(nFAD/r)(\partial u/\partial r)_{r=r_o} \quad (3.2.37)$$

the first term being the spherical contribution to the current and the latter term being the linear contribution, the current can be simplified to:-

$$i_s = i_p + nFADc_\alpha^*(D/r_o)\varphi(\sigma t) \quad (3.2.38)$$

with $\phi(\sigma t)$ defined as

$$\varphi(\sigma t) = (1-S_{\sigma\lambda}(\sigma t))/(1+\theta S_{\sigma\lambda}(\sigma t)) \quad (3.2.39)$$

and i_p is the current at a planar electrode as defined by eqn. (3.1.35). i.e. the approximate solution for i_p, *c.f.* the exact solution presented by Reinmuth. Thus by a simple adaption of the computer program that was used to solve eqn. (3.1.41) the spherically corrected current was evaluated and compared with that found for the solution presented in 3.2.1. In both cases the current are normalised to the expected diffusion limited current at a hemisphere, which is given by

$$i_l = nFADc_\alpha^*/r_o \qquad (3.2.40)$$

thus the normalised currents evaluated are

$$i_R/i_l = \pi^{1/2}\chi(\sigma t)\ \rho + \varphi(\sigma t) = \chi_R \qquad (3.2.41)$$

for Reinmuth's solution, χ_R, and the solution presented in 3.2.1, χ_S, respectively. ρ being defined as $1/\phi$, see 3.2.1

It is found that for values of $\rho >= 0.9865$, and using a dimensionless potential/time step, δ, of 0.01, as recommended by Nicholson and Shain [48], that χ_R and χ_S agreed to within 1% over the scan limits used, see figure 3.2.1. However as a steady state response is approached , i.e. $\rho < 0.9865$, the error between the two solutions increases dramatically, and it is found that for ρ of 0.099 that there is a 40% difference between the two sets of results. This discrepancy arises due to the evaluation of the integral (3.2.33), the spherical factor, since as a steady state is approached the spherical component becomes more important. As explained in 3.2.1 this integral is evaluated in a staircase manner, and therefore an accumulative error occurs which becomes more important as ρ is decreased. In order to minimise this error for smaller values of ρ, the dimensionless step size, δ, is decreased. The effect of decreasing δ on the accuracy of the results for $\rho >= 0.3120$ is shown in table 3.2.2. It can be seen that for $\rho = 0.3120$ that a δ of 0.001 is required to bring χ_S to within 1% of

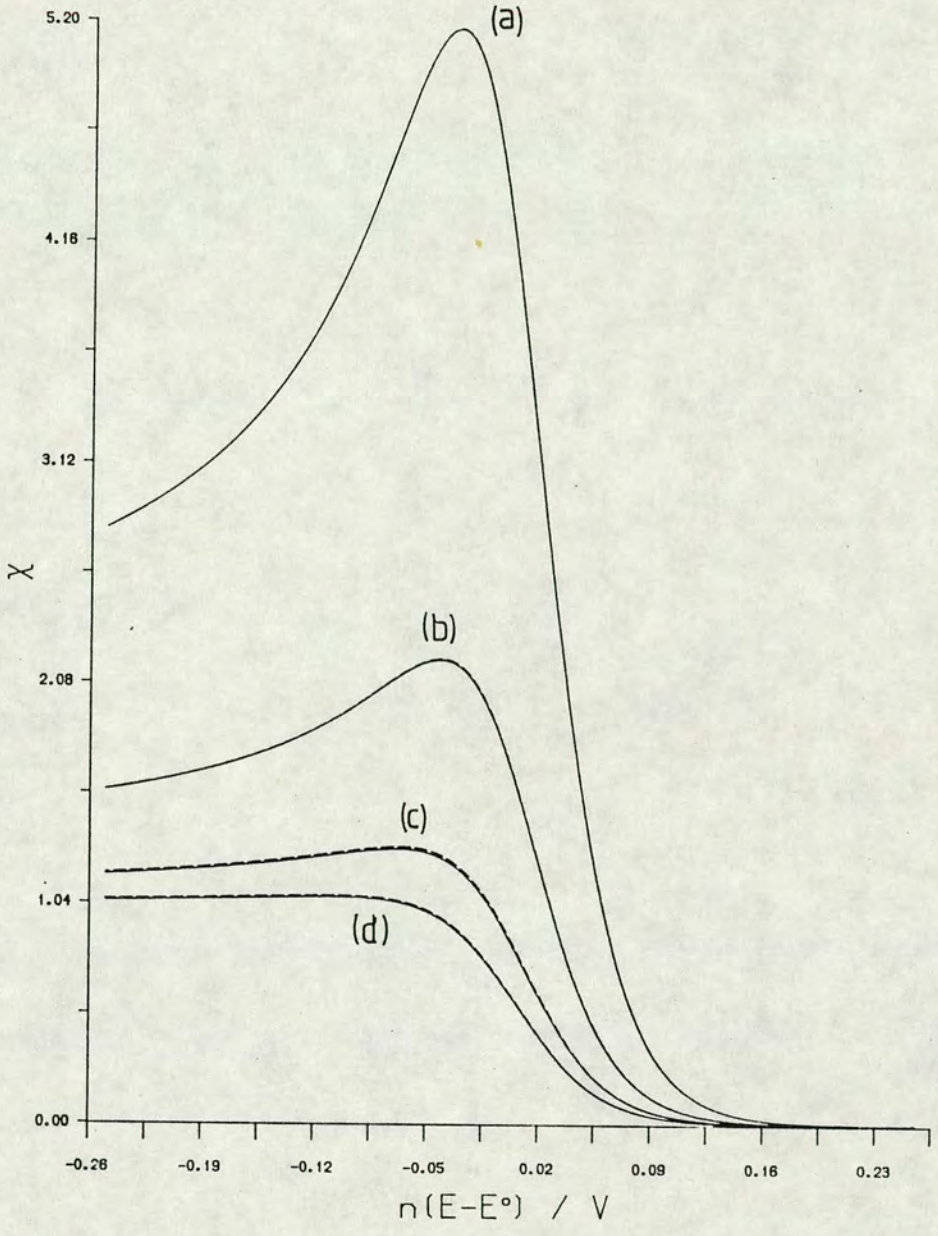

Figure 3.2.1 Plot of χ *vs.* $n(E-E^{\circ})$ for linear sweep voltammograms from the pseudo-analytical solution (——), and Reinmuth's solution (---). The four voltammograms being for (a) ρ=9.865, (b) ρ=3.120, (c) ρ=0.9865, (d) ρ= 0.3210.

			χ_R		χ_S			
ρ	Equivalent ν /Vs^{-1}	δ	χ_p	χ_I	χ_p	χ_I	%difference, χ_p	%difference, χ_I
0.312	0.1	0.01	1.0786	1.0572	1.0242	1.0068	5	5
		0.005			1.0434	1.0303	3	3
		<u>0.001</u>			1.0719	1.0511	0.6	0.6
0.986	1.0	<u>0.01</u>	1.3093	1.1810	1.2984	1.1731	0.8	0.7
3.120	10.0	<u>0.01</u>	2.1957	1.5729	2.1913	1.5715	0.2	0.09
9.865	100.0	<u>0.01</u>	5.1732	2.8116	5.1699	2.8113	0.06	0.01

Table 3.2.2 Table showing the effect of varying δ on the accuracy of the pseudo-analytical solution as compared to the results for Reinmuth's solution as under the same conditions. The optimal values of δ for each value of ρ, presented in figure 3.2.1, are underlined.

χ_R. For values of ρ less than 0.312, δ has to be made so small, to be within 1% of χ_R, that it becomes computationally impractical to evaluate linear sweep voltammograms, or cyclic voltammograms, due to the large number of steps required by the integration. This difficulty could however be overcome by using more sophisticated integration techniques. Table 3.2.2 thus shows the optimal values of δ which should be used to produce results which are accurate to within 1% of those predicted by Reinmuths solution.

It is clear from this that for the correct value of δ, for a given value of ρ, that it is possible to generate cyclic, or linear sweep, voltammograms for diffusion to a spherical/hemi-spherical electrode by this method, which are at least as accurate as those produced from Reinmuth's solution.

3.2.3 Quasi-Reversible Ion Transfer

Until now kinetic studies at microelectrodes have been confined to either steady-state conditions or very fast sweep rates, i.e. $>1 kVs^{-1}$. The former study has been treated for microdisc [55,56], microband [57,58], and microsphere [59,44] electrodes, and the later has recently been reviewed by Andrieux *et al* [60]. As discussed in 3.2.2, analytical solutions have been presented for reversible cyclic voltammetry at a spherical electrode [54]. Due to the nature of the Reinmuth correction it is not possible to apply the spherical correction to the quasi-reversible case, and to date solutions for this have not been presented. Here it will be shown that it is possible to apply the same numerical integration methods, as derived in 3.2.1, for the reversible case, to quasi-reversible charge tranfer reactions at a spherical electrode.

In this case the same boundary conditions as in 3.2.1 apply i.e. eqns (3.2.1) to (3.2.5), however the present expression for the surface concentrations is no longer the Nernst relationship, due to it no longer being a reversible reaction.

Therefore here it is replaced by the kinetic term

$$i(t)/nFA = D_\alpha[\,\partial c_\alpha(r,t)/\partial r\,]_{r=r} = k_f c_\alpha^* - k_b c_\beta^* \qquad (3.2.42)$$

given that the reaction being studied is

$$I_\alpha \underset{k_b}{\overset{k_f}{\rightleftharpoons}} I_\beta \qquad (3.2.43)$$

The other difference, compared to the reversible case is that c_α^* is not assumed to zero for the conditions $r>=r_o$ $t=0$. If it is then assumed that the Butler-Volmer relationship accounts for the kinetics of the above reaction then the same substitutions that were made in 3.1.2 can be made i.e. eqns (3.1.48) and (3.1.49), to give

$$i(t)/nFA = k\,\exp[\,-(\alpha nF/RT)(E-E^\circ)\,][\,c_\alpha^*(r_o,t) - \exp(nF/RT)(E-E^\circ)c_\beta(r_o,t)\,] \qquad (3.2.44)$$

Given that the potential relationship is as defined in 3.1.1 for cyclic voltammetry eqn. (3.2.44) can be written as

$$i(t)/nFA = k(\theta S_\lambda(t))^{-\alpha}\,[\,c_\alpha(r_o,t) - \theta S_\lambda(t) c_\beta(r_o,t)\,] \qquad (3.2.45)$$

where $S_\lambda(t)$ is defined as in (3.1.14) and $\theta=c_\alpha^*/c_\beta^*$, which can be defined for the the initial conditions by the Nernst relationship.

Expressions for the surface concentrations, $c_\alpha(r_o,t)$ and $c_\beta(r_o,t)$ can be derived in the same manner as in 3.2.1, and are given by

$$c_\alpha(r_o,t) = c_\alpha^* - 1/(nFA\sqrt{D_\alpha})\int_0^t i(\tau)\Big[1/(\pi(t-\tau))^{1/2} - (D_\alpha/r_o)^{1/2}\exp[\,(D_\alpha/r_o^2)(t-\tau)\,]\mathrm{erfc}[\,(D_\alpha^{1/2}/r_o)(t-\tau)^{1/2}\Big]d\tau \qquad (3.2.46)$$

$$c_\beta(r_o,t) = c_\beta^* + 1/(nFAD_\beta^{1/2})\int_0^t i(\tau)\Big[1/(\pi(t-\tau))^{1/2} - (D_\beta/r_o)^{1/2}\,\exp[\,(D_\beta/r_o^2)(t-\tau)\,]\mathrm{erfc}[(D_\beta^{1/2}/r_o)(t-\tau)^{1/2}\Big]d\tau \qquad (3.2.47)$$

the difference in this case being the non-zero bulk concentration of I_α, c_α^*. These equations for the bulk concentrations can then be substituted into (3.2.45) to give

$$i(t)/nFA = k(\theta S_\lambda(t))^{-\alpha}\Big\{ c_\alpha^* - 1/(nFA\sqrt{D_\alpha})\int_0^t i(\tau)\Big[1/(\pi(t-\tau))^{1/2} - (D_\alpha^{1/2}/r_o)\exp[(D_\alpha/r_o^2)(t-\tau)]\operatorname{erfc}[(D_\alpha^{1/2}/r_o)(t-\tau)^{1/2}]\Big]d\tau$$

$$-\theta S_\lambda(t)\Big[c_\beta^* + 1/(nFA\sqrt{D_\beta})\int_0^t i(\tau)[1/(\pi(t-\tau))^{1/2} - (D_\beta^{1/2}/r_o)\exp((D_\beta/r_o^2)(t-\tau))\operatorname{erfc}((D_\beta^{1/2}/r_o)(t-\tau)^{1/2})\Big]\Big\} \quad (3.2.48)$$

This expression can be simplified by substituting f(t)=i(t)/nFA, and eqn. (3.2.27), for $D_\alpha=D_\beta$ to result in

$$f(t)/c_\alpha^* = k(\theta S_\lambda(t))^{-\alpha}\Big\{ - 1/c_\alpha^*\sqrt{D}\int_0^t f(\tau)[1/(\pi(t-\tau))^{1/2} - H(t-\tau)]d\tau - S_\lambda(t) - \theta S_\lambda(t)/c_\alpha^*\sqrt{D}\int_0^t f(\tau)[1/(\pi(t-\tau))^{1/2} \quad H(t-\tau)]d\tau\Big\} \quad (3.2.49)$$

A change of variables as in 3.1.1 is then carried out i.e. eqns (3.1.30) and (3.1.31), to evaluate a current potential relationship, thus resulting in

$$g(\sigma t)(\theta s_{\sigma\lambda}(\sigma t))^\alpha/c_\alpha^* k = 1 - S_{\sigma\lambda}(\sigma t) - \int_0^{\sigma t} g(z)[1/(\pi(t-\tau))^{1/2} - \varphi\exp(\varphi^2(\sigma t-t))\operatorname{erfc}(\varphi(\sigma t-t)^{1/2})]d\tau \quad x \quad (1+\theta S_{\sigma\lambda}(\sigma t)/(\sigma D)^{1/2}c_\alpha^*) \quad (3.2.50)$$

ϕ being defined as in 3.2.1. This can then be made dimensionless by the substitution of $\psi(\sigma t)$, the dimensionless current, as defined in (3.2.30) to obtain

$$\psi(\sigma t)(\theta S_{\sigma\lambda}(\sigma t))^\alpha(\sigma D)^{1/2} = 1 - S_{\sigma\lambda}(\sigma t) - \int_0^{\sigma t}\psi(z)/(\pi(\sigma t-z))^{1/2}dz\ (1 + \theta S_{\sigma\lambda}(\sigma t)) + \int_0^{\sigma t}\varphi\psi(z)\exp(\varphi^2(\sigma t-z))\operatorname{erfc}(\varphi(\sigma t-z)^{1/2})dz\ (1+\theta S_{\sigma\lambda}(\sigma t)) \quad (3.2.51)$$

Eqn. (3.2.51) can now be evaluated for $\psi(\sigma t)$, numerically by the same substitutions as in 3.1.1, i.e. eqns. (3.1.36) and (3.1.37), and the integrals can be replaced by their finite sums as in 3.2.1, i.e. by eqns (3.1.40) and (3.2.33). This results in the the final expression for the evaluation of $\psi(\sigma t)$ being given by

$$(\sigma D)^{1/2}\psi(\delta n)(\theta S_{\delta\lambda}(\delta n))^{\alpha/k} = 1 - S_{d\lambda}(\delta n) - (1 + \theta S_{\delta\lambda}(\delta n))$$

$$x \left\{ 2(\delta/\pi)^{1/2} \left[\psi(1)n^{1/2} + \sum_{i=1}^{n-1} (n-i)^{1/2}[\psi(i+1) - \psi(i)] \right] \right.$$

$$\left. + \delta\varphi \left[\sum_{i=1}^{n-1} \psi(i)\exp[\varphi^2\delta(n-i)]\operatorname{erfc}[\varphi(\delta(n-i))^{1/2}] \right] \right\} \qquad (3.2.52)$$

The current can then be obtained from

$$i(\delta n) = nFADc_{\alpha}^{*}(D\sigma)^{1/2}\psi(\delta n) \qquad (3.2.53)$$

having computationally evaluated $\psi(\sigma t)$.

The routines involved in solving (3.2.52) are identical to those used in 3.2.1 for the evaluation of equation (3.2.34), and the program used is presented in Appendix 1.4. Thus the errors introduced in evaluating the integral for the spherical contribution should be the same as discussed in 3.2.2 and therefore the values of ρ and δ used must be carefully noted, when the cyclic voltammograms are analysed. Thus the analysis of steady-state voltammograms must be done bearing this in mind, however, as described earlier, kinetic analysis of voltammograms in steady-state conditions has already been carried out by an alternative approach [12,13]. Due to the excessively large computation times required for the generation of steady-state curves, i.e. small δ values, it is not practical to use the present technique to analyse steady state curves, and therefore the solution presented will only be discussed for values of $\rho > 0.3120$.

To illustrate the effect of the charge tranfer rate constant, k^o, figure 3.2.2 shows the effect of varying k^o over the range 10^2 - $10^{-4}cms^{-1}$, for four different sweep rates i.e. 0.1, 1.0, 10.0 and 100 Vs^{-1}, the values of α, D and r_o being held constant in each case, i.e. α=0.5, D=10^{-5} cm^2s^{-1}, and r_o=5x10^{-4}cm. The corresponding plots of $\ln((i_{ss}-i)/i)$ *vs.* $E-E^o$ are shown in figure 3.2.3. It can be seen for each of the sweep rates presented the value of $\chi_{1/2}$, i.e. the normalised current is equal to 0.5, when the system is seen to become irreversible, moves 118mV per decade change in the rate constant. It can also be seen for the system presented that steady-state measurements (figure 3.2.2(a)) do not allow values of k of less than $10^{-2}cms^{-1}$ to be evaluated. However at faster sweep rates more resolution of the faster reactions can be achieved.

In order to establish a method to estimate rate constants, from a sweep rate dependence, at a hemi-/spherical electrode, the variation of ΔE_p was examined. It is shown, in figure 3.2.4 that as the sweep rate is increased the difference in the peak potentials ΔE_p, decreases to a minimum and then increases again, due to the planar contribution becoming the dominant factor. This trend being more pronounced for slower rate constants over the range of sweep rates examined. It is therefore possible to construct working curves of $\Delta E_{p,min.}$ *vs.* k, for different values of r_o and D, from which it is possible to evaluate k from the $\Delta E_{p,min.}$ observed experimentally. An example of such a working curve for the data presented in figure 3.2.4 is shown in figure 3.2.5, along with data for D=$10^{-5}cm^2s^{-1}$, r_o=10^{-3}cm and D=$10^{-6}cm^2s^{-1}$, r_o=5x10^{-4}cm. The data is also tabulated in Table 3.2.3.

It can be seen in these working curves that at the irreversible limit, for the rate constants, that the function becomes linear with a gradient of 236mV per decade, twice that observed for the $E_{1/2}$ shift. At the other extreme the peak

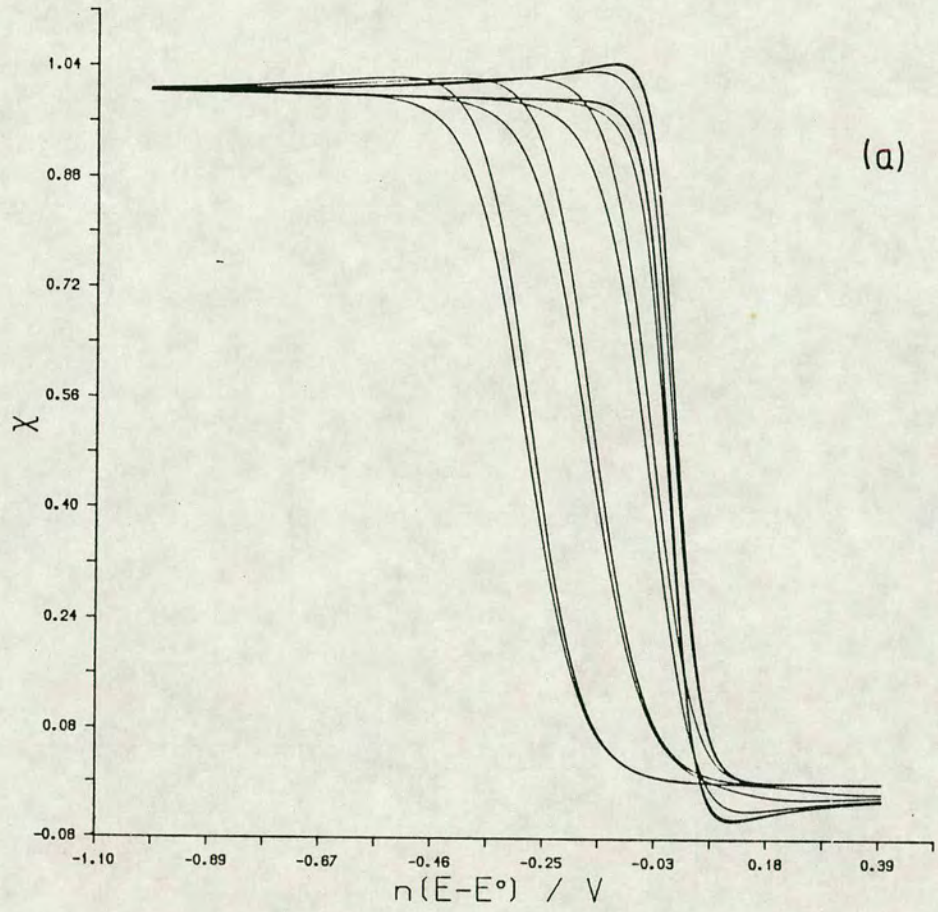

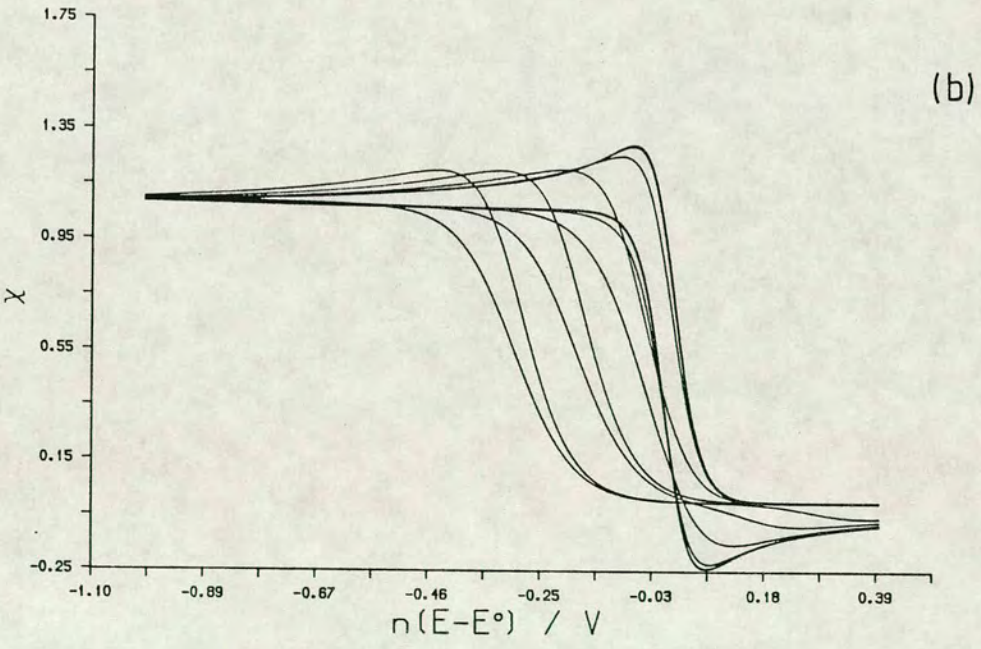

Figure 3.2.2 Plots of χ *vs.* $n(E-E^{\circ})$ of cyclic voltammograms of a quasi-reverisble reaction for spherical diffusion for k° varying from 10^{2}–10^{-4}cms^{-1}, for 4 different sweep rates. (a) 0.1Vs^{-1}, (b) 1.0Vs^{-1}, (c) 10.0Vs^{-1}, (d) 100.Vs^{-1}. (α=0.5, D=1x10^{-5}cm^{2}s^{-1}, r_o=5x10^{-4}cm.)

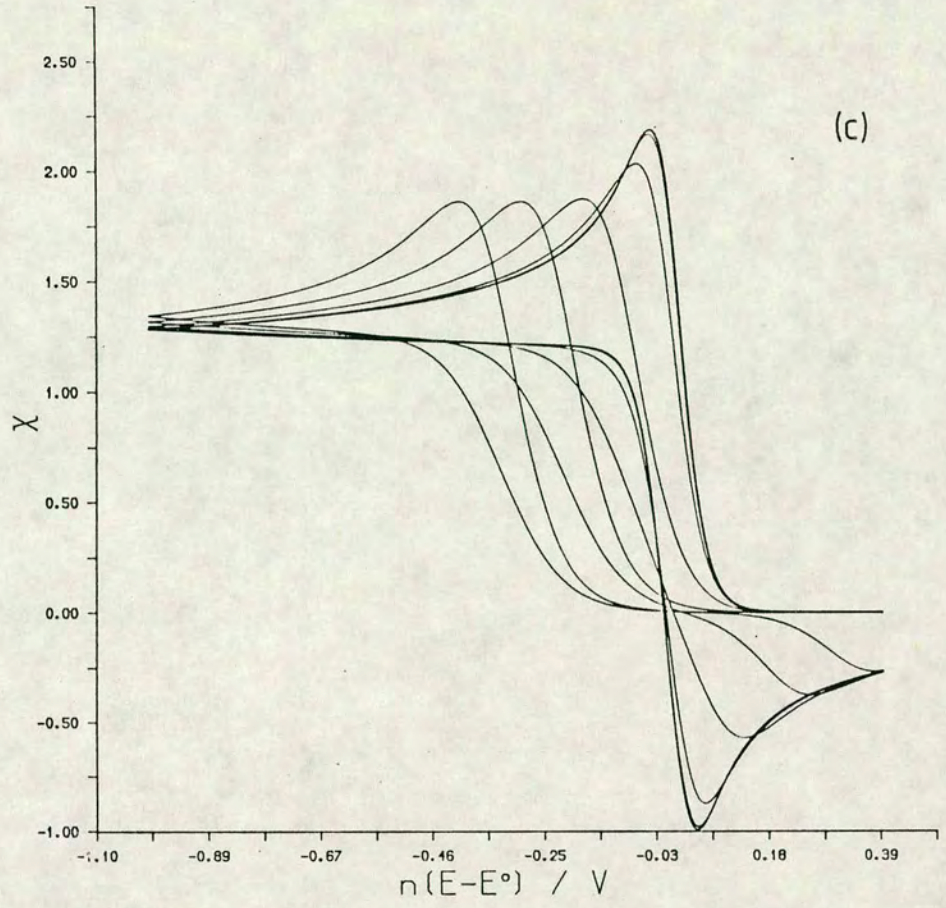
(c)
2.50
2.00
1.50
1.00
0.50
0.00
-0.50
-1.00
χ
-1.10
-0.89
-0.67
-0.46
-0.25
-0.03
0.18
0.39
n(E-E°) / V

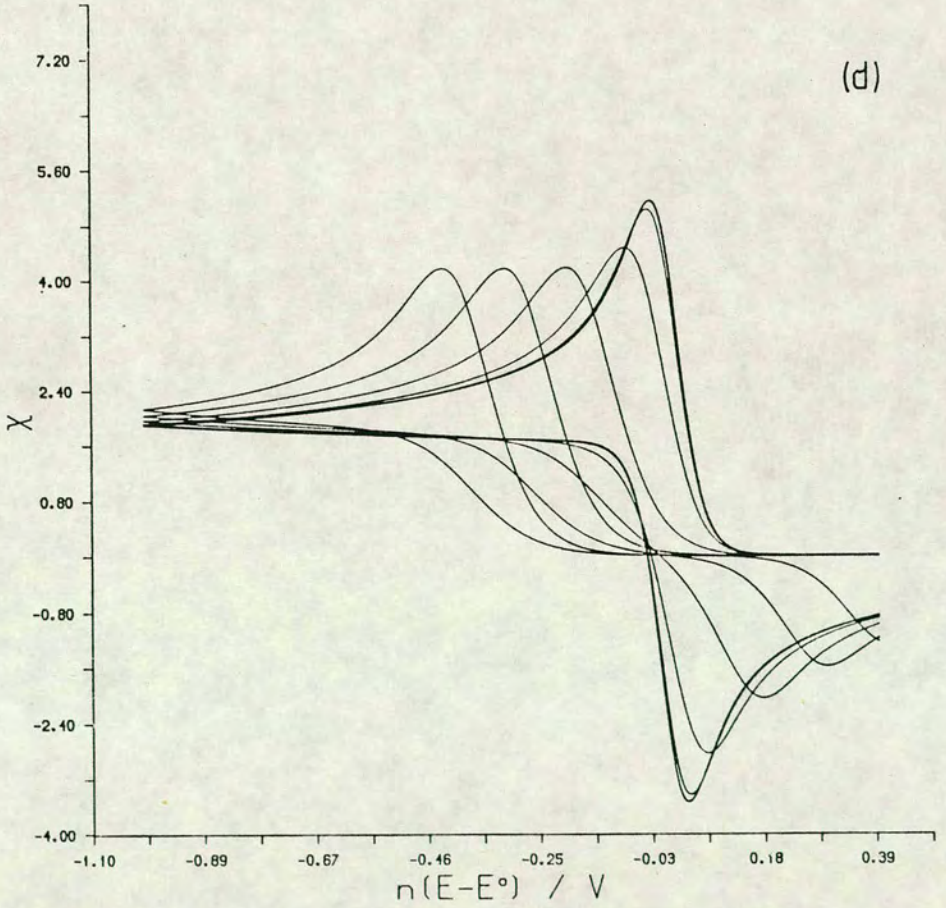
(d)
7.20
5.60
4.00
2.40
0.80
-0.80
-2.40
-4.00
χ
-1.10
-0.89
-0.67
-0.46
-0.25
-0.03
0.18
0.39
n(E-E°) / V

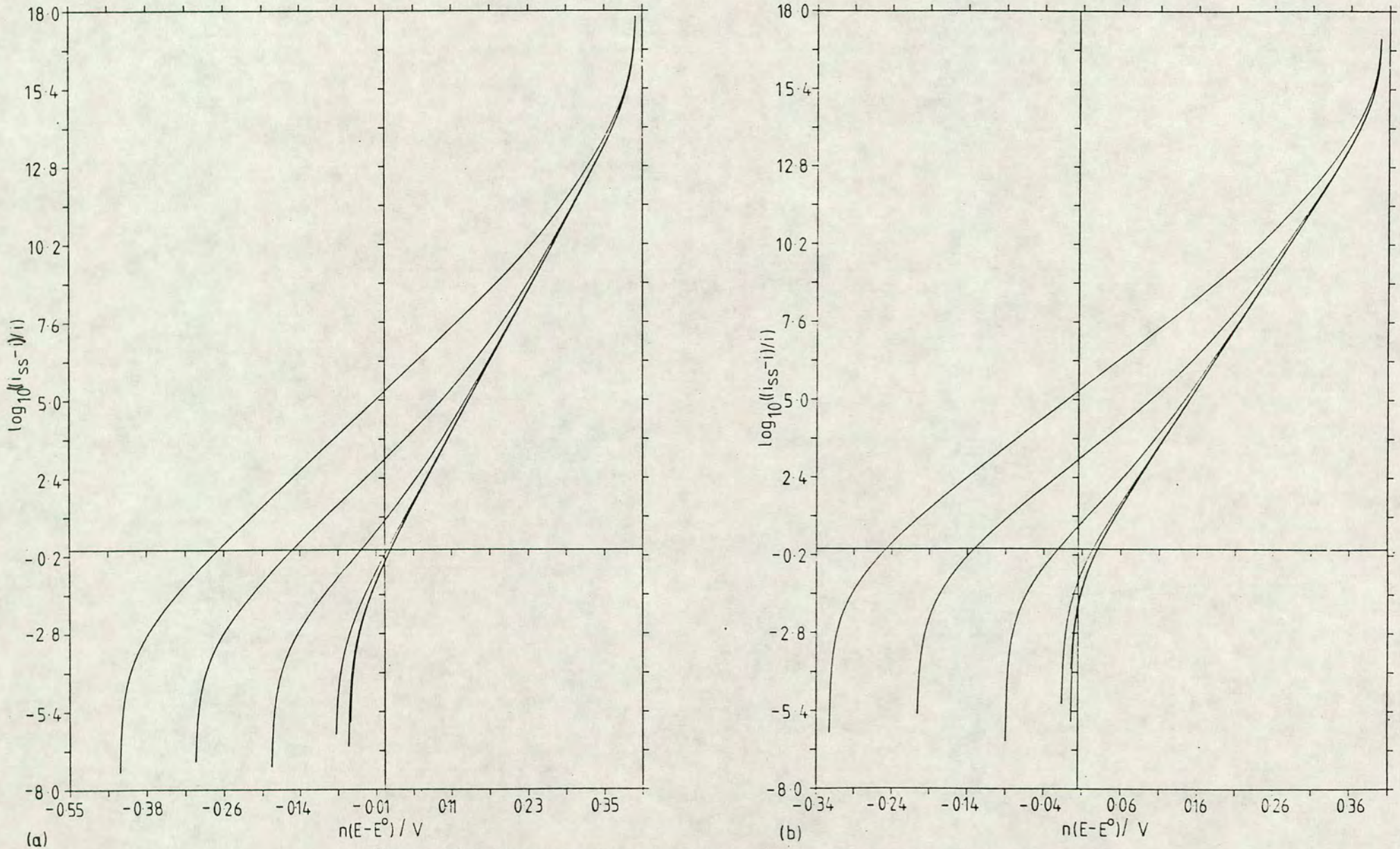

Figure 3.2.3 Corresponding plots of $\log_{10}((i_{ss}-i)/i)$ *vs.* $n(E-E^{o})$ for the cyclic voltammograms in figure 3.2.2 (a)-(d).

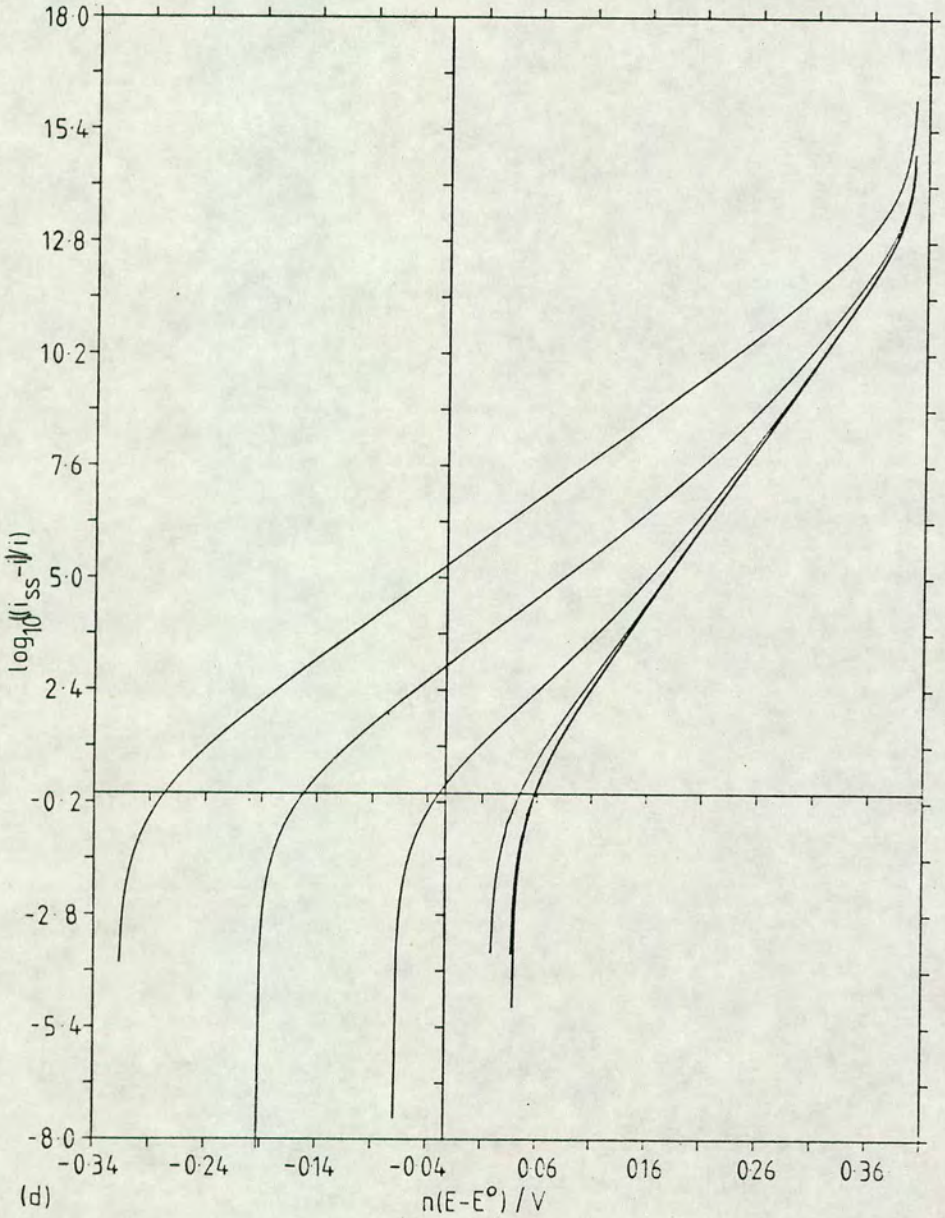
18·0
15·4
12·8
10·2
7·6
5·0
2·4
-0·2
-2·8
-5·4
-8·0
$\log_{10}((i_{ss}-i)/i)$
-0·34
-0·24
-0·14
-0·04
0·06
0·16
0·26
0·36
n(E-E°) / V
(d)

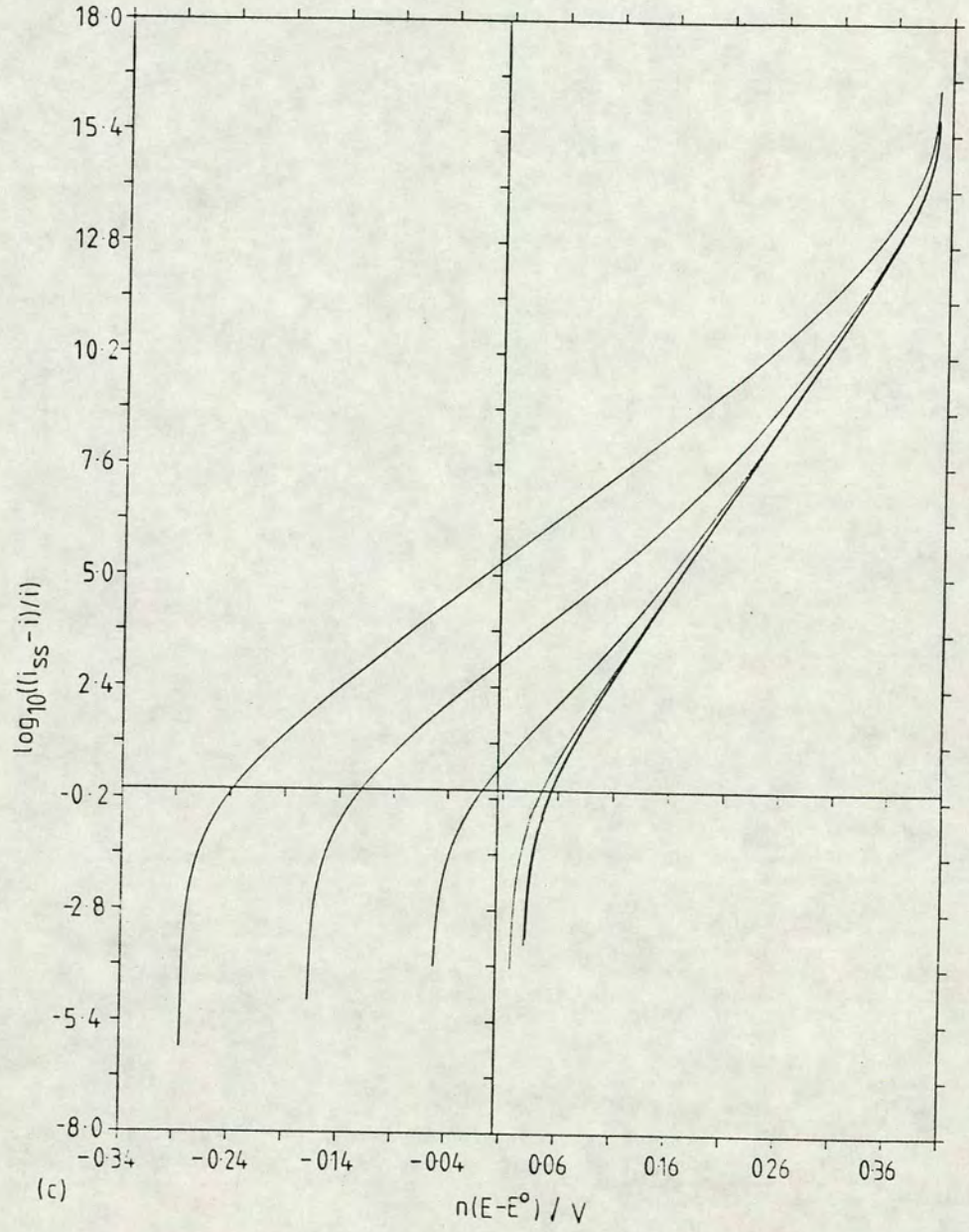
18·0
15·4
12·8
10·2
7·6
5·0
2·4
-0·2
-2·8
-5·4
-8·0
$\log_{10}((i_{ss}-i)/i)$
-0·34
-0·24
-0·14
-0·04
0·06
0·16
0·26
0·36
n(E-E°) / V
(c)

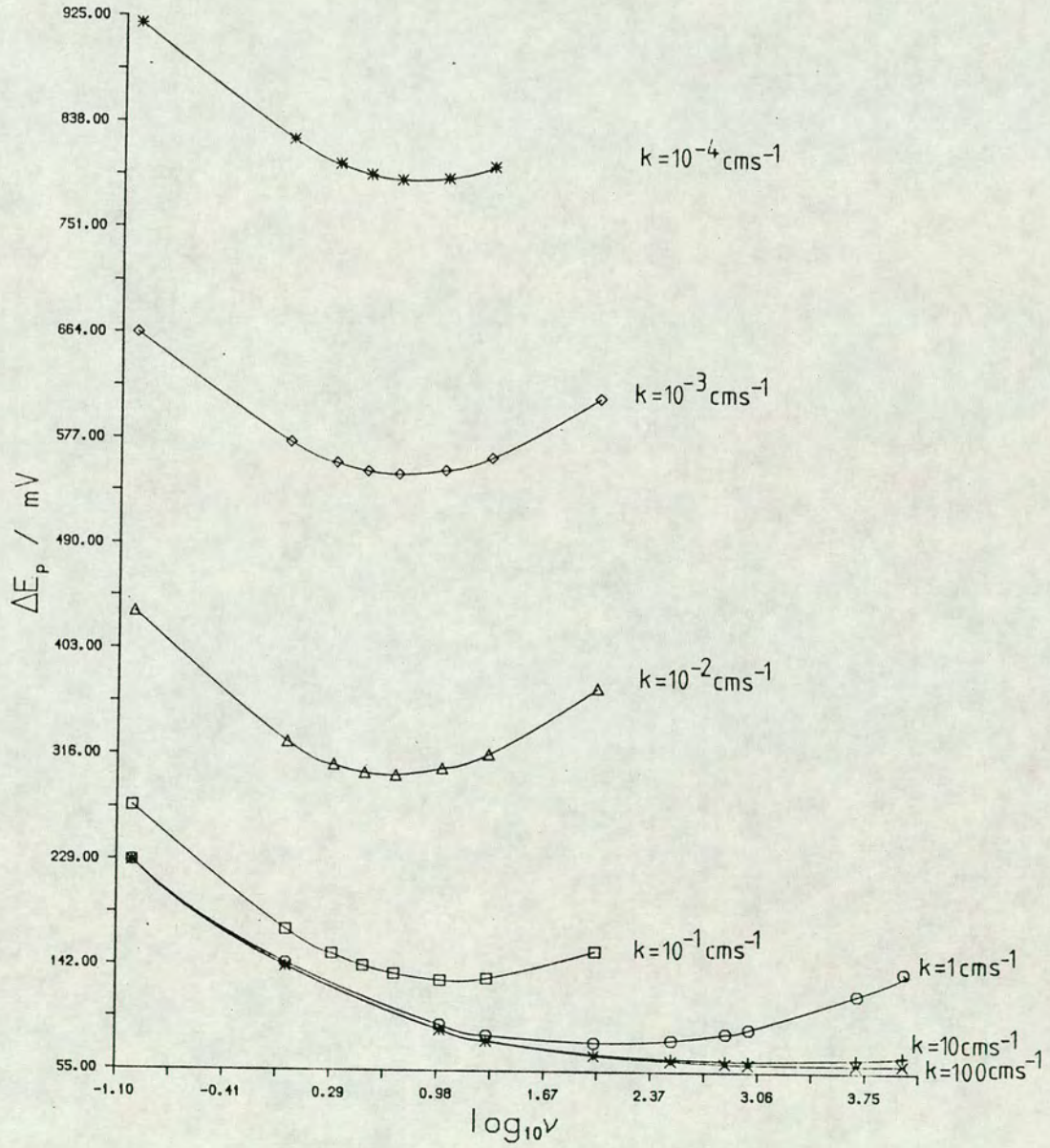

Figure 3.2.4 Plots of ΔE_p *vs.* $\log_{10}\nu$ for k^o values of 10^{-4}–10^2cms^{-1}. (α=0.5, D=1x10^{-5}cm^{2}s^{-1}, r_o=5x10^{-4}cm).

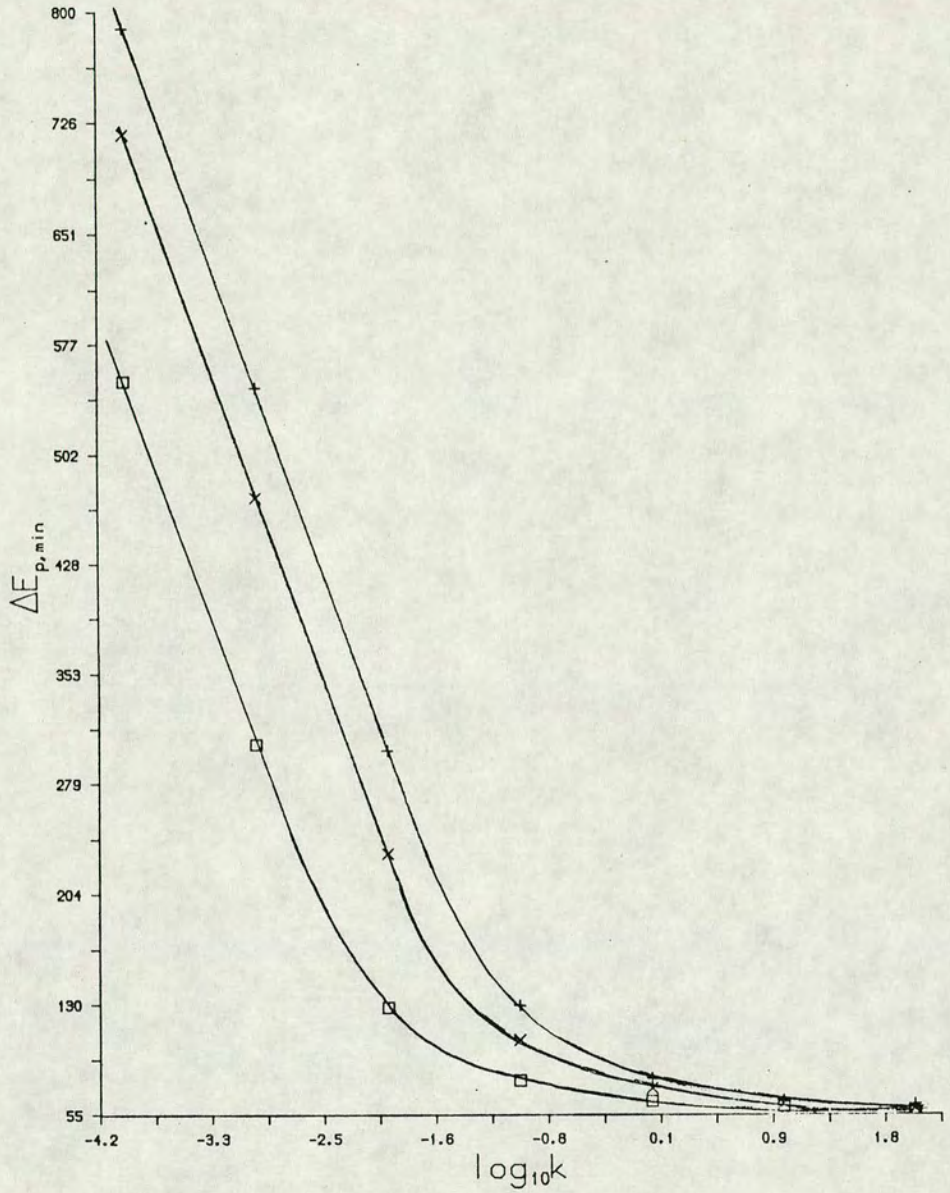

Figure 3.2.5 Working curve plots of $\Delta E_{p,min}$ *vs.* $\log_{10}k^{o}$ for (a) $r=5x10^{-4}cm$, $D=1x10^{-5}cm^{2}s^{-1}$ (+), (b) $r=5x10^{-4}cm$, $D=1x10^{-6}cm^{2}s^{-1}$ (□), (c) $r=10x10^{-4}cm$, $D=1x10^{-5}cm^{2}s^{-1}$ (X).

$D=10^{-5}$ cm^2s^{-1}, $r=5x10^{-4}cm$		$D=1x10^{-5}cm^2s^{-1}$, $r=10x10^{-4}cm$	
$log_{10}k^o$	$\Delta E_{p,min.}$	$log_{10}k^o$	$\Delta E_{p,min.}$
2	61.8	2	58.6
1	64.8	1	62.2
0	79.4	0	73.0
-1	128.7	-1	105.4
-2	300.9	-2	231.4
-3	546.9	-3	472.6
-4	788.8	-4	717.4

$D=1x10^{-6}cm^2s^{-1}$, $r=5x10^{-4}cm$	
$log_{10}k^o$	$\Delta E_{p,min.}$
2	58.3
1	60.0
0	64.1
-1	78.3
-2	127.3
-3	305.21
-4	551.3

Table 3.2.3 Table showing the variation of $\Delta E_{p,min}$ with k^o, for three systems, i.e. $D=1x10^{-5}cm^2s^{-1}$, $r=5x10^{-4}cm$; $D=1x10^{-5}cm^2s^{-1}$, $r=10x10^{-4}cm$; $D=1x10^{-6}cm^2s^{-1}$, $r=5x10^{-4}cm$.

separation reaches the asymptotic limit of 58mV, at 25°C. The minimum peak separation observed for the system r_o=5μm, D=$10^{-5}cm^2s^{-1}$ is equal to 129 and 79mV for k=10^{-1} and 1 cms^{-1} respectively. This results illustrates that cyclic voltammetry at micro electrodes can be used to access this range of rate constants. Unfortunately it is difficult to produce a universal working curve as the $\Delta E_{p,min}$ *vs.* $\log_{10}k$ dependence is a function of both the radius of the electrode and the diffusion coefficient, as can be seen in figure 3.2.5 and Table 3.2.3. However the algorithim can be simply evaluated on a microcomputer for a given set of experimental conditions, i.e. r_o and D.

All of the data presented so far has been a charge transfer coefficient, α, of 0.5, however it should be noted that α has a profound effect on both the peak current and the peak positions, see figure 3.2.6. This effect has been shown to occur for both high sweep rates and those where the steady state is approached.

Thus it can be seen that this solution for spherical diffusion can be used to predict rate constants up to *c.a.* 1 cms^{-1}, if the correct experimental conditions are chosen.

3.2.4 Experimental Results For Oxidation/Reduction at a Microdisc Electrode

In order to check the validity of the possible kinetic analysis of data for spherical/hemi-spherical electrodes the oxidation of $K_4Fe(CN)_6$ at a 25μm radius Pt disc electrode has been examined. The approximation that the diffusion limited current at a microdisc and micro hemi-spherical electrode are equivalent, for $r_{hemisphere}=(2/\pi)r_{disc}$, as used by Oldham and Zoski [62], has been assumed to hold for non-steady state conditions. Thus the results for a disc were compared with those for a hemi-sphere of equivalent radius, i.e. 12.5μm radius disc equivalent to an 8μm hemispherical electrode.

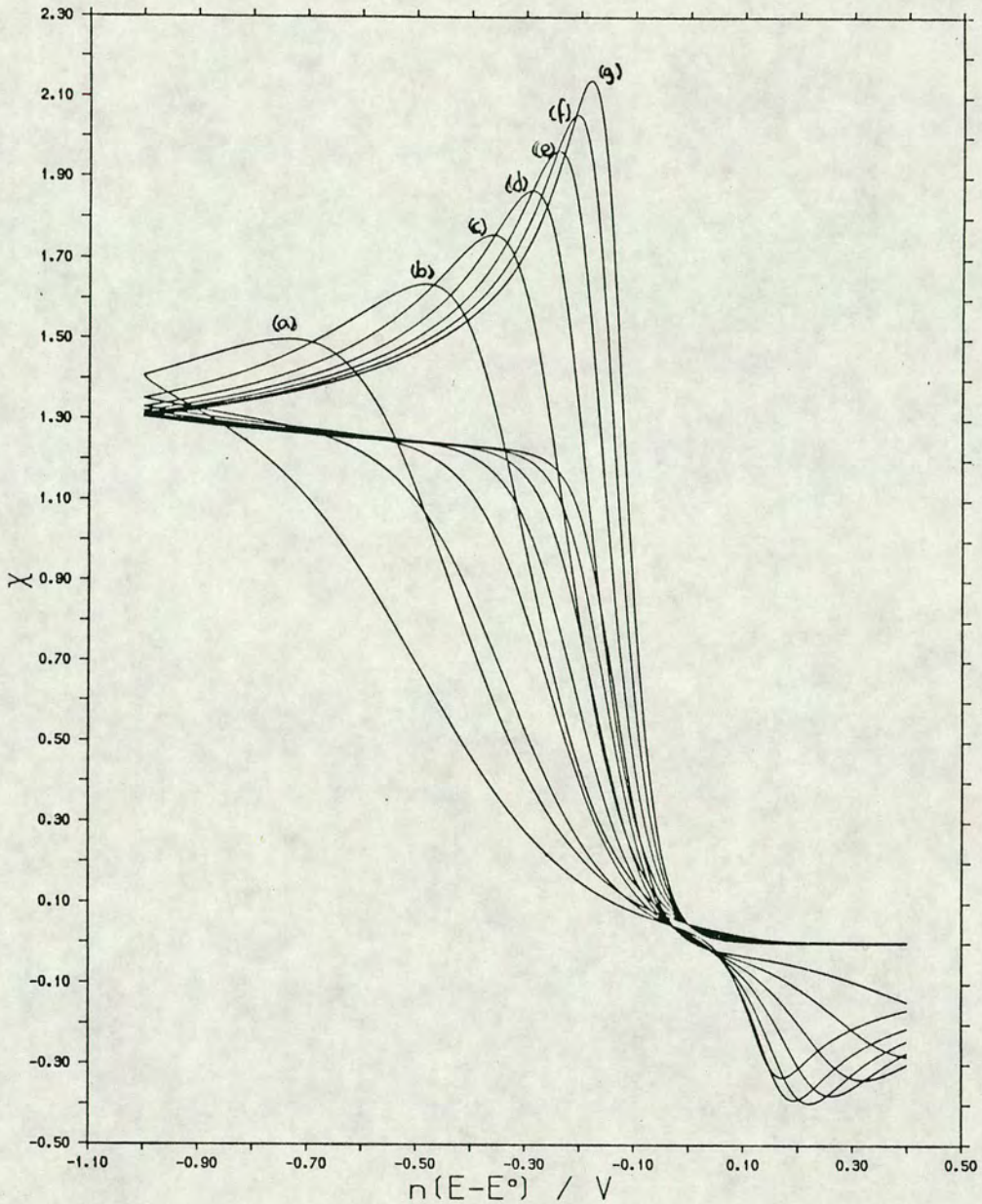

Figure 3.2.6 Cyclic voltammograms for spherical diffusion, under kinetic control, showing the effect of varying α. α=0.2, 0.3, 0.4, 0.5, 0.6, 0.7, 0.8, for (a)– (g) respectively. ($D=1x10^{-5}cm^2s^{-1}$, $k=0.001cms^{-1}$, $r=5x10^{-4}cm$, $\nu=10Vs^{-1}$).

Figure 3.2.7 shows the ΔE_p *vs.* $\log_{10}\nu$ relationship for this system. It can be seen that this relationship goes through a minimum as predicted by the analytical solution. By constructing a working curve, as explained in 3.2.3, for a hemispherical electrode; r_o=8μm, D=5.8x10^{-6}cm^{2}s^{-1}, of $\Delta E_{p,min.}$ *vs.* $\log_{10}k$, see figure 3.2.8, it was possible to evaluate the rate constant for the oxidation of $[Fe(CN)_6]^{4-}$ to $[Fe(CN)_6]^{3-}$. This was found to be 3.8x10^{-3}cms^{-1}.

As well as evaluating the rate constant in the manner described above it was also evaluated by analysing the "steady state" wave i.e. ν=0.1Vs^{-1}, see figure 3.2.9. For this curve a $\log_{10}((i_l-i)/i)$ *vs.* E relationship was evaluated for the same conditions, over a range of rate constants and an attempt to fit the reciprocal gradients of the semi-log plots for each value of k^o was made. This results in a rate constant constant of 1.8x10^{-3}cms^{-1} being found. This is in the same order of magnitude as that evaluated by the other approach. The reason why the two values do not agree more closely is due to the assumption that the equivalence of a disc and micro hemisphere holds for non-steady state systems, which has not been proven to be correct.

The value of the rate constant found for the oxidation/reduction of the ferro-/ferri cyanide couple is exceptionally slow compared to that expected, since this couple is normally found to be reversible at a Pt electrode. This low value may be explained by surface of the Pt disc electrode being contaminated since the electrode was not thoroughly cleaned prior to use.

These results demonstrate that the results predicted by this relationship are the same as those found experimentally. However the experimental results presented do not produce a reasonable order of magnitude value of the rate constant due to the reasons outlined above.

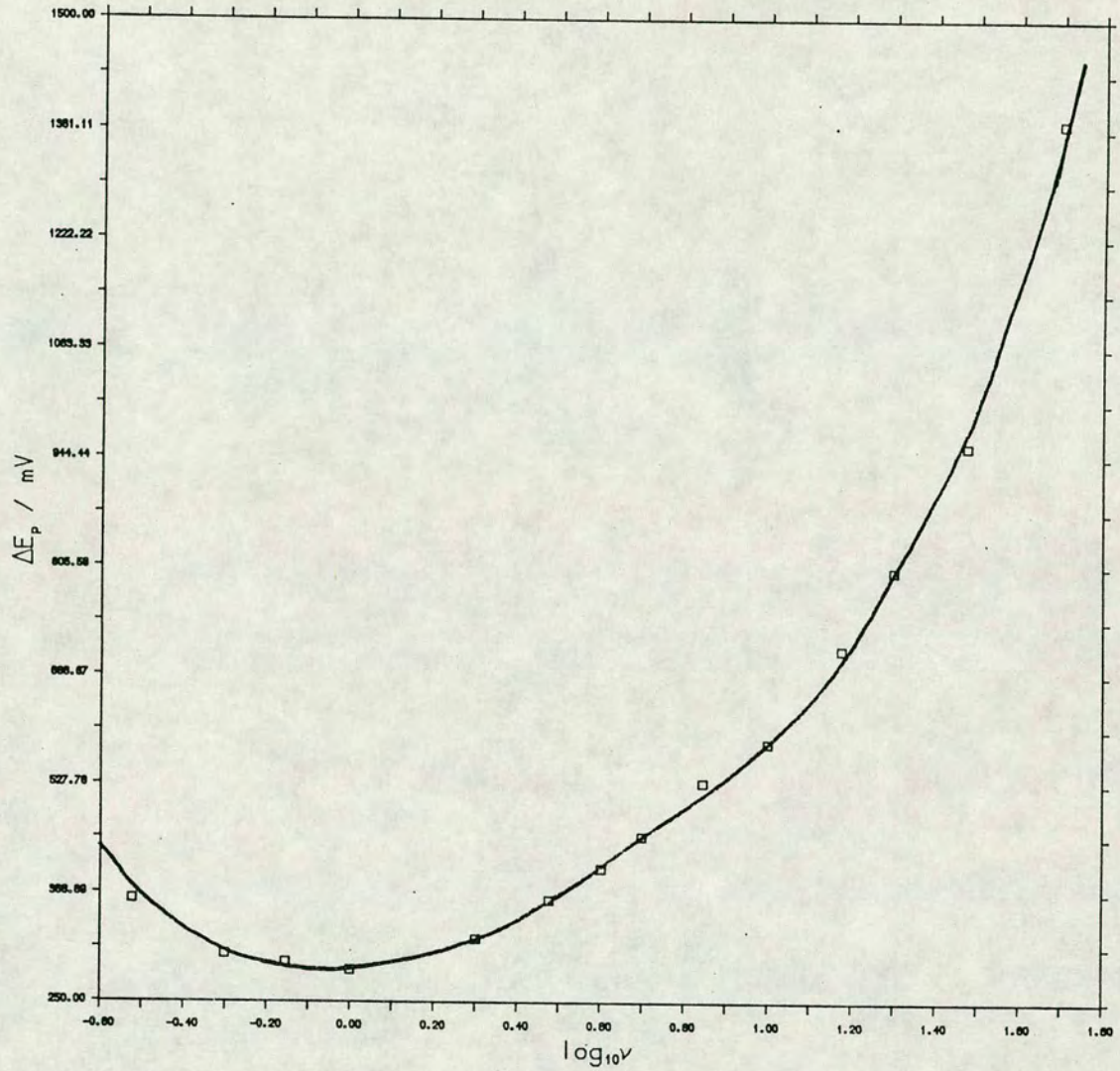

Figure 3.2.7 Plot of ΔE_p *vs.* $\log_{10}\nu$ from the cyclic voltammograms for the oxidation/reduction of potassium ferricyanide at 12.5µm radius Pt disc electrode.

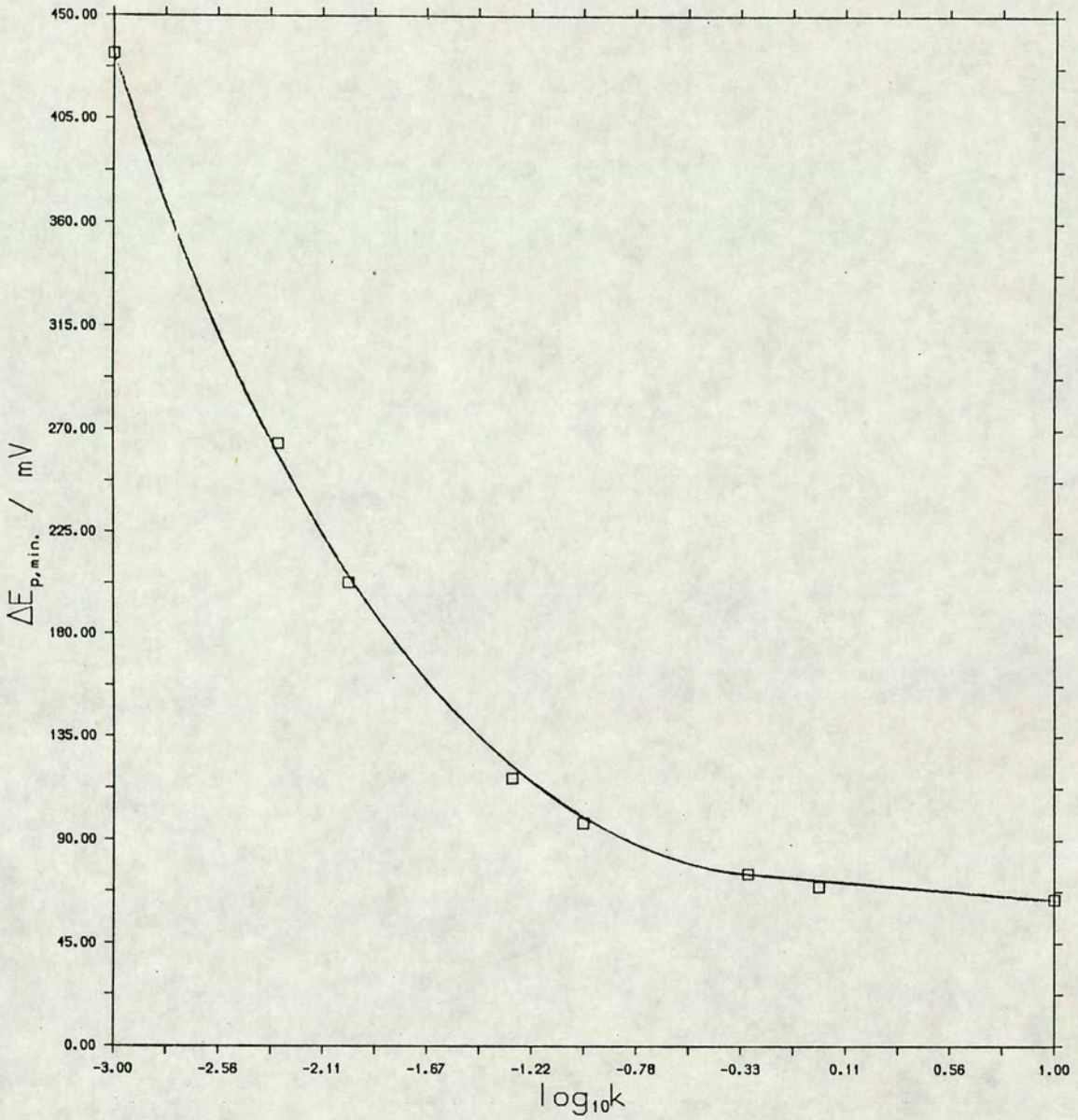

Figure 3.2.8 Working curve of $\Delta E_{p,min}$ *vs.* $\log_{10}k$ from the analytical solution for the experimental parameters of the experiment analysed in figure 3.2.7.

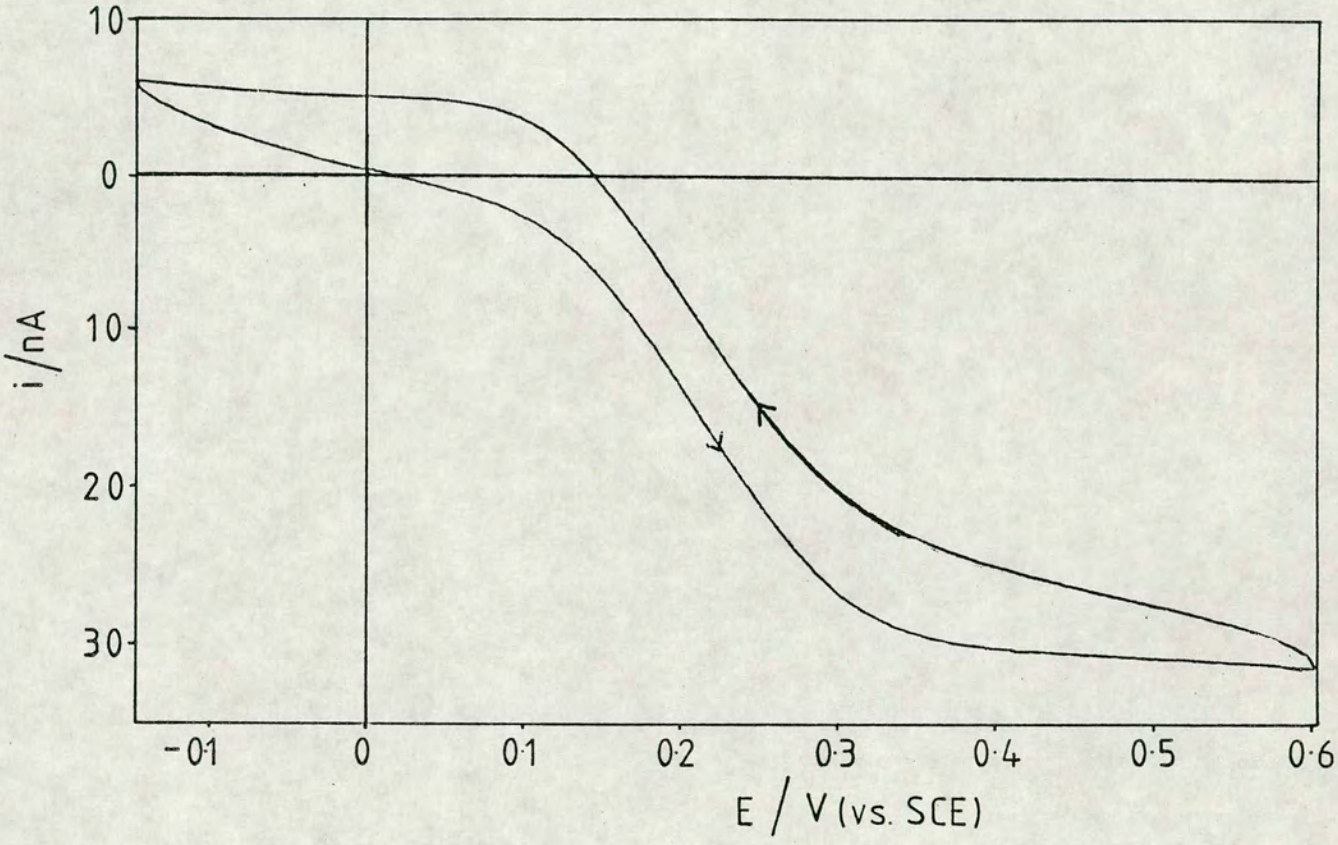

Figure 3.2.9 Steady state cyclic voltammogram for the oxidation of potassium ferrocyanide at a 12.5μm radius Pt disc electrode (ν=100mVs^{-1}).

3.3 Voltammetry For Ion Transfer For ITIES Supported AT The Tip Of A Micropipette

As described in chapter 2, ITIES which are supported at the tip of a micropipette show unique diffusion characteristics. Here ITIES of this type are characterised for linear sweep and cyclic voltammetry experimentally and also an approximate numerical solution is presented. The experimental results will be presented first, followed by the theoretical treatment, and they will then be compared with the experimental results.

3.3.1 Experimental Results

3.3.1.1 Linear Sweep For Ingress Transfer

The movement of ions towards the interface prior to transfer is similar to that of reactants for redox reactions at a microdisc electrode. The main difference is that the transferred ion moves away from the interface in a linear motion inside the pipette whereas the products of the redox reactions diffuse away in the same pattern as the arrival of the reactants. Figure 3.3.1 shows that despite the difference of the mass transport of the products a steady state wave is obtained. Figure 3.3.2 illustrates that the wave can be analysed in the classical manner for a steady state wave i.e.

$$E=E_{1/2}+(RT/nF)\ln((i_d-i)/i) \qquad (A)$$

It can be seen that the plot shows a linear relationship however the slope of this line is not equivalent to 58mVdecade^{-1} as expected for a fully reversible system but is slightly higher. Also the line does not pass through zero on the potential axis i.e. the $E_{1/2}$ value for the pipette does not appear to be the same

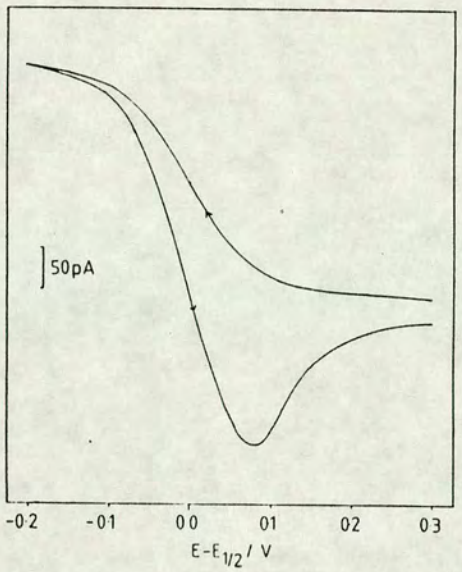

Figure 3.3.1 Cyclic voltammogram for the ingress transfer of TEA^+, first, for the cell Ag/AgCl/TPBNa(1mM),NaCl(10mM)/CVTPB(1mM),TEATPB(60μM)// LiCl(1mM)/AgCl/Ag at a 15μm radius pipette. $E=\Delta_o^w\phi$. (This definition of E will be used throughout.)

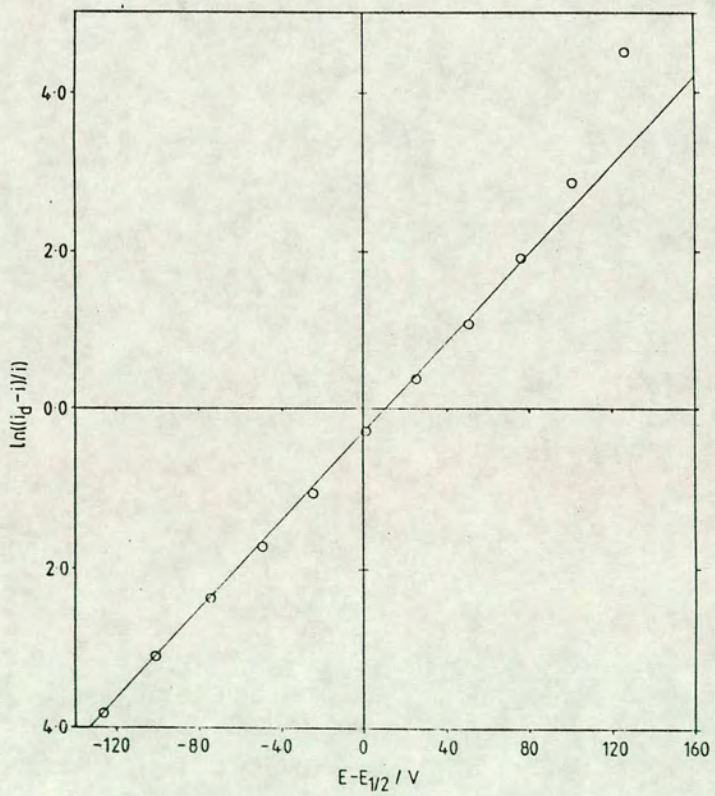

Figure 3.3.2 Plot of $\ln((i_d-i)/i)$ *vs.* $(E-E_{1/2})$ for the voltammetric wave shown in fig. 3.3.1. Slope = 80.0mVdecade^{-1}.

as the $E_{1/2}$ evaluated from a macro ITIES experiment. If this wave is analysed in the same manner as the steady-state wave for the oxidation of potassium ferrocyanide in 3.2.4, i.e. by fitting the reciprocal slopes of $\ln((i_l-i)/i)$ vs. E to the experimental results, it is possible to evaluate a rate constant for TEA^+ transfer from 1,2-dichloroethane to water. This is found to be *c.a.* $0.009 cms^{-1}$, again this is inconsistant with results from other experiments which suggests that the system is reversible. A reason for this anomaly may be that the iR drop in the pipette is significant. This iR drop may be caused by the pipette used in this experiment having a long shank, as discussed in 2.5.1.2, or by the accumulation of debris from the reference electrode near the tip of the pipette, see figure 3.3.3. If it is the latter case which is the major contributor to iR then the resistance in the tip of the pipette will be much higher than expected due to a vast reduction of the internal cross sectional area, as illustrated in figure 3.3.3. In order to overcome this drawback of iR the design of a low noise, small current, 2 or 4 electrode system should be considered.

The radius dependence of the plateau current, i_{ss}, has been compared to that of hemispherical and microdisc electrodes and it can be seen in figure 3.3.4 that the results obtained lie between the two limits given by

$$i_{ss}=2\pi nFDc^*r_{hs} \qquad (B)$$

and

$$i_{ss}=4nFDc^*r_d \qquad (C)$$

for hemisphere and a microdisc, where F is the Faraday constant, D is the diffusion coefficient, and c^* is the concentration of the transfering ion and r_{hs} and r_d represent the radius of the hemisphere and the disc respectively. We believe that the observed current is higher, on one hand, due to a certain degree of curvature of the liquid/liquid interfaces which, despite numerous experimental procedures, cannot be avoided due to surface tension effects, and

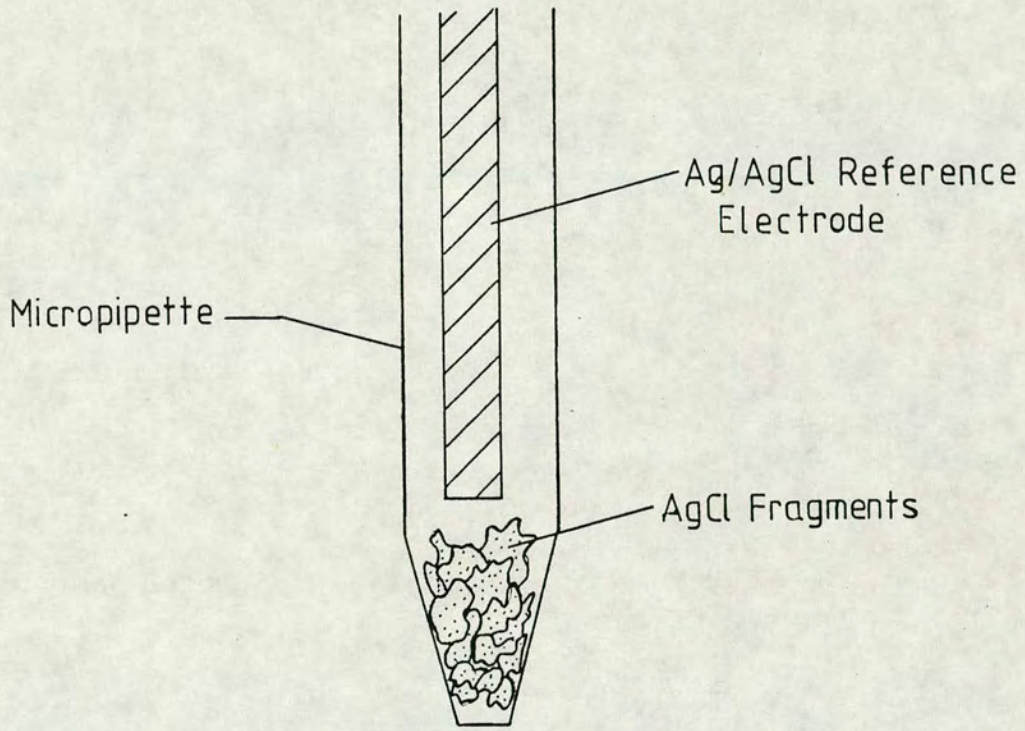

Figure 3.3.3 Diagram showning the tip of a micropipette in which small fragments of debris have accumulated, thus increasing the resistance within the pipette.

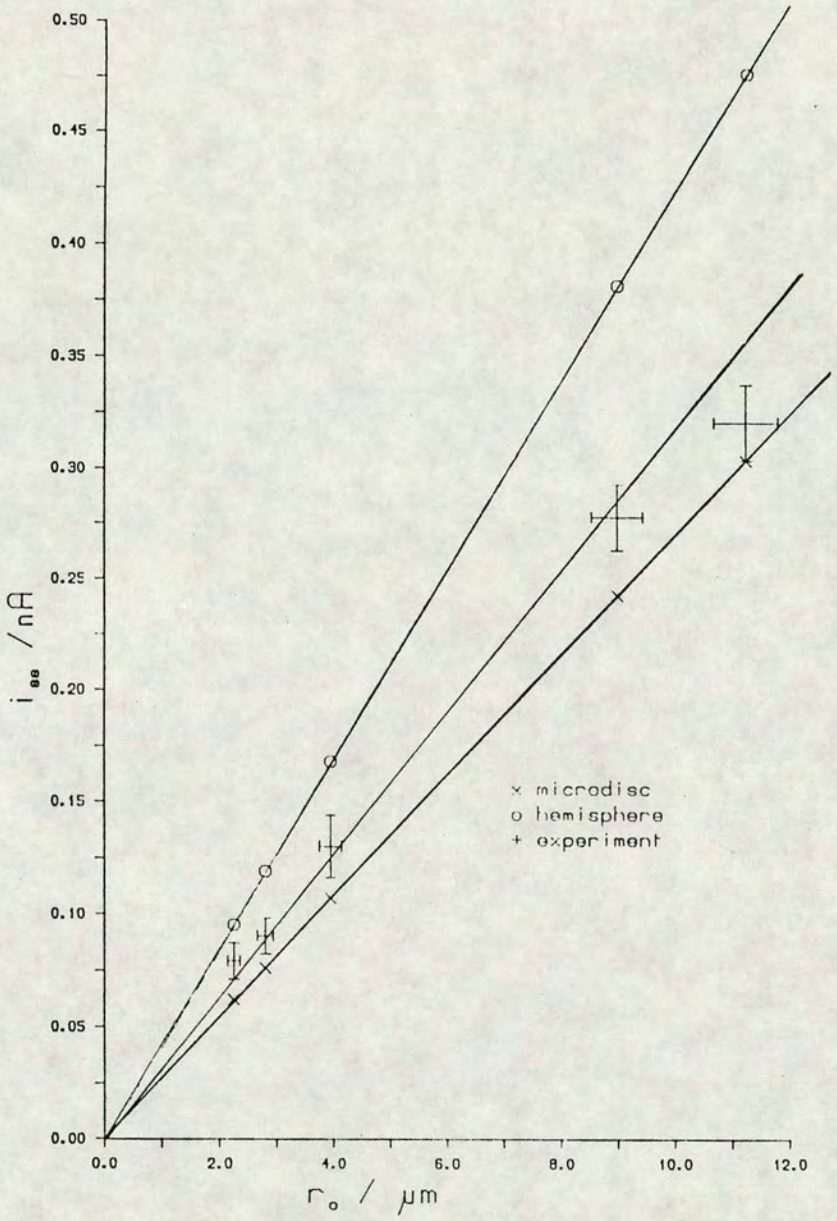

Figure 3.3.4 Dependence of i_{ss} on the radius of the pipette for ingress transfer. A comparison between the experimental data (+), with that expected for a hemisphere (o) and a microdisc (x). The cell used was the same as that described in figure 3.3.1 with a TEA^+ concentration of 100µM.

are difficult to overcome, even when using micrometer controlled syringes to adjust the position of the interface. On the other hand the current being larger than that predicted for a disc in a semi infinite insulating plane could also be explained by the finite wall thickness of the pipette enhancing the microdisc edge effects. This phenomenon has already been observed [61] for the case of insulated carbon microdisc electrodes where the insulating layer thickness was of the same dimensions as the carbon fibre.

The concentration dependence of the plateau current for a given pipette is found to be linear within experimental error as seen in figure 3.3.5. The experimental error stems from differences in the interface curvature caused by changing the solutions.

These results for ingress transfer at a pipette illustrate that the diffusion for this transfer displays the same characteristics as are found for the diffusion to a microdisc electrode. As described by Oldham and Zoski [62], microdisc and microsphere interfaces are equivalent in the steady state mode. We can therefore conclude that liquid microITIES supported at a micro pipette tip behave like a microelectrode with a response falling between that of a microdisc and that of a microhemisphere i.e.

$$4nFDc^{*}r > i > 2\pi nFDc^{*}r.$$

3.3.1.2 Linear Sweep For Egress Transfer

The transfer of ions from inside the pipette is controlled by linear diffusion giving rise to a peak shaped linear sweep voltammogram, as seen in figure 3.3.6.

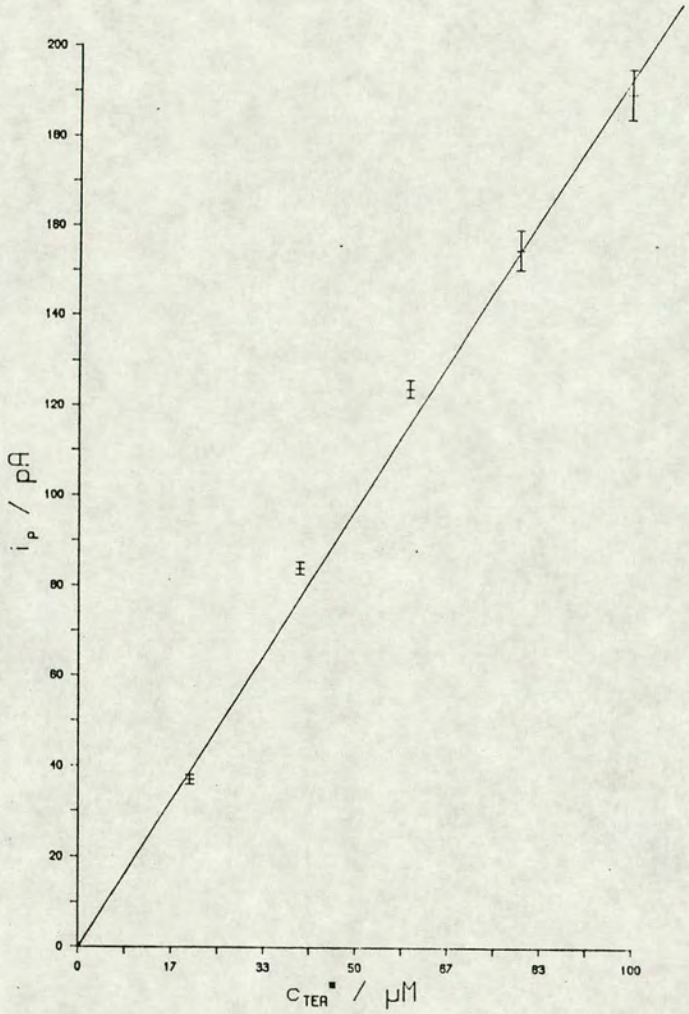

Figure 3.3.5 Concentration dependence of plateau current, i_{ss}, for TEA^+ ingress transfer, for the cell shown in figure 3.3.1 over the concentration range 10–100µM.

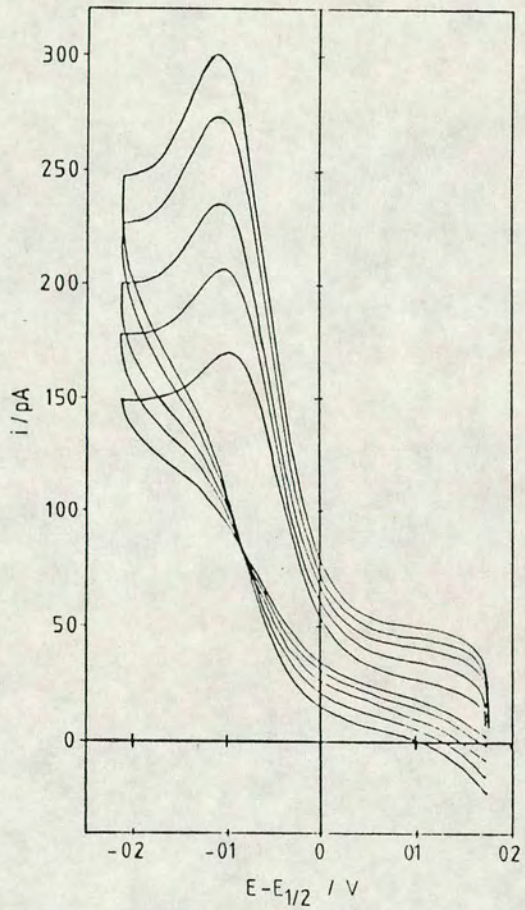

Figure 3.3.6 Cyclic voltammograms, showing sweep rate dependence, for egress transfer of TEA^+. Sweep rates 0.02, 0.04, 0.06, 0.08, 0.10 Vs^{-1}. The cell used was Ag/AgCl/TPBNa(1mM),NaCl(10mM)/CVTPB(1mM)//TEACl,(15µm)LiCl(1mM)/AgCl/Ag.

The sweep rate dependence (fig. 3.3.7) shows that the peak current is proportional to the square root of sweep rate as in classical linear sweep voltammetry i.e. it obeys a Randles-Sevcik type relationship,

$$i_p = 2.69 \times 10^5 n^{3/2} c_\alpha^* D^{1/2} \nu^{1/2} \quad (D)$$

The difference between the results obtained at the micropipette and those obtained at a large flat interface is approximately 1%, when comparing slopes, and can be entirely attributed to an error arising from the scatter of the points in each case. We can therefore conclude that egress motion obeys the equation obtained for semi-infinite linear diffusion.

3.3.1.3 Cyclic Voltammetry

Due to the asymmetry of the diffusion field cyclic voltammetry is not a useful technique for the study of ion transfer at a liquid/liquid interface supported at the tip of a micropipette. As shown in figure 3.3.1 the reverse scan of a steady state wave is not a wave itself, as found at a microdisc electrode, but a peak shaped voltammogram. The sweep rate dependence shows that the reverse peak of an ingress/egress transfer does not increase in the classical manner with the square root of the sweep rate. The reason for this is that fewer coulombs are passed on the forward sweep as the sweep rate increases, thus limiting the size of the return peak. Conventional cyclic voltammetry at a planar electrode is a useful tool for the determination of the reversibility of the system. Experimental evidence of reversibility criteria were difficult to assess in the present study due to the inherent presence of iR drop.

Alternatively the return scan of an egress/ingress transfer, see figure 3.3.6, cannot be clearly observed as the mass transfer for ingress motion is much faster than that for egress. Any quantivative analysis of the experimental data

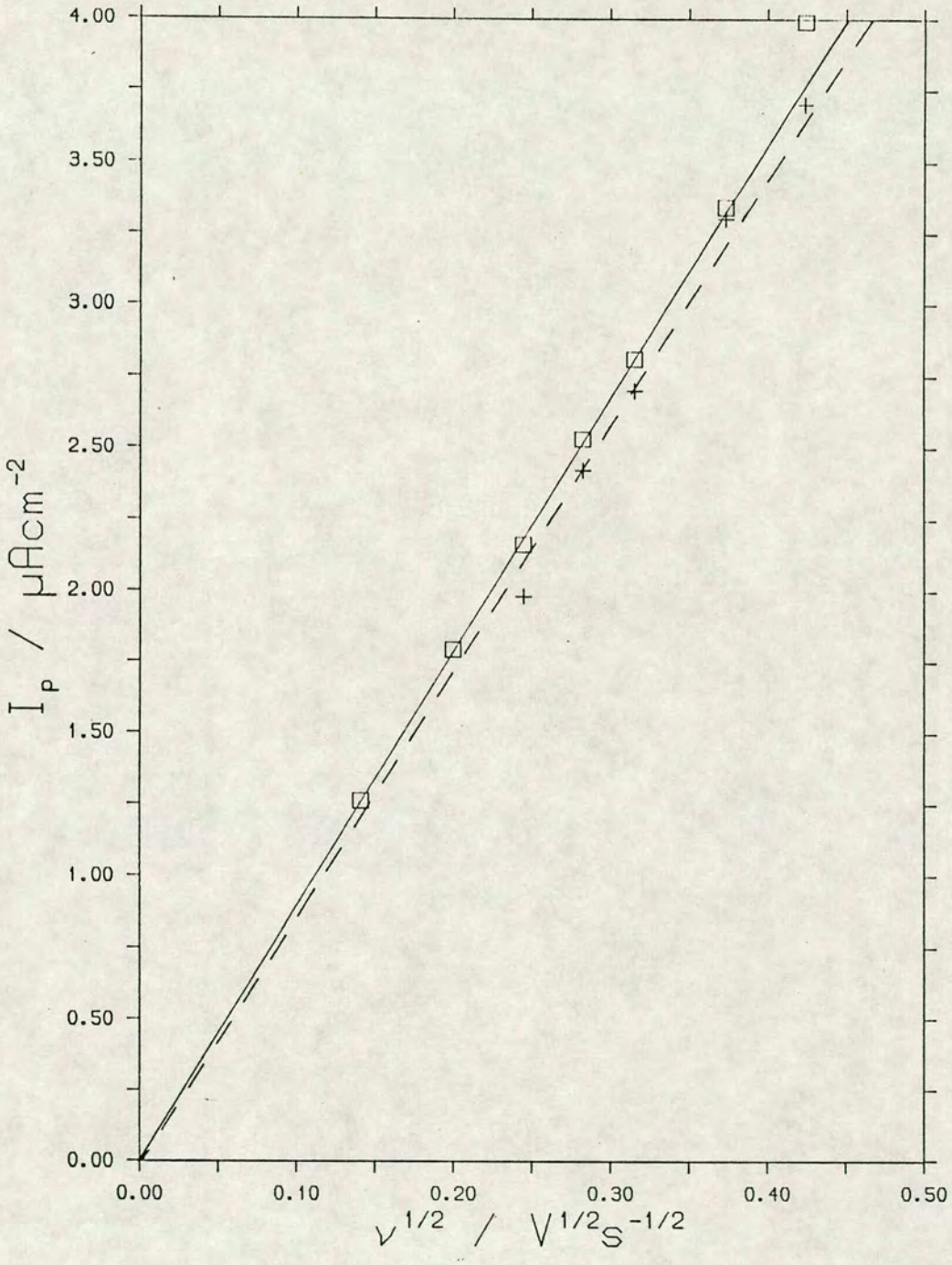

Figure 3.3.7 Plot of I_p *vs.* $\nu^{1/2}$ for the voltammograms shown in figure 4 (microITIES$_{(\square)}$ and those for a macroITIES$_{(+)}$ experiment for the same cell. Slopes are 8.5×10^{-6} and 8.0×10^{-6} $C^{3/2}cm^3s^{-1/2}J^{-1/2}$ for the micro and macro ITIES respectively.

is also difficult because of the variation of the capacitive current with sweep rate.

The cyclic voltammetric technique for ingress/egress transfer which may find analytical application is asymmetric sweep rate cyclic voltammetry. In this case the forward sweep is carried out at a constant sweep rate, and the reverse sweep rate is varied. It is then observed that the reverse scan obeys the classical dependence on the square root of sweep rate sweep rate (see figure 3.3.8). It should be pointed out that the height of the reverse peak is dependent on the limit of the forward sweep as it is a constant plateau current.

Any quantification of the size of the reverse peak is complicated as it depends on the radius of the pipette, the limit of the forward scan and the sweep rate of both the forward and return scans.

3.3.2 Pseudo Analytical Solution

An approximate solution for cyclic voltammetry of ion transfer at a micropipette has been evaluated. The solution involves approximating the diffusion of the ions for ingress transfer to that for a hemispherical interface, and for egress transfer planar diffusion. The assumption that the diffusion to a microdisc electrode can be approximated to that for a microhemispherical electrode was made by Oldham and Zoski [62] for electrodes of equivalent size, i.e. a microdisc electrode of radius r_d is equivalent to a micro hemispherical electrode of radius $(\pi/2)r_d$, and they showed that the two systems gave almost identical steady state voltammetric responses. The micropipette is therefore modelled as shown in figure 3.3.9 where the boundary conditions are the equality of the flux across the hemisphere and the disc, and the Nernst equation for the surface concentration on the hemisphere and the disc respectively. It should be stressed that this model is a mathematical

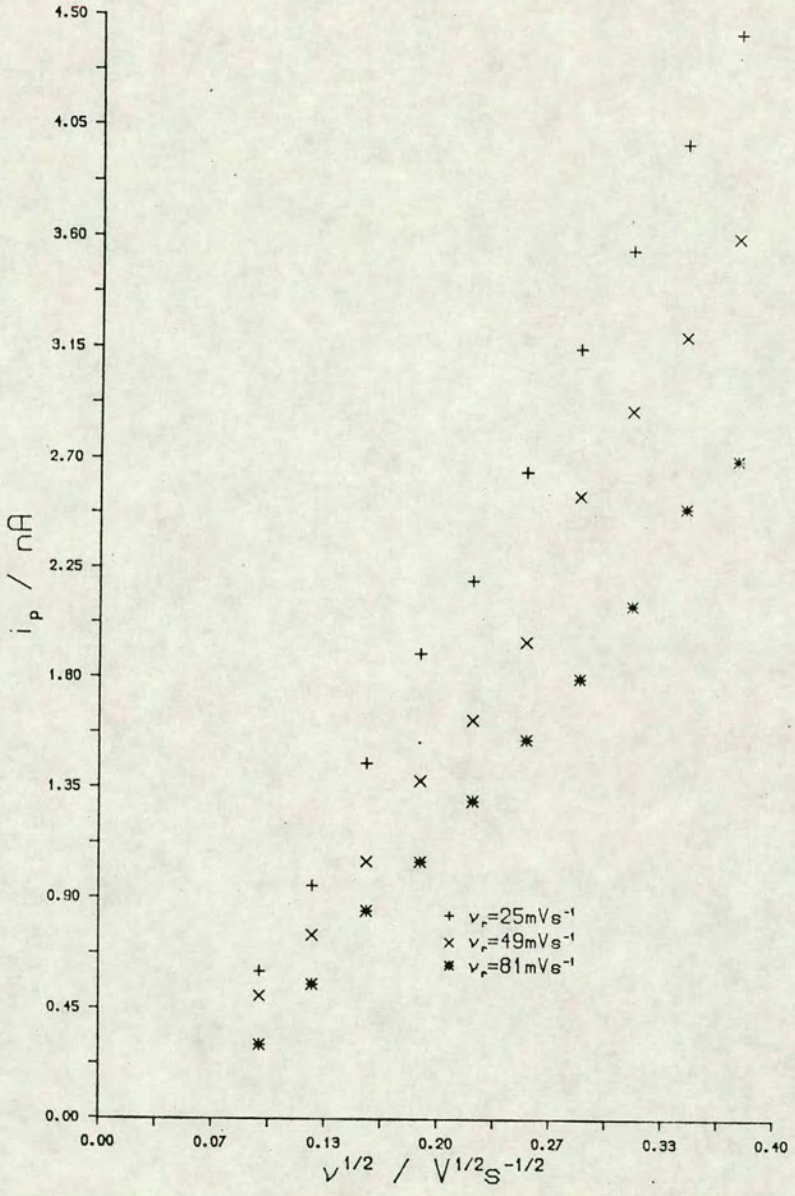

Figure 3.3.8 Plot of i_p *vs.* $\nu_r^{1/2}$ for an asymmetric sweep experiment with three different forward sweeps. (+) 25mVs^{-1}, (x) 49mVs^{-1}, (*) 81mVs^{-1}. Pipette radius 9µm. Cell:-

Ag/AgCl/TPBNa(10mM),NaCl(0.1M)/BTPPATPB(10mM),TEATPB(1mM)//LiCl(10mM)/AgCl/Ag.

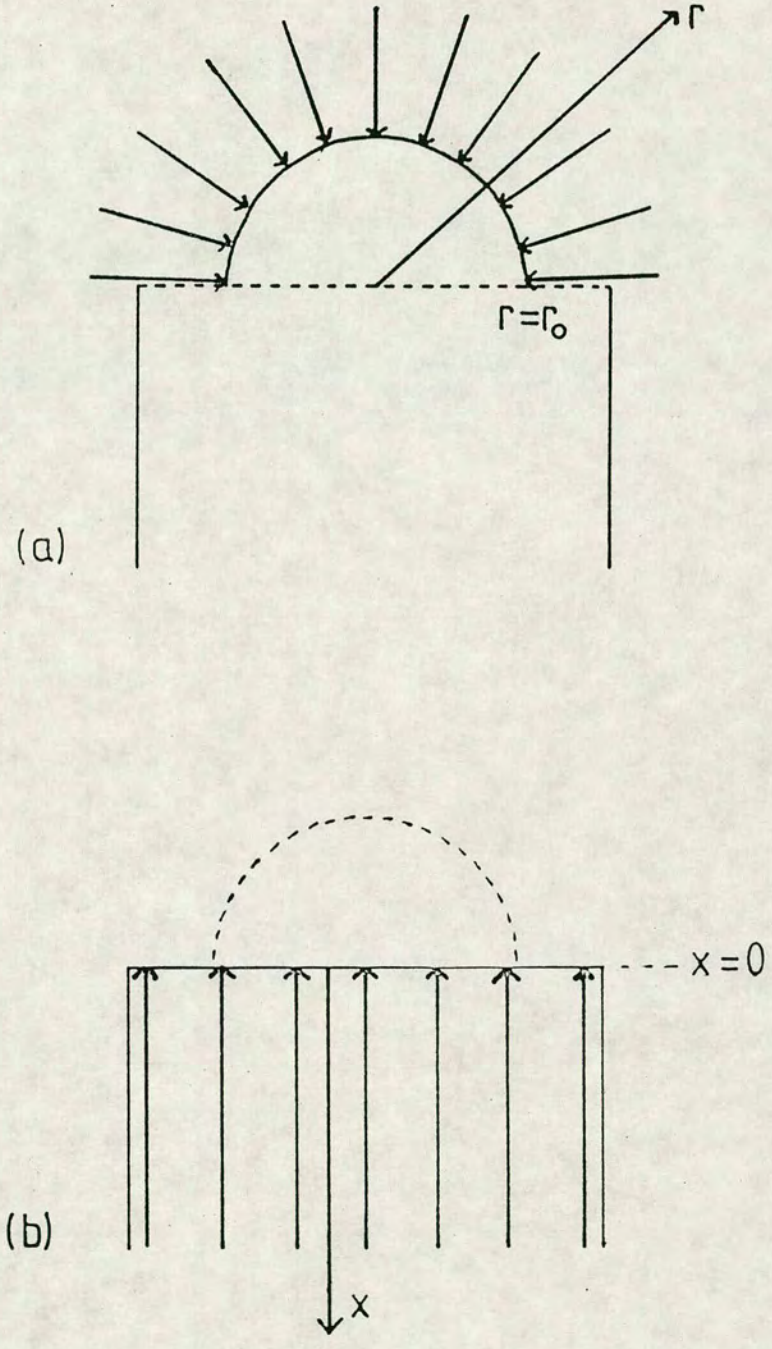

Figure 3.3.9 Schematic diagram showing the model used for the pseudo analytical solution. (a) spherical diffusion to a hemisphere for ingress transfer and (b) linear diffusion to a plane for egress transfer.

simplification of the true diffusion equations and is not an exact analytical solution.

This problem was approached using a combination of the solutions which are presented in 3.1.1 and 3.2.1 for linear and spherical diffusion respectively, and many of the methods used in these case be utilised in this case. For this case the boundary conditions are given by

$$[\partial c_\alpha(r,t)/\partial t] = D_\alpha[(\partial^2 c_\alpha(r,t)/\partial r^2) + (2/r)(\partial c_\alpha(r,t)/\partial r)] \qquad (3.3.1)$$

$$[\partial c_\beta(x,t)/\partial t] = D_\beta[\partial^2 c_\beta(x,t)/\partial x^2] \qquad (3.3.2)$$

$$t = 0,\ r \geq r_o : c_\alpha = c_\alpha^*$$
$$x = 0 : c_\beta = c_\beta^* \ (\approx 0) \qquad (3.3.3)$$

$$t \geq 0,\ r \to \infty : c_\alpha \to c_\alpha^*$$
$$x \to \infty : c_\beta \to 0 \qquad (3.3.4)$$

$$t > 0,\ r = r_o,\ x=0 : A_{hs}D_\alpha[\partial c_\alpha(r,t)/\partial r]_{r=r_o} + A_d D_\beta[\partial c_\beta(x,t)/\partial x]_{x=0} \qquad (3.3.5)$$

$$c_\alpha(r_o,t)/c_\beta(0,t) = \exp[(nF/RT)(E-E^\circ)] \qquad (3.3.6)$$

Equation (3.3.5) arises from the equality of the fluxes. Again for cyclic voltammetry the potential-time function is given by eqns. (3.1.7) and (3.1.8), and if the same simplifications are made as in 3.1.1 the following relationship results

$$c_\alpha(r_o,t)/c_\beta(0,t) = \theta S_\lambda(t) \qquad (3.3.7)$$

It is then possible to evaluate an expression for $c_\alpha(r=r_0,t)$ using the procedure described in 3.2.1 to give

$$c_\alpha(r_o,t) = c_\alpha^* - 1/(nFA_{hs}D_\alpha^{1/2}) \int_0^t i(\tau)\left[1/(\pi(t-\tau))^{1/2} - a\exp(a^2(t-\tau))\operatorname{erfc}(a(t-\tau)^{1/2})\right] d\tau \qquad (3.3.8)$$

and to evaluate $c_\beta(o,t)$ by the procedure described in 3.1.1 resulting in

$$c_\beta(0,t) = 1/(nFA_dD_\beta^{1/2})\int_0^t i(\tau)/(\pi(t-\tau))^{1/2}\, d\tau \qquad (3.3.9)$$

a being given as $\sqrt{D}/r_o$ for $D_a=D_b=D$. Equations (3.3.8) and (3.3.9) can then be substituted into eqn.(3.3.7) resulting in

$$c_\alpha^* - 1/(nFA_{hs}D_\alpha^{1/2})\int_0^t i(\tau)\left[1/(\pi(t-\tau))^{1/2} - a\exp[a^2(t-\tau)]\right.$$
$$\left.\operatorname{erfc}[a(t-\tau)^{1/2}]\right] d\tau = \theta S_\lambda(t)/(nFA_dD_\beta^{1/2}) \int_0^t i(\tau)/(\pi(t-\tau))^{1/2}\, d\tau \qquad (3.3.10)$$

In eqn. (3.3.10) we see that the areas of both the hemisphere, A_{hs}, and the disc, A_d are required to be known, but since we know the relationship between the radii of both it is possible to express the area of the hemisphere in terms of the area of the disc, i.e. $A_{hs}=(8/\pi^2)A_d$. Thus introducing $A_d=A$ and $f(\tau)=i(\tau)/nFA$ eqn. (3.3.10) then becomes

$$1 - \pi^2/(8c_\alpha^*D^{1/2}) \int_0^t f(\tau)/(\pi(t-\tau))^{1/2}\, d\tau$$
$$+ \pi^2/(8c_\alpha^*D^{1/2}) \int_0^t f(\tau)a\exp[a^2(t-\tau)]\operatorname{erfc}[a(t-\tau)^{1/2}]\, d\tau$$
$$= \theta S_\lambda(t)/c_\alpha^*\sqrt{D} \int_0^t f(\tau)/(\pi(t-\tau))^{1/2}\, d\tau \qquad (3.3.11)$$

As in section 3.1.1 in order to evaluate the current-potential relationships instead of current-time relationships a change of variable must be carried out, i.e. the calculations must be made with respect to σt. The integral can then be

made dimensionless in order to be solved numerically by the following substitution

$$\psi(\sigma t) = g(\sigma t)/(\sigma D)^{1/2} c_\alpha^* \qquad (3.3.12)$$

thus eqn. (3.3.11) becomes

$$1 - \pi^2/8 \int_0^{\sigma t} \psi(z)/(\sigma t - z)^{1/2}\, dz + \pi^2/8 \int_0^{\sigma t} \psi(z)\varphi \exp[\varphi^2(\sigma t - z)]$$
$$\operatorname{erfc}[\varphi(\sigma t - z)^{1/2}]\, dz = \theta S_{\sigma\lambda}(\sigma t)/\pi^{1/2} \int_0^{\sigma t} \psi(z)/(\sigma t - z)^{1/2}\, dz \qquad (3.3.13)$$

with $\phi = a/\sqrt{\sigma}$. This expression can then be solved for the dimensionless current, $\psi(z)$, numerically using the methods used in 3.1 and 3.2 , by replacing the integrals by their finite sums. This results in

$$1 - \delta\varphi\pi^2/8 \left[\sum_{i=1}^{n-1} \psi(i) \exp[\alpha^2(n-i)] \operatorname{erfc}[\alpha(n-i)] \right] =$$
$$2(\delta/\pi)^{1/2} \left[\psi(1) n^{1/2} + \sum_{i=1}^{n-1} (n-i)^{1/2} [\psi(i+1) - \psi(i)] \right] [\theta S_{\sigma\lambda}(\sigma n) + (\pi^2/8)] \qquad (3.3.14)$$

this can be evaluated computationally, and the current is given by the expression

$$i(\sigma t) = nFAc_\alpha^* (D\sigma)^{1/2} \psi(\sigma t) \qquad (3.3.15)$$

The results produced from this solution have been compared to both the experimental results and, for the forward scan i.e. ingress transfer, to the results produced by the solution of Reinmuth's equation based on a spherical electrode [54] of radius $2r_d/\pi$. As well as comparing this solution to these two sets of results the "steady-state" current was compared to the steady state current predicted by eqn.(C) for a microdisc i.e. the results evaluated computationally are in the form i/nFc_α^* thus the comparative steady-state current is given by $4Dr_d$. The program used to carry out this evaluation is shown in Appendix A.5.

Figure 3.3.10 shows a set of voltammograms, giving a variation of sweep rate, for a 20μm (r_d) electrode for the pseudo-analytical solution. It can be seen that this solution neither gives a true steady state current nor is the ingress transfer independent of sweep rate. Comparing this set of voltammograms with experimental results it would be expected that the steady state current be independent of sweep rate, allowing for the effects of capacitance. However from these experimental results it is not clear whether or not a true steady state current is reached and thus indicating that the pseudo analytical solution may be correct in this case. Also comparing figure 3.3.10 with 3.3.11, the results for Reinmuth's solution, we see a similar relationship with sweep rate. For electrode sizes greater than 20μm (r_d) and sweep rates greater than $0.02Vs^{-1}$ the pseudo analytical results are in agreement to within 5% of Reinmuth's results when comparing the "peak" current values. A better representation of this can be seen in figure 3.3.12. This figure also shows that the wave obtained for a pipette is moved to more negative potentials relative to E^o. It should be noted that cyclic voltammetry at a small hemisphere electrode calculated by Reinmuth's algorithm only produces true steady state at infinitely small sweep rates, as the linear component of the equation only

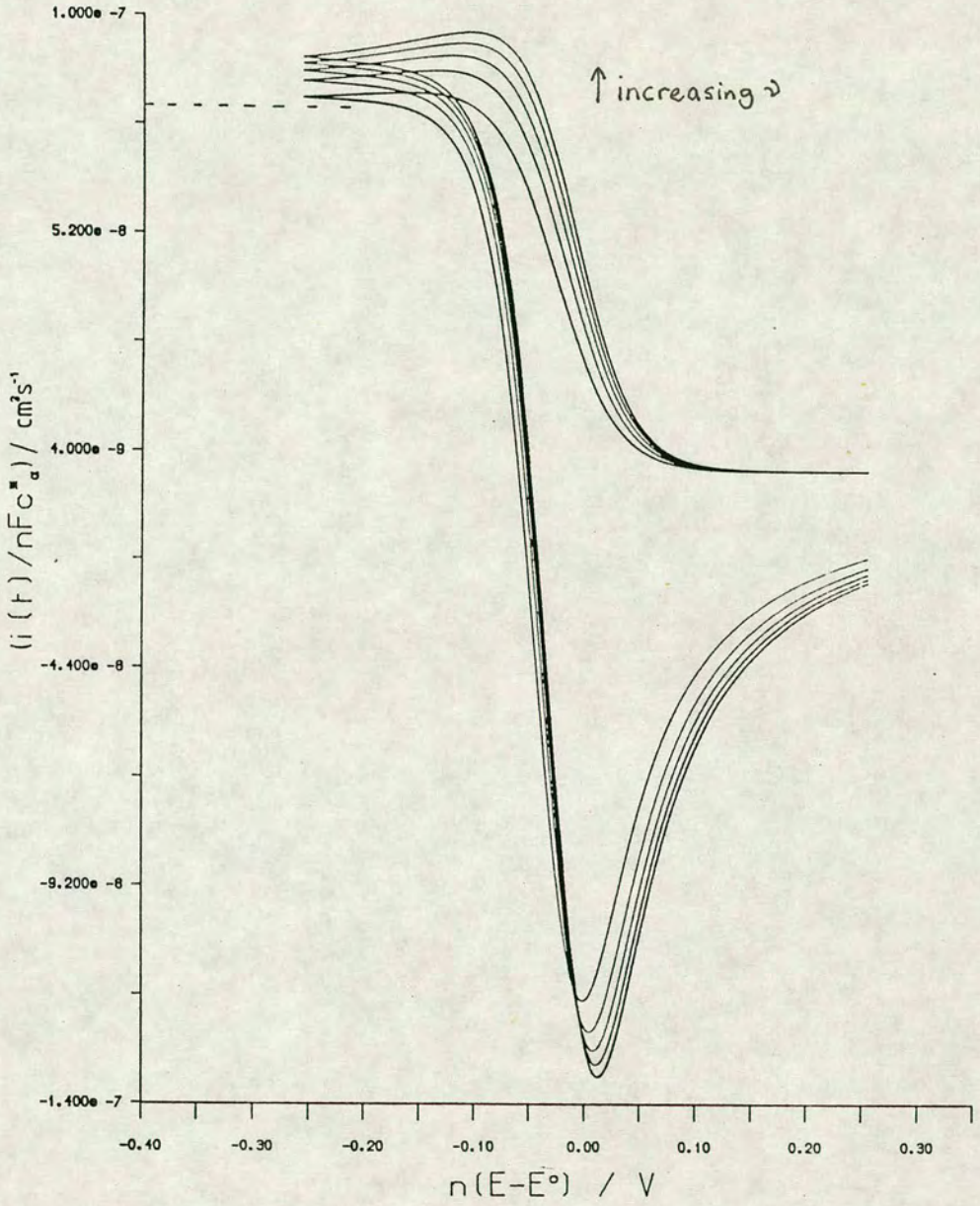

Figure 3.3.10 Cyclic voltammograms produced by the pseudo analtyical solution showing a sweep rate dependence. Input parameters $\ln\theta=10.0$, $D=1\times10^{-5}cm^2s^{-1}$, $r_d=20\mu m$ and $\nu=0.02,0.04,0.06,0.08,\ 0.10Vs^{-1}$.

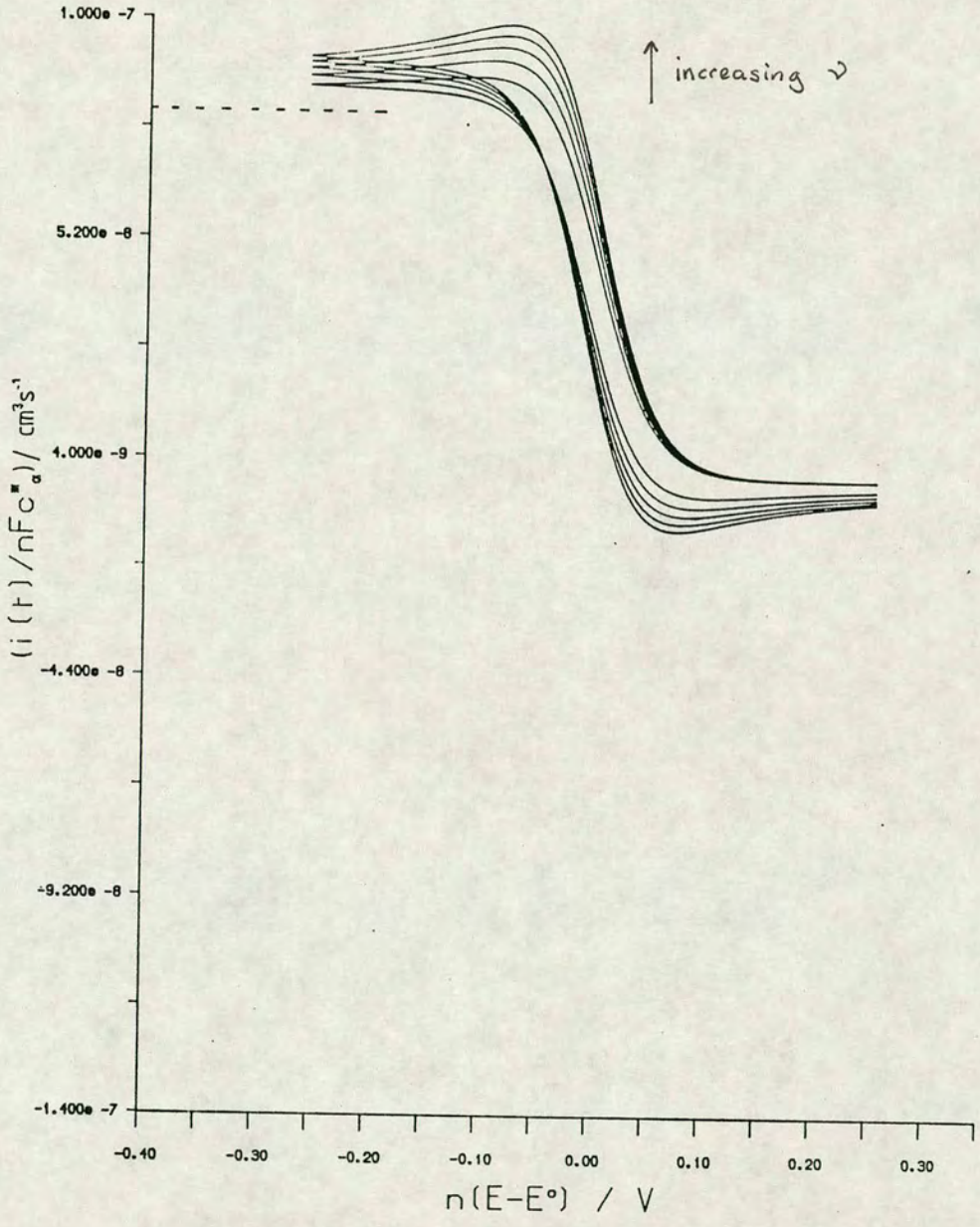

Figure 3.3.11 Cyclic voltammograms produced by Reinmuth's solution for a spherical electrode, showing a sweep rate dependence for the same input parameters as in figure 3.3.10. The line (-----) shows the expected steady state current for a micro disc electrode.

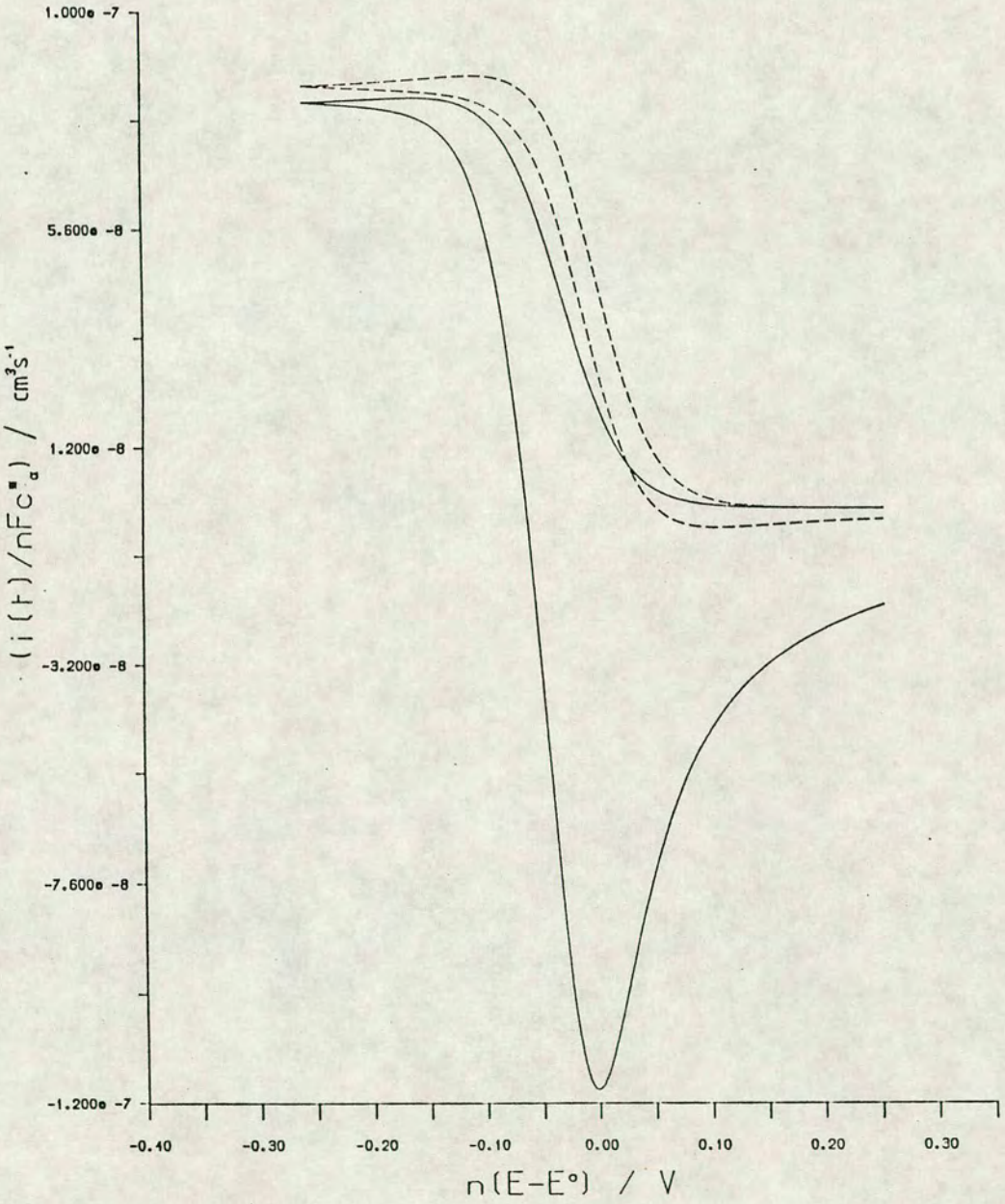

Figure 3.3.12 Cyclic voltammograms comparing the pseudo analytical solution (——) and that for Reinmuth's solution for a sphere (----). $\ln\theta=10.0$, $D=1\times10^{-5}cm^2s^{-1}$, $r_d=20\mu m$ and $\nu=0.02Vs^{-1}$.

becomes negligible in these conditions, as seen in figure 3.3.11.

The shape of the wave obtained by the pseudo analytical solution for the pipette and the Reinmuth algorithm have been analysed by plotting $\ln((i_d - i)/i)$ *vs* potential as shown in figure 3.3.13. The discrepancy for the half wave potential as calculated by the Reinmuth algorithm is due to the residual linear diffusion component. The shift obtained for the pseudo analytical case appears to be inherent to the mathematical analysis. The former has a slope of $60.6 mV decade^{-1}$ for the linear part of the diagram and the latter is $61.3 mV decade^{-1}$.

The radius dependence of the plateau current obtained by the pseudo analytical solution was investigated by plotting the last point of the forward scan, which is only approximately the true steady state value, *versus* the radius. The data obtained illustrated in figure 3.3.14 show that a micropipette behaves in a similar fashion to a microhemisphere.

The linear concentration dependence of the current at a micropipette is implicit from eqn. (3.3.15).

The extension of the above pseudo analtyical solution to a case where we have egress transfer on the forward scan is straight forward and will not be explicitly derived here. Cyclic voltammograms for such a derivation is shown in figure 3.3.15 and the resulting dependence of the peak current on square root of sweep rate is shown in figure 3.3.16. These results compare well with those found experimentally. It should be noted that when comparing the results with the classical Randles-Sevcik equation the pseudo analytical solution gives a slope, $i/nFc^*_\alpha \nu^{1/2}$, which is within 3% of that predicted.

For the reasons outlined in section 3 the return peak in the cyclic

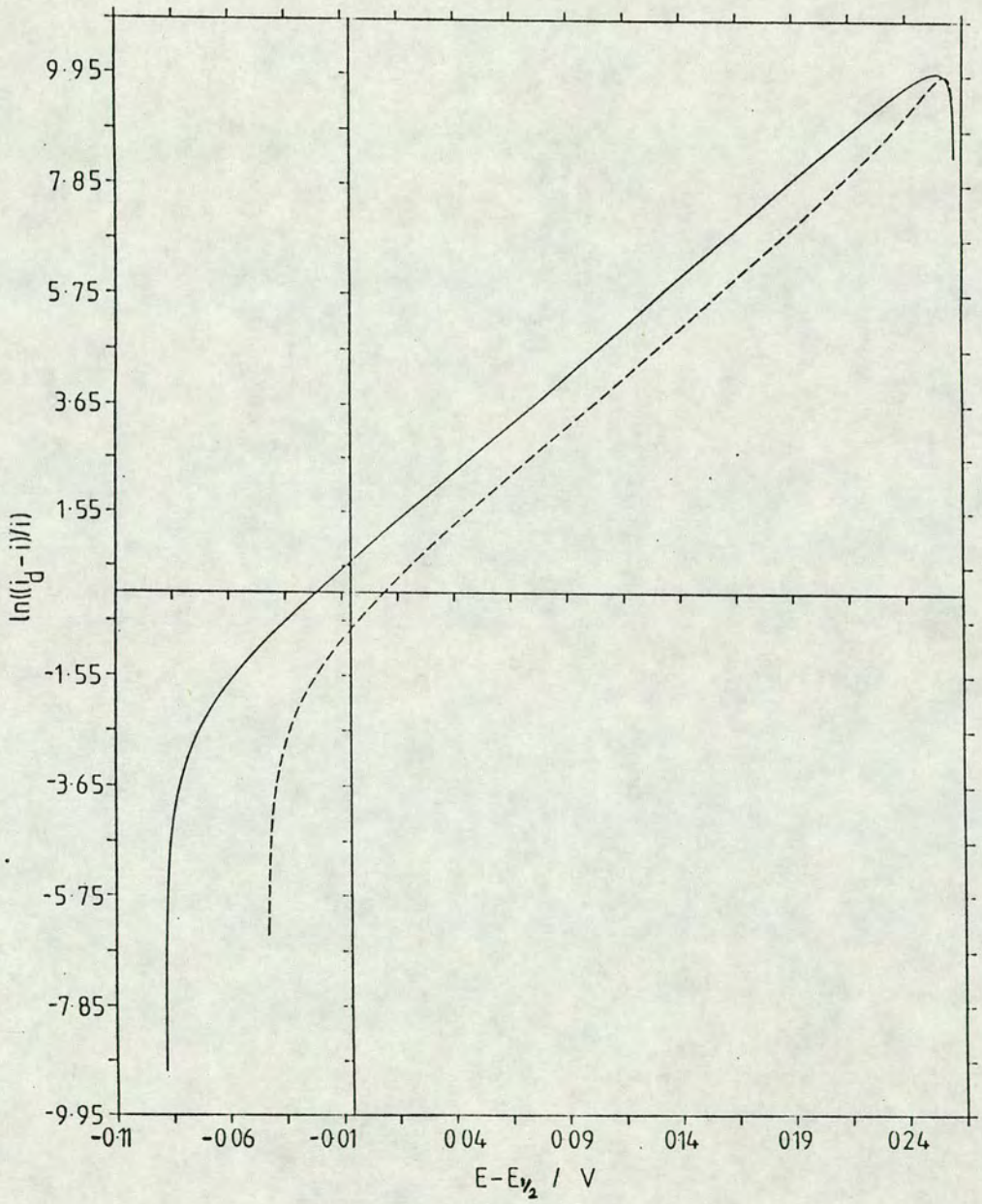

Figure 3.3.13 Plot of $\ln((i_d-i)/i)$ *vs.* $(E-E_{1/2})$ for analysis of "steady state" waves produced by the pseudo analytical solution for a pipette (——) and Reinmuth's solution for a spherical electrode (----). The waves analysed were for conditions the same as those for figure 3.3.2.

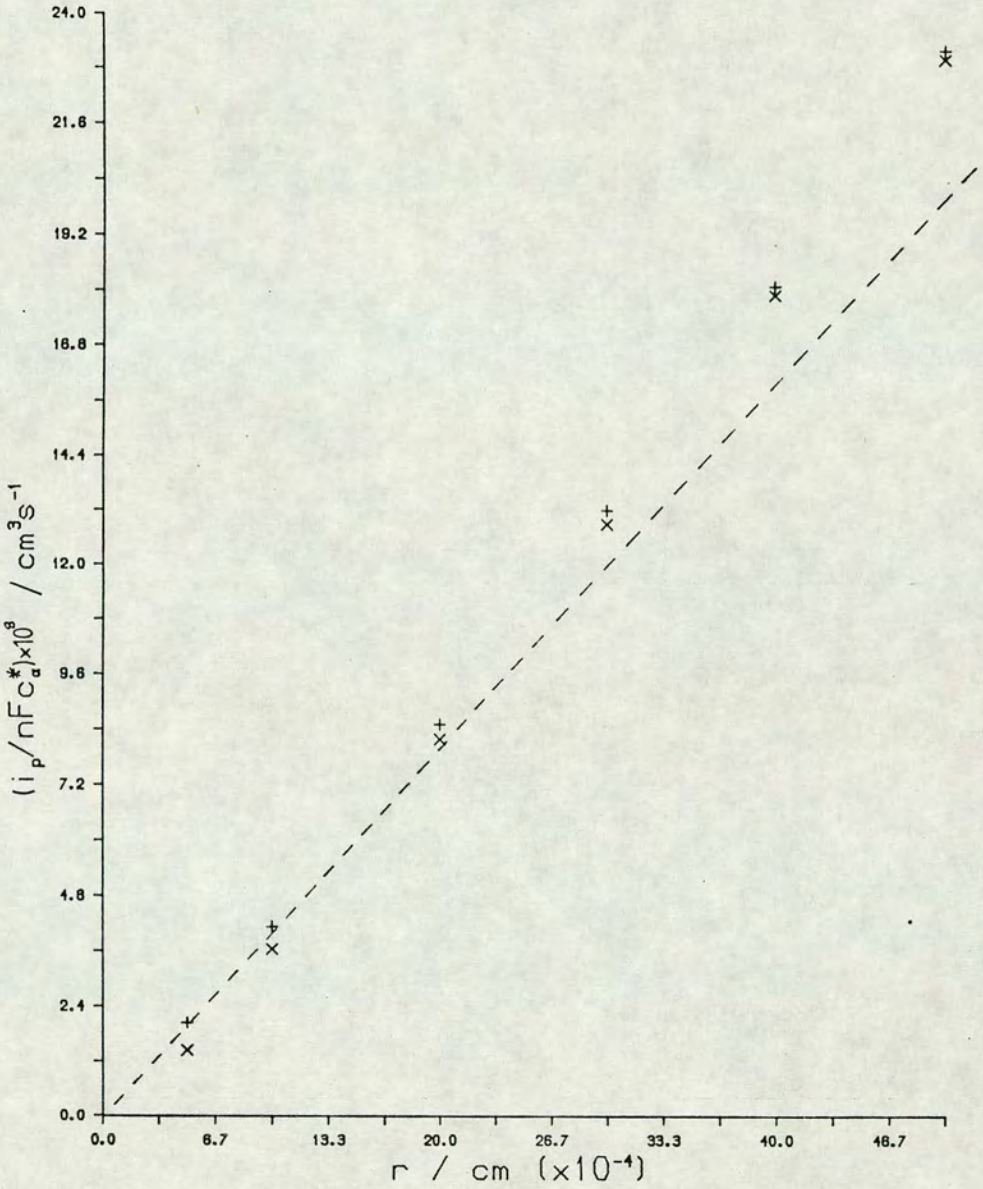

Figure 3.3.14 Plot of i_p/nFc_α^* *vs.* r_d for the pseudo analytical solution (x) and Reinmuth's solution for a spherical electrode (+). Also shown is the steady state current *vs.* radius relationship for a microdisc electrode (-----).

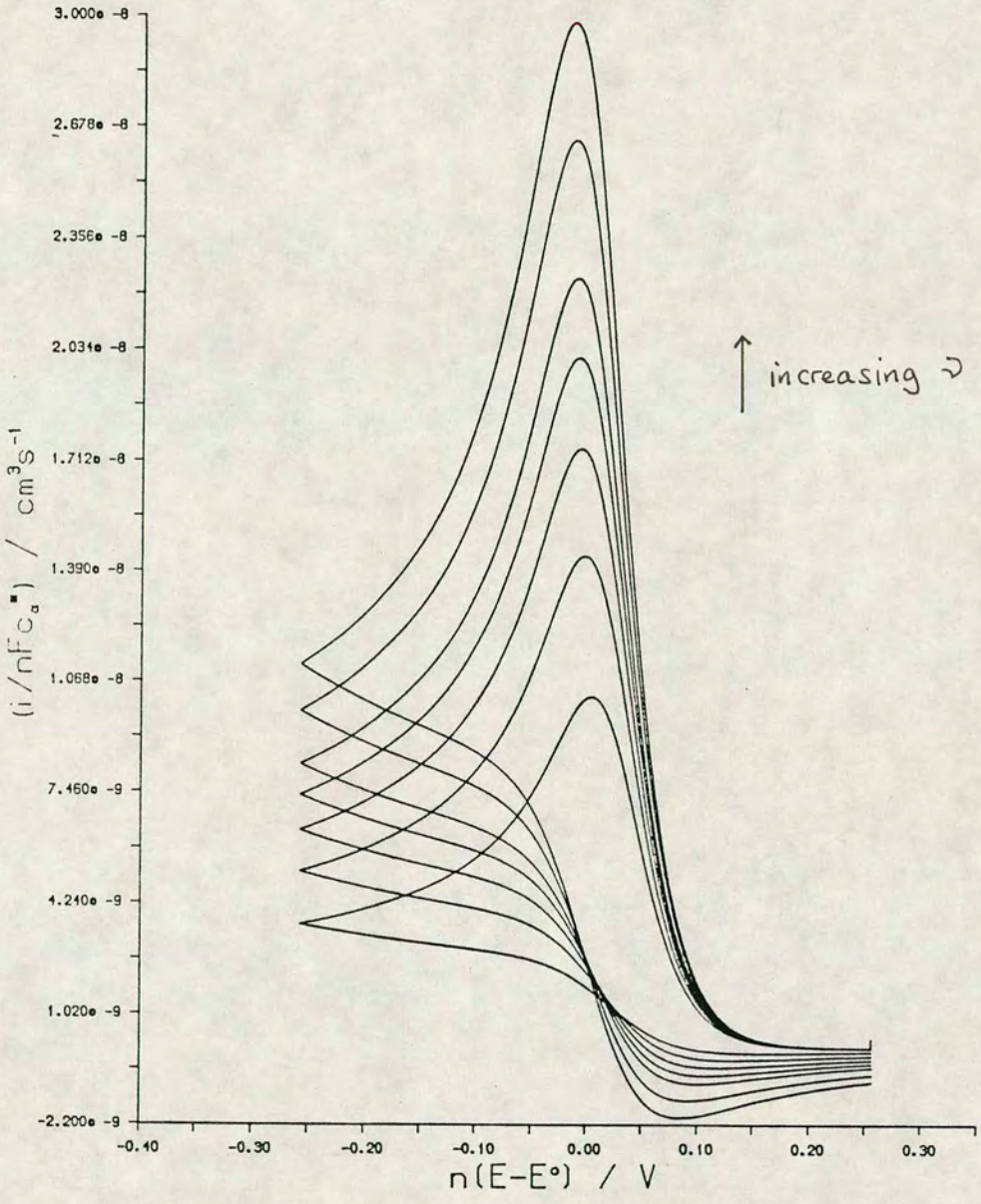

Figure 3.3.15 Cyclic voltammograms for egress transfer, for the pseudo analytical solution, showing a sweep rate dependence. $\ln\theta=10.0$, $D=7\times10^{-6}cm^{2-1}$, $r_d=17\mu m$ and sweep rates of 0.02, 0.04, 0.06, 0.08, 0.10, 0.14, $0.18Vs^{-1}$. (i.e. the same conditions as used in the experiment for egress transfer.)

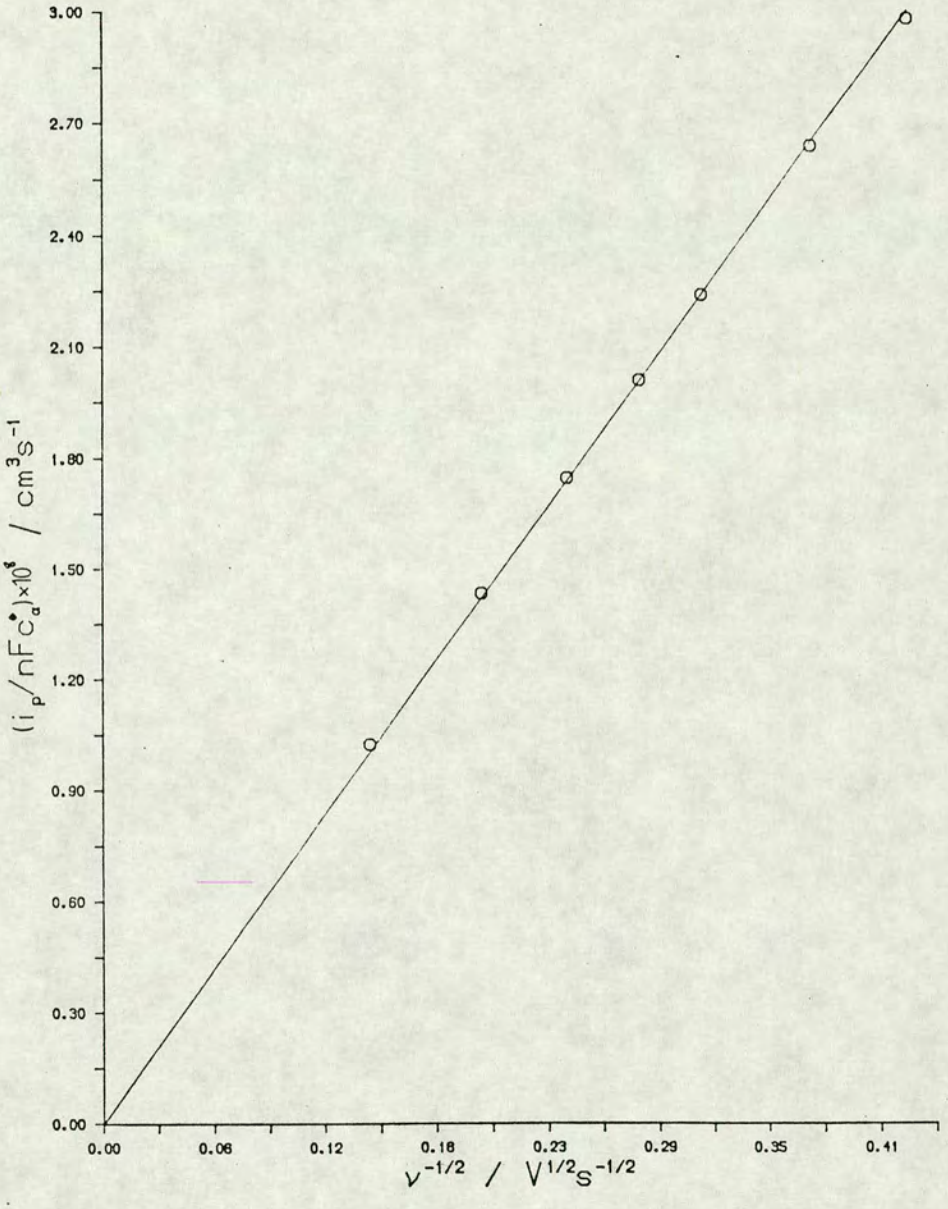

Figure 3.3.16 Plot of i_p/nFc^*_α *vs.* $\nu^{1/2}$ for the cyclic voltammograms shown in figure 3.3.15.

voltammogram for ingress/egress transfer does not increase proportionately with sweep rate, but increases to a constant value. This relationship is also seen for this solution as is shown in figure 3.3.10, thus confirming that analysis of the return peak in cyclic voltammetry at a micropipette is not a suitable analytical tool.

The final comparison between the pseudo analytical solution and the experimental results is for asymmetric sweep cyclic voltammetry, however in order to make this comparison the potential function for the solution must be redefined and also the function $S_l(t)$ i.e.

$$E = E_i - \nu_1 t \qquad : 0 < t \leq \lambda \qquad (3.3.16)$$

$$E = E_i - \nu_1 \lambda + (t-\lambda)\nu_2 \qquad : t \geq \lambda \qquad (3.3.17)$$

$$S_\lambda(t) = \begin{cases} \exp[-\sigma_1 t] & : 0 < t \leq \lambda \\ \exp[-\sigma_1 \lambda + \sigma_2(t-\lambda)] & : t \geq \lambda \end{cases} \qquad (3.3.18)$$

A resulting cyclic voltammogram for this solution, using the same parameters as used experimentally for fig.3.3.8, is given in figure 3.3.17 and the sweep rate dependence is shown for the same conditions is shown in figure 3.3.18. This shows that there is a linear relationship between $i_{p,r}$ and $\nu_r^{1/2}$ for $\nu_r > \nu_f$ and for $\nu_r < \nu_f$ the $i_{p,r}$ limits to a value greater than zero. However again the experimental and the pseudo analytical solution agree to within 10% for this type of voltammetry and they both show similar trends.

3.3.3 Conclusions

It has been shown the way which an ITIES supported at the tip of a micropipette responds to different types of linear sweep voltammetry, and given an approximate analytical solution to this problem. The results of linear sweep voltammetry for ingress transfer have shown that the steady state

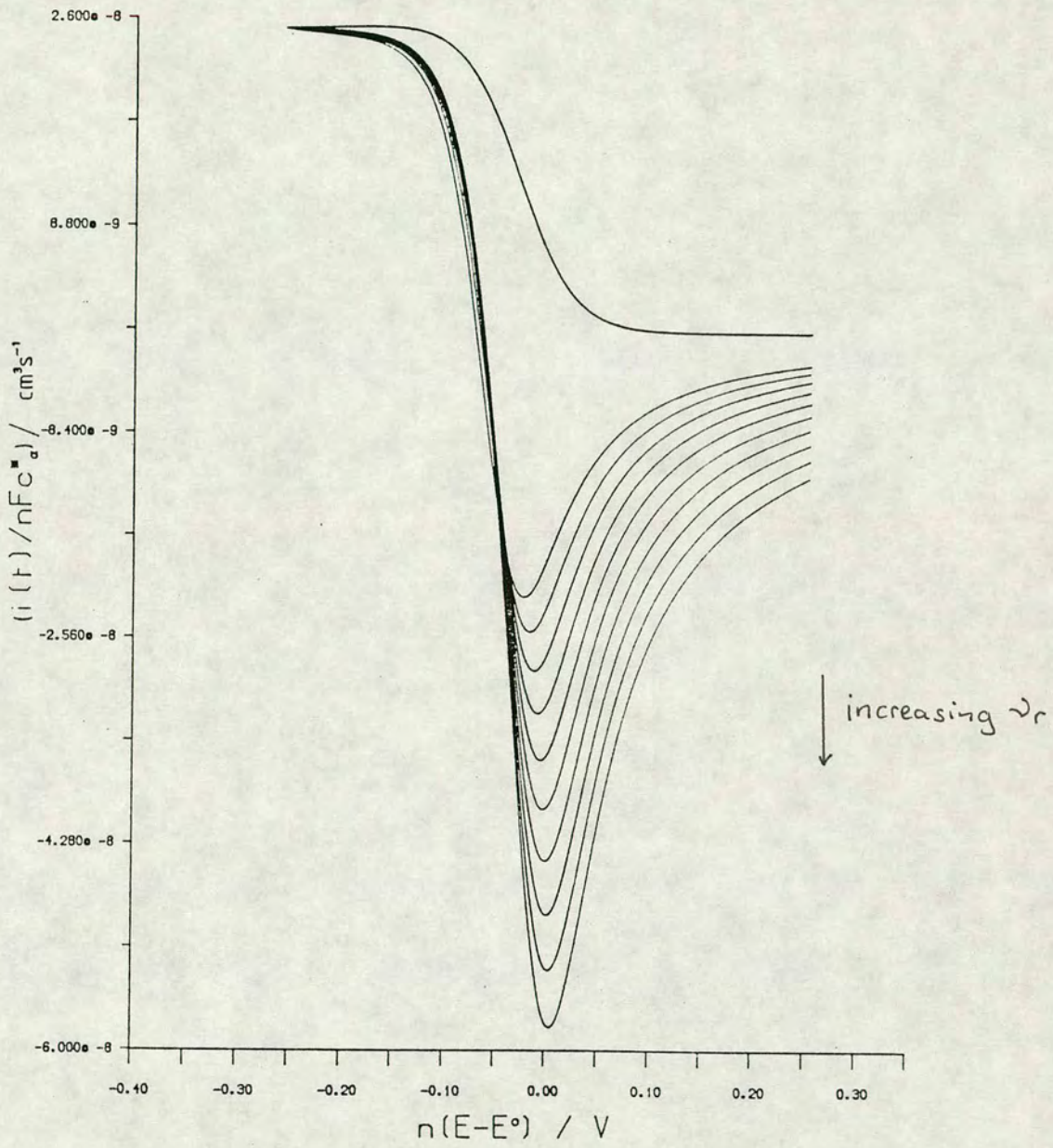

Figure 3.3.17 Asymmetric sweep voltammograms, from the pseudo analytical solution, for conditions the same as those shown in figure 3.3.8, i.e. $\ln\theta=10.0$, $D=7\times10^{-6}cm^2s^{-1}$, $r_d=9\mu m$, $\nu_f=0.049Vs^{-1}$, and $\nu_r=0.016,0.36,0.64,0.10,0.144\ Vs^{-1}$.

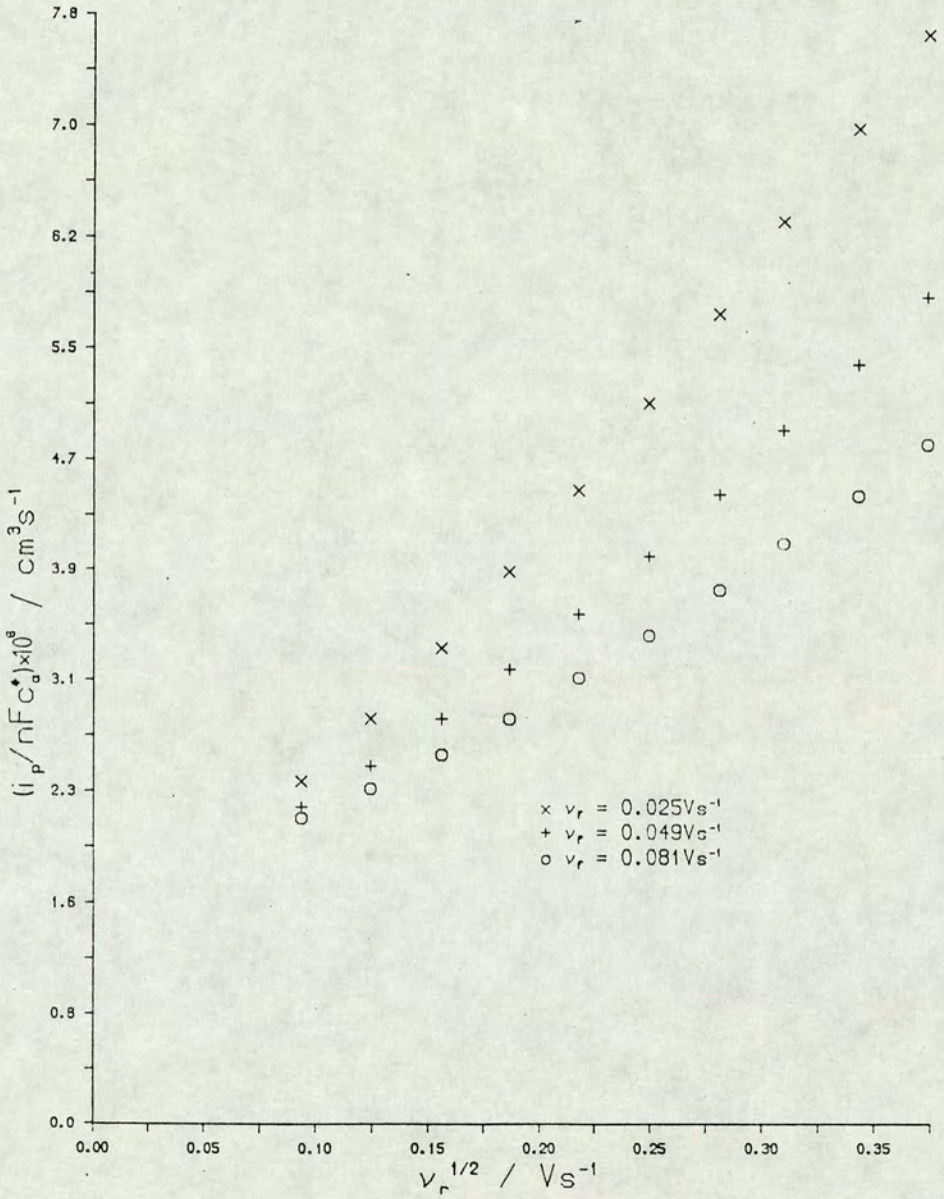

Figure 3.3.18 Plot of i_p/nFc_α^* *vs.* $\nu_r^{1/2}$ for asymmetric sweep voltammetry with ν_f=0.025,0.049, 0.081Vs^{-1}. The other input parameters are the same as in figure 3.3.17.

current response is very close to that found for a microdisc electrode and that the methodology developed to analyse steady state waveforms at microdisc electrodes for both kinetic and analytical information does apply. On the other hand the results for linear sweep egress transfer appear to obey the Randles-Sevcik relationship and can therefore find interesting applications for analysis of small volume samples.

Cyclic voltammetry is most useful for ingress/egress transfer when using an asymmetric waveform with a constant forward sweep rate. In this case the return peak is proportional to both the concentration and the square root of sweep rate.

The approximate pseudo analytical solution is relatively accurate, despite the nature of the approximation on which it is based (see figure 3.3.8). It is useful to predict the approximate relationships for cyclic voltammetry at a micropipette. However this analysis does not alleviate the need for an accurate simulation method to analyse the experimental results.

3.4 Cyclic Voltammetry For Electron Transfer At ITIES

3.4.1 Reversible Electron Transfer At A Planar ITIES

The interface between two immiscible electrolyte solutions (ITIES) has proven to be a suitable interface at which to study heterogeneous electron transfer, as discussed in chapter 2, the general scheme for which is outlined in fig. 3.4.1.

When the concentration of the reactants in the two adjacent phases is of the same magnitude, diffusion of both reactants to the interface should be

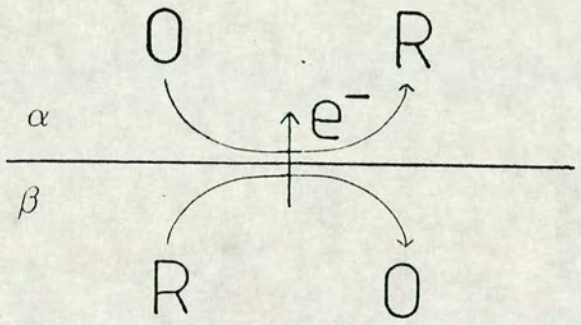

Figure 3.4.1 Schematic diagram showing an electron transfer reaction across an ITIES i.e. from phase β to phase α.

taken into account. It is shown that the combined diffusion of the reactants produces cyclic voltammograms which do not obey the classical behavior as derived by Nicholson and Shain [48], see 3.1.1.

If we assume that the diffusion of the reactants and products for the process illustrated in fig. 3.4.1 is linear, the concentration for any of the four species is given by a modified version of (3.1.15), i.e.

$$\bar{c}_i(x,s)=c_i^*/s + A(s)[x(s/D_i)] \qquad (3.4.1)$$

Where c_i^* represents the bulk concentration of species i, $\bar{c}_i$ the Laplace transform of the concentration, D_i the diffusion coefficient and x the absolute value of the distance from the interface. The constants $A_i(s)$ have to be determined from the boundary conditions which in the present case are given by the mass balance at the interface:

$$\bar{i}(s)=nFAD_O^{\alpha}[\partial\bar{c}_O^{\alpha}/\partial x]_{x=0} = -nFAD_R^{\alpha}[\partial\bar{c}_R^{\alpha}/\partial x]_{x=0}$$

$$=nFAD_R^{\beta}[\partial\bar{c}_R^{\beta}/\partial x]_{x=0} = -nFAD_O^{\beta}[\partial\bar{c}_O^{\beta}/\partial x]_{x=0} \qquad (3.4.2)$$

where $\bar{i}(s)$ is the Laplace transform of the current. The superscripts α and β refer to the phase, and the subscripts O and R refer to the oxidised and the reduced species respectively.

By combining equations (3.4.1) and (3.4.2) the interfacial concentration of the four species can be written as:

$$c_O^{\alpha}(0,t) = c_O^{\alpha *} - I(t)/D_O^{\alpha 1/2} \qquad (3.4.3)$$

$$c_R^{\alpha}(0,t) = c_R^{\alpha *} + I(t)/D_R^{\alpha 1/2} \qquad (3.4.4)$$

$$c_O^{\beta}(0,t) = c_O^{\beta *} + I(t)/D_O^{\beta 1/2} \qquad (3.4.5)$$

$$c_R^{\beta}(0,t) = c_R^{\beta *} - I(t)/D_R^{\beta 1/2} \qquad (3.4.6)$$

where I(t) is the convoluted current defined as

$$I(t) = \pi^{-1/2} \int_0^t f(\tau)(t-\tau)^{-1/2}\, d\tau \qquad (3.4.7)$$

and f(t) being define as in 3.1.

Assuming a totally reversible system the concentrations of the four species are related via the Nernst equation

$$E = E^{o'} + RT/nF \ln ((c_O^{\alpha} c_R^{\beta})/(c_R^{\alpha} c_O^{\beta})) \qquad (3.4.8)$$

E and $E^{o'}$ being as defined as in 3.1.1. where n is the number of electrons exchanged at the interface

$$n = z_O^{\alpha} - z_R^{\alpha} = z_O^{\beta} - z_R^{\beta} \qquad (3.4.9)$$

By defining the parameters θ, σ and $S_\lambda(t)$ as in 3.1.1, i.e. eqns. (3.1.11), (3.1.12) and (3.1.14), it is possible to express the Nernst equation as

$$\theta S_\lambda(t) = c_O^{\alpha} c_R^{\beta} / c_R^{\alpha} c_O^{\beta} \qquad (3.4.10)$$

By substituting eqns(3.4.3-6) into eqn(3.4.10), we obtain the following quadratic expression for the convoluted current

$$AI(t)^2 + BI(t) + C = 0 \qquad (3.4.11)$$

with the constants A, B and C defined as

$$A = \theta S_\lambda(t)/(D_R{}^\alpha D_O{}^\beta)^{1/2} - 1/(D_O{}^\alpha D_R{}^\beta)^{1/2} \qquad (3.4.12)$$

$$B = \theta S_\lambda(t)[c_R{}^{\alpha*}/D_O{}^{\beta 1/2} + c_O{}^{\beta*}/D_R{}^{\beta 1/2}] + c_O{}^{\alpha*}/D_R{}^{\beta 1/2} + c_R{}^{\beta*}/D_O{}^{\alpha*1/2} \qquad (3.4.13)$$

$$C = c_R{}^{\alpha*} c_O{}^{\beta*} \theta S_\lambda(t) - c_O{}^{\alpha*} c_R{}^{\beta*} \qquad (3.4.14)$$

Obviously eqn. (3.4.11) has two roots, one of which being the convoluted current. The choice between the two roots stems from the continuity condition of the convoluted current and therefore the correct solution reads

$$I(t) = (-B + (B^2 - 4AC)^{1/2})/2A \qquad (3.4.15)$$

The continuity of I(t) is verified for A=0 by taking I(t) equal to -C/B.

In order to integrate eqn.(3.4.15) in the general case the following dimensionless coefficients are introduced

$$\alpha = c_O{}^{\alpha*}/c_\alpha \qquad (3.4.16)$$

with c_α the total concentration of the redox couple in α given by

$$c_\alpha = c_O{}^{\alpha*} + c_R{}^{\alpha*} \qquad (3.4.17)$$

and

$$\beta = c_O{}^{\beta*}/\kappa c_\alpha \qquad (3.4.18)$$

where κ represents the ratio of the total concentrations of the redox couples, i.e.

$$\kappa = (c_O^{\beta*} + c_R^{\beta*})/c_\alpha = c_\beta/c_\alpha \qquad (3.4.19)$$

The diffusion coefficients of the reactants and products can also be expressed by a set of dimensionless parameters

$$\xi^\alpha = (D_O^\alpha/D_R^\alpha)^{1/2} \qquad (3.4.20)$$

$$\xi^\beta = (D_O^\beta/D_R^\beta)^{1/2} \qquad (3.4.21)$$

$$\zeta = (D_O^\alpha/D_O^\beta)^{1/2} \qquad (3.4.22)$$

These dimensionless coefficients can be substituted into eqns. (3.4.12-14) to give

$$A = (\xi^\alpha/\xi^\beta)\ \theta S_\lambda(t) - 1 \qquad (3.4.23)$$

$$B = \theta S_\lambda(t)[((1-\alpha)c_\alpha D_O^{\alpha 1/2})/\xi^\beta + c_\alpha \kappa \beta D_O^\alpha(\xi^\alpha/\xi^\beta\zeta)] \qquad (3.4.24)$$

$$C = (\kappa c_\alpha^2 D_O^\alpha/\xi^\alpha\zeta)[(1-\alpha)\beta\theta S_\lambda(t) - \alpha(1-\beta)] \qquad (3.4.25)$$

It can be shown that the convoluted current is proportional to $c_\alpha\sqrt{D_o^\alpha}$.

Equation (3.4.15) can be written in full as

$$\pi^{-1/2} \int_0^t f(\tau)(t-\tau)^{-1/2} d\tau = (-B+(B^2-4AC)^{1/2})/2A \qquad (3.4.26)$$

The integral can be evaluated in the same manner as in 3.1.1, thus (3.4.26) can be written as

$$\chi(n)\Lambda + \sum_{i=1}^{n-1} (n-i)^{1/2}(\chi(i+1)-\chi(i)) =$$

$$1/(2\delta^{1/2})[\,(-B+(B^2+4AC))/2A\,] \qquad (3.4.27)$$

with the integral being replaced by its finite sum (see 3.1.1). Due to the changes of variables $S_\lambda(t)$ in A, B and C can now be written as $S_{\sigma\lambda}(\delta n)$. The integration of eqn. (3.4.27) leads to a dimensionless current parameter $\chi(\sigma t)$ which is related to the current by

$$i(\sigma t) = nFA(\pi D_O{}^{\alpha}\sigma)^{1/2}c_{\alpha}\chi(\sigma t) \qquad (3.4.28)$$

It can be seen fron (3.4.28) that a normal sweep rate dependence is applicable, i.e. i_p *vs.* $\nu^{1/2}$ gives a linear relationship. The values of the dimensionless current $\chi(\sigma t)$ have been calculated as a function of potential for a range of values of the parameters α, β, and κ. The program used to calculate values of $\chi(\sigma t)$ is shown in Appendix A.6. All the results presented assume the equality of the diffusion coefficients of the reactants and products i.e.

$$\zeta = \xi^{\alpha} = \xi^{\beta} = 1 \qquad (3.4.29)$$

3.4.1.1 Case 1 α=1, β=0

Case 1 represents the simple reaction with a zero initial concentration of the products (i.e. the situation normally assumed in classical cyclic voltammetry).

The data for this system was acquired before it was realised that in fixing α and β as input parameters, we were essentially choosing our initial starting

potential, due to the relationship

$$\theta S_{\lambda}(t) = c_O^{\alpha} c_R^{\beta} / c_R^{\alpha} c_O^{\beta} \qquad (3.4.30)$$

which for t=0 is reduced to

$$\theta = c_O^{\alpha^*} c_R^{\beta^*} / c_R^{\alpha^*} c_O^{\beta^*} \qquad (3.4.31)$$

Now the bulk concentrations of all the species can be defined in terms of α, β , κ and c_{α} to give

$$\theta = \alpha(1-\beta)/\beta(1-\alpha) \qquad (3.4.32)$$

Thus for this case θ should be undefined, i.e. $\theta \rightarrow 1$. However for the results presented here the condition $\ln\theta=10$ was used which is equivalent to $\alpha=0.99999$, $\beta=0.00001$, thus no great loss of accuracy of the results occurred. However in all future work this was kept in mind and $\ln\theta$ was evaluated directly from the values of α and β, and not input directly.

In this case the coefficient κ represents the ratio of concentrations of the reactants $c_o^{\alpha} / c_R^{\alpha}$. Equation (3.4.28) then reads

$$i(\sigma t) = nFA(\pi D_O^{\alpha} \sigma)^{1/2} \chi(\sigma t) \qquad (3.4.33)$$

and shows that the peak current is proportional to the square root of the sweep rate with a slope value of $nFA\sqrt{(\pi D_O^{\alpha} nF/RT)}\chi_p(\sigma t)$ where $\chi_p(\sigma t)$ is the dimensionless peak current, given in Table 3.4.1 for different values of κ. Figure 3.4.2 illustrates this dependence for $\kappa=1$.

When the concentration of the reactants is equal (i.e. $\kappa=1$) it can be seen

from table 3.4.1 that the mid-peak potential, $E_{1/2'}$ is equal to the formal potential and that the peak separation ΔE_p is equal to 116mV. This is in fact equivalent to a classical cyclic voltammogram with n=1/2 as the concentration profiles of the reactants in the adjacent phases are symmetrical. This symmetry also holds for the products and consequently the ratio in eqn. (3.4.10) reads $(c_O^{\alpha}/c_O^{\beta})^2$. The sweep rate dependence illustrated in figure 3.4.2 follows eqn. (3.4.33) and can be used to evaluate either the diffusion co-efficient D_O^{α} or the bulk concentration of the oxidised species in phase α.

When the concentration of the reduced species in phase β exceeds that of the oxidised species in phase α (i.e. $\kappa>1$) the mid-peak potential shifts towards positive values as high as 131mV when κ equal to 100. On the other hand, the peak separation decreases and the peak current approaches a limiting value of 0.217. This is due to the electron tranfer now being limited mainly, but not totally, by the arrival of c_O^{α} at the interface. This behaviour is illustrated in figure 3.4.3.

Conversely when the concentration of the oxidised species in the phase α exceeds that of the reduced species in the phase β (i.e. $\kappa < 1$), the normalised current $\chi(\sigma t)/\kappa$ however shows a similar behavior to that described above i.e. shift of mid-peak potentials to positive values, decrease of the peak separation and the same limiting value of the normalised plateau current. Thus in this case we are now being mainly limited by the arrival of c_R^{β} at the interface.

This shows that even under pseudo first order conditions, in either phase, the electron transfer reaction cannot be compared to an electron transfer at a metal/electrolyte interface, where it might be expected that the diffusion of the species in one phase controls the electron transfer and the phase with the high concentration would thus behave like a metal with a non-diffusion limited

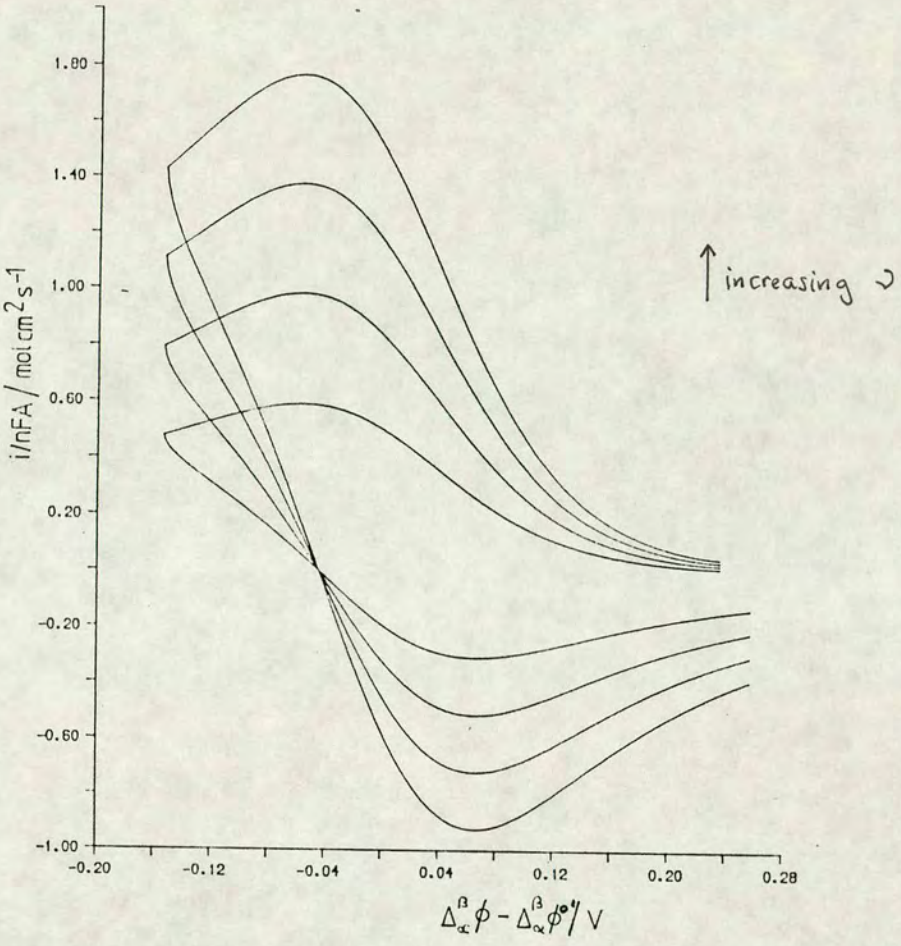

Figure 3.4.2 Cyclic voltammograms, i/nFA *vs.* $(\Delta_\alpha^\beta\phi - \Delta_\alpha^\beta\phi^{o'})$, showing sweep rate dependence for $\alpha=1,\beta=0$ and $\kappa=1$. Scan rates 0.009,0.0025,0.0049 and 0.0081Vs^{-1}.

κ	$E_{p,f}$/mV	$E_{p,b}$/mV	ΔE_p/mV	$E_{1/2}$/mV	$\chi(\sigma t)_{f,p}$	$\chi(\sigma t)_{f,p}/\kappa$
0.01	88.3	172.4	84.1	130.4	0.00217	0.217
0.05	46.0	131.5	85.5	88.8	0.0108	0.216
0.1	27.2	113.8	86.6	70.5	0.0215	0.215
0.5	−26.5	71.7	98.2	22.6	0.103	0.206
1.0	−57.0	58.8	115.8	0.9	0.178	0.178
2.0	−27.0	72.2	99.2	22.6	0.206	
10.0	26.5	114.3	87.8	70.4	0.215	
20.0	45.7	132.3	86.6	89.0	0.216	
100.0	87.9	173.7	85.8	130.8	0.217	

Table 3.4.1 Dimensionless current function $\chi(\sigma t)$ and other cyclic voltammogram characteristics for case 1 ($\alpha=1,\beta=0$), E= $\Delta_\alpha^\beta\phi-\Delta_\alpha^\beta\phi^{o'}$, scanning from E=+500mV to −500mV, step increment 0.3mV.

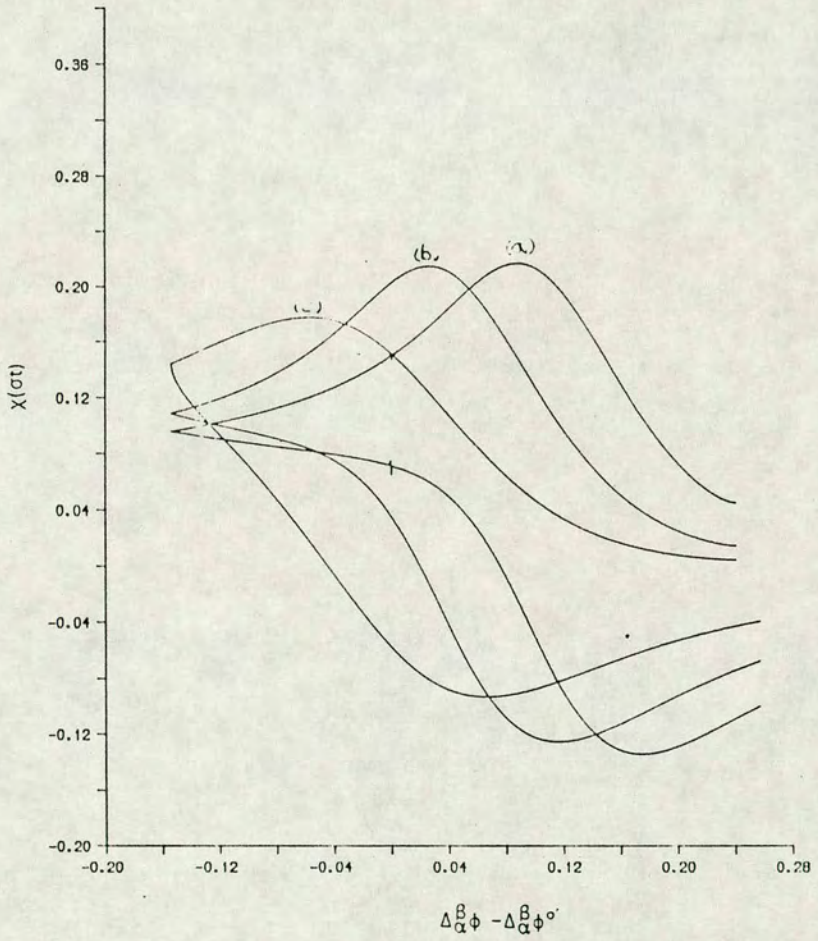

Figure 3.4.3 Cyclic voltammograms of $\chi(\sigma t)$, dimensionless current, *vs.* $(\Delta_\alpha^\beta\phi - \Delta_\alpha^\beta\phi^o)$ for $\alpha=1,\beta=0$, with varying κ; (a) $\kappa=1$ (b) $\kappa=10$ (c) $\kappa=100$.

supply of electrons or "electron holes".

This shows that it is only possible to use cyclic voltammetry to evaluate the formal potential under very specific conditions of the concentrations in each phase, i.e. $\kappa=1$.

3.4.1.2 Case 2: $\alpha=0.5$ $\beta=0.0$

Another interesting situation for the study of the electron transfer reactions at ITIES is when one phase contains an equimolar concentration of electron donor and acceptor, and the other phase only contains the reactant i.e. $\alpha=0.5$, $\beta 0$. It can be seen, for this case, in Table 3.4.2 that when this equimolar mixture is in excess, compared to the reduced species in β then the system is truely controlled by the arrival of the latter reactant. Thus the system approaches that of a metal/electrolyte interface where phase α, is behaving as the solid. i.e. ΔE_p, $E_{1/2}=0$, and $\chi(\sigma t)/\kappa=0.251$. When the value of κ is increased the peak separation moves to a maximum value of 98mV at $\kappa=0.5$ and the $E_{1/2}$ values move positively for values of $\kappa>1$.

Thus it is shown that for electron transfer with cyclic voltammetry at ITIES the results produced are vastly different from those found for electron transfer at a metal/electrolyte interface. Even under pseudo first order conditions the usual criteria for reversibility at a planar electrode i.e. $\Delta E_p=58$mV and $E_{1/2}=E^{o'}$, only applies when both forms of the redox couple in one phase are present in large excess over the reactant of the other phase.

They also show that peak separations greater than 60mV can be observed, under reversible conditions, due to the effect of the concentration of the reactants and products in each phase, and thus their diffusion. Hence this criteria should not be taken as an indication of a kinetically controlled reaction.

κ	$E_{p,f}$/mV	$E_{p,b}$/mV	ΔE_p/mV	$E_{1/2}$/mV	$\chi(\sigma t)_{f,p}$	$\chi(\sigma t)_{f,p}/\kappa$
0.01	−29.5	29.0	58.5	−0.3	0.00251	0.251
0.05	−33.4	28.3	61.7	−2.6	0.0123	0.246
0.1	−37.8	27.5	65.3	−5.2	0.0241	0.241
0.5	−70.1	27.5	97.6	−21.3	0.0955	0.191
1.0	−41.3	42.1	83.4	0.4	0.111	0.111
2.0	−15.9	59.3	75.2	21.7	0.115	
10.0	30.1	101.0	70.9	65.6	0.118	
20.0	48.6	119.7	71.1	84.2	0.118	
100.0	90.4	161.6	71.2	126.0	0.118	

Table 3.4.2 Dimensionless current function $\chi(\sigma t)$ and other cyclic voltammogram characteristics for case 2 ($\alpha=0\leq\beta=0$), E= $\Delta_{\alpha}^{\beta}\phi-\Delta_{\alpha}^{\beta}\phi^{o'}$, scanning from E=+500mV to −500mV, step increment 0.3mV.

	Experimental Results		Analytical Results	
$\kappa(=c_\beta/c_\alpha)$	ΔE_p/mV	$E_{1/2}$/mV	ΔE_p/mV	$E_{1/2}$/mV
9.09	85	318	87	75
18.18	85	318	86	88
45.45	85	298	85	111
90.91	85	285	85	128
181.82	85	263	84	145

Table 3.4.3 Comparison of ΔE_p and $E_{1/2}$ values from experiment (ref:63) and from the analytical solution, α=0.90909, β=0, For κ values ranging from 9 to 182.

Therefore before the results for electron transfer at ITIES are analysed the concentrations of all species should be taken into account.

3.4.2 Comparison Of Theoretical Cyclic Voltammogram With Experimental Results For Electron Transfer[63]

In 1979 Samec *et al* [63] presented experimental results for cyclic voltammetry of electron transfer at an ITIES for the system, ferricyanide in water and ferrocene in nitrobenzene. The trends observed in these results have been compared with the results predicted by the analytical solution for cyclic voltammetry presented in 3.4.1.

Due to the E^o value for this electron transfer not being known for this system it is not possible to directly compare the potentials from both sets of results, since in the analytical solution all the potentials are referred to E^o. Therefore it is only possible to compare trends and the values of ΔE_p.

Table 3.4.3 shows the effect of increasing the bulk concentration of ferrocene, while keeping the concentration of the redox couple in the aqueous phase constant. This is equivalent to keeping α and β constant and varying κ in the analytical solution, in this case α=0.90909 and β'0.0, and κ varies from 9.1 to 181.82. from this it can be seen that the ΔE_p values agree very well between theory and experiment, although the theory predicts a slight downward trend in ΔE_p with increasing κ which is not seen experimentally. This may be explained by the normal error expected in measuring the peak potentials of ±1mV. Since the change predicted over this range of κ values is only 3mV the change in the experimental results may be masked by this error.

The theoretical results also predict a movement of the mid-peak potential, $E_{1/2}$ with an increase in κ of 70mV. The experimental results also show a change in $E_{1/2}$ with κ but in this case the change is only 55mV. Also these

changes appear to be in opposite directions, however this is not actually the case, since the potential scales use different conventions in each case i.e. the experimental results quote the potentials as $\Delta_o^w\phi$ whereas the theoretical results quote the potentials as $\Delta_w^o\phi$. Therefore the trends in the theoretical voltammograms match those predicted experimentally, in size of the changes of peak potentials and in the direction which these potentials move.

3.4.3 Quasi-Reversible Electron Transfer At A Planar ITIES

In a manner similar to that used in 3.1 and 3.2 it is possible to adapt the solution for the reversible electron transfer at an ITIES to a solution for kinetically controlled electron transfer. Thus in this case the Nernst equation in 3.4.1 is replaced by a kinetic term to describe the boundary conditions for mass balance at the interface i.e.

$$i(t)/nFA = k_f c_O^{\alpha} c_R^{\beta} - k_b c_R^{\alpha} c_O^{\beta} \qquad (3.4.34)$$

given that the reaction that we are studying is

$$A_O^{\alpha} + B_R^{\beta} \underset{k_b}{\overset{k_f}{\rightleftharpoons}} A_R^{\alpha} + B_O^{\beta} \qquad (3.4.35)$$

Assuming that the kinetics are controlled in a Butler-Volmer relationship eqns. (3.1.48) and (3.1.49) can be substituted into (3.4.34) to give

$$i(t)/nFA = k^o \exp[-\alpha(nF/RT)(E-E^o)](c_O^{\alpha} c_R^{\beta} - \exp[(nF/RT)(E-E^o)] c_R^{\alpha} c_O^{\beta}) \qquad (3.4.36)$$

If the system is at equilibrium initially then the concentration of the four

species can be related to the resting/initial potential and *vice versa*, by the Nernst equation

$$E_i = E^o + RT/nF \ln(c_O^{\alpha^*} c_R^{\beta^*} / c_R^{\alpha^*} c_O^{\beta^*}) \qquad (3.4.37)$$

If the ratio of bulk concentrations of the reactants and products is equated to θ then (3.4.37) can be written

$$\theta = \exp[(nF/RT)(E_i - E)] \qquad (3.4.38)$$

Given that the potential function with time is the normal expression for cyclic voltammetry, i.e. eqns. (3.1.7) and (3.1.8), the usual substitutions can be made, i.e. eqns. (3.1.12) and (3.1.11), to result in (3.4.36) becoming

$$i/nFA = k^o(\theta S_\lambda(t))^{-\alpha}[c_O^{\alpha} c_R^{\beta} - \theta S_\lambda(t) c_R^{\alpha} c_O^{\beta}] \qquad (3.4.39)$$

Given that the species are diffusing to the interface in a planar manner the expressions for the surface concentrations of each species can be given as in 3.4.1, eqns. (3.4.3) to (3.4.6), to give

$$\begin{aligned} 0 = {} & c_O^{\alpha^*} c_R^{\beta^*} - \theta S_\lambda(t) c_R^{\alpha^*} c_O^{\beta^*} - i(t)(\theta S_\lambda(t))^{\alpha}/nFAk^o \\ & - I(t)[\, c_R^{\beta^*}/D_O^{\alpha}1/2 + c_O^{\alpha^*}/D_R^{\alpha^*}1/2 \\ & + \theta S_\lambda(t)(c_R^{\alpha^*}/D_O^{\beta}1/2 + c_O^{\beta^*}/D_R^{\alpha}1/2)\,] \\ & - I(t)^2[\, \theta S_\lambda(t)/(D_R^{\alpha} D_O^{\beta})^{1/2} - (D_O^{\alpha} D_R^{\beta})^{-1/2}\,] \end{aligned} \qquad (3.4.40)$$

which is a quadratic expression similar to that found in 3.4.1, i.e.

$$I(t)^2 A + I(t)B + C = 0 \qquad (3.4.41)$$

where

$$A = \theta S_\lambda(t)/(D_R^{\alpha} D_O^{\beta})^{1/2} - (D_O^{\alpha} D_R^{\beta})^{1/2} \qquad (3.4.42)$$

$$\begin{aligned} B = {} & c_R^{\beta^*}/D_O^{\alpha}1/2 + c_O^{\alpha^*}/D_R^{\beta}1/2 + \\ & \theta S_\lambda(t)[\, c_R^{\alpha^*}/D_O^{\beta}1/2 + c_O^{\beta^*}/D_R^{\alpha}1/2\,] \end{aligned} \qquad (3.4.43)$$

$$C = i(t)(\theta S_\lambda(t))^{\alpha}/nFAk^o + \theta S_\lambda(t) c_R^{\alpha^*} c_O^{\beta^*} - c_O^{\alpha^*} c_R^{\beta^*} \qquad (3.4.44)$$

It can be seen, by comparison with the reversible case, in 3.4.1, that only C is effected by the introduction of kinetics. Thus by introducing the same

dimensionless coefficients as in 3.4.1, i.e. eqns. (3.4.42) to (3.4.44), it is possible to redefine A, B and C as

$$A = S_\lambda(t)\xi^\beta/(1-\alpha)\beta\kappa\xi^\beta - 1/\alpha(1-\beta)\kappa \qquad (3.4.45)$$

$$B = c_\alpha D_O{}^{\alpha 1/2}\{1/\kappa(1-\beta) + 1/\alpha\xi^\beta\zeta + S_\lambda(t)[\xi^\alpha/(1-\alpha)\xi^\beta\zeta + 1/\beta\kappa\xi^\beta]\} \qquad (3.4.46)$$

$$C = D_O{}^\alpha c_\alpha{}^2/\xi^\beta\zeta\ [i(t)(\theta S_\lambda(t))^\alpha/nFAk^o{}_\alpha c_\alpha{}^2\kappa(1-\beta) + S_\lambda(t) - 1] \qquad (3.4.47)$$

If the convoluted current is written out in full and making the substitution f(t)=i(t)/nFA, eqn. (3.4.41) becomes

$$\pi^{1/2}\int_0^t f(\tau)(t-\tau)^{1/2}\,d\tau = (-B+(B^2-4AC)^{1/2})/2A \qquad (3.4.48)$$

with C now given as

$$C = (c_\alpha{}^2 D_O{}^\alpha/\xi^\beta\zeta)[f(t)(\theta S_\lambda(t))^\alpha/k^o{}_\alpha c_\alpha{}^2\kappa(1-\beta) + S_\lambda(t) - 1] \qquad (3.4.49)$$

The integral in (3.4.48) can be replaced by its finite sum, as described in 3.1 which results in

$$\chi(1)\sqrt{n} + \sum_{i=1}^{n-1}(n-i)^{1/2}(\chi(i+1) - \chi(i)) = 1/(2\sqrt{\delta})[(-B+(B^2-4AC))/2A] \qquad (3.4.50)$$

With the coefficients A, B and C now defined as

$$A = S_{\delta\lambda}(\delta n)\xi^{\beta}/(1-\alpha)\beta\kappa\xi^{\beta} - 1/\alpha(1-\beta)\kappa \tag{3.4.51}$$

$$B = 1/\kappa(1-\beta) + 1/\alpha\xi^{\beta}\zeta + S_{\delta n}(\delta n)[\,\xi^{\alpha}/(1-\alpha)\xi^{\beta}\zeta + 1/\beta\kappa\xi^{\beta}\,] \tag{3.4.52}$$

$$C = (\xi^{\beta}\zeta)^{-1}[\,\chi(n)(\pi\sigma D_O{}^{\alpha})^{1/2}(\theta S_{\delta\lambda}(\delta n))^{\alpha}/\alpha(1-\beta)\kappa k^{o}c_{\alpha} + S_{\delta\lambda}(\delta n) - 1\,] \tag{3.4.53}$$

Now we have an expression to evaluate $\chi(n)$ which is involved in the solution of the quadratic equation as well as in the finite sum expression. It is therefore necessary to carry out the following routine to evaluate $\xi(n)$.

The left hand side of equation (3.4.50) can be written as

$$\chi(n) + SUM \tag{3.4.54}$$

thus eqn.(3.4.50) becomes

$$\chi(n) + SUM = (-B+(B^2-4AC)^{1/2})/4A\ \delta^{1/2} \tag{3.4.55}$$

Now by defining

$$SUM + B/4A\sqrt{\delta} = SUM' \tag{3.4.56}$$

eqn. (3.4.55) becomes

$$4A\sqrt{\delta}(\chi(n)+SUM')^{2} = (B^2-4AC)^{1/2} \tag{3.4.57}$$

which can be expanded to become

$$16\delta A^2\chi(n)^2 + 32\delta A^2 SUM'\chi(n) + 16\delta A^2 SUM' - B^2 + 4AC = 0 \tag{3.4.58}$$

It is now necessary to split C into two parts i.e. one containing $\chi(n)$ and the other not, thus

$$C = C_1 + C_2\chi(n) \qquad (3.4.59)$$

with C_1 and C_2 defined as

$$C_1 = (\xi\beta\zeta)^{-1}(S_{\delta\lambda}(\delta n) - 1) \qquad (3.4.60)$$

$$C_2 = (\xi\beta\zeta)^{-1}\left[((\pi\sigma D_O{}^{\alpha})^{1/2}(\theta S_{\delta\lambda}(\delta n))^{\alpha})/\alpha k^{o} c_{\alpha}{}^{\kappa(1-\beta)}\right] \qquad (3.4.61)$$

This results in a quadratic equation which can be solved for $\chi(n)$

$$16\delta A^2\chi(n)^2 + (32\delta A^2 SUM' + 4AC_2)\chi(n)$$

$$+ 16\delta A^2 SUM'^2 + B + AC_1 = 0 \qquad (3.4.62)$$

thus

$$\chi(n) = (-B' + (B'^2 - 4A'C')^{1/2})/2A' \qquad (3.4.63)$$

where A', B' and C' are defined as

$$A' = 16\delta A^2 \qquad (3.4.64)$$

$$B' = 32\delta A^2 SUM' - B^2 + 4AC_2 \qquad (3.6.65)$$

$$C' = 16\delta A^2 SUM'^2 - B^2 + 4AC_2 \qquad (3.4.66)$$

It is also possible to redefine C_2 by introducing a dimensionless rate term, ψ, thus

$$C_2 = (\xi\beta\zeta)^{-1}((\theta S_{\sigma\lambda}(\delta n))^2/\alpha(1-\beta)\kappa\psi) \qquad (3.6.67)$$

$$\psi = k^{o} c_{\alpha}/(\pi\sigma D_O{}^{\alpha})^{1/2} \qquad (3.6.68)$$

This problem can be solved computationally and the program used to carry this out is shown in Appendix A.7.

As for reversible electron transfer at planar ITIES, i.e. 3.4.1, quasi electron transfer was examined for two cases i.e. α=1,β=0 and α=0.5,β=0.

3.4.3.1 Case1: α=0.99999,β=0.000001

For this case the cyclic voltammograms were investigated for ψ values ranging from 100 to 0.001, i.e reversible reactions to irreversible reactions, and the data presented for three different values of κ is presented in table 3.4.4. This shows that for each case the peak separation increases as ψ decreases, and for smaller values of κ ΔE_p being greater at low values of κ. For each value of κ presented the ΔE_p found limits towards the value found for the reversible case, for high values of ψ, as expected. The data in Table 3.4.4 can be presented in a manner similar to that by Nicholson [49] for electron transfer at a metal/electrolyte interface, i.e. working curves of ΔE_p *vs.* $\log_{10}\psi$, from which it is possible to evaluate k for a given set of experimental conditions. Examples of such curves for the data presented in Table 3.4.4 can be seen in figures (3.4.4) to (3.4.6).

3.4.3.2 Case2: α=0.5, $\beta=10^{-7}$

The cyclic voltammograms were produced for the same set of conditions as in Case 1 , i.e. variation of ψ from 100 to 0.001 for κ = 1, 0.1, 0.01. The effect of these parameters on ΔE_p is presented in Table 3.4.5. It can be seen that ΔE_p increases as ψ decreases, and that the values limit towards the reversible situation as ψ increases, again as expected. Thus it is possible to construct working curves of ΔE_p *vs.* $\log_{10}\psi$ from which it is possible to evaluate k for a set of experimental conditions, as is seen in figures (3.4.7) to (3.4.9).

α=0.99999, β=0.00001		ΔE_p/mV		
ψ	$\log_{10}\psi$	κ=1.0	κ=0.1	κ=0.01
100	2	116.1	87.4	87.4
50	1.699	116.7	87.4	89.9
10	1	118.2	93.8	109.2
5	0.699	120.5	101.5	131.0
1	0	140.5	159.3	213.7
0.1	−1	299.4	382.8	503.6
0.05	−1.301	374.1	458.6	578.1
0.01	−2	550.0	633.3	782.8
0.005	−2.301	625.6	708.3	826.0
0.001	−3	802.1	883.3	>940.3

Table 3.4.4 Table showing variation of ΔE_p with the kinetic parameter, ψ, for κ=1,0.1,0.01, and α=0.9999, β=0.00001. ψ varying from 100 to 0.001.

α=0.5, $\beta=10^{-7}$		ΔE_p/mV		
ψ	$\log_{10}\psi$	κ=1.0	κ=0.1	κ=0.01
100	2	84.5	66.5	59.1
50	1.699	84.8	67.1	59.1
10	1	86.8	71.2	63.2
5	0.699	89.9	75.8	68.3
1	0	111.5	111.0	105.9
0.1	−1	258.7	289.8	285.2
0.05	−1.301	329.4	360.9	356.1
0.01	−2	498.7	528.3	522.2
0.005	−2.301	571.4	600.0	594.7
0.001	−3	739.9	766.9	761.0

Table 3.4.5 Table showing variation of ΔE_p with the kinetic parameter ψ, κ=1,0.1,0.01, and α=0.5, $\beta=10^{-7}$. ψ varying from 100 to 0.001.

These two sets of results shows that it is possible to evaluate rate constants, for a given set of experimental parameters, by the use of working curves which show the variation of ΔE_p with ψ. However these results are only presented for $\alpha_{t.c.} = 0.5$ and it is expected that variation of $\alpha_{t.c.}$ will produce changes in the peak separation of voltammograms and thus working curves would have to be produced for different values of $\alpha_{t.c.}$, before a definite rate constant could be evaluated. As well as this it should be noted that similar effects of ΔE_p as found for varying ψ can also be produced by varying the composition of both phases. Thus great care should be exercised before this technique is used to evaluate rate constants for electron transfer at planar ITIES.

Figure 3.4.4 Working curve of ΔE_p *vs.* $\log_{10}\psi$ for the evaluation of kinetic parameters, for electron transfer reactions under kinetic control.

α=0.99999,$\beta=10^{-5}$. κ=1.

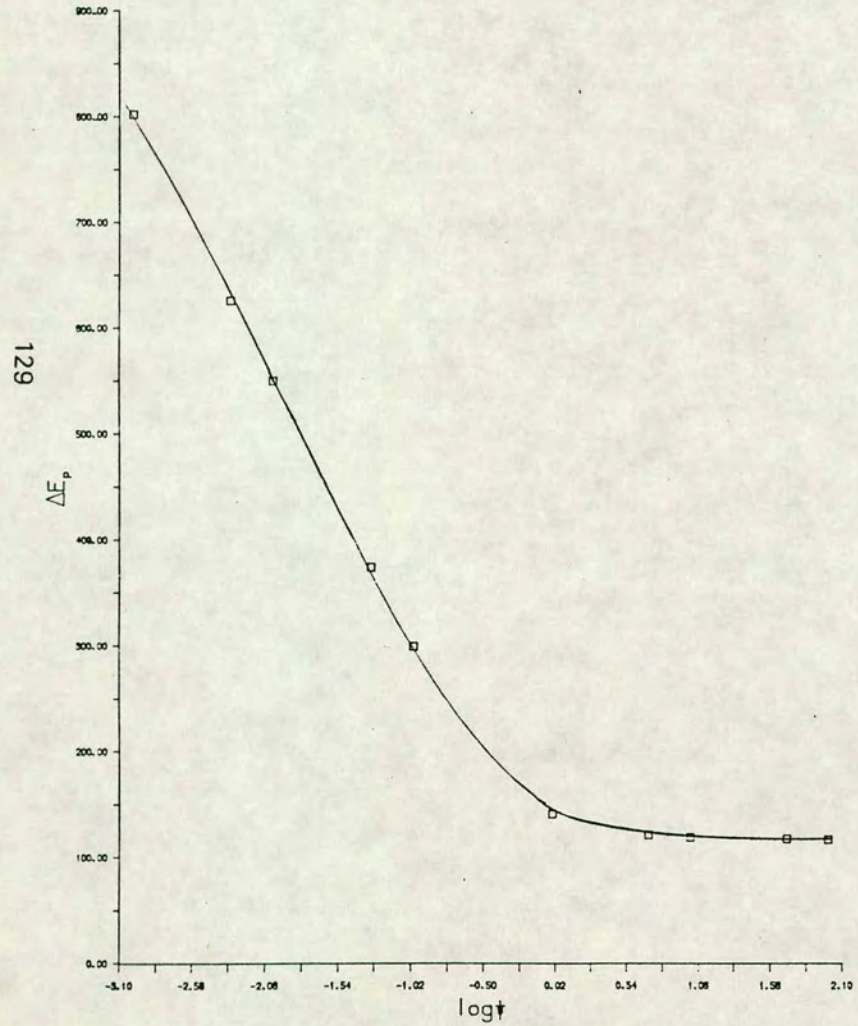

Figure 3.4.5 Working curve of ΔE_p *vs.* $\log_{10}\psi$ for the evaluation of kinetic parameters, for electron transfer reactions under kinetic control.

α=0.99999,$\beta=10^{-5}$. κ=0.1.

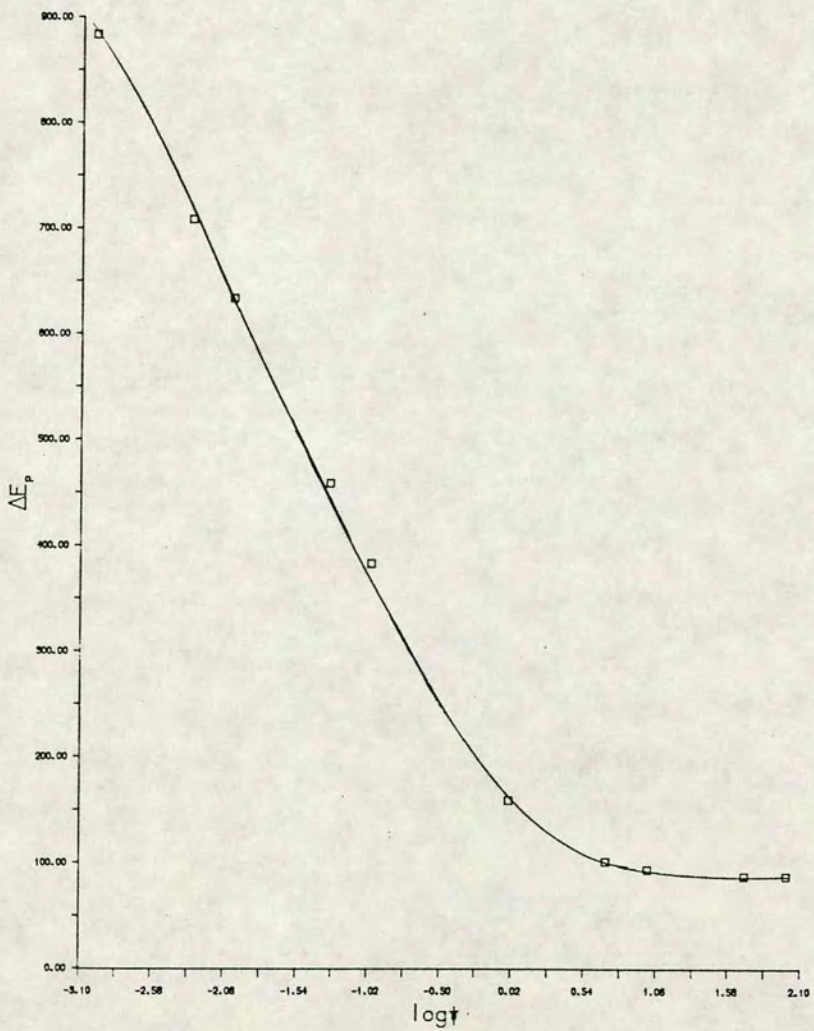

Figure 3.4.6 Working curve of ΔE_p *vs.* $\log_{10}\psi$ for the evaluation of kinetic parameters, for electron transfer reactions under kinetic control. $\alpha=0.99999, \beta=10^{-5}$. $\kappa=0.01$.

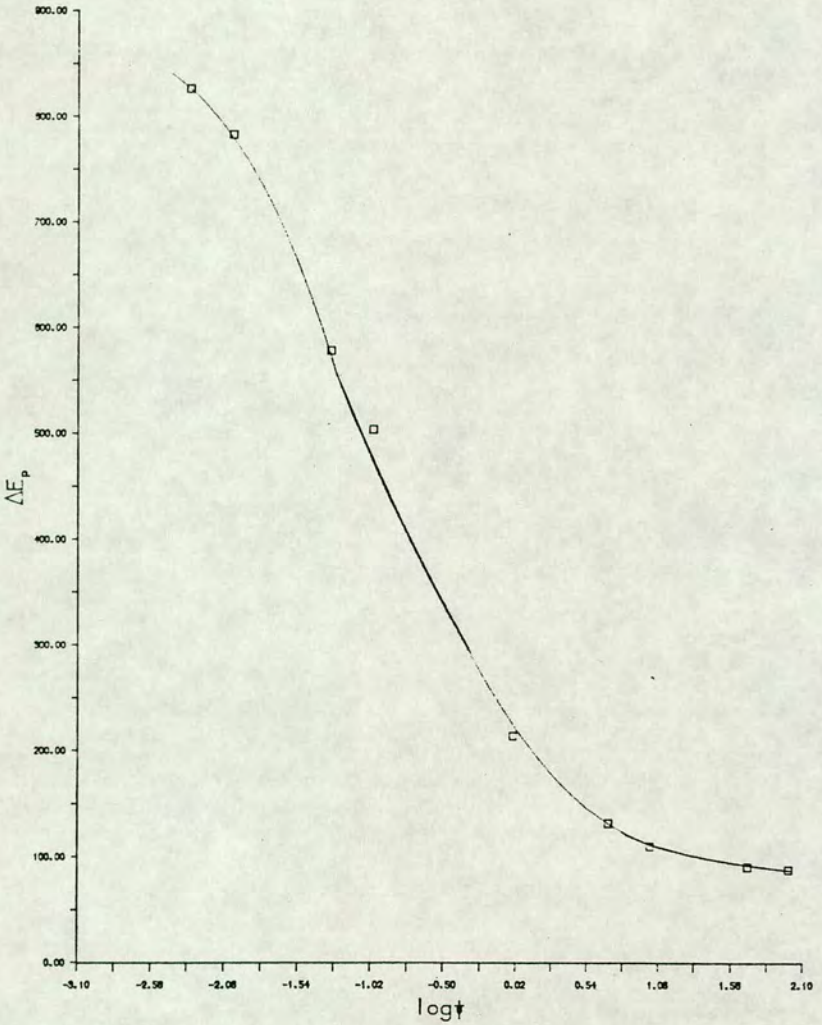

Figure 3.4.7 Working curve of ΔE_p *vs.* $\log_{10}\psi$ for the evaluation of kinetic parameters, for electron transfer reactions under kinetic control. $\alpha=0.5, \beta=10^{-7}$ $\kappa=1$.

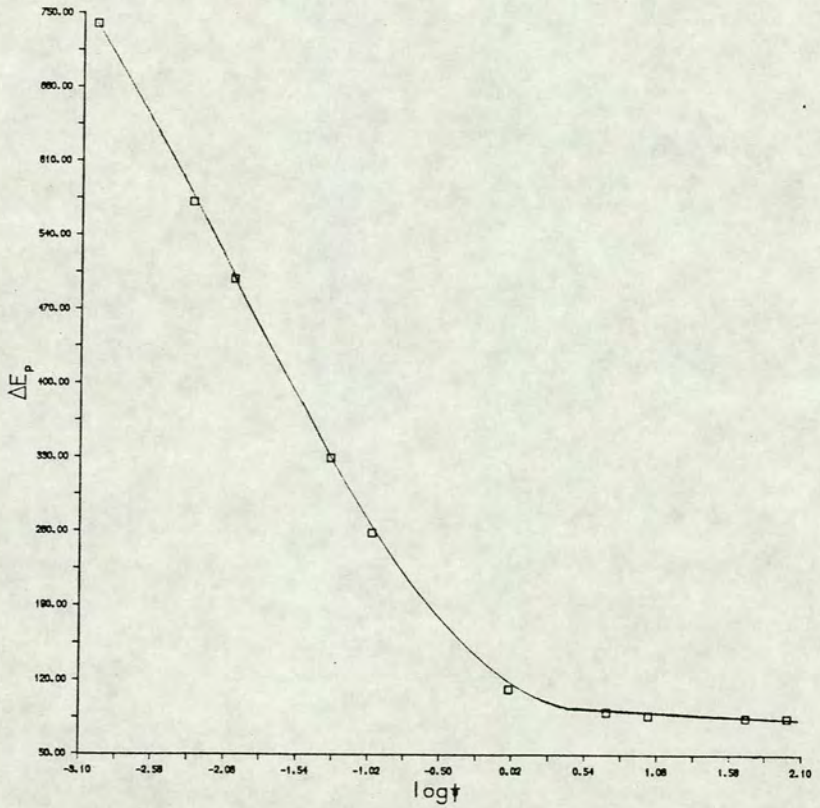

Figure 3.4.8 Working curve of ΔE_p *vs.* $\log_{10}\psi$ for the evaluation of kinetic parameters, for electron transfer reactions under kinetic control. $\alpha=0.5, \beta=10^{-7}$. $\kappa=0.1$.

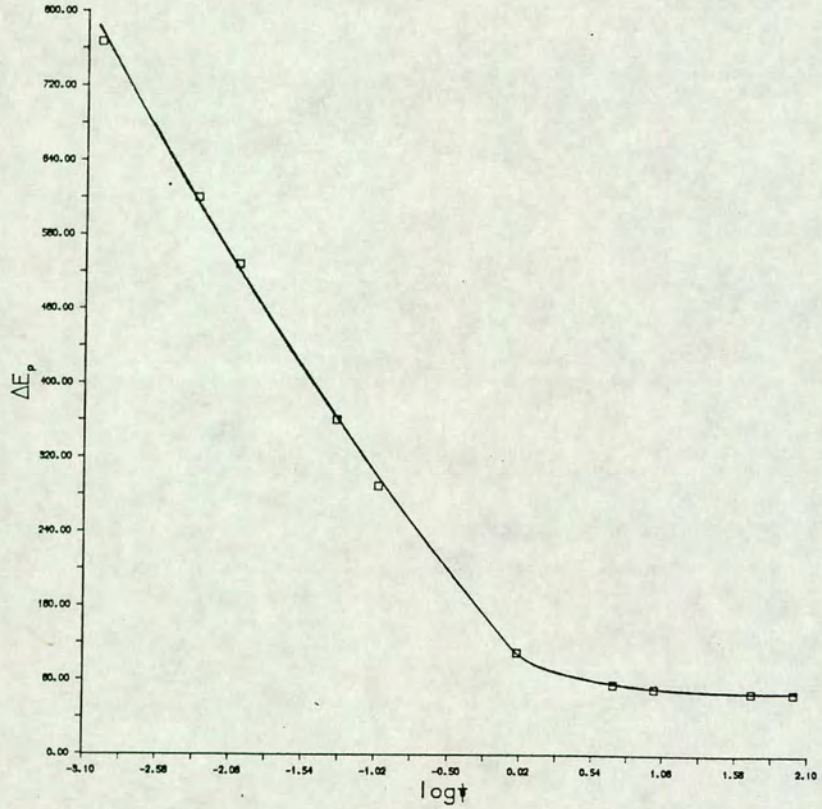

Figure 3.4.9 Working curve of ΔE_p *vs.* $\log_{10}\psi$ for the evaluation of kinetic parameters, for electron transfer reactions under kinetic control. $\alpha=0.5, \beta=10^{-7}$. $\kappa=0.01$.

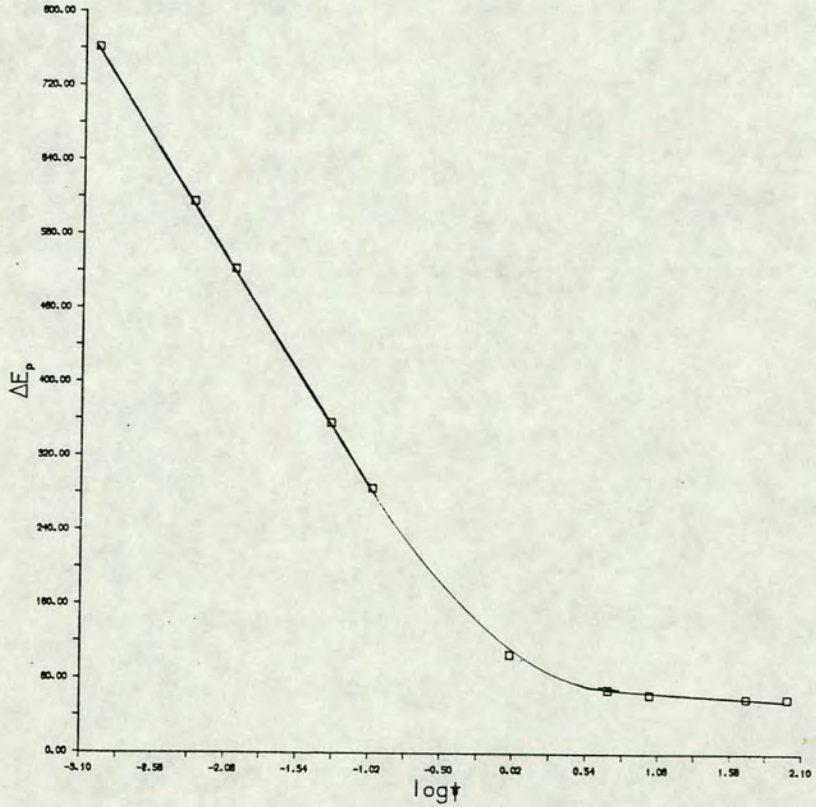

Chapter 4
Facilitated Ion Transfer At MicroITIES

As discussed in chapter two, facilitated ion transfer can be useful for several reasons i.e. evaluation of association constants, ligand-ion stoichiometries and quantity of an ion in solution, however the measurement of the kinetics of facilitated ion-transfer has proved difficult, due to the rates of such reactions. In the past the methods used to evaluate fast rate constants at metal electrodes have been limited by mass transport of the reactants to the interface. This has been overcome by rapid variation of electrode potentials, e.g. chronoamperometry, a.c. polarography, a.c. impedance, or by increasing the rate of arrival of the reactants to the interface, e.g. rotating disc, wall jet and micro electrodes. For ion/facilitated ion transfer only the former types of techniques have been used since, until recently, the latter techniques have not been available at ITIES.

In chapter three it was shown that it is now possible to carry out cyclic voltammetry at ITIES which are suspended at the tip of a micropipette, and to get a steady state response for transfers which are limited by mass transfer of the species outside the pipette. This allows the mass transport limitations mentioned to be overcome by using micro electrode techniques, and a method is presented to analyse steady state voltammograms for facilitated ion transfer [1]. This technique is then used to investigate the rates of transfer of K^+, facilitated by dibenzo-18-crown-6, and Li^+, facilitated by both ETH1810 and 2,9-dibutyl-1,10-phenanthroline.

4.1 Theory For The Analysis of Steady-State Response For Facilitated Ion Transfer At A MicroITIES [64]

In a system where the concentration of the transfering ion in one phase is in large excess over the concentration of the complexing agent in the other phase, only the diffusion of the complexing agent to the interface will limit the transfer of the ion. Therefore the observed current for facilitated ion transfer, in such systems, is equal to the rate of departure, from the interface, of the complexed ion. For spherical diffusion, i.e. if the aqueous phase is within the pipette containing the ion to be transfered, this current is given by

$$i = (z_i FAD_C/r)\ (c_C^b - c_C^\sigma) = (z_i FAD_{CI}/r)\ (c_{CI}^\sigma - c_{CI}^b) \qquad (4.1.1)$$

where it is assumed that the Nernst diffusion layer thickness constant. The subscripts C and CI refer to the ionophore and the complexed ion, respectively, the superscripts b and σ refer to the bulk and the surface concentrations, F,D and A have their usual meanings, and r is the radius of the tip of the pipette. The observed limiting current i.e. when the the concentration of the ionophore at the interface, c_C^σ, is approximately zero, can be given by

$$i_d = (z_i FAD_C/r)\ c_C^b = (z_i FAD_{CI}/r)\ c_{CI}^\sigma \qquad (4.1.2)$$

assuming that the initial concentration of complexed ion in the bulk organic phase, c_{OI}^* is zero.

The kinetic expression for the current can be classically defined as

$$i = z_i FA(\overrightarrow{k_{app}} c_C^\sigma - \overleftarrow{k_{app}} c_{CI}^\sigma) \qquad (4.1.3)$$

where $\vec{k}_{app}$ $\overleftarrow{k}_{app}$ are apparent forward and reverse electrochemical rate constants. However it should be noted that $\vec{k}_{app}$ is a pseudo first order rate constant, since c_I^{σ} is very large it can be assumed constant throughout the experiment, i.e.

$$\overrightarrow{k_{app}} = \overrightarrow{k_{app}}' c_I^{\sigma} \qquad (4.1.4)$$

Equations (4.1.2) and (4.1.3) can now be substituted into (4.1.1) to give

$$i = z_i F A c_c^{b} [\overrightarrow{k_{app}}(1-i/i_d) - \overleftarrow{k_{app}} \xi i/i_d] \qquad (4.1.5)$$

with ξ being the ratio D_C/D_{CI}.

The dependence of electrochemical rate constants, for charge transfer reactions at an ITIES, on potential has been the subject of great debate [65]. In this case we are looking at the rate of transfer from a position in the water phase which has potential ϕ^w, to a position in the organic phase with a potential ϕ^o, see figure 4.1.1, and not transfer across the mixed solvent layer, where the complexation reaction is assumed to take place.

If we model the reaction according to activated complex theory, for the apparent standard case, where the activation energy barrier is symmetrical and the concentration of the ionophore is equal to that of the complexed ion, the equilibrium can be described by

$$\overrightarrow{k_{app}} c_C^{\sigma} = \overleftarrow{k_{app}} c_{CI}^{\sigma} \qquad (4.1.6)$$

The apparent standard rate constant can be defined as

$$k^o_{app} = \overleftarrow{k_{app}} = \overrightarrow{k_{app}} = Z\exp(-\Delta G^o_A/RT) \qquad (4.1.7)$$

Also for the apparent standard case the Galvani potential difference between the

two phases is defined as the formal potential, $\Delta^{o}_{w}\phi^{o'}$; this being related to the standard potential for ion transfer, $\Delta^{o}_{w}\phi_{i}$, by the expression

$$\Delta^{o}_{w\varphi}{}^{o'} = \Delta^{o}_{w\varphi_i} - RT/z_iF \ lnK_c + RT/z_iF \ ln\gamma C/\gamma CI \qquad (4.1.8)$$

with K_c being the complexation constant in the organic phase, and γ the activity coefficient.

If the Galvani potential difference between the two phases is varied from the formal potential, such that the potential of the organic phase is changed with respect to the water phase, see figure 4.1.1, then the electrochemical potential of the uncharged ionophore remains constant, i.e. zero, and that of the complexed ion is changed by the amount $-(\Delta^{o}_{w}\phi-\Delta^{o}_{w}\phi^{o'})$. This causes the Gibbs energy of the complexed ion to change by $z_iF(\Delta^{o}_{w}\phi-\Delta^{o}_{w}\phi^{o'})$, as is shown schematically in figure 4.1.2. The activation energy for ion transfer to oil phase, $\Delta\vec{G}_A$, is changed by a fraction of the Gibbs-energy difference:

$$\Delta\vec{G}_A = \Delta G^{o}_{A} + \alpha_{app}z_iF(\Delta^{o}_{w\varphi} - \Delta^{o}_{w\varphi}{}^{o'}) \qquad (4.1.9)$$

and the barrier to the back reaction is changed proportionately to

$$\overleftarrow{\Delta G}_A = \Delta G^{o}_{A} - (1-\alpha_{app})z_iF(\Delta^{o}_{w\varphi} - \Delta^{o}_{w\varphi}{}^{o'}) \qquad (4.1.10)$$

Eqns. (4.1.9) and (4.1.10) can be combined to give an expression for the reverse rate constant in terms of the forward rate constant

$$\overleftarrow{k_{app}} = \overrightarrow{k_{app}} \ exp[\,(z_iF/RT)(\Delta^{o}_{w\varphi} - \Delta^{o}_{w\varphi}{}^{o'})\,] \qquad (4.1.11)$$

This expression is seen to produce the correct trends in rate constants since it would be expected to show, for cation transfer from water to oil, that the rate

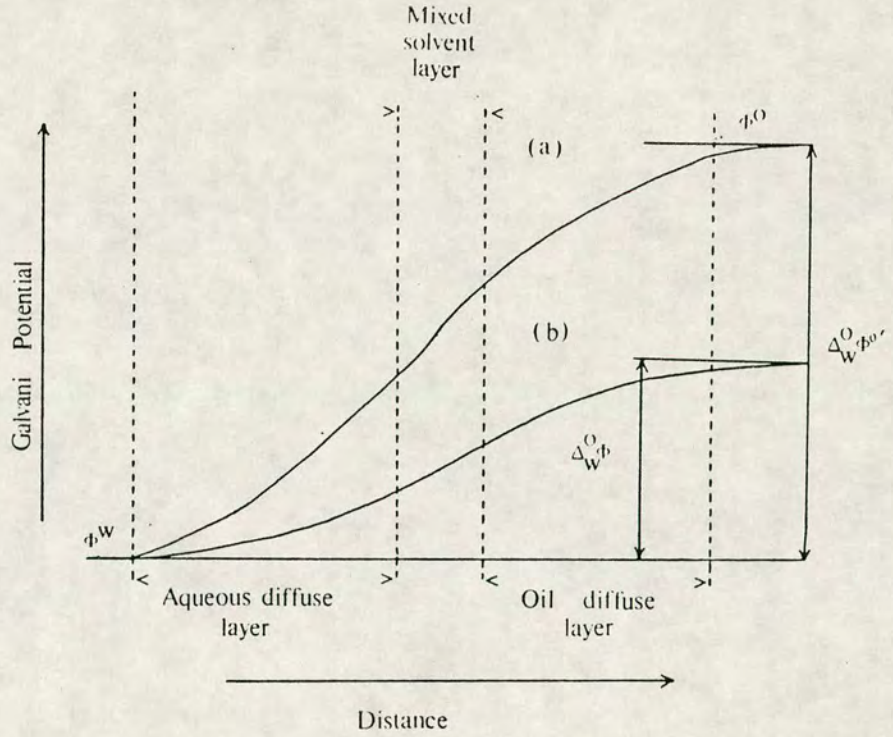

Figure 4.1.1 Schematic diagram showing the Galvani potential distribution across an ITIES. The solid lines shows the distribution for the formal case i.e. $\Delta^{o}_{w}\phi=\Delta^{o}_{w}\phi^{o'}$. The dashed line shows the distribution when the potential of the organic phase has been altered relative to the aqueous phase, so that the potential difference between the phases is now $\Delta^{o}_{w}\phi$.

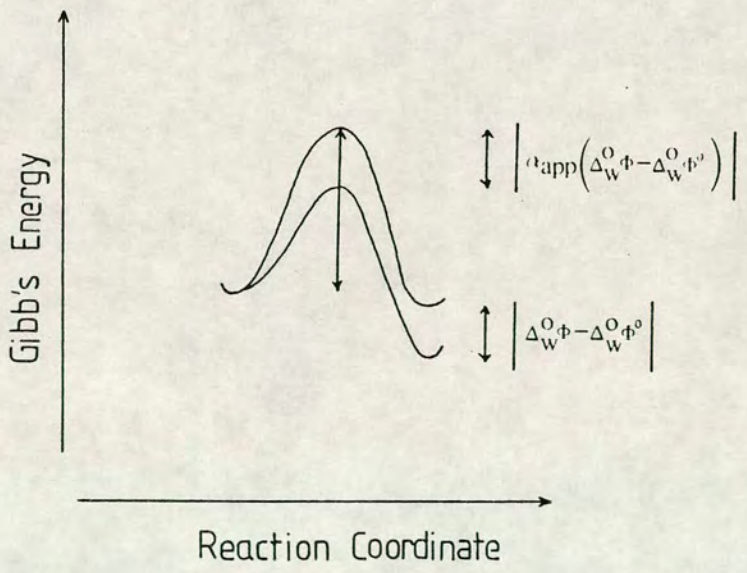

Figure 4.1.2 Simple representation of potential energy of Gibbs-energy change during an ion-ionophore reaction at an ITIES, where the potential difference between the phases is altered from the formal potential.

would be expected to increase as the potential of the organic phase is made more negative i.e. $\Delta^{o}_{w}\phi < \Delta^{o}_{w}\phi^{o'}$. For this condition the argument of the exponential term in (4.1.11) is negative, and becomes more negative as $\Delta^{o}_{w}\phi$ gets smaller, and thus either the back reaction decreases or the forward reaction increases, as expected. Eqn. (4.1.11) can be substituted into eqn.(4.1.5) to give an expression for the current for a current-potential curve,

$$i = Z_i F A c_C^b \overrightarrow{k_{app}} [(1-i/i_d) - \xi \exp((z_i F/RT)(\Delta^{o}_{w}\varphi - \Delta^{o}_{w}\varphi^{o'}))] \qquad (4.1.12)$$

which for irreversible reactions i.e. $\vec{k}_{app}$ =0, can be expressed as

$$i = z_i F A c_C^b \overrightarrow{k_{app}} (1-i/i_d) \qquad (4.1.13)$$

From these expressions it is possible to evaluate the potential dependent apparent rate constants for either quasi-reversible or irreversible facilitated ion transfers. Later in this chapter a method to use these apparent rate constants, and apparent charge transfer coefficients, to evaluate the true rate constants and charge transfer coefficients will be discussed.

4.2 Evaluation Of Apparent Rate Constant For DB18C6 Facilitated K^+ Transfer

A cyclic voltammogram showing the response for dibenzo-18-crown-6 (DB18C6) facilitated K^+ transfer across a water/1,2-dichloroethane interface supported at the tip of a micropipette is shown in figure 4.2.1. This is for a system where the K^+ is present in a large excess over the concentration of DB18C6 i.e. the cell is as shown below

Ag/AgCl/$MgSO_4$(0.1M),KCl(10mM)//TBATPB(1mM),DB18C6(0.1mM)

//TBATPB(1mM),DB18C6(0.1mM)/TBACl(1mM)/AgCl/Ag

Therefore we are in the pseudo first order conditions which are described in 4.1. It can be seen from this figure that steady-state properties are observed for K^+ transfer out of and into the pipette. This behaviour is due to spherical diffusion mass transfer control of the forward and the return charge transfers which can be explained by the transfer out of the pipette being controlled by the arrival of the ionophore by spherical diffusion to the tip, and the transfer into the pipette being controlled by the arrival of the ion-ionophore complex again by spherical diffusion. This contrasts with the behaviour described in chapter 3 for non-assisted ion transfer at a micropipette. The steady state voltammogram has been analysed by the theory described in 4.1 i.e. knowing i_d, it is possible to evaluate, at each potential chosen, relative to $\Delta^o_w\phi^{o'}$, a value of

$\vec{k}_{app}$, the potential dependent forward apparent rate constant, by manipulation of eqn. (4.1.12), i.e.

$$\overrightarrow{k_{app}} = i_d/z_iFAc_C{}^b \left[i_d/i - 1 - \exp((z_iF/RT)(\Delta^o_{w\varphi}-\Delta^o_{w\varphi}{}^{o'})) \right] \qquad (4.2.1)$$

k^o_{app} can be evaluated for these results from the equation

$$\overrightarrow{k_{app}} = k^o{}_{app} \exp[(-\alpha_{app}z_iF/RT)(\Delta^o_{w\varphi}-\Delta^o_{w\varphi}{}^{o'})] \qquad (4.2.2)$$

and figure 4.2.2 shows the $\ln\vec{k}_{app}$ *vs.* $\Delta^o_w\phi-\Delta^o_w\phi^{o'}$ relationship. This is seen to be linear and the intercept on the abscissa allows the evaluation of the standard apparent rate constant. To be able to evaluate $\vec{k}_{app}$, and thus k^o_{app}, $\Delta^o_w\phi^{o'}$ must be known accurately, which is not always the case for these types of reactions. It is therefore necessary to develop a method to evaluate the formal potential of the system. There are two ways to carry this out, one involves relating the potential scale to a real Galvani potential-difference scale, using

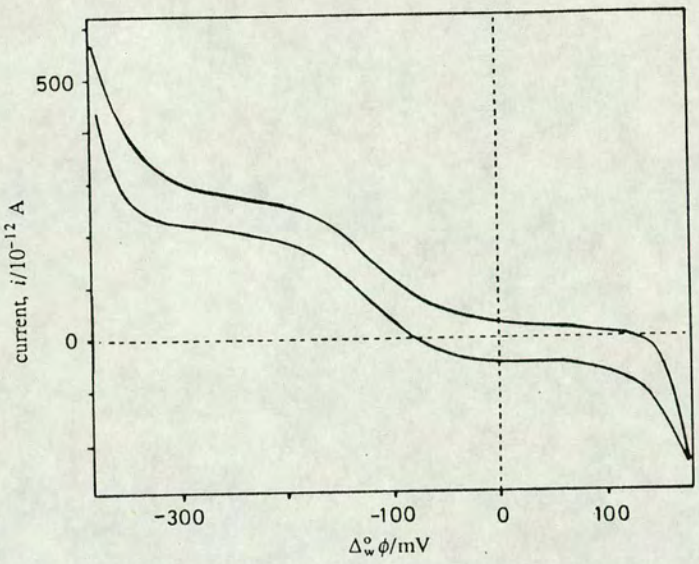

Figure 4.2.1 Cyclic voltammogram for DB18C6- facilitated K^+ transfer at an microITIES suspended at the tip of a micropipette. The cell used was that given in section 4.2. ν=0.05Vs^{-1}.

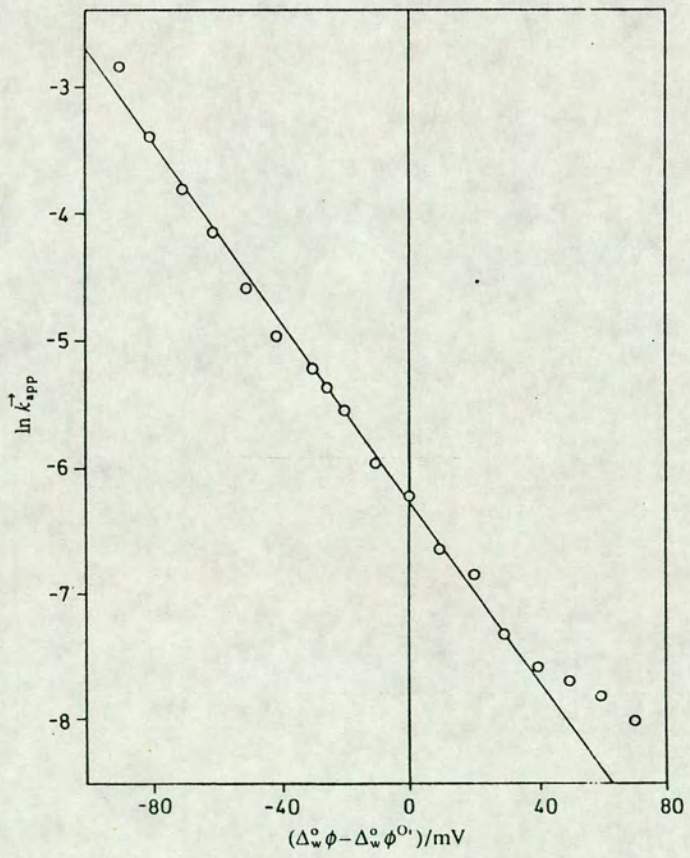

Figure 4.2.2 Plot of $\ln\vec{k}_{app}$ *vs.* $\Delta^o_w\phi-\Delta^o_w\phi^{o'}$ for the cyclic voltammogram shown in figure 4.2.1.

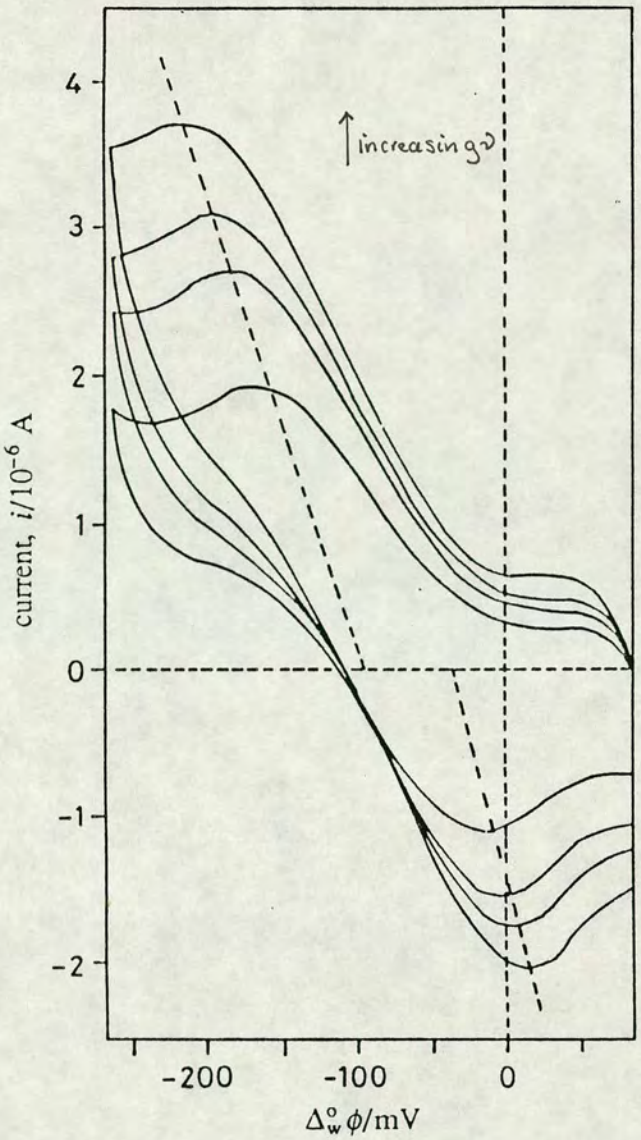

Figure 4.2.3 Cyclic voltammograms for the cell shown in section 4.2 at a large planar ITIES, used to evaluate the formal potential. ν=0.025,0.049, 0.064,0.100Vs^{-1}.

$\Delta_w^o \Phi^{o\prime}$/V	k^o_{app}/cm s^{-1}	α_{app}
−0.050	9.92×10^{-4}	0.92
−0.055	1.15×10^{-3}	0.92
−0.060	1.52×10^{-3}	0.91
−0.065[a]	1.96×10^{-3}[a]	0.91[a]
−0.070	2.46×10^{-3}	0.90
−0.075	3.08×10^{-3}	0.89
−0.0080	4.46×10^{-3}	0.87

[a] Values for the formal Galvani potential obtained by the mid-peak potential method.

Table 4.2.1 Values of k^o_{app} and α_{app} obtained for a range of formal potentials.

either the Grunwald assumption or by measuring the potential of zero charge, and then evaluate the formal potential from the standard potential for ion transfer of the species and the association constant using eqn. (4.1.8). However this involves the approximation of the activity coefficients and, as described in chapter 2, this can lead to large inaccuracies in the resulting value of $\Delta^{o}_{w}\phi^{o'}$. The other approach is drawn from the empirical method to evaluate $E^{o'}$ for reversible systems i.e. by measurement of the mid-peak potential for cyclic voltammetry at a large planar interface. However in this case, since it is a quasi-reversible system this method is not strictly correct since the peak positions are sweep rate dependent. If the positions of these peaks are extrapolated to zero sweep rate , see figure 4.2.3, then it is possible to obtain a good estimate of the formal potential. The latter method is that which is used here to evaluate the formal potential ($\Delta^{o}_{w}\phi^{o'}$) and it produces a value of -201mV. If the system is reversible then a plot of $\ln((i_d-i)/i)$ *vs.* $\Delta^{o}_{w}\phi$ allows the formal potential to be evaluated from the half wave potential i.e. $\Delta^{o}_{w}\phi_{1/2}=\Delta^{o}_{w}\phi^{o'}$, however for quasi-reversible systems there is a shift in $\Delta^{o}_{w}\phi_{1/2}$ away from $\Delta^{o}_{w}\phi^{o'}$. The steady state wave in figure 4.2.1 is analysed in this way and from this the $\Delta^{o}_{w}\phi_{1/2}$ is -236mV, which is 35mV more negative than the formal potential evaluated above, which is in the direction expected for a kinetically controlled reaction.

The potential scales reported in figures 4.2.1 and 4.2.3 can be converted to an absolute scale by measurement of the p.z.c. (potential of zero charge) for this system. It was measured by the streaming method, as described in ref. [66], and found to be -136mV, thus the standard potential is -65mV on an absolute potential scale. Table 4.2.1 shows the effect of an error in the formal potential on the standard apparent rate constant, and also on the apparent charge transfer coefficient. It can be seen that for the formal potential

evaluated that the rate constant is 1.96×10^{-3} cm s^{-1} and that the charge transfer coefficient is 0.91.

This technique has therefore produced an apparent charge transfer rate constant of the order of magnitude expected for this facilitated charge transfer reaction.

4.3 Investigation Of ETH1810 Facilitated Li^+ Transfer

Interest in N,N-dicyclohexyl-N',N-diisobutyl-*cis*-cyclohexane-1,2-carboxamide (ETH1810) comes from its identification, by Simon *et al* [67], as a good selective ionophore for lithium, used in potentiometric assays. It should, therefore, be a good ionophore to facilitate Li^+ transfer, and thus allow Li^+ transfer to occur within the polarisation of an ITIES, and be assayed amperometrically. In order to be able to do this its response at a liquid/liquid interface is characterised.

In the same way as the apparent rate constant for K^+ transfer, facilitated by DB18C6, was found, the apparent rate constant for Li^+ transfer facilitated by ETH1810 was evaluated. In this case the cell used was

Ag/AgTPBCl/TBATPBCl(1mM),ETH1810(1mM)//LiCl(0.1M)/AgCl/Ag
Q.C.E. Water

Figure 4.3.1 shows the cyclic voltammogram for such a cell for an ITIES at a micropipette, i.e. the same steady-state response for transfer into and out off the pipette as in 4.2. The equivalent cyclic voltammogram for a large planar ITIES is shown in figure 4.3.2. Inspection of the potential scales from these two figures shows that there appears to be a large potential shift of the polarisation range between the two experiments, i.e. in figure 4.3.1 the potential range is from +600 to -100 mV ($\Delta_w^o\phi$) and in figure 4.3.2 the range is from +100 to

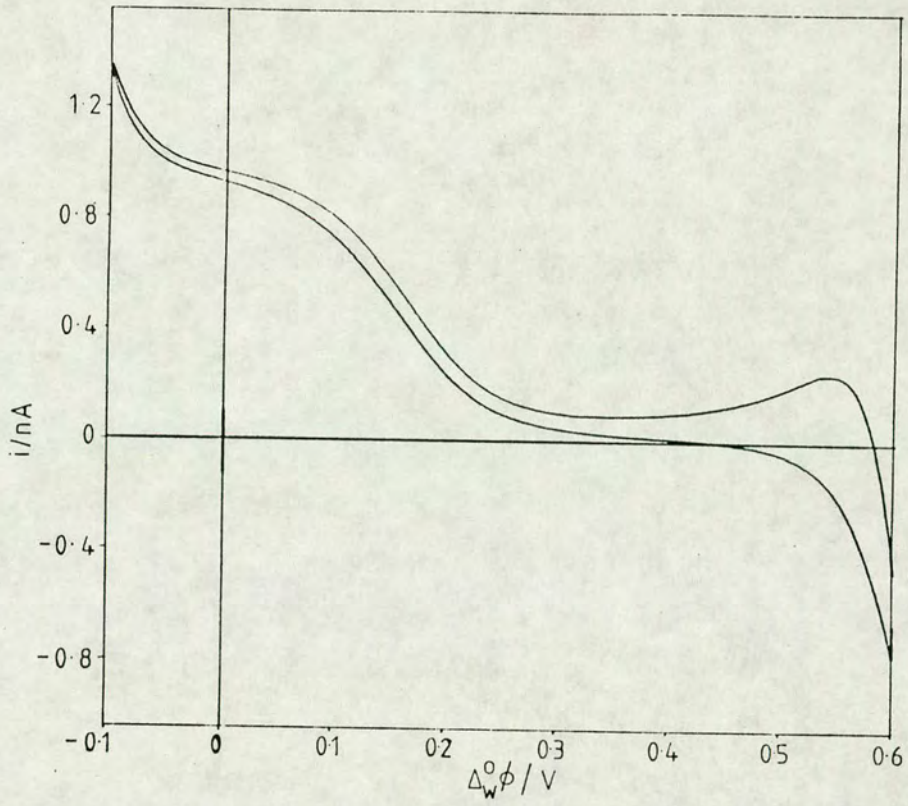

Figure 4.3.1 Cyclic voltammogram for ETH1810-facilitated Li^+ transfer at a microITIES supported at the tip of a micropipette. The cell being that described in section 4.3. ν=0.05Vs^{-1}.

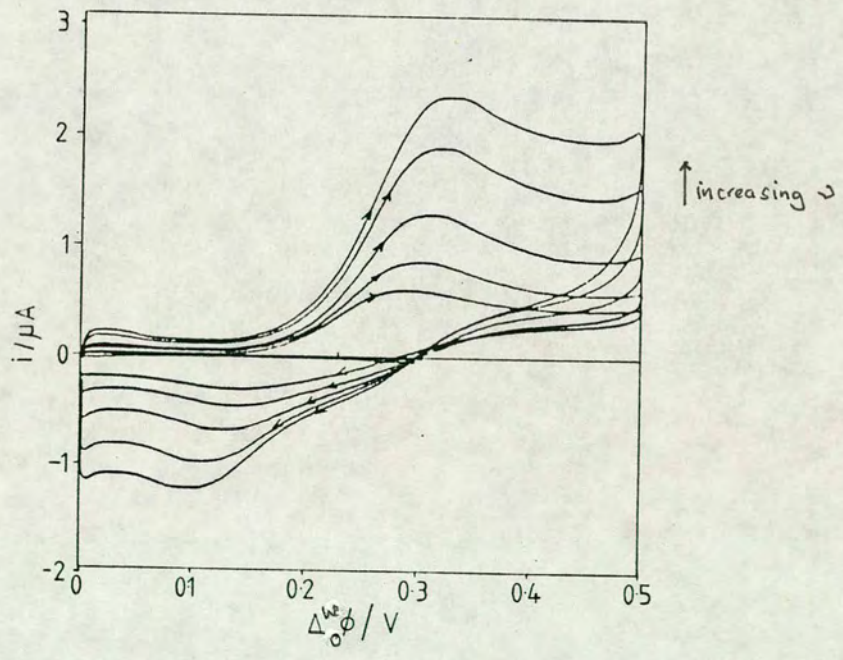

Figure 4.3.2 Cyclic voltammograms for the cell shown in 4.3 at a large planar ITIES, used for the evaluation of the formal potential. ν=0.025,0.050, 0.100,0.200,0.300Vs^{-1}.

-600mV. This can be explained by the instability of the Ag/AgTPBCl reference electrode to light and thus the composition of the electrode will change with time, thus altering its potential. In an attempt to match the potential scales from both experiments, cyclic voltammograms showing full potential windows, were superimposed, see figure 4.3.3. This however introduces a certain error, with there being a range of 150mV over which these windows could be superimposed. Figure 4.3.3 shows the "best" overlay of these windows. If it is then assumed that the large ITIES has the correct potential scale as is shown in 4.3.3, then by using the same extrapolation of peak potentials to zero sweep rate then $\Delta^{O}_{w}\phi^{o'}$ is found to be -228mV. This point is illustrated in figure 4.3.3 by a cross on the potential scale. Then by using this potential as $\Delta^{O}_{w}\phi^{o'}$ in the micropipette experiment is was possible to evaluate an approximate value of k^{o}_{app} for ETH1810 assisted Li^{+} transfer. The plot of $\log_e \vec{k}_{app}$ *vs.* $\Delta^{O}_{w}\phi$ is shown in figure 4.3.4, which was used to evaluate the apparent standard rate constant, and table 4.3.1 shows k^{o}_{app} values for other possible $\Delta^{O}_{w}\phi^{o'}$'s and thus indicates the error introduced by using this window matching technique. It can be seen that there is an order of magnitude change in the apparent standard rate constant when $\Delta^{O}_{w}\phi^{o'}$ is changed by 0.05V. It is shown that for the $\Delta^{O}_{w}\phi^{o'}$ value estimated for this transfer reaction that k^{o}_{app} is 0.014 cms^{-1}, and α_{app} is 0.49, however the error in this value must be stressed.

Shao *et al* [68], has also studied the facilitated transfer of Li^{+} at a 1,2-dichloroethane/water interface. We have shown that the voltammetric response for this system shows a dependence on pH. For low pH's only a reversible response is observed, which has been shown to correspond to facilitated ion transfer. At higher pH's i.e. 10.25, only a quasi-reversible/irreversible cyclic voltammogram is seen, with $\Delta^{o}_{w}\phi^{1/2}$ being at a more positive potential than at the low pH, this must correspond to Li^{+}

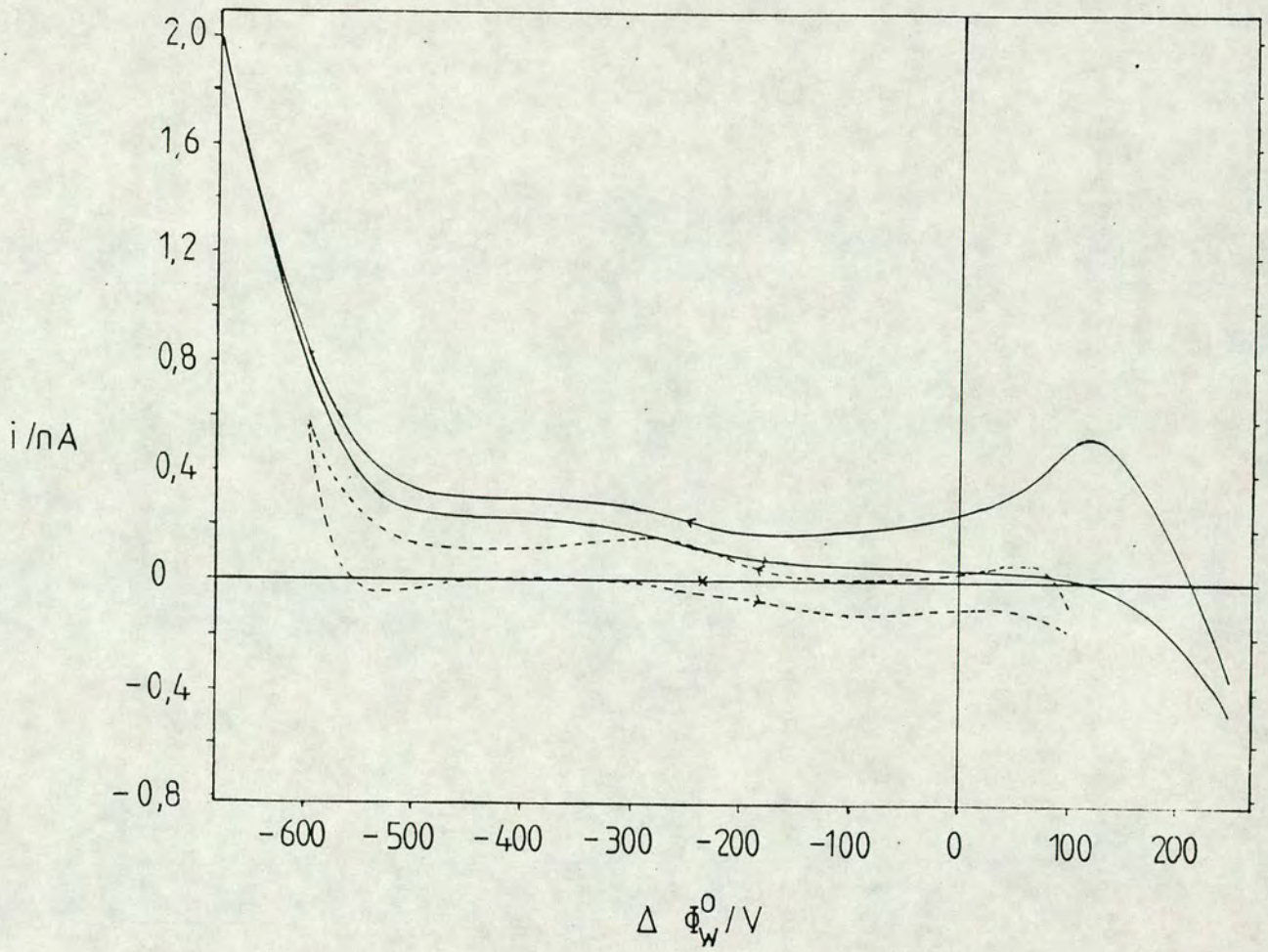

Figure 4.3.3 Superimposition of potential windows for both large and microITIES used to match potential scales for the cell in 4.3.

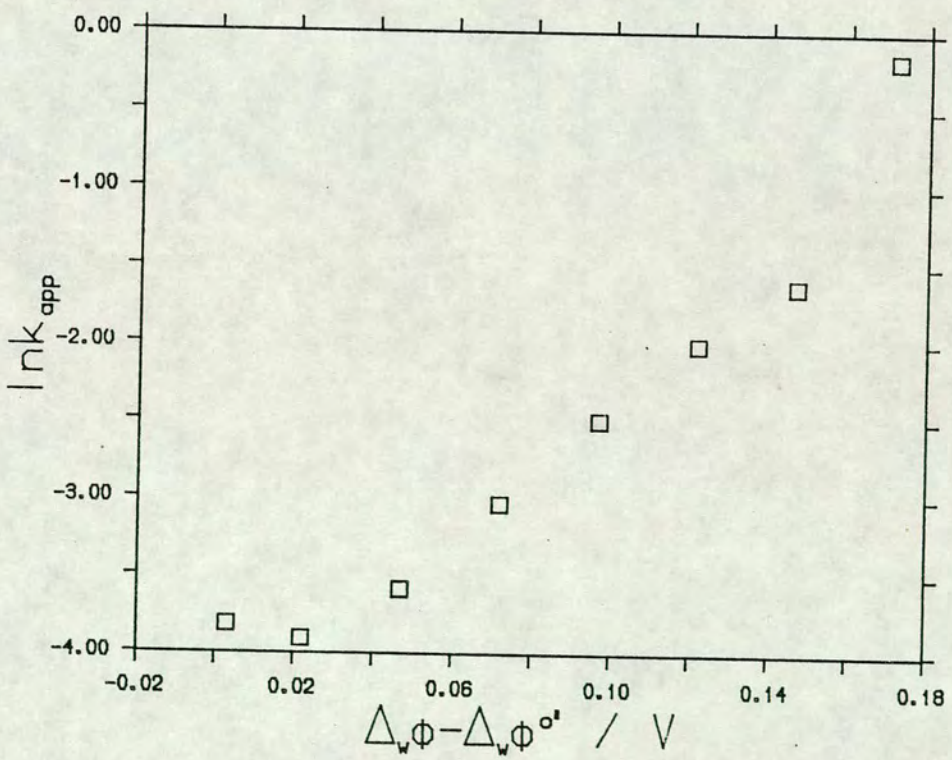

Figure 4.3.4 Plot of $\ln \vec{k}_{app}$ *vs.* $\Delta^{o}_{w}\phi - \Delta^{o}_{w}\phi^{o'}$ for the cyclic voltammogram shown in figure 4.3.1.

facilitated transfer only. The pH of the solutions used in the micro ITIES experiment is c.a. 6.6 and Shao has suggested that at this intermediate pH, the voltammetric wave produced is due to the mixed transfer of Li^+ and H^+, both being facilitated by ETH1810. If large concentrations of Li^+ are used, relative to H^+, then it would be expected that the wave should become more characteristic of Li^+ transfer, however this may not occur at the Li^+ concentrations expected due to ETH1810 being approximately 10 times more selective towards protons than lithium ions. As well as making these observations about the effect of pH on the reaction taking place Shao has also investigated the rate constants for transfer, and charge transfer coefficients using chronocoulometry [36]. He has evaluated α_{app} to be 0.45 and $k^o_{app} \simeq 5.9 \times 10^{-3} cms^{-1}$. Again there is an error in $\Delta^o_w\phi^{o'}$ due to the approximation discussed in 4.2, however in this case there is no need to window match, thus these values are more accurate than those found by the micropipette techniques. Comparison with the results from the micropipette experiment suggest that the $\Delta^o_w\phi^{o'}$ value used in the micro ITIES experiment is wrong by approximately 30mV and this could be explained by incorrect matching of the potential windows.

From these results it can be assumed that the apparent rate of charge transfer is approximately 5×10^{-3} cms^{-1} and that α_{app} is *c.a* 0.5. Assuming that the conclusions, about mixed transfer at pH 6.6, are correct then it can be said that this transfer of H^+ and Li^+ is a relatively slow reaction and that the transfer of H^+ is a fast, reversible reaction when facilitated by ETH1810.

4.4 Evaluation Of The Rate Of Transfer Of Li^+ Transfer Facilitated By 2,9-Dibutyl-1,10-Phenanthroline

Another group of ligands which have been shown to be good selective ionophores are 1,10-phenathroline derivatives,[69], with the most selective

$\Delta^{o}_{w}\phi^{o'}$ / V	k^{o}_{app} / cms^{-1}	α_{app}
−0.200	0.0044	0.57
−0.210	0.0071	0.52
−0.220	0.0087	0.54
−0.228	0.0140	0.49
−0.240	0.0213	0.45
−0.250	0.0450	0.32

Table 4.3.1 Values of k^{o}_{app} and α_{app} obtained for a range of formal potentials.

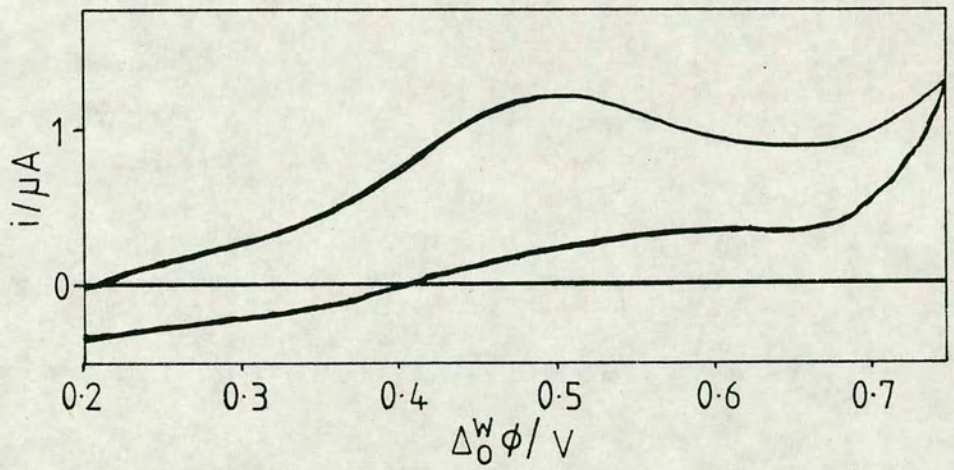

Figure 4.4.1 Cyclic voltammogram for the cell shown in section 4.4 (the ionophore being 2,9-dibutyl-1,10-phenanthroline), at a large planar ITIES. ν=0.100Vs^{-1}.

species, towards Li^+, being the 2,9-dibutyl derivative. Here its use as an ionophore to facilitate Li^+ at a 1,2 dichloroethane/water interface using the method presented in 4.1 is investigated, and its apparent rate constant for transfer is estimated.

In order to evaluate $\Delta^o_w\phi^{o'}$ a macro ITIES experiment was carried out using the cell

Ag/AgTPBCl/TBATPBCl(1mM),ionophore(1mM)//LiCl(0.1M)/AgCl/Ag

the resulting cyclic voltammogram is shown in figure 4.4.1. It can be seen from this that there is no return peak suggesting that this is an irreversible process, and hence it is not possible to estimate a value for $\Delta^o_w\phi^{o'}$ in the way described in 4.1.

The micro ITIES experiment was carried out using the same cell as described above, and the cyclic voltammogram for this is shown in figure 4.4.2. It can be seen that again a steady state response is found for both ingress and egress facilitated ion transfer. From this voltammogram it is possible to evaluate $\Delta^o_w\phi_{1/2}$, the half wave potential, which is known for an irreversible system to be shifted from the $\Delta^o_w\phi^{o'}$ value. The steady state wave is then analysed as for an irreversible process, i.e. eqn. (4.1.13), yielding a range of potential dependent $\vec{k}_{app}$ values. It is then possible to evaluate k^o_{app} and α_{app} by plotting $\ln k^o_{app}$ *vs.* $\Delta^o_w\phi$ (see figure 4.4.3) from the relationship

$$\ln\vec{k}_{app} = \ln k^o{}_{app} - (\alpha_{app}z_iF/RT)\Delta^o_{w\varphi} + (\alpha_{app}z_iF/RT)\Delta^o_{w\varphi}{}^{o'} \qquad (4.4.1)$$

assuming $\Delta^o_w\phi^{o'}$ is known. Table 4.4.1 shows the values of k^o_{app} evaluated by this method for values of $\Delta^o_w\phi^{o'}$ which are shifted by 0,20,40,60 and 80mV from the $\Delta^o_w\phi_{1/2}$ value, i.e. -60mV. This shows that the values of k^o_{app}

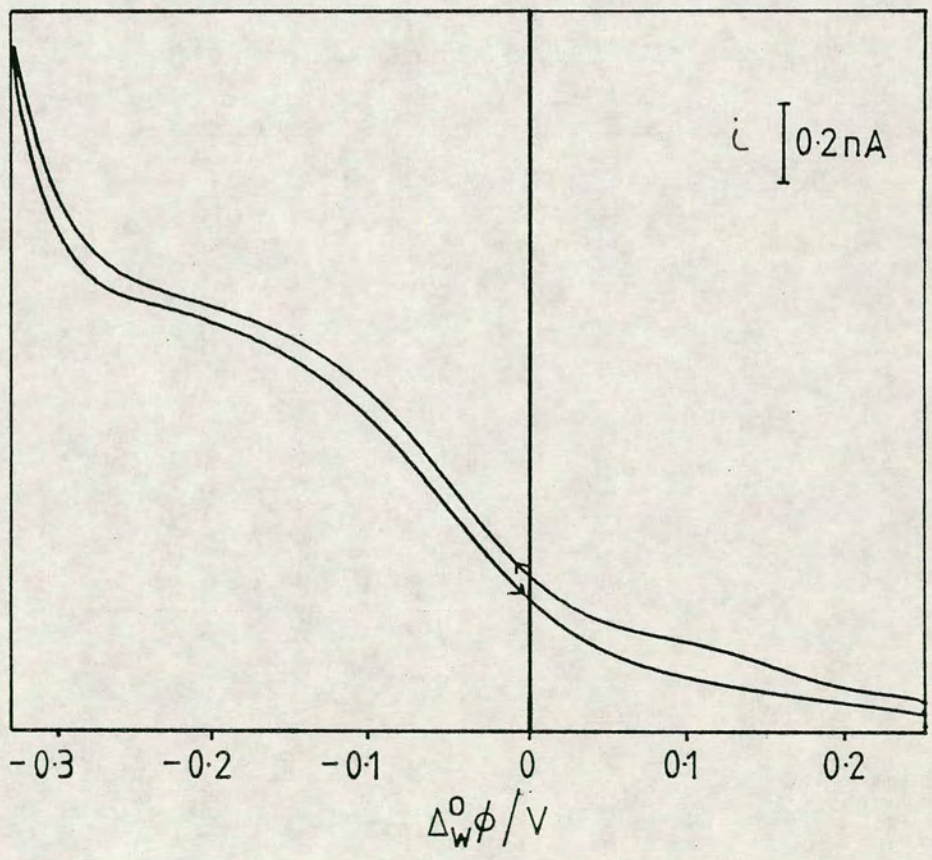

Figure 4.4.2 Cyclic voltammogram for the same as used in figure 4.4.1, at a microITIES. ν=0.05Vs^{-1}.

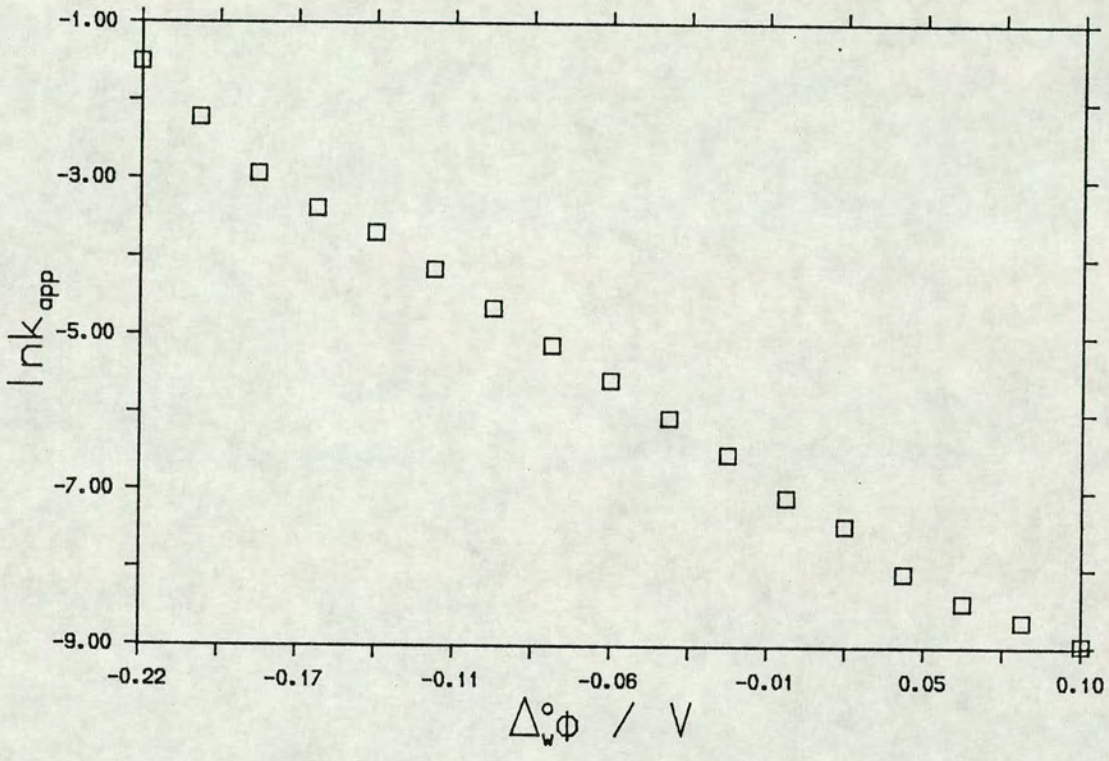

Figure 4.4.3 Plot of $\ln \vec{k}_{app}$ *vs.* $\Delta^{\circ}_{w}\phi$ for the cyclic voltammogram shown in figure 4.4.2.

range between $3.6x10^{-3}$ to $5.4x10^{-4}$ cms^{-1}, which indeed suggest that the facilitated transfer of Li^+ by 9,2-dibutyl- 1,10-phenanthroline ia an irreversible process. This implies that Li^+ becomes very strongly complexed by the ionophore, only being released as high over-potentials are applied, Li^+ being able to return to the aqueous phase after either being decomplexed by the ionophore and then crossing, or by dragging the ionophore into the aqueous phase. If it is the former process then the activation energy for de-complexation must be large, or if it is the latter then the activation energy for transfer must be large, as would be expected to force a very hydrohpobic molecule to cross into the aqueous phase.

These results show that, although it is not possible to accurately determine the apparent rate constant for facilitated ion transfer, the reaction is slow enough to be classed as irreversible.

$\Delta^{o}_{w}\phi$ / V	$\vec{k}_{app}$ / cms^{-1}
0.10	$1.27x10^{-4}$
0.08	$1.72x10^{-4}$
0.06	$2.18x10^{-4}$
0.04	$3.15x10^{-4}$
0.02	$5.83x10^{-4}$
0.00	$8.31x10^{-4}$
-0.02	$1.45x10^{-3}$
-0.04	$2.29x10^{-3}$
-0.06	$3.74x10^{-3}$
-0.08	$5.91x10^{-3}$
-0.10	$9.38x10^{-3}$
-0.12	$1.55x10^{-2}$
-0.14	$2.48x10^{-2}$
-0.16	$2.48x10^{-2}$
-0.18	$3.41x10^{-2}$
-0.20	$5.27x10^{-2}$
-0.22	$1.09x10^{-1}$

Table 4.4.1 Values of k^{o}_{app} obtained for a range of formal potentials.

Chapter 5
Electrochemical Determination Of Catecholamines

5.1 Introduction

The ability to accurately determine the quantities of certain species in biological fluids is of great importance to be able to gain an understanding of both the functions of these species and also the ability of drugs to effect the levels of such species in the body. One of the most common groups of such species, called neurotransmitters, are the catecholamines which are responsible for the control of large areas of both the peripheral and central mammalian nervous systems. In particular, catecholamines have been linked to various types of mental disorders e.g. depression, schizophrenia and recently a link between a deficiency in the catecholamine, dopamine, in the caudate nucleus and Parkinson's disease has been postulated [70]. Therefore a technique which allows the determination of catecholamines in these areas of the central nervous system (C.N.S.) either by extraction of the extra cellular fluid and then analysis, or by direct *in vivo* analysis, is important.

Until around the mid 1970's there were five techniques which were used for quantitative analysis of catecholamines i.e. bioassay, spectrophotometry, spectrofluorometry, gas and high performance liquid chromatography and radio assay. These provided a sensitivity range of 10μg, for spectrophotometry, to 1pg, for gas chromatography and radio assays. The main drawback of such techniques is that none can be used for *in vivo* applications and thus require removal of fluid, or tissue, from the region of interest and then analysis, usually after a pretreatment of the solution.

It was not until the mid 1970's that electrochemistry was used to directly monitor catecholamines, without pretreatment of solutions, although their electrochemical properties had been widely studied before this time [71,72], and it also had been used as the detection system for HPLC. With the advent of microelectodes, the direct electrochemical monitoring of catecholamines [73] became possible, due to the size of such electrodes allowing them to be employed *in vivo*. The reason why electrochemistry seemed such a suitable tool to analyse solutions containing catecholamines was their ease of oxidation and, as mentioned above, their oxidation reactions have been widely studied, as well as the oxidations of their precursors and metabolites.

The use of electrochemistry to analyse solutions containing catecholamines however has some limitations. The major problem being that the oxidation which occurs is that of the aromatic hydroxyl groups to carbonyl groups, i.e.

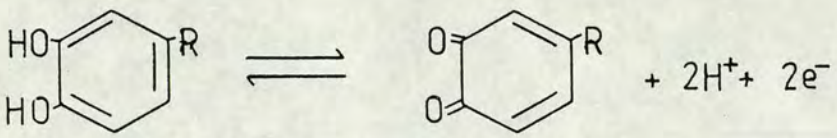

and that these hydroxyl groups are common not only to the catecholamines which are neuroactive, but also to their precursors and metabolites. Therefore the oxidation potentials of most of these compounds are within *c.a.* 50mV, thus making the determination of one species in a solution containing the precursors and metabolites, very difficult. Another similar problem is that in areas where catecholamines are commonly found in the mammalian C.N.S., ascorbic acid is also found at much higher concentrations and this has an oxidation potential which is very close to those of catecholamines. Several techniques have been used to overcome these problems, most of which involve some kind of modification of the electrode surface being used. Three pretreatment methods have dominated this modification process each having

different effects on the selectivity of the surface towards the active and interfering species.

Electrochemical pretreatment, by rapidly cycling between 0 and +3V,at 70Hz, for 20s, at a carbon fibre microelectrode, alters the surface groups of the electrode such that the oxidation potential of ascorbic acid becomes more negative than that of the catecholamines and their metabolites [74,75].

The second pretreatment used involves the immobilisation of ascorbic acid oxidase on the electrode surface, which causes any ascorbic acid which is in the vicinity of the electrode to be converted into dehydroascorbate, which is electroinactive. Thus allowing catecholamines to be detected without interference for ascorbic acid [76].

The third method involves chemically altering the electrode surface either by incorporating stearic acid into a carbon paste mixture [77–79] or by coating the electrode surface with an ion exchange membrane [80–82]. The basis of this method is that the interfering ions i.e. the catecholamine metabolites, and precursors, and ascorbic acid are anions at physiological pH, whereas the catecholamines are cations. Thus these species will be repelled by a surface which is overall negatively charged. In the case of stearic acid modified carbon paste electrode it is the negative charge of the stearate which causes the repulsion. In the latter case the ion exchange membrane is usually Nafion, which is a perfluorosulphonated form of teflon, and it is a cation exchanger, i.e. if the electrode surface is coated with this, only the cationic catecholamines will be able to reach the electrode surface.

Although these techniques have been sucessful in eliminating the interference from ascorbic acid and the anionic catecholamine species, it is still difficult to distinguish between cationic catecholamine species. In this chapter

two alternative techniques to determine catecholamines will be discussed, one involves the use of liquid/liquid interfaces and the other uses enzymes which are active on catecholamines.

5.2 The Determination Of Catecholamines By Ion Transfer At An ITIES

As discussed in the introduction to this chapter the catecholamines of importance are cationic at physiological pH and that the major interferents of these species were anionic. Thus it would be expected that it should be possible to distinguish between these species very easily by investigating their ion transfer at a liquid/liquid interface. It had been shown by other studies that the standard Gibb's free energies of transfer [32] suggest that it should be possible to have the catecholamines dopamine, epinephrine and norepinephrine crossing within a suitable polarisation window. The structures of these three species are shown below.

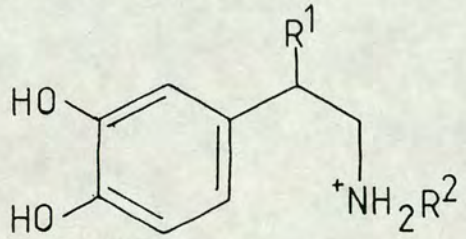

R^1=H,R^2=H Dopamine

R^2=H,R^1=OH Norepinephrine

R^2=Me,R^1=OH Epinephrine

The transfer of these species at both nitrobenzene/water and 1,2-dichloroethane/water interfaces have been investigated using the following cell, where the ITIES is supported at the tip of a micropipette.

Ag/AgCl/TBACl(1mM)/TBATPBCl(1mM)/

/catecholamine(500µM),LiCl(1mM)/AgCl/Ag

A typical cyclic voltammogram produced for such a system is shown in figure 5.2.1 for dopamine. It can be seen from this figure that the transfer of these

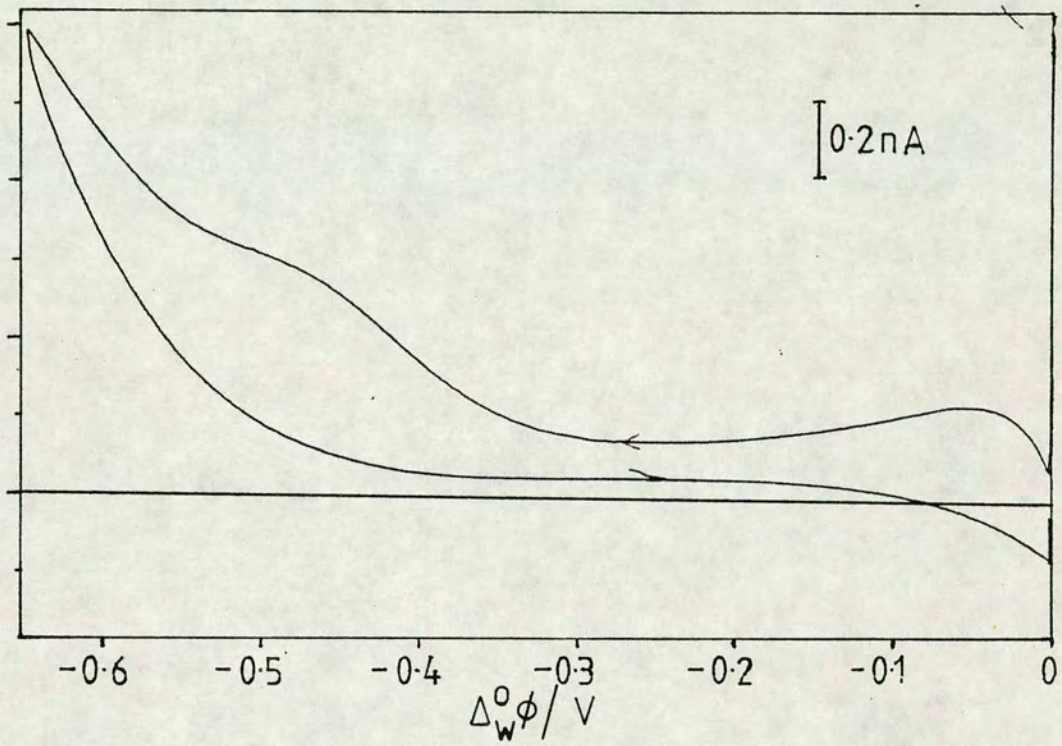

Figure 5.2.1 Cyclic voltammogram for the cell shown in section 5.2 for ion transfer at an ITIES suspended at the tip of a micropipette. The catecholamine in this case being dopamine.

ions occurs at potentials which are very close to the polarisation limit of the potential window, which in this case is limited by Li^+ transfer from the aqueous to the organic phase. Thus it is very difficult to use this system to quantitatively determine these species in solution. The problem with the transfer potentials being too near the end of the potential window will become accentuated if a solution near, in composition, to that of extra-cellular fluid, was to be used. This would be due to the presence of other alkali metal ions in solution, instead of Li^+ e.g. Na^+ and K^+. These ions further shorten the potential window of the system, and thus neither DA, NE or E would cross within this window. Therefore simple ion transfer will not provide a suitable method to determine the concentrations of these species, although it can be shown that individually they transfer at potentials far enough apart for them to be resolved. (See figure 5.2.2).

As described in chapter 4 a possible way to alter the potential at which an ion will cross a liquid/liquid interface is by the use of an ionophore in one or the other of the phases, (usually the organic). It is known that quaternary nitrogen groups can be complexed by crown ethers and therefore each of the three species being investigated, which contain quaternary nitrogens, should be complexed by a suitable crown ether e.g. DB18C6. Thus the transfer potential of these ions can be altered by the use of a crown ether in the organic phase. However again we expect to see an interference in the facilitated transfer due to the presence of Na^+ and K^+ ions, both of which are complexed by crown ethers. This leads to the requirement of a much more selective complexing agent in the organic phase for catecholamines. One such complexing agent has been designed by Kimura *et al* [83] and it involves a molecule which has two active complexing groups i.e. a hexaaza macrocycle and a crown ether, which bind the catechol moiety and the quaternary nitrogen respectively. This ditopic

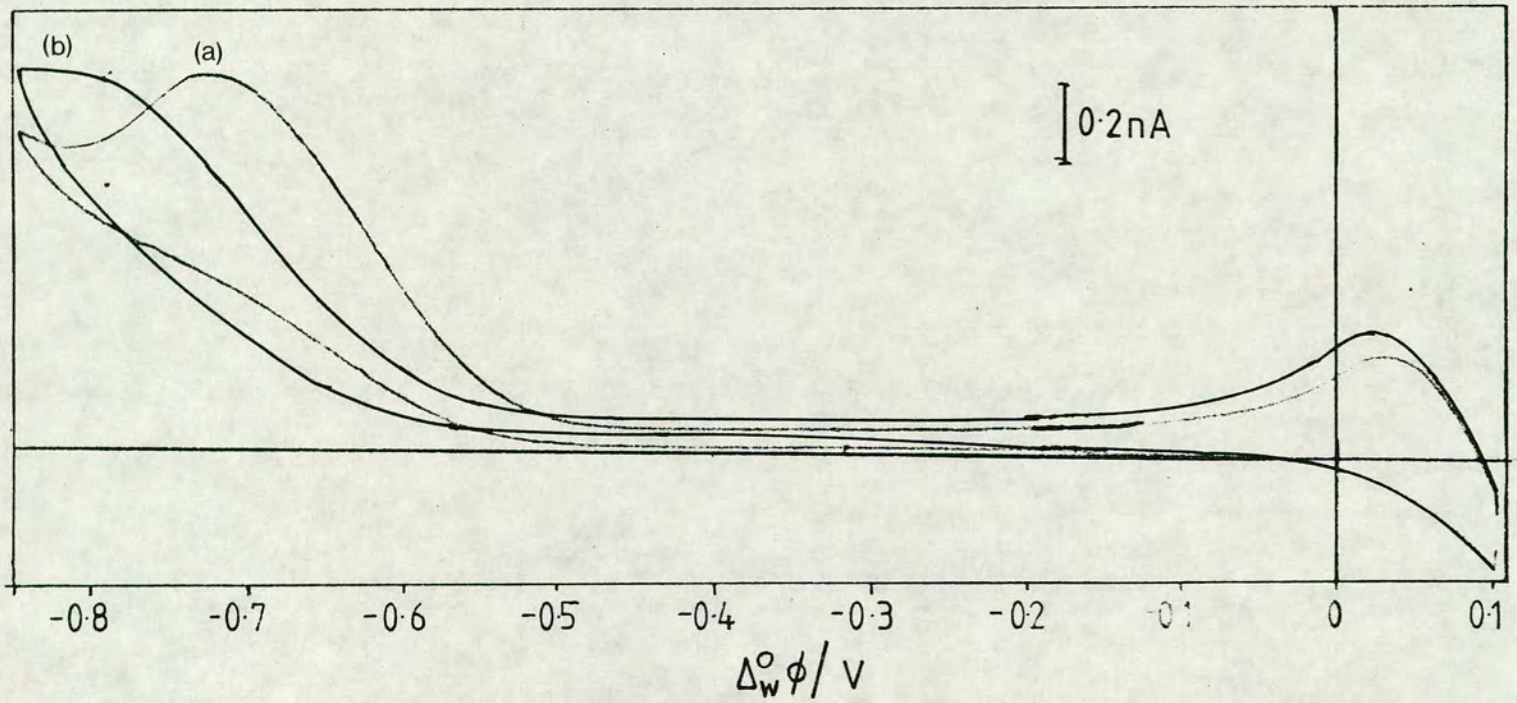

Figure 5.2.2 Superimposition of cyclic voltammograms of cell Ag/AgCl/TBACl(1mM)/TBATPBCl(1mM)//catecholamine(10mM)/AgCl/Ag, where the scan has been taken past the "end" of the polarisation window to show the transfers of (a) dopamine, (b) norepinephrine, (No supporting electrolyte in water phase).

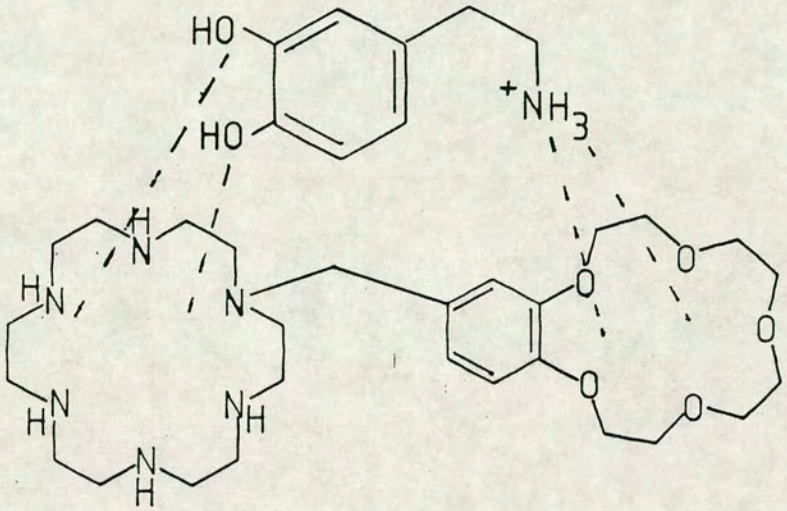

Figure 5.2.3 Diagram of the ditopic receptor designed by Kimura *et al.*, showing the postulated complexation position of dopamine.

receptor molecule is shown in figure 5.2.3 with the postulated complexed position of dopamine. The use of this molecule to facilitate DA transfer has been investigated at a DCE/water interface, however with little success. The problem which appears to arise is that in the pH ranges investigated the hexaaza ring becomes protonated and thus this half of the molecule prefers to be solvated in the aqueous phase, whilst the crown ether prefers to be in the organic phase. This leads to the molecule straddling the interface and not being able to facilitate the transfer of the catecholamine molecules. Essentially the ditopic receptor is adsorbed at the interface thus disrupting any ion transfer reactions across this interface. It may be possible to overcome this problem with the hexaaza ring by alkylating the nitrogens in this ring and thus making it sufficiently hydrophobic to remain dissolved in the organic phase. However, to date, this molecule has not been synthesised.

These results suggest that the direct detection of catecholamines at a liquid/liquid interface is unlikely, due to the problems outlined. However with the design of a more specific ionophore for these molecules it is likely that techniques used at ITIES will be able to determine catecholamines in solution. This, along with the use of ITIES supported at tips of micropipettes, should allow their determination *in vivo*.

5.3 Use Of Enzymes For The Determination Of Catecholamines

As discussed in section 5.2 the detection of catecholamines by ion transfer techniques is not as straight forward as had been expected and certain obstacles have been found to prevent its use. Another possible way to specifically allow the detection of catecholamines is by incorporating an enzyme into the system which specifically acts on catecholamines. The

electrochemical determination may then involve the direct detection of the products of the enzymatic reaction by either oxidation/reduction or by an ion transfer technique, or by the oxidation/reduction of the enzyme itself.

Four enzymes which are active on catecholamines are discussed here i.e. dopamine-β-hydroxylase, catechol-O-methyl transferase (COMT), monoamine oxidase (MAO), and tyrosinase. Biologically these enzymes are involved in either the metabolism of catecholamines to other active species or to inactivate species. A brief summary of the actions of these enzymes on dopamine is shown schematically in figure 5.3.1.

5.3.1 Actions Of Dopamine-β-Hydroxylase

Dopamine-β-hydroxylase is involved in the biosynthesis of norepinephrine from dopamine. It is a copper-dependent mono-oxygenase redox enzyme which contains two Cu^{2+} ions in its inactive state, which have to be reduced to Cu^{+} in order to activate the enzyme towards hydroxylation. Naturally this is carried out by ascorbate which gets oxidised to dehydroascorbate, the Cu^{+} ions then bind dioxygen and activate it towards the hydroxylation of dopamine. The hydroxylation then occurs and the enzyme is oxidised to its inactive state, with the production of one molecule of water.

The products of this process are norepinephrine and dehydroascorbate. The former having a very similar oxidation potential to dopamine, and thus the same problems are associated with its determination, and the latter not being electroactive since the oxidation of ascorbate is an irreversible process. As well as the products not being suitable for the determination of catecholamines, it is most unlikely that it should be possible to electrochemically reactivate the enzyme, i.e. $Cu^{2+}+e^{-}\rightarrow Cu^{+}$, due to the presence of ascorbate, the natural activator, in very high concentrations *in vivo*.

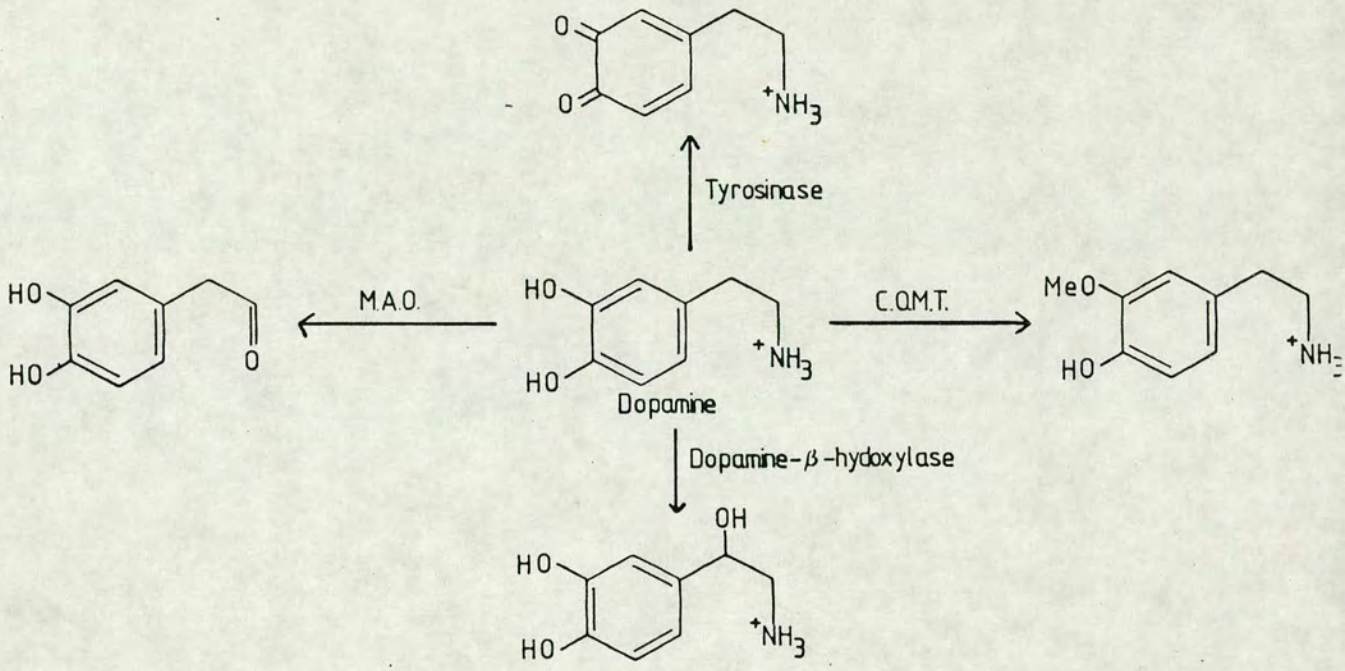

Figure 5.3.1 Schematic diagram summarising the action of the enzymes dopamine-β-hydroxylase, catechol-*O*-methyl tranferase, monoamine oxidase and tyrosinase on dopamine.

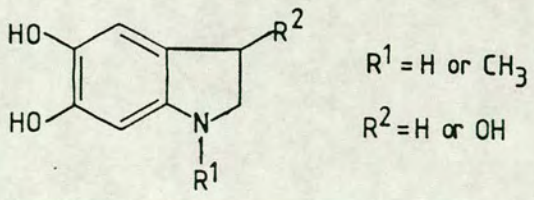

Figure 5.3.2 Leukochrome, product of catecholamine oxidation.

For the reasons outlined above it is assumed that this enzyme is unsuitable for the electrochemical determination of catecholamines.

5.3.2 Actions Of Tyrosinase (Polyphenol Oxidase)

Tyrosinases are cuproenzymes which catalyse ortho-diphenols (e.g. catecholamines), in a two electron process, to ortho-quinones, i.e. the standard oxidation products of catecholamines. The net stoichiometry of the reaction is that 2 moles of diphenol are dehydrogenated per mole of dioxygen consumed, thus O_2 undergoes a net 4-electron reduction to give 2 molecules of water. Studies have shown that for this reaction the copper, present in the enzyme as Cu^+, does not undergo any detectable valence change, and therefore the enzyme itself is not being oxidised/reduced. The mechanism proposed for this reaction involves the exchange of one of the phenol oxygen atoms with an oxygen atom from dioxygen.

As the enzyme does not undergo any redox reaction it is not possible to detect quantities of catecholamines by the direct electrochemistry of the enzyme. The product of the reaction i.e. the o-quinone, is known to undergo a ring closure reaction, at physiological pH [71], which gives a product, a leuko-chrome (see figure 5.3.2) which has an oxidation potential which is lower than that of the parent catecholamine. This potential is sufficiently altered from the catecholamines and their interferents, that it may be possible to indirectly determine the quantity of catecholamine by oxidation of the leuko-chrome product. However so far it has not been possible to correlate quantities of catecholamines present to the oxidation current for the leuko-chrome. A possible reason for this maybe that, due to its low oxidation potential, the leuko-chrome product is able to reduce the o-quinone product. This complicates the following chemical reactions since it will reduce the

concentrations of o-quinone which can then undergo ring closure and also the amount of leuko-chrome which can be electrochemically oxidised. Also it is likely that the leuko-chrome product, having such a low oxidation potential, will be oxidised by any oxygen which is dissolved in the solution. Further studies of the following reactions would have to be made before this system could be used as a method for catecholamine detection.

5.3.3 Action Of Mono-Amine Oxidase (MAO)

Mono-amine oxidase (MAO) is a flavoprotein oxidase which converts neuroactive amines into inactive aldehydes, these aldehydes are then either oxidised or reduced, to their final products, (the reaction scheme is shown in figure 5.3.3). The initial product of the oxidation is an aldimine, which is rapidly hydrolysed to the aldehyde and ammonia. The enzyme, now in a reduced state, is then oxidised back to its active form by dioxygen, with the formation of one mole of hydrogen peroxide (H_2O_2).

The products of this enzymatic reaction are dihydroxyphenylethanol or dihydroxyphenylacetic acid, for reduction and oxidation of the aldehyde, respectively. Both of these products undergo the same oxidation as the parent catecholamine, i.e to the o-quinone, and these occur at potentials very close to that of the parent catecholamine. This makes the measurement of these productsan unsuitable method to evaluate catecholamines. It may however be possible to evaluate the quantity of the reduced form of the enzyme either by its direct electrochemical oxidation or by evaluation of the quantity of H_2O_2, produced by the reactivation of the enzyme, electrochemically. One of the problems of using the latter method, i.e. oxidation of H_2O_2, is that the determination is dependent on the concentration of dioxygen in solution. Other flavoprotein enzymes have been used in systems to determine different species

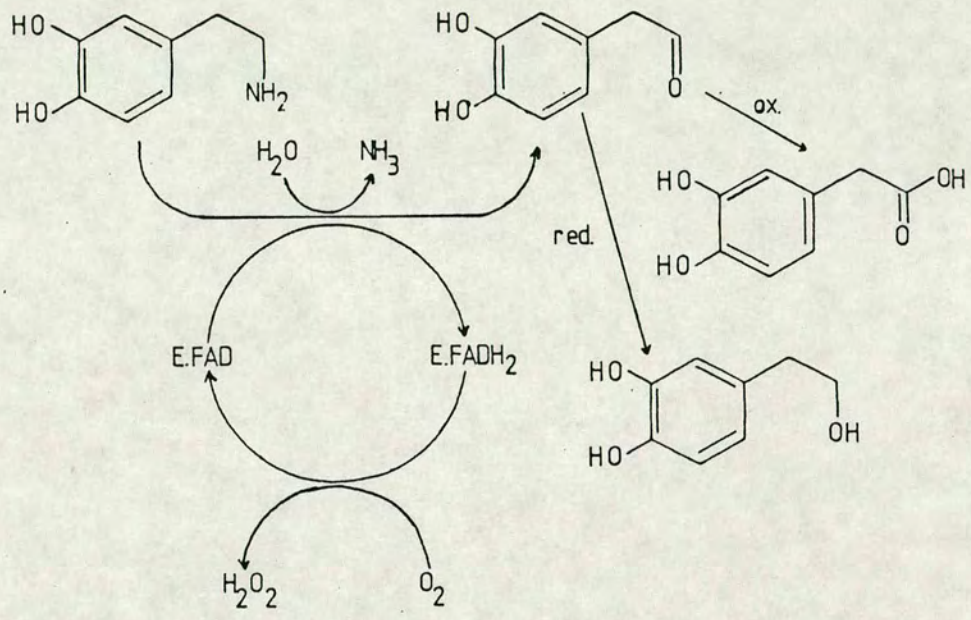

Figure 5.3.3 Reaction scheme showing the action of mono-amine oxidase on a catecholamine.

in solution e.g. glucose using glucose oxidase [84], and the problem with O_2 concentrations has been overcome by using mediators to oxidise the enzyme back to its active state. Figure 5.3.4 shows schematically a comparison of the two systems. These mediators have a much higher affinity for the enzyme than O_2 and therefore is the dominant reaction. The type of mediators which have mainly been used for such systems are substituted ferrocenes, e.g. ferrocene carboxylic acid. It may therefore be possible to find such a mediator to be active on MAO and thus be used for the determination of catecholamines.

The direct electrochemical oxidation/reduction of MAO has been investigated by cyclic voltammetry at a pyrolytic carbon electrode. As can be seen in figure 5.3.5 MAO gives no electrochemical signal over the polarisation range -200mV to +500mV (vs. Ag/AgCl). Thus this is not a suitable method to regenerate the enzyme to determine the quantity of a catecholamine.

The determination of catecholamines by measurement of levels of H_2O_2, electrochemically, is difficult due to their ease of oxidation, i.e. their oxidation occurs at a potential which is less than H_2O_2. Therefore any oxidation of H_2O_2 will also cause an oxidation of catecholamines, thus reducing the levels of them that can react with the enzyme. Thus it is necessary to find a mediator which can be used for this system. So far all of the species tested as mediators have an oxidation potential greater than that of the catecholamines and therefore the same problem as found with H_2O_2 arises. Figure 5.3.6 shows cyclic voltammograms for dopamine and ferrocenecarboxylic acid which hightlight this problem. The type of mediator which is required is a water soluble species which, in its reduced form, has an oxidation potential which is less than the that of the catecholamines. The problem with such species is that they tend not to be stable in aqueous solutions, as they are oxidised by any dissolved O_2.

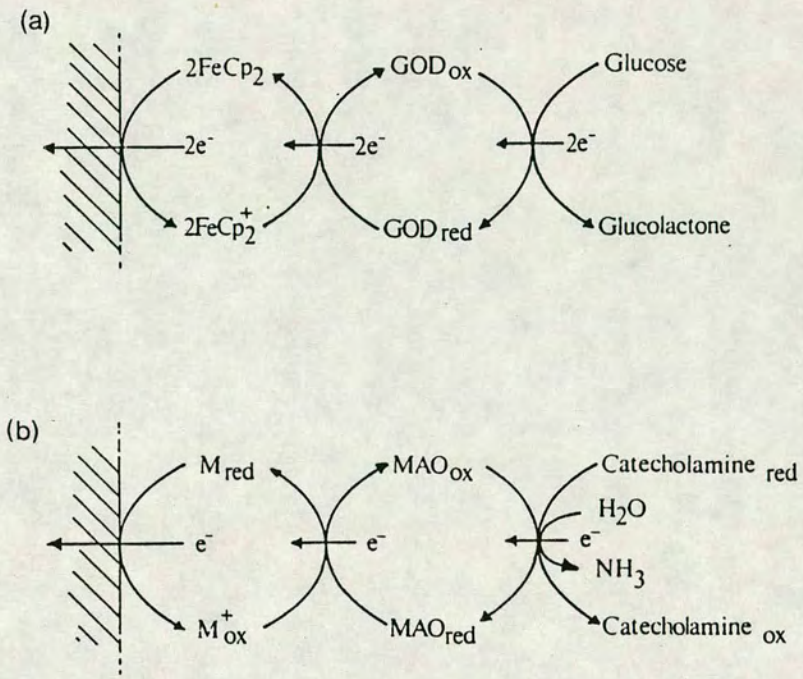

Figure 5.3.4 (a) Reaction scheme showing the mediation/reactivation of the enzyme glucose oxidase by the mediator Ferrocene. (b)Reaction scheme showing the desired equivalent mediation reaction on mono-amine oxidase by a mediator,M.

Figure 5.3.5 Cyclic voltammogram of MAO in a phosphate buffered solution (pH 7.4). The solution contains 140mM NaCl,20mM potassium phosphate buffer, MAO. (pyrolytic carbon working electrode).

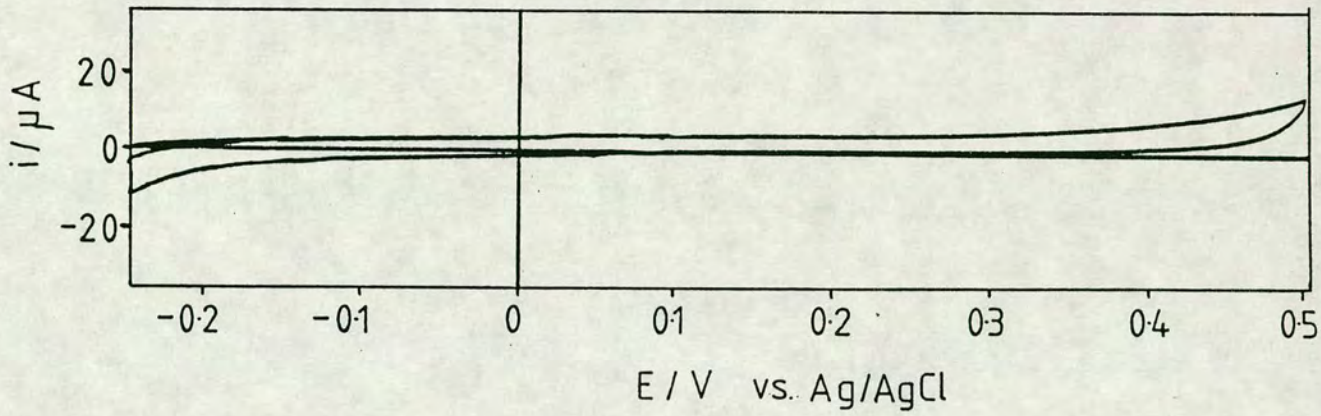

Figure 5.3.6 Cyclic voltammograms of dopamine and ferrocene carboxylic acid in a phosphate buffered solution (pH 7.4) superimposed. (pyrolytic carbon working electrode).

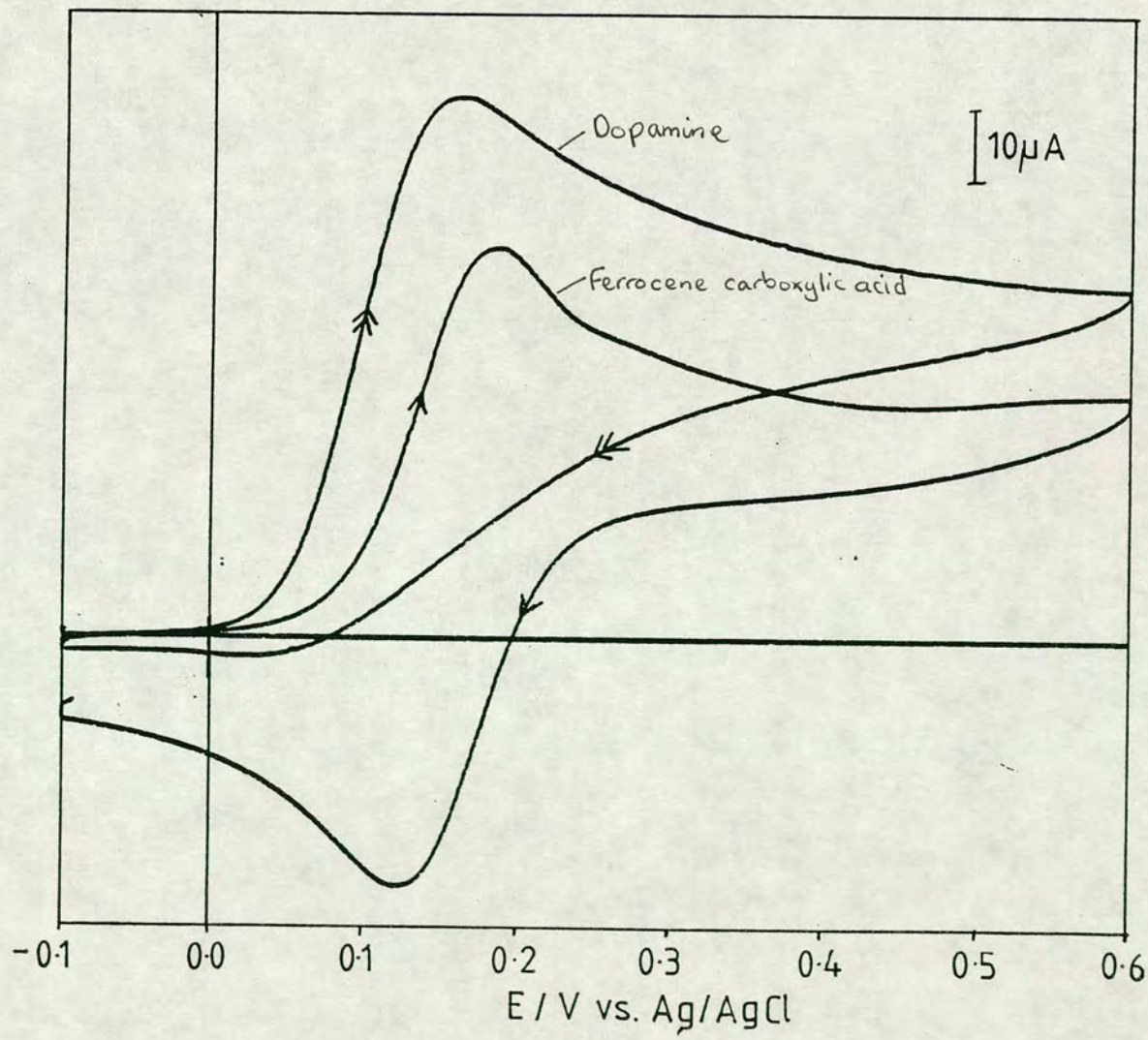

Until a suitable mediator is found the use of MAO as a suitable enzyme to allow electrochemical determination of catecholamines is not possible.

5.3.4 Action Of Catechol-*O*-Methyl Transferase

Catechol-*O*-methyl transferase (COMT) is a non-redox enzyme which catalyses the transfer of the methyl group of S-adenosylmethionine (SAM) to the 3-hydroxy group of a catecholamine, and it is one of the enzymes that inactivates catecholamines at nerve synapses. It has been shown that the presence of a divalent cation is essential for the functioning of COMT, although what role it plays is unclear. The natural ion is Mg^{2+}, however it has been found that both Co^{2+} and Mn^{2+} both give more efficient enzymatic reactions.

Since COMT is a non-redox enzyme it is not possible to electrochemically monitor it in order to determine catecholamine concentrations. It may be possible to determine the quantity of the methylated product either by its oxidation or by its ion transfer.

It has been shown previously by other groups [72] that 3-methoxycatecholamines have oxidation potentials which are *c.a* 250mV more positive than catecholamines, at physiological pH, as illustrated in figure 5.3.7. Therefore this may be a possible route to the determination of catecholamines.

It would be expected that the replacement of the 3-hydroxyl by a methoxy group should make the molecule more hydrophobic, and thus lower its Gibbs energy of transfer from water to an immiscible organic solvent. This should allow its detection at an ITIES.

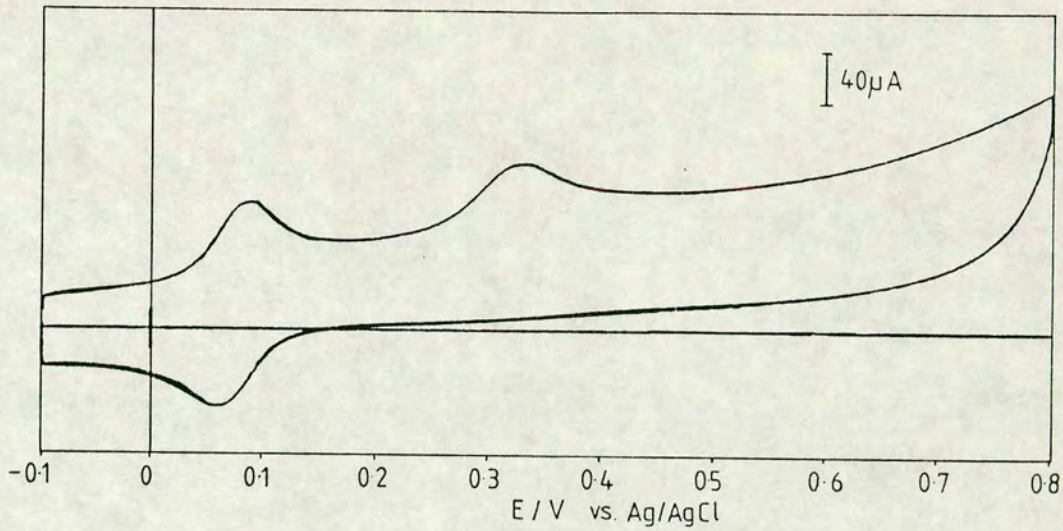

Figure 5.3.7 Cyclic voltammogram of the solution 140mM NaCl,20mM potassium phosphate buffer (pH 7.4), DA.HCl (1mM) and MeDA (1mM), ν=49mVs^{-1}.

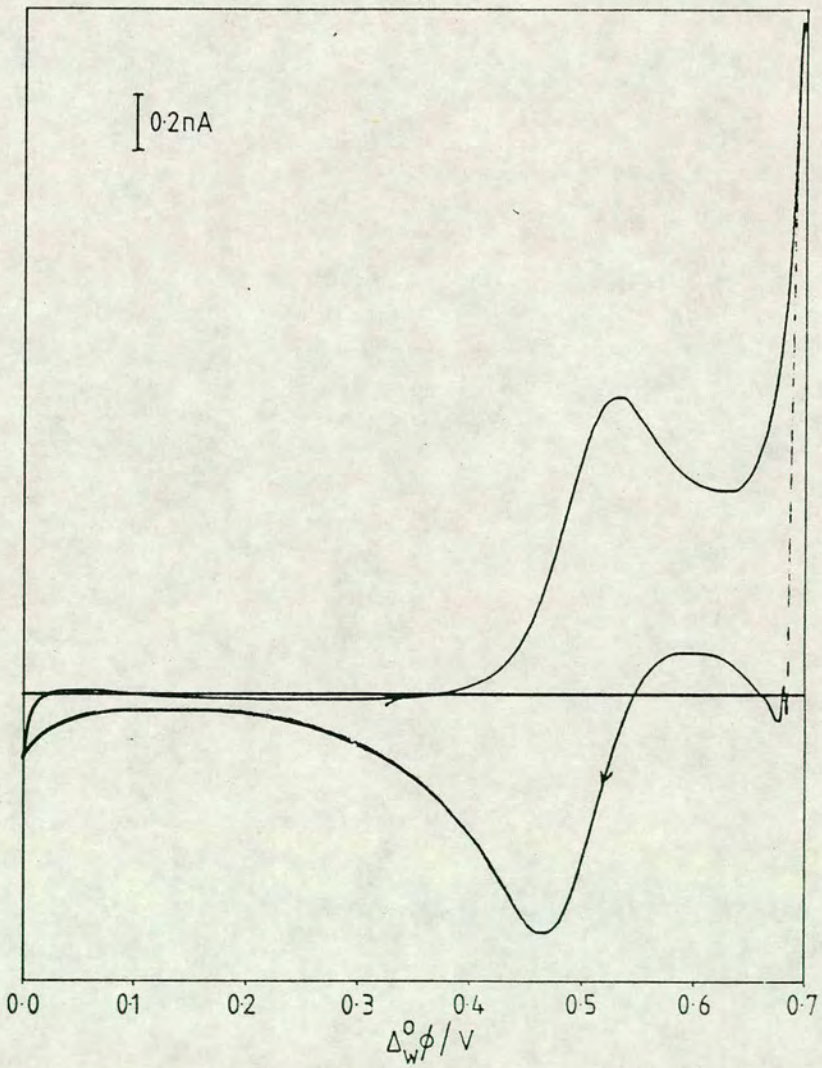

Figure 5.3.8 Cyclic voltammogram of the cell shown in section 5.3.4 at a large planar ITIES, showing the transfer of MeDA within the polaristion window.

The transfer of 3-methoxydopamine (MeDA) has been studied at both large and micro-ITIES using the cell:-

Ag/AgCl/TBACl(1mM)/TBATPBCl(1mM)//LiCl(10mM),MeDA(1mM)/AgCl/Ag

It can be seen in figure 5.3.8 that it does cross within the potential window, and therefore this technique, in combination with COMT, may be used to detect catecholamines in solution.

For the reasons outlined above catechol-*O*-methyl transferase seems to be the most suitable enzyme which could be used, in conjunction with electrochemistry, to detect catecholamines.

Chapter 6
Conclusions and Future Work

It has been shown that liquid/liquid interfaces can now be used in many different geometries for different functions i.e. assay techniques, a route to the evaluation of complexation constants and the rates of ion transfer.

In chapter 3 approximate analytical solutions have been presented for the different geometries of liquid/liquid interfaces. It has been shown that although these solutions are only approximate, that they do produce results which show the correct trends and can be accurate to within a fraction of a percent, as has been shown for ion transfer at the tip of a micropipette. They have also revealed trends for kinetically controlled reactions that suggest that with the use of microelectrodes that it should be possible to evaluate the rate of charge transfer, and this should not only apply at an ITIES but also at metal/electrolyte interfaces. The kinetic analysis of electron transfer at an ITIES has also been examined by the same approximate analytical type procedure. It has been shown that the kinetic analysis of such a system is very complicated with similar trends as observed for the kinetic case being seen for the reversible case, by simply changing the concentrations in each phase.

In order to be able to characterise these liquid/liquid interfaces more fully a more accurate digital simulation method is required.

As discussed there is a scope for the use of ITIES as analytical devices, however their use in the determination of catecholamines has proved limited. However with the possible synthesis of a ditopic receptor which is more hydrophobic i.e. by alkylation of the existing species, it may be possible to use facilitated ion transfer to circumvent the problems encountered. One of the

major drawbacks to using ITIES as practical sensing devices is the instability of the liquid phase, it would therefore be ideal if one of the phases could be replaced by some kind of conducting polymer, which was hydrophobic, or hydrophilic, to be used without mixing with the other phase. This should be investigated in future work.

Another possible application of ITIES is, not only to sense species in solution, but also to deliver them, eg ionic drugs. This could be particularly relevant with the use of micropipettes *in vivo*, and be used as part of a feedback system to stabilise levels of an active species in, for example, blood.

The work on the detection of catecholamines, although not amenable to detection at ITIES, shows that using enzymes, particularly catechol-*O*-methyl transferase and monoamine oxidase, has promise, but again more work must be carried out in order to produce a working device.

Appendix A
Computer Programs

A.1 Program To Solve Eqn. (3.1.41)

```
1    c   NUMERICAL SOLUTION FOR LINEAR DIFFUSION FROM SHAIN AND
2    c   NICHOLSON I.E. NUMERICAL EVALUATION  OF THE INTEGRAL IN
3    c   EQN(3.1.41) FROM 0 - N. DELTA TAKEN TO BE 0.01, DELTA
4    c   BEING THE INTEGRATION STEP SIZE
5        implicit double precision (a-h,o-z)
6        dimension a(8000),x(8000)
7    c   INPUTING VALUE FOR LN(THETA)
8        read(5,*) dlntheta
9        theta=exp(dlntheta)
10   c   EVALUATION OF THE NUMBER OF STEPS FOR THE INTEGRATION
11       c=4*dlntheta/0.01
12       ic=c
13   c   SETTING VALUES OF CONSTANTS R,F,T, AND (PI) ^ 1/2
14       r=8.314
15       f=96485.
16       t=298.16
17       pi=sqrt(3.1416)
18   c   LOOP FOR THE EVALUATION OF THE COEFFICIENTS OF CHI(i)
19           do 15 g=0,(c-1)
20            j=g
21            p = ic-g
22            q = ic-(g+1)
```

```
23              a(j+1)=sqrt(p)-sqrt(q)
24      15      continue
25  c   MAIN LOOP FOR THE CALCULATION OF CHI(i)
26          do 20 d=1,c
27              sum=0
28              i=d
29  c       CALCULATION OF RHS FOR ALL VALUES OF N
30              if (d*0.01.lt.((c/2)+1)*0.01)then
31                s=exp(-0.01*d)
32              else
33                s=exp((0.01*d)-(c*0.01))
34              endif
35              b=1/(1+(theta*s))
36              b=b/0.2
37  c       CALCULATION OF THE EQUIVALENT POTENTIAL VALUE FOR N
38              dpot=((r*t)/f)*log(theta*s)
39  c       LOOP FOR THE EVALUATION OF THE SUM
40  c       THE PREVIOUS N-1 CHI(I)
41              do 40 g=1,(d-1)
42                j=g
43                prod=x(j)*a(ic-(i-j))
44                sum=sum+prod
45      40      continue
46  c       EVALUATION OF CHI(I)
47              x(i)=(b-sum)
48              xpi=pi*x(i)
49  c       PRINTING OUT THE VALUES OF N,E-EO,CHI(N), AND (PI)1/2*CHI(N)
50              write(6,*) i,dpot,x(i),xpi
```

```
      20 continue
         end
```

A.2 Program to solve eqn. (3.1.55)

```
c     NUMERICAL SOLUTION FOR KINETICLLY CONTROLLED ELECTRON
c     TRANSFER AT A METAL/ELECTROLTYE INTERFACE
c     WITH LINEAR DIFFUSION i.e. SOLUTION OF EQN. (3.1.55).
c
      implicit double precision (a-h,o-z)
c     SETTING ARRAYS FOR THE COEFFICIENTS OF CHI FOR THE
c     SUM i.e. a(i), chi(i) AND THE POTENTIAL RELATIVE
c     TO E0 (dpot(i)).
c
      dimension a(8010),x(8010),dpot(8010)
c     Input OF VALUES dlntheta, THE CHARGE TRANSFER COEFFICIENT,
c     phi AND zeta. dlntheta DICTATES STARTING POTENTIAL.
c     phi IS A "CONSTANT" THAT INCORPORATES THE RATE
c     CONSTANT, DIFFUSION COEFFICIENT, AND SWEEP RATE.
c     zeta IS THE RATIO OF THE DIFFUSION COEFFICIENTS OF THE
c     REACTANT AND PRODUCT.
      read(5,*) dlntheta,transco,phi,zeta
      theta=exp(dlntheta)
c     EVALUATING THE NUMBER OF POINTS FOR THE INTEGRATION SO
c     THAT THE POTENTIAL SWEEP LIMITS ARE EQUIDISTANT
c     FROM E0.
      c=2.*(int(log(theta**2)/0.01))
c     DELTA TAKEN TO BE 0.01
```

```
c     SETTING VALUES OF CONSTANTS R,F, AND T.
      r=8.314
      f=96485.
      t=298.16
c     MAIN LOOP FOR THE CALCULATION OF chi(I)
      do 20 d=1,c
       sum=0
       i=d
       if (d*0.01.lt.(((c/2)+1)*0.01))then
       s=exp(-0.01*d)
       else
       s=exp((0.01*d)-(0.02*(c/2.)))
       endif
      b1=(1.+(zeta*theta*s))*0.2
      b2=(1-s)
      b3=((theta*s)**transco)/phi
c     CALCULATION OF THE POTENTIAL RELATIVE TO E0
       dpot(i)=((r*t)/f)*(log(s*theta))
c     LOOP FOR THE EVALUATION OF THE COEFFICIENTS
c     OF chi(i) FOR N
       do 30 g=0,(d-1)
        j=g
        p = d-g
        q = d-(g+1)
        a(j+1)=sqrt(p)-sqrt(q)
   30   continue
c     LOOP FOR THE EVALUATION OF THE SUM THE PREVIOUS
c     N-1 chi(i)
```

```
52              do 40 g=1,(d-1)
53                j=g
54                prod=x(j)*a(j)
55                sum=sum+prod
56        40      continue
57      c       PRINTING OUT THE VALUES OF N,E-E0 AND CHI(N)
58              x(i)=(b2-(b1*sum))/(b3+b1)
59              write(6,*) i,dpot(i),x(i)
60        20    continue
61            end
```

A.3 Program to evaluate eqn. (3.2.34)

```
1     c     NUMERICAL SOLUTION FOR SPHERICAL/SPHERICAL DIFFUSION
2     c     FOR THE METHOD DEVELOPED FROM REINMUTHS SPHERICAL
3     c     CORRECTION OF SHAIN AND NICHOLSON'S LINEAR DIFFUSION
4     c     CASE. SEE TEXT FOR DETAILS .i.e. NUMERICAL SOLUTION
5     c     OF THE INTEGRALS IN EQN(3.2.32) FROM 0 - N.
6           implicit double precision (a-h,o-z)
7           dimension a(80000),cc(80000),x(80000)
8     c     SETTING VALUES OF CONSTANTS R,F,T
9           es=0
10          r=8.314
11          f=96485.
12          t=298.16
13    c     INPUTING VALUE FOR STARTING POTENTIAL, SCAN LIMIT,
14    c     DIMENSIONLESS TIME STEP PARAMETER AND THE KINETIC
15    c     PARAMETER
```

```
      read(5,*) dinpot,scanlim,delta,rho
      dlntheta=(f/(r*t))*dinpot
      theta=dexp(dlntheta)
c     EVALUATION OF THE NUMBER OF STEPS FOR THE INTEGRATION
      c=2.*((((f/(r*t))*(-1.*scanlim))+dlntheta)/delta)
      ic=c
      wc=0
c     EVALUATION OF THE CONSTANT ALPHA
      alpha=(1./rho)*dsqrt(delta)
c     EVALUATION OF THE CONSTANT MULTIPLIERS FOR THE FINITE
c     SUMS
      y1=(2*dsqrt(delta))/sqrt(3.1416)
      y2=(1./rho)*delta
c     EVALUATION OF A(i)
        do 30 j=0,(ic-1)
          g=j
          p =ic-g
          q =ic-(g+1)
          a(j+1)=dsqrt(p)-dsqrt(q)
   30     continue
c     LOOP FOR THE EVALUATION OF THE COEFFICIENTS OF
c     PHI(I) FOR THE EVALUATION OF EXP[X**2]*ERFC[X]
        do 40 j=1,ic-1
          g=j
          fn=((alpha**2)*(ic-g))
          if (dsqrt(fn).gt.3) then
c     EVALUATION OF EXP[X**2]ERFC[X] FOR X>3.
            fn=dsqrt(fn)
```

```
44              cc(j)=1/(sqrt(3.1416)*fn)
45              ser1=1./(2.*(fn**2))
46              ser2=3./(4.*(fn**4))
47              ser3=15./(8.*(fn**6))
48              cc(j)=cc(j)*(1.-ser1+ser2-ser3)
49             else
50    c      EVALUATION OF EXP[X**2]ERCF[X] FOR X<=3 USING THE
51    c      DIRECT MANNER i.e. USING EXPONENTIAL AND THE
52    c      DEFINED FUNCTION ERF
53              cc(j)=dexp(fn)
54              cc(j)=cc(j)*(1.-erf(dsqrt(fn)))
55             endif
56        40   continue
57    c      MAIN LOOP FOR THE CALCULATION OF PHI(I)
58            do 20 i=1,c
59              sum=0
60              sum2=0
61              d=i
62              if(d.lt.(c/2)+1)then
63               s=dexp(-delta*d)
64              else
65               s=dexp((delta*d)-(c*delta))
66              endif
67              b=1./(1.+(theta*s))
68    c      CALCULATION OF THE EQUIVALENT POTENTIAL VALUE FOR N
69              dpot=((r*t)/f)*dlog(theta*s)
70    c      CALCULATION OF PHI(1)
71             if (i.eq.1) then
```

```
72              x(1)=b/y1
73              else
74      c       CALCULATION OF PHI(N) FOR N>1
75              do 70 j=1,i-1
76               g=j
77               prod=x(j)*a(ic-(i-j))
78               sum=sum+prod
79               prod2=x(j)*cc(ic-(i-j))
80               sum2=sum2+prod2
81           70  continue
82              tl=b-(y1*sum)+(y2*sum2)
83              bl=y1
84              x(i)=tl/bl
85              endif
86      c       WRITING THE VALUES OF RELATIVE POTENTIAL AND CURRENT
87      c       PARAMETERS i.e. n(E-E0) AND PHI(i), TO OUTPUT CHANNEL 7
88              write (7,*) dpot,x(i)
89           20 continue
90              end
91      c
92      c       FUNCTION FOR THE EVALUATION OF ERF(X)
93      c



94              function erf(x)
95              implicit double precision (a-h,o-z)
96              data p,a1,a2,a3,a4,a5 / 0.3275911, 0.254829592d0,
97             * -0.284496736d0, 1.421413741d0, -1.453152027d0,
```

```
98          *  1.061405429d0 /
99      c
100             x=dabs(x)
101             if(x.gt.1.0E-07) goto 10
102              erf = 0.0
103              return
104         10   if(x.lt.5.0) goto 20
105              erf=1.0
106              return
107         20    t=1.0/(1.0+p*x)
108             tpow=t
109             sum=a1*t
110             tpow=tpow*t
111             sum=sum+a2*tpow
112             tpow=tpow*t
113             sum=sum+a3*tpow
114             tpow=tpow*t
115             sum=sum+a4*tpow
116             tpow=tpow*t
117             sum=sum+a5*tpow
118             erf=1.0-sum*dexp(-x*x)
119             return
120             end
```

A.4 Program for evaluation of eqn.(3.2.52)

```
1     c     NUMERICAL SOLUTION FOR SPHERICAL/SPHERICAL DIFFUSION
2     c     FOR THE METHOD DEVELOPED FROM REINMUTHS SPHERICAL
```

```
3     c     CORRECTION OF SHAIN AND NICHOLSON'S LINEAR DIFFUSION
4     c     CASE, FOR QUASI-REVERSIBLE REACTIONS.
5           implicit double precision (a-h,o-z)
6           dimension a(40000),cc(40000),x(40000)
7     c     SETTING VALUES OF CONSTANTS R,F,T
8           r=8.314
9           f=96485.
10          t=298.16
11    c     INPUTING THE INITIAL POTENTIAL, THE SCAN LIMIT, THE
12    c     DIFFUSION COEFFICIENT, ELECTRODE RADIUS, SWEEP RATE,
13    c     CHARGE TRANSFER COEFFICIENT, RATE CONSTANT AND DELTA.
14          read(5,*) dinpot,scanlim,diffco,rad,v,transco,rateco
15          read(5,*) delta
16    c     EVALUATION OF THE VALUE OF THETA
17          dlntheta=(f/(r*t))*dinpot
18          theta=dexp(dlntheta)
19    c     EVALUATION OF THE NUMBER OF STEPS FOR THE INTEGRATION
20          c=2*((((f/(r*t))*(-1.*scanlim))+dlntheta)/delta)
21          ic=c
22          es=0
23    c     EVALUATION OF THE CONSTANTS SIGMA, PSI, PHI AND ALPHA
24          sigma=(f/(r*t))*v
25          phi=rateco/(dsqrt(diffco*sigma))
26          psi=dsqrt(diffco)*(1./(rad*dsqrt(sigma)))
27          alpha=psi*(dsqrt(delta))
28    c     LOOP FOR THE EVALUATION OF EXP[X**2]*ERFC[X]
29            a(1)=dsqrt(c)-dsqrt(c)
30          do 40 j=1,ic-1
```

```
31              g=j
32               p =ic-g
33               q =ic-(g+1)
34               a(j+1)=dsqrt(p)-dsqrt(q)
35              fn=((alpha**2)*(ic-g))
36              if (dsqrt(fn).gt.3) then
37      c       EVALUATION OF EXP[X**2]ERFC[X] FOR X>3.
38               fn=dsqrt(fn)
39               cc(j)=1/(sqrt(3.1416)*fn)
40               ser1=1./(2.*(fn**2))
41               ser2=3./(4.*(fn**4))
42               ser3=15./(8.*(fn**6))
43               cc(j)=cc(j)*(1.-ser1+ser2-ser3)
44              else
45      c       EVALUATION OF EXP[X**2]ERCF[X] FOR X<=3 BY
46      c       THE DIRECT METHOD.
47               cc(j)=dexp(fn)
48               cc(j)=cc(j)*(1.-erf(dsqrt(fn)))
49              endif
50        40    continue
51      c       MAIN LOOP FOR THE CALCULATION OF PHI(I)
52              do 20 i=1,c
53                sum=0
54                sum2=0
55                d=i
56      c       CALCULATION OF LHS, OF EQN(3.2.52), FOR ALL VALUES OF N
57                if (d*delta.lt.((c/2)+1)*delta)then
58                 s=dexp(-delta*d)
```

```
59              else
60               s=dexp((delta*d)-(c*delta))
61              endif
62      c       EVALUATION OF THE CONSTANT MULTIPLIERS FOR THE FINITE
63      c       SUMS
64              y1=((theta*s)**transco)/phi
65              y3=((2*dsqrt(delta))/sqrt(3.1416))*(1+(theta*s))
66              y4=(1+(theta*s))*delta*psi
67              y2=1-s
68      c       CALCULATION OF THE EQUIVALENT POTENTIAL VALUE FOR N
69              dpot=((r*t)/f)*dlog(theta*s)
70      c       CALCULATION OF PHI(1)
71              if (i.eq.1) then
72              x(1)=y2/(y1+y3)
73              else
74      c       CALCULATION OF PHI(N) FOR N>1
75              do 70 j=1,i-1
76               g=j
77               prod=x(j)*a(ic-(i-j))
78               sum=sum+prod
79               prod2=x(j)*cc(ic-(i-j))
80               sum2=sum2+prod2
81        70     continue
82              tl=y2-(y3*sum)+(y4*sum2)
83              bl=y1+y3
84              x(i)=tl/bl
85              endif
86      c       WRITING THE VALUES OF RELATIVE POTENTIAL AND CURRENT
```

```
c     PARAMETERS i.e. n(E-E0) AND PHI(i), TO OUTPUT CHANNEL 7
       write (7,*) dpot,x(i)*(1./psi)
 20    continue
       end
c
c     FUNCTION FOR THE EVALUATION OF ERF(X)
c
       function erf(x)
       implicit double precision (a-h,o-z)
       data p,a1,a2,a3,a4,a5 / 0.3275911, 0.254829592d0,
     * -0.284496736d0, 1.421413741d0, -1.453152027d0,
     * 1.061405429d0 /
c
       x=dabs(x)
       if(x.gt.1.0E-07) goto 10
        erf = 0.0
        return
 10    if(x.lt.5.0) goto 20
        erf=1.0
        return
 20     t=1.0/(1.0+p*x)
       tpow=t
       sum=a1*t
       tpow=tpow*t
       sum=sum+a2*tpow
       tpow=tpow*t
```

```
113          sum=sum+a3*tpow
114          tpow=tpow*t
115          sum=sum+a4*tpow
116          tpow=tpow*t
117          sum=sum+a5*tpow
118          erf=1.0-sum*dexp(-x*x)
119          return
120          end
```

A.5 Program to evaluate eqn. (3.3.14)

```
 1    c     NUMERICAL SOLUTION FOR SPHERICAL/LINEAR DIFFUSION
 2    c     FOR THE METHOD DEVELOPED FROM A COMBINATION OF THE
 3    c     SPHERICAL/SPHERICAL AND LINEAR/LINEAR CASES.
 4          implicit double precision (a-h,o-z)
 5          dimension a(9000),cc(9000),dpot(9000),s(9000),x(9000)
 6    c     INPUTING VALUES FOR LN(THETA), DIFFUSION COEFFICIENT,
 7    c     ELECTRODE RADIUS AND SWEEP RATE
 8          read(5,*) dlntheta,diffco,rad,v
 9          theta=dexp(dlntheta)
10          ad=(3.1415927*(rad**2))
11          rad=(2*rad)/3.1415927
12    c     EVALUATION OF THE NUMBER OF STEPS FOR THE INTEGRATION
13          c=4*dlntheta/0.01
14          ic=c
15    c     SETTING VALUES OF CONSTANTS R,F,T AND (Pi) ^ 1/2
16          r=8.314
17          f=96485.
```

```
18          t=298.16
19          pi=sqrt(3.141527)
20          afact=(3.141527**2)/8
21    c     EVALUATION OF THE CONSTANTS SIGMA, PSI AND APLHA
22          sigma=(f/(r*t))*v
23          psi=sqrt(diffco)*(1./(rad*sqrt(sigma)))
24          alpha=psi*0.1
25    c     EVALUATION OF THE CONSTANT MULTIPLIER Y1
26          y1=0.01*psi*afact
27    c     EVALUATION OF S(i) FOR ALL VALUES OF N
28          do 10,d=1,c
29            i=d
30            if(d*0.01.lt.((c/2)+1.)*0.01)then
31             s(i)=exp(-0.01*d)
32            else
33             s(i)=exp((0.01*d)-(c*0.01))
34            endif
35     10    continue
36    c     LOOP FOR THE EVALUATION OF THE COEFFICIENTS OF PHI(I)
37            do 30 g=0,(c-1)
38              j=g
39              p = ic-g
40              q = ic-(g+1)
41              a(j+1)=sqrt(p)-sqrt(q)
42     30      continue
43    c     LOOP FOR THE EVALUATION OF EXP[X**2]ERFC[X]
44            do 40 g=1,c-1
45              j=g
```

```
46                fn=((alpha**2)*(ic-g))
47                if (sqrt(fn).gt.2) then
48      c       EVALUATION OF EXP[X**2]ERFC[X] FOR X>3.
49                fn=sqrt(fn)
50                cc(j)=1/(sqrt(3.1416)*fn)
51                ser1=1/(2*(fn**2))
52                ser2=3/(4*(fn**4))
53                ser3=15/(8*(fn**6))
54                cc(j)=cc(j)*(1-ser1+ser2-ser3)
55               else
56      c       EVALUATION OF EXP[X**2]ERFC[X] FOR X<=3 USING BY
57      c       THE DIRECT METHOD
58                cc(j)=exp(fn)
59                ef=sqrt(fn)
60                cc(j)=cc(j)*(1-erf(ef))
61               endif
62       40      continue
63      c       MAIN LOOP FOR THE CALCULATION OF PHI(I)
64              do 20 d=1,c
65                sum=0
66                sum2=0
67                i=d
68      c       EVALUATION OF THE "CONSTANT" MULTIPLIER Y2
69                y2=(0.2/pi)*((theta*s(i))+afact)
70      c       CALCULATION OF THE EQUIVALENT POTENTIAL VALUE FOR N
71                dpot(i)=((r*t)/f)*dlog(theta*s(i))
72      c       CALCULATION OF PHI(1)
73                if (d.eq.1) then
```

```
74              x(1)=1/y2
75             else
76      c      CALCULATION OF PHI(N) FOR N>1
77              do 70 g=1,d-1
78               j=g
79               prod=x(j)*a(ic-(i-j))
80               sum=sum+prod
81               prod2=x(j)*cc(ic-(i-j))
82               sum2=sum2+prod2
83       70      continue
84              tl=1+(y1*sum2)-(y2*sum)
85              bl=y2
86              x(i)=tl/bl
87             endif
88       20    continue
89      c      WRITING THE VALUES OF RELATIVE POTENTIAL AND CURRENT
90      c      PARAMETERS i.e. n(E-E0) AND i/nFC*, TO OUTPUT CHANNEL 7
91             do 80 i=1,c
92              write (6,*) dpot(i),x(i)*sqrt(diffco*sigma)*ad
93       80    continue
94             end
95      c
96      c
97      c      FUNCTION FOR THE EVALUATION OF ERF(X)


98             function erf(x)
99             real erf
```

```
      data p,a1,a2,a3,a4,a5/0.3275911,0.254829592d0,
     * -0.284496736d0,1.421413741d0,-1.453152027d0,1.061405429d0/
c
      x=abs(x)
      if(x.gt.1.0E-07) goto 10
       erf = 0.0
      return
10     if(x.lt.5.0) goto 20
       erf=1.0
      return
20     t=1.0/(1.0+p*x)
      tpow=t
      sum=a1*t
      tpow=tpow*t
      sum=sum+a2*tpow
      tpow=tpow*t
      sum=sum+a3*tpow
      tpow=tpow*t
      sum=sum+a4*tpow
      tpow=tpow*t
      sum=sum+a5*tpow
      erf=1.0-sum*exp(-x*x)
      return
      end
```

A.6 Program to evaluate eqn.(3.4.28)

```
1     c     NUMERICAL SOLUTION FOR REVERSIBLE ELECTRON TRANSFER
```

```
2     c     AT A LIQUID/LIQUID INTERFACE.
3           implicit double precision (a-h,o-z)
4           dimension b(8010),s(8010),a(8010),x(8010),dpot(8010),
5          * curr(8010)
6     c     INPUT OF THE DIMENSIONLESS CONCENTRATION PARAMETERS
7     c     AND THE DIMENSIONLESS DIFFUSION COEFFICIENTS
8           read(5,*) alpha,beta,dkappa,zeta,zetaa,zetab
9     c     SETTING VALUES OF CONSTANTS R,F,T, AND PI ^ 1/2
10          r=8.314
11          f=96485.
12          t=298.16
13          pi=sqrt(3.1416)
14    c     EVALUATION OF LN(THETA)
15          theta=(alpha*(1-beta))/(beta*(1-alpha))
16          dlntheta=log(theta)
17    c     EVALUATION FOR SCAN LIMITS SYMMETRICAL ABOUT E0
18          c=2.*(int(log(theta**2)/0.01))
19    c     CALCULATION OF S(t)
20          do 10,d=1,c
21            i=d
22            if (d*0.01.lt.(((c/2)+1)*0.01))then
23             s(i)=exp(-0.01*d)
24            else
25             s(i)=exp((0.01*d)-(0.02*(c/2.)))
26            endif
27    c     CALCULATION OF THE EQUIVALENT POTENTIAL VALUE FOR N
28            dpot(i)=((r*t)/f)*(log(s(i)*theta))
29    c     EVALUATION OF THE CONVOLUTED CURRENT, I(t)
```

```
30    c     i.e. THE RHS OF EQN.(3.4.26)
31          aa=((zetaa/zetab)*theta*s(i))-1.
32          cd=(dkappa/(zeta*zetab))
33          cd=cd*(((1-alpha)*theta*s(i)*beta)-(alpha*(1-beta)))
34          bb=((1-alpha)/zetab)+((beta*dkappa*zetaa)/(zetab*zeta))
35          b1=(theta*s(i)*bb)+(alpha+(((1-beta)*dkappa)/(zetab*zeta)))
36          srt=(b1**2)-(4*aa*cd)
37          b(i)=-(b1-sqrt(srt))/(2*aa)
38    c     EVALUATION OF THE CONVOLUTED CURRENT AT THE
39    c     DISCONTINUITY I.E. A=0 AT E-E0 IS c.a. ZERO
40          if (abs((r*t/f)*log(theta*s(i))).lt.1.e-5)then
41           b(i)=dkappa*(alpha*(1-beta)-beta*(1-alpha))
42           bdiv=alpha*zetab*zeta+dkappa*beta*zetaa+(1-alpha)*zeta
43           b(i)=b(i)/(dkappa*(1-beta)+bdiv)
44          endif
45          b(i)=b(i)/0.2
46     10   continue
47    c     MAIN LOOP FOR THE CALCULATION OF CHI(I)
48          do 20 d=1,c
49           sum=0
50           i=d
51    c     EVALUATION OF THE COEFFICIENTS OF CHI(I)
52           do 30 g=0,(d-1)
53            j=g
54            p = d-g
55            q = d-(g+1)
56            a(j+1)=sqrt(p)-sqrt(q)
57     30    continue
```

```
c      CALCULATION OF CHI(1)
         if (d.eq.1) then
          x(1)=b(1)/a(1)
c      CALCULATION OF CHI(I) FOR N>1
         else
c     EVALUATION OF THE SUM THE PREVIOUS N-1 CHI(I)
         do 40 g=1,(d-1)
          j=g
          prod=x(j)*a(j)
          sum=sum+prod
   40    continue
         if (b(i).eq.0) then
          x(i)=0.0
         else
          x(i)=(b(i)-sum)/a(i)
         endif
        endif
c      OUTPUT OF THE VALUES OF E-E0 AND CHI(N) FOR EACH N
          write (6,*) i,dpot(i),x(i)
   20  continue
       end
```

A.7 Program for the evaluation of eqn. (3.4.63)

```
c     NUMERICAL SOLUTION FOR QUASI-REVERSIBLE ELECTRON
c     TRANSFER AT A LIQUID/LIQUID INTERFACE.
      implicit double precision (a-h,o-z)
      dimension a(8010),x(8010)
```

```
5     c     INPUT OF THE CHARGE TRANSFER COEFFICIENT AND DPHI.
6     c     DPHI IS A 'CONSTANT' THAT COMBINES THE RATE CONSTANT,
7     c     DIFFUSION COFFICIENT, SWEEP RATE, AND CONCENTRATION.
8           read(5,*) transco,dphi
9     c     INPUT OF THE DIMENSIONLESS CONCENTRATION PARAMETERS
10    c     AND THE DIMENSIONLESS DIFFUSION COEFFICIENTS
11          read(5,*) alpha,beta,dkappa,zeta,zetaa,zetab
12    c     SETTING VALUES OF CONSTANTS R,F AND T
13          r=8.314
14          f=96485.
15          t=298.16
16    c     EVALUATION LN(THETA)
17          theta=(alpha*(1-beta))/(beta*(1-alpha))
18          dlntheta=log(theta)
19    c     EVALUATION OF c FOR SCAN LIMITS SYMMETRICAL ABOUT E0
20          c=2.*(int(log(theta**2)/0.01))
21          ic=c
22    c     EVALUATION OF THE COEFFICIENTS OF CHI(I)
23            do 15 g=0,ic-1
24              j=g
25              p = ic-g
26              q = ic-(g+1)
27              a(j+1)=sqrt(p)-sqrt(q)
28       15   continue
29    c     LOOP FOR THE CALCULATION OF CHI(I)
30          do 20 d=1,c
31            sum=0
32            i=d
```

```
33    c     EVALUATION OF S(t)
34          if (d*0.01.lt.(((c/2)+1)*0.01))then
35          s=exp(-0.01*d)
36          else
37          s=exp((0.01*d)-(0.02*(c/2.)))
38          endif
39    c     CALCULATION OF THE POTENTIAL RELATIVE TO E0.
40          dpot=((r*t)/f)*(log(s*theta))
41    c     EVALUTION OF THE CONSTANTS FOR THE QUADRATIC
42    c     EQUATIONTO SOLVE FOR I(t) i.e A, B and
43    c     C=C1+C2chi(i) ARE aa,bb,cc1 AND cc2 RESPCTIVELY.
44          aa=-(1./(alpha*dkappa*(1.-beta)))
45          aa=aa+((s*zetaa)/((1-alpha)*beta*dkappa*zetab))
46          bb=(1./(dkappa*(1-beta)))+(1./(alpha*zetab*zeta))
47          b1=s/(beta*dkappa*zetab)
48          b1=b1+((s*zetaa)/((1-alpha)*zetab*zeta))
49          bb=b1+bb
50          cd1=1./(zeta*zetab)
51          cd2=s-1
52          cc1=cd1*cd2
53          cd3=(theta**transco)*(s**transco)
54          cd4=cd3/(dphi*dkappa*(1-beta)*alpha)
55          cc2=cd1*cd4
56    c     EVALUATION OF THE SUM THE PREVIOUS N-1 CHI(I)
57            do 40 g=1,(d-1)
58              j=g
59              prod=x(j)*a(ic-(i-j))
60              sum=sum+prod
```

```
61      40      continue
62      c       EVALUATION OF CHI(i) AT THE DISCONTINUITY A=0,
63      c       i.e. E-E0 IS c.a. ZERO
64              if (abs(dpot).lt.1e-4)then
65              tl=(-0.2*bb*sum)-cc1
66              bl=(0.2*bb)+cc2
67              x(i)=tl/bl
68              else
69      c       EVALUTION OF CHI(I) FOR ALL OTHER VALUES BY EVALUATION
70      c       OF THE QUADRATIC equation for chi(i), the coefficients
71      c       BEING a1, b1, AND c1.
72              sum1=sum+(bb/(0.4*aa))
73              a1=0.16*(aa**2)
74              b1=(32.*(aa**2)*0.01*sum1)+(4.*aa*cc2)
75              c1=(16.*(aa**2)*0.01*(sum1**2))-(bb**2)+(4.*aa*cc1)
76              if (dpot.gt.0.0)then
77              tl=-b1+sqrt((b1**2)-(4.*a1*c1))
78              else
79              tl=-b1-sqrt((b1**2)-(4.*a1*c1))
80              endif
81              bl=2.*a1
82              x(i)=tl/bl
83              endif
84      c       OUTPUT OF CHI(I) AND EQUIVALENT POTENTIAL.
85              write(6,*) dpot,x(i)
86      20      continue
87              end
```

References

1. W.Nernst and E.H.Riesenfield - Ann. Phys. 8(1902),600

2. M.Cremer - Z. Biol. 47(1906),562

3. B.Beutner - Trans. Am. Electrochem. Soc. 21(1912),219

4. E.Baur - Z.Elektrochem. 24(1918),100

5. G.Ehrensvard and D.F.Cheesman - Science 94(1941),23

6. E.J.W.Verwey and K.F.Niesson - Philos. Mag. 28(1939),435

7. M.Kahlweit and H.Strenlow - Z. Elektrochem. 58(1954),658

8. C.Gavach, T.Mlodnicka and J.Guastalla - C. R. Acad. Sci C266(1968),1196

9. R.M. Wightman and D.O.Wipf - Electroanal. Chem., Vol.15, pp267-353.

10. J.A.Campbell and H.H.Girault - J. Electroanal. Chem. 266 (1989), 465

11. G.Taylor and H.H.Girault - J. Electroanal. Chem. 208 (1986), 179

12. M.Senda, T.Kakutani, T.Osakai and T.Ohkouchi - Proceedings 1st Bioelectroanal. Symp., Matrafured, 1986.

13. C.Gavach and F.Henry - J. Electroanal. Chem. 54 (1974), 361

14. C.Gavach - J. Chim. Phys. 70 (1973), 1478

15. C.Gavach, P.Seta and F.Henry - Bioelectrochem. Bioenerg. 1 (1974), 329

16. C.Gavach, B.D'Epenoux and F.Henry - J. Electroanal. Chem. 64 (1975), 107

17. J.Koryta, P.Vangsek and M.Brezina - J. Electroanal. Chem.67 (1976), 263

18. Z.Samec, V.Marecek, J.Koryta and M.W.Khalil - J. Electroanal. Chem. 83 (1977), 393

19. Z.Samec, V.Marecek and J.Weber - J. Electroanal. Chem. 100 (1979), 841

20. Z.Samec, V.Marecek, J.Weber and D.Homolka - J. Electroanal. Chem. 99 (1979), 385

21. D.Homolka and V.Marecek - J. Electroanal. Chem. 112 (1980), 91

22. T.Kakutani, T.Osakai and M.Senda - Bull. Chem. Soc. Jpn. 56 (1983), 991

23. B.Hundhammer, T.Solomon and H.Alemu - J. Electroanal. Chem. 149

(1983), 179

24. T.Osakai, T.Kakutani and M.Senda - Bull. Chem. Soc. Jpn. 57 (1984), 370

25. V.Marecek and Z.Samec - Anal. Chim. Acta 151 (1983), 265

26. J.Koryta - Electrochim. Acta 24 (1979), 293

27. Z.Samec, V.Marecek and J.Weber - J. Electroanal. Chem. 96 (1977), 245

28. E.Grunwald, G.Baughman and G.Kohnstam - J. Amer. Chem. Soc. 82

(1960), 5801

29. A.A.Stewart, Y.Shao, C.M.Pereira and H.H.Girault - J. Electroanal. Chem. -

in press

30. Z.Samec, V.Marecek and M.P.Colombini - J. Electroanal. Chem. 257 (1988), 147

31. Z.Samec and V.Marecek - J. Electroanal. Chem. 200 (1986), 17

32. D.Homolka, V.Marecek, Z.Samec, K.Base and H.Wendt - J. Electroanal. Chem.

163 (1984), 159

33. Y.N. Kozolc and J.Koryta - Anal. Lett. 16(B3) (1983), 255

34. Z.Samec, D.Homolka and V.Marecek - J. Electroanal. Chem. 158 (1983), 28

35. V.Marecek and Z.Samec - Anal. Lett. 14(B15) (1981), 1241

36. Y.Shao and H.H.Girault - J. Electroanal. Chem. 282 (1990), 59

37. A.Hofmanoua, L.Q.Hung and M.W.Kahil - J. Electroanal. Chem. 135 (1982), 257

38. Z.Samec, D.Homolka and V.Marecek - J. Electroanal. Chem. 135 (1982), 265

39. M.Guainazzi, G.Silvestri and G.Suvalle - J. Chem. Soc. D. (1975), 200

40. A.A.Stewart, J.A.Campbell, H.H.Girault and M.Eddows - Ber. Bunsenges. Phys.

Chem. 94 (1990), 83

41. P.N.Swan, Ph.D. Dissertation, University of Southampton, 1980

42. R.N.Adams - Anal. Chem. 48 (1976), 1126A

43. J-L.Ponchon, R.Cespaglia, F.Gonon, M.Jouvet and J-F.Pujol - Anal. Chem.

51 (1979), 1483

44. C.G.Zoski, K.B.Oldham, P.J.Mahon, T.L.E.Henderson and A.M.Bond -

J. Electroanal. Chem. - in press

45. T.Hepel and J.Osteryoung - J. Electroanal. Chem. 125 (1981), 315

46. M.Fleischmann, S.Bandyopadhyay and S.Pons - J. Phys. Chem. 89 (1985), 5537

47. P.M.Kovach, W.L.Caudill, P.G.Peters and R.Wrightman - J. Electroanal. Chem. 185 (1985), 285

48. R.S.Nicholson and I.Shain - Anal. Chem. 36 (1964), 706

49. R.S.Nicholson - Anal. Chem. 37 (1965), 1351

50. G.Mamantov - M.Sc. Thesis (1954)

51. H.D.Hurwitz - J. Electroanal. Chem. 7 (1964), 368

52. I.Shain and K.J.Martin - J. Phys. Chem. 65 (1961), 254

53. J.R.Delmastro and D.E.Smith - Anal. Chem. 38 (1966), 169

54. W.H.Reinmuth - J. Am. Chem. Soc. 79 (1957), 6358

55. K.Aoki, K.Tokuda and H.Matsuda - J. Electroanal. Chem. 235 (1987), 87

56. A.M.Bond, K.B.Oldham and C.G.Zoski - J. Electroanal. Chem. 245 (1988), 71

57. K.R.Wehmeyer, M.R. Deakin and R.M.Wrightman - Anal. Chem. 57 (1985), 1913

58. M.R.Deakin, R.M.Wrightman and C.A.Amature - J. Electroanal. Chem. - 215 (1986), 49

59. A.M.Bond and K.B.Oldham - J. Electroanal. Chem. - 158 (1983), 193

60. C.P.Andrieux, P.Hapiot and J-M.Sauveant - Chem. Rev. 90 (1990), 723

61. D.Shoup and A.Szabo - J. Electroanal. Chem. 160 (1984), 27

62. K.B.Oldham and C.G.Zoski - J. Electroanal. Chem. 256 (1988), 11

63. Z.Samec, V.Marecek and J.Weber - J. Electroanal. Chem. 103 (1979), 11

64. J.A.Campbell, A.A.Stewart and H.H.Girault - J. Chem. Soc.,Faraday Trans.I, 85 (1989), 843

65. H.H.Girault and D.J.Schiffrin - J. Electroanal. Chem. 195, (1985) 213

66. H.H.Girault and D.J.Schiffrin - J. Electroanal. Chem. 161, (1984) 415

67. E.Metzger, D.Ammann, R.Asper and W.Simon - Anal. Chem. 58 (1986), 132

68. Private communication from Y.Shao, University of Edinburgh.

69. H.Sugihara, T.Okada and K.Miratani - Chem. Letts. 12 (1987), 2391

70. H.Ehringer and O.Hornykiewicz - Klim. Wischr. 38 (1960), 1236

71. M.D.Hawley, S.V.Tatawawadi, S.Piekarski and R.N.Adams - J. Am. Chem. Soc. 89 (1967), 447

72. A.W.Sternson, R.M^{c}Creery, B.Feinberg and R.D.Adams - J. Electroanal. Chem. 46 (1973), 313

73. R.M.Wrightmann, E.Strope, P.M.Plotsky and R.N.Adams - Nature 267 (1976), 145

74. F.Gonon, M.Buda, R.Cespuglio, M.Jouvet and J.F.Pujol - Nature 286 (1980), 902

75. F.Gonon, M.Buda, R.Cespuglio, M.Jouvet and J.F.Pujol - Brain Res. 223 (1981), 69

76. G.Nagg, M.E.Rice and R.N.Adams - Life Sci. 31 (1982),2611

77. C.D.Blaha and R.F.Lane - Eur. J. Pharm. 98 (1984), 113

78. M.B.Gelbert and D.J.Carran - Anal. Chem. 58 (1986), 1028

79. P.A.Broderick - Neurosci. Lett. 95 (1988), 275

80. G.A.Gerhardt, A.F.Oke, G.Nagg, B.Moghaddam amd R.D.Adams - Brain Res. 290 (1984), 390

81. G.Nagg, G.A.Gerhardt, A.F.Oke, M.E.Rice, R.N.Adams, R.B.Moore III, M.N.Szentirmay and C.R.Martin - J.Electroanal. Chem. 188 (1985), 85

82. R.M.Wrightmann, E.W.Kristensen, L.J.May and W.G.Kuhr - Proc. 1st Bioelectroanal. Symp., Matrafured, 1986, pp 187-208.

83. E.Kimura, H.Fujoka and M.Kodama - J. Chem. Soc. Comm. - 1986, 1158

84. A.E.G.Cass, G.Davis, G.D.Francis, H.A.O.Hill, W.J.Aston, I.J.Higgins, E.V.Plotkin, L.D.L.Scott and A.P.F.Turner - Anal. Chem. 56 (1984), 667

List of Courses Attended

"Electroanalytical Chemistry", by Dr. H.H. Girault.

"Membrane Science and Separation Techniques", by Dr. H.H. Girault

"Current Topics in Physical Chemistry", by Dr J. Tietje-Girault and Dr A. Jones.

"Computers in Chemistry", by Dr A.J. Blake, Dr. R. Gould, Dr. K.P. Lawley and Dr. K. McKendrick

"Solid State Chemistry", by Dr. G. McDougall

Butler Post-Graduate Electrochemistry Meetings, Edinburgh, 1988,1989,1990.

Department of Chemistry, Physical Chemistry Seminar Evenings.

39th International Society of Electrochemistry Conference, Strathclyde, 1988.

Royal Society of Chemistry, Electrochemistry Group, Spring Informal Meeting, Warwick, 1989.

NATO Advanced Studies Institue: Microelectrodes-Theory and Applications, Alvor, 1990.